Phenotypic characterization of SHOC2 inactivation in adult mice

Sibel Sari

Submitted in fulfilment of the requirements

for the Degree of

Doctor of Philosophy

University College London

2021

Declaration

I, Sibel Sari, confirm that the work presented in this thesis is my own. Where information has been derived from other sources, I confirm that this has been indicated in the thesis.

London, January 2021

In loving memory of my father…

To my mum and grandparents…

Abstract

The RAS/RAF/MEK/ERK signaling pathway plays an important role throughout mammalian development, from embryogenesis to tissue-specific cellular homeostasis and its aberrant activation is a major driver of human cancer.

RAF activation is a complex process that involves multiple regulatory steps in addition to RAS binding. Key among them is the dephosphorylation of a conserved inhibitory site by a phosphatase complex comprised of SHOC2, MRAS and PP1 (SHOC2 complex).

In order to study the role of Shoc2 in vivo, we have generated two mouse models of conditional Shoc2 inactivation. Shoc2 knock-out (KO) and knock-in (KI) mice are embryonic lethal indicating Shoc2 function is required during mouse development. To examine Shoc2 function in adult tissue homeostasis, Shoc2 KO and KI mice were crossed with animals carrying an inducible ubiquitously expressed $CreER^{T2}$ recombinase. Treatment with tamoxifen leads to efficient recombination in all tissues examined, except brain. Significantly, Shoc2 inactivation is tolerated well in the short term although, pleiotropic phenotypes do emerge after sustained Shoc2 inhibition. Histopathological analysis revealed that Shoc2 KO and KI mice display skin dermatitis characterized by marked inflammation, epidermal hyperproliferation and keratinocyte differentiation defects, as well as hair cycle impairment.

Post-mortem studies also show those mice have splenomegaly and lymphadenopathy which could be secondary to the progressively more severe skin inflammation. Male KO mice also have enlarged bladders full of urine suggesting a sexually dimorphic role for Shoc2 in urinary function.

Collectively, our results help validate SHOC2 as a therapeutic target for RAS-driven cancers and suggest that future SHOC2 targeted therapies may be tolerated relatively well-compared to other core components of ERK-pathway. However, our studies also indicate that sustained inhibition may lead to toxicities and underscore the importance of optimizing treatment windows as well as close monitoring of some particularly sensitive tissues.

Impact statement

The data presented in this thesis provides a better understanding of the previously unexplored physiological roles of Shoc2 in tissue homeostasis by characterising phenotypic changes related to systemic genetic Shoc2 inactivation.

We have generated KO and KI Shoc2^{D175N} mouse models to examine the role of Shoc2 at the organismal level under physiological conditions. Our results revealed that constitutive deficiency of Shoc2 in mice results in embryonic lethality at E8.5 demonstrates the importance of Shoc2 in embryonic development. We also show for the first time that inactivation of Shoc2 by the D175N mutation, which selectively disrupts SHOC2 holophosphatase complex formation, also results in embryonic lethality at the same stage of embryogenesis, suggesting lethality upon Shoc2 inhibition is dependent on its RAF phosphatase function.

In contrast to core components of the MAPK/ERK cascade (RAF, MEK, ERK), systemic Shoc2 inactivation in adult mice using either KO or KI Shoc2^{D175N} mouse models appears better tolerated in the short term, suggesting that redundant Shoc2-independent mechanisms of ERK pathway activation have important contributions to tissue homeostasis. However, our studies unveil an essential role of Shoc2 in skin homeostasis as Shoc2 KO and KI mice develop a skin dermatitis with features of atopic dermatitis and psoriasis with Shoc2 KI mice having a milder phenotype than KO mice. Systemic inflammation, likely secondary to skin inflammation, has also been detected in Shoc2 KO and KI mice with splenomegaly and lymphadenopathy. Furthermore, we have discovered a sexually dimorphic role of Shoc2 in urinary function, with male but not female KO mice developing enlarged urinary bladders. Hence, these study reveals a previously unknown role for Shoc2 in immune cell, skin and bladder homeostasis by using *in vivo* mouse models.

Our data shows that Shoc2 KI mice show a lower penetrance and delayed emergence of phenotypes compared to Shoc2 KO mice which correlates with greater median survival compared to the KO model. This may have important implications for future therapies as the Shoc2 KI model better recapitulates pharmacological inhibition of the SHOC2 phosphatase complex in the clinic. Overall, this study suggests SHOC2 targeted therapies may be relatively well-tolerated in the short term. However, our studies also reveal new roles for Shoc2 in physiological processes and suggest pleiotropic phenotypes likely to emerge after sustained inhibition.

Table of contents

List of figures

List of tables

Abbreviations

4-OHT	4-hydroxy-tamoxifen
AML	Acute myeloid leukemia
ARF	ADP Ribosylation factors
ATP	Adenosine triphosphate
BM	Bone marrow
BMMs	Bone marrow-derived macrophages
BSA	Bovine Serum Albumin
CD	Cluster of differentiation
cDNA	Complementary deoxyribonucleic acid
CLP	Common lymphoid progenitor
CMP	Common myeloid progenitor
CMV	Cytomegalovirus
COSMIC	Catalogue of somatic mutations in cancer
CR1/2/3	Conserved region 1/2/3
CRC	Colorectal cancer
CRD	Cysteine rich domain
DAB	Diaminobenzidine
DMEM	Dulbecco’s modified Eagle’s medium
DMSO	Dimethyl sulfoxide
DNA	Deoxyribonucleic acid
dNTPs	Deoxyribose nucleoside triphosphate
DTT	Dithiothreitol
DUSP	Dual-specificity phosphatase
ECL	Enhanced chemiluminescence
EDTA	Ethylenediaminetetraacetic acid
EGF	Epidermal growth factor
EGFR	Epidermal growth factor receptor
EMT	Epithelial-mesenchymal transition
ER	Estrogen receptor
ERK	Extracellular signal-regulated kinase
FACS	Fluorescence-activated cell sorting
FBS	Fetal bovine serum
FDA	Food and drug administration
FGF	Fibroblast growth factor
FGFR	Fibroblast growth factor receptor
GAP	GTPase activating protein
GDP	Guanosine diphosphate
GEF	Guanine nucleotide exchange factors
GEMM	Genetically engineered mouse model
GMP	Granulocyte/macrophage progenitor

GPCR	G-protein coupled receptor
GRB2	Growth factor receptor bound protein 2
GTP	Guanosine triphosphate
H&E	Hematoxylin and eosin
HEPES	Hydroxyethyl piperazineethanesulfonic acid
HER2	Human epidermal growth factor receptor 2
HRAS	Harvey rat sarcoma viral oncogene homolog
HSC	Hematopoietic stem cell
HRP	Horseradish peroxidase
HSP90	Heat shock protein 90
HVR	Hypervariable region
ICMT	Isoprenylcysteine carboxylmethyl-transferase
IF	Immunofluorescence
IFN	Interferon
IL	Interleukin
IP	Immunoprecipitation
IP	Intraperitoneal
JAK	Janus kinase
KD	Knockdown
KO	Knockout
KI	Knockin
KRAS	Kirsten rat sarcoma viral oncogene homologue
KSR	Kinase suppressor of RAS
LRR	Leucine-rich repeat
LSL	Lox-stop-lox
LUAD	Lung adenocarcinoma
MAPK	Mitogen-activated protein kinase
MEK	Mitogen-activated protein kinase kinase/ MAPK kinase
MPP	Multipotent progenitor
mRNA	Messenger ribonucleic acid
NF1	Neurofibromatosis type 1
NRAS	Neuroblastoma RAS viral oncogene homologue
NSCLC	Non-small-cell lung cancer
o/n	Overnight
PAGE	Polyacrylamide gel electrophoresis
PAK	p21-activated kinase
PBS	Phopsphate Buffered Saline
PCR	Polymerase chain reaction
PDAC	Pancreatic ductal adenocarcinoma
PFA	Paraformaldehyde
PI3K	Phosphatidylinositol 3-kinase
PKA	Protein kinase A
PKC	Protein kinase C
PMA	Phorbol myristate acetate
PMK	Primary murine keratinocytes

PP1	Protein phosphatase 1
PP2A	Protein phosphatase 2A
RAF	Rapidly accelerated fibrosarcoma
RAN	Ras related nuclear protein
RAS	c-Rat sarcoma viral oncogene homolog
RBD	Ras binding domain
RHO	Ras-homologous
RCE1	Ras converting enzyme
RNA	Ribonucleic acid
RPMI	Roswell park memorial institute medium
RSK	Ribosomal protein S6 kinase
RT	Room temperature
RTK	Receptor tyrosine kinase
SDS	Sodium dodecyl sulfate
SH2	Scr homology 2
SH3	Scr homology
SHOC2	Soc-2 suppressor of clear homolog
SOS	Son of sevenless homolog
TCR	T-cell receptor
TGF	Transforming growth factor
TRP53	Transformation related protein 53
TNF	Tumour necrosis factor
WT	Wild-type

Chapter 1 Introduction

RAS family GTPases

The RAS superfamily of small GTPases comprises over 150 different proteins divided into five distinct subfamilies: RAS, RHO, RAB, RAN, and ARF. These proteins play critical roles in regulation of cell proliferation, cell polarity, migration, signal transduction, nuclear transport and vesicular trafficking (Figure 1-1A) (Vigil et al. 2010; Wuichet and Sogaard-Andersen 2014).

The RAS subfamily was the first described and prototypical members includes the Harvey rat sarcoma viral oncogene homolog (HRAS), neuroblastoma RAS viral (v-ras) oncogene homolog (NRAS) and Kirsten rat sarcoma viral oncogene homolog (KRAS) genes together with the closely related MRAS, RRAS and TC21 (Karnoub and Weinberg 2008; Castellano and Santos 2011).

In the mammalian genome, three *RAS* genes encode four highly homologous, ubiquitously expressed ~21 kDa RAS isoforms: HRAS, NRAS, two KRAS isoforms that arise from alternative RNA splicing KRAS4A and KRAS4B. These proteins are >90% identical in the first 168–169 amino acids (known as the G domain) which contains the GTP–GDP binding site and interaction sites for effector proteins, but highly divergent in the C-terminal 20 amino acids, which are known as the hypervariable region (HVR) (Figure 1-1B) (Pylayeva-Gupta et al. 2011; Cox et al. 2014). The HVR commonly terminates with a CAAX (C, cysteine; A, aliphatic amino acid; X, terminal amino acid) tetrapeptide motif that undergoes posttranslational modifications (Papke and Der 2017). These modifications include the covalent addition of farnesyl group (isoprenoid) to the cysteine residue of the CAAX motif mediated by protein farnesyltransferase (Zhang and Casey 1996). The addition of the prenyl groups enhances hydrophobicity and promote RAS association with the plasma membrane (Konstantinopoulos et al. 2007).

After prenylation, the last three amino acid residues (AAX) are cleaved by RCE1 (RAS converting CAAX endopeptidase 1) (Boyartchuk et al. 1997), and then farnesylated cysteine residue undergoes carboxymethylation mediated by ICMT (isoprenylcysteine carboxyl methyltransferase) (Gutierrez et al. 1989; Dai et al. 1998; Simanshu et al. 2017). Additionally, H, N and KRAS4A are also modified with palmitoyl groups at C-terminal cysteine residues, which is required for further contribution of membrane-anchoring (Hancock et al. 1990). However, KRAS4B does not undergo palmitoylation (due to lack of C-terminal cysteine residues to accept

palmitoylation modification) but instead interacts directly to the plasma membrane by associating its positively charged polylysine region (polybasic region) in the HVR with the negatively charged head groups of membrane lipids through electrostatic interaction (Ehrhardt et al. 2002; Zhao et al. 2015).

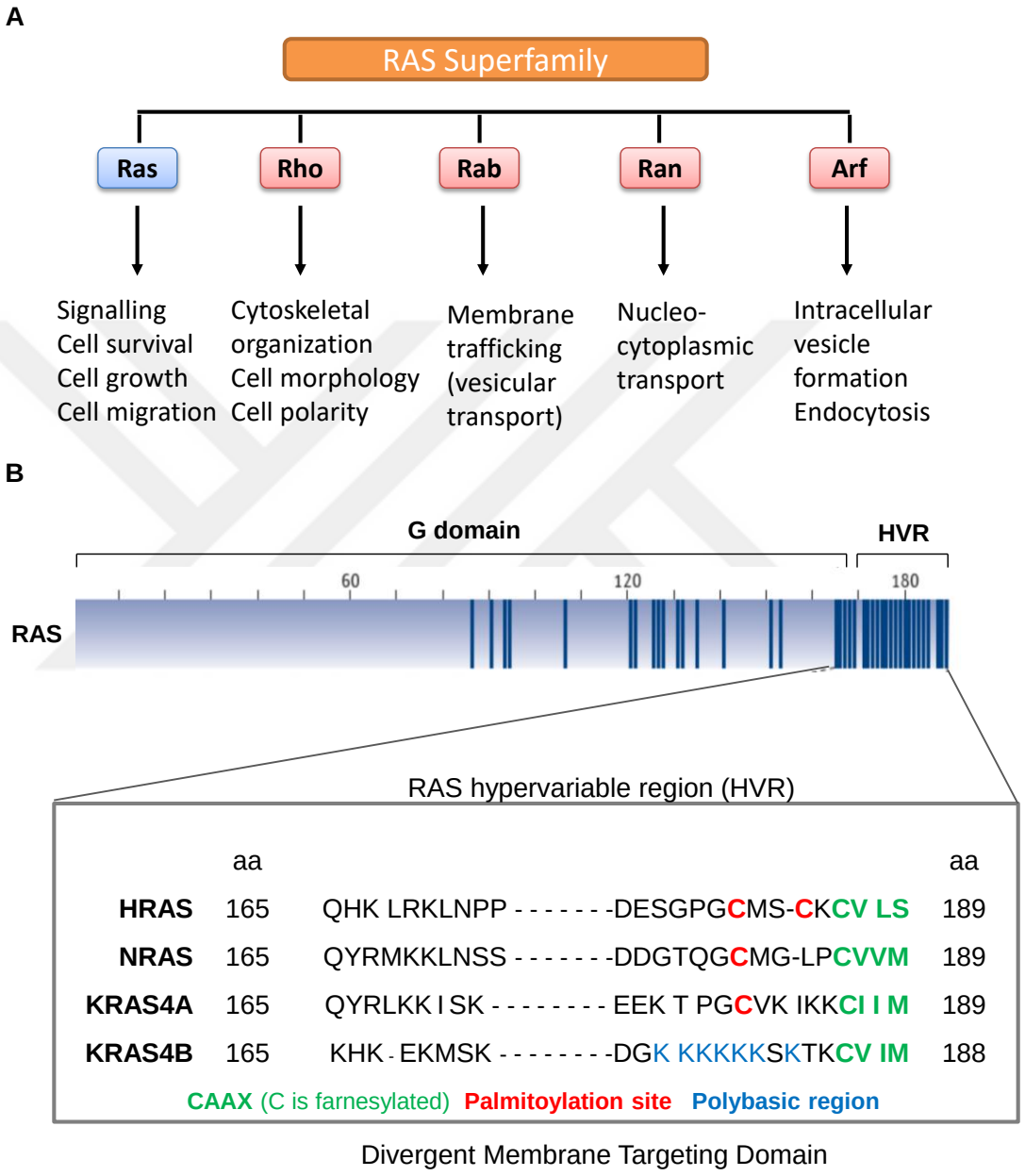

Figure 1-1. The RAS superfamily and post-translationally modified RAS proteins

A. Major subfamilies and functions of the RAS superfamily. Adapted from (Vigil et al. 2010).
B. The four RAS proteins: HRAS, NRAS, KRAS4A and KRAS4B share >90% overall sequence identity in their G-domains (blue vertical lines indicate amino acid non-identity). However, the ~24 amino acid C-terminal HVR domain contains divergent membrane targeting signals. Highlighted in green is the first post translational modification motif, the cysteine residue forming the membrane targeting CAAX motif,

which is farnesylated. For HRAS, NRAS and KRAS4A, the second signal consists of cysteine residues that are palmitoylated (highlighted in red). For KRAS4B, the second signal consists of a polybasic region made up of a stretch of lysines (highlighted in blue). Adapted from (Cox et al. 2014).

The RAS proteins oscillate between an active GTP-bound and inactive GDP-bound state to function as molecular switches at the inner leaflet of the plasma membrane (Zhou and Hancock 2015). This switch is tightly regulated by GTPase-activating proteins (GAPs) and guanine nucleotide exchange factors (GEFs) (Figure 1-2A) (Downward et al. 1990b). Signal transduction by Receptor Tyrosine Kinases (RTKs), G-Protein Coupled Receptors (GPCRs) and cytokine receptors can activate RAS. This activation can occur primarily at the plasma membrane, but also other membrane sites, such as Golgi membranes and endosomal membranes (Burke et al. 2001; Chiu et al. 2002). Ligand engagement to an RTK, for example EGF binding to EGFR, leads to receptor autophosphorylation on multiple tyrosine residues. One of the SH2 domain proteins, GRB2, binds to these tyrosine-phosphorylated residues and then binds to GEF SOS (Son of Sevenless), translocating it to the plasma membrane. This translocation is believed to bring SOS into close proximity with RAS, leading to the activation of RAS (Margolis and Skolnik 1994).

Termination of RAS signalling occurs through hydrolysis of GTP to GDP by GAPs (eg. Neurofibromin 1 - NF1) which accelerate the weak intrinsic GTPase activity of RAS by nearly 100-fold, returning RAS to the inactive, GDP-bound state (Bos et al. 2007). GAPs function by inserting an ‘arginine finger’ into the active site of the GTPase whereby it neutralises the negative charge of the γ-phosphate and stabilises the transition state (Ahmadian et al. 1997).

In response to extracellular signals from growth factors, hormones and cytokines, active RAS binds effectively with a series of cytoplasmic target or effectors thereby regulating cell growth, differentiation, proliferation, migration etc. Among the various RAS effectors, RAF is one of the best characterized-effectors identified downstream of RAS (Figure 1-2B) (Vojtek et al. 1993).

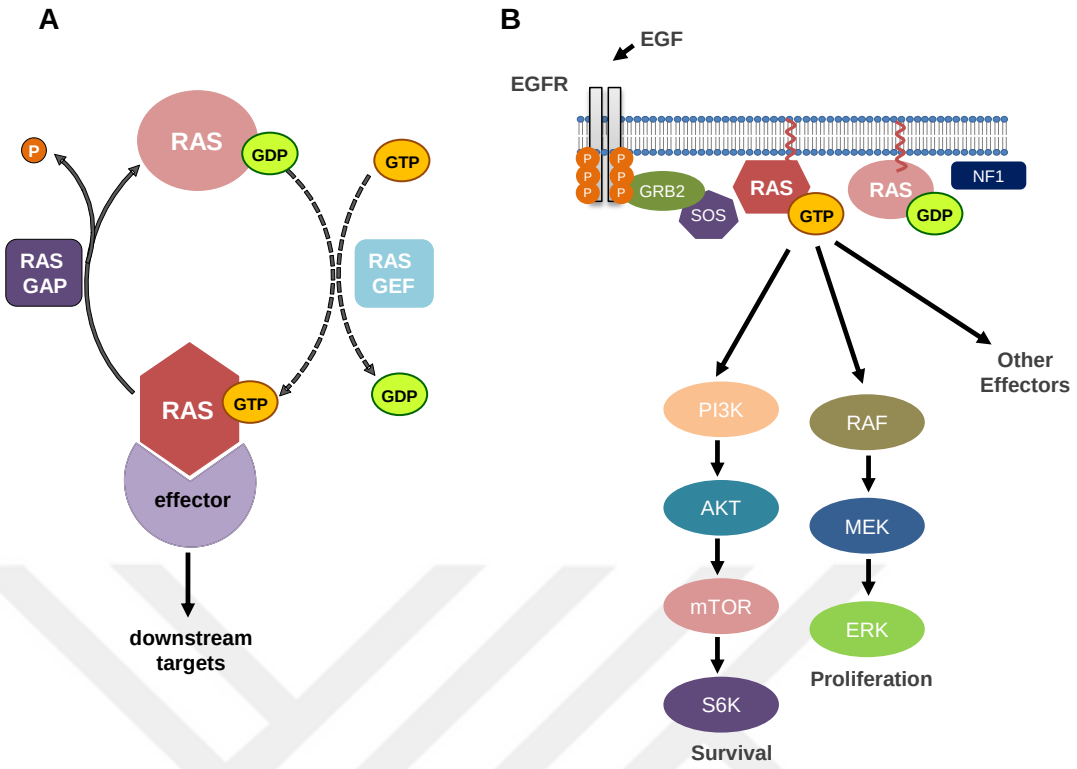

Figure 1-2. Regulation of the RAS GDP–GTP cycle and its effector pathways

A. RAS proteins cycling between active and inactive states is mediated by GAPs and GEFs. Active GTP-bound RAS binds and activates downstream effectors. Adapted from (Cox et al. 2014).
B. RAS-GTP activates numerous effector pathways of which the RAF/MEK/ERK and PI3K/AKT pathways are the best characterized. Adapted from (Karnoub and Weinberg 2008).

The RAS/RAF/MEK/ERK signalling pathway

RAS and its downstream kinase cascade RAF/MEK/ERK or, MAPK/ERK pathway, transduces extracellular signals to control a wide range of cellular responses (Ferraiuolo et al. 2017). Ligand-binding to a cell surface receptor tyrosine kinase, results in the generation of phosphotyrosine binding sites for adaptor proteins, causing activation of the membrane bound GTPase RAS (Cseh et al. 2014). Following RAS activation, RAF (Rapidly Accelerated Fibrosarcoma) is recruited to the cell membrane and activated RAF phosphorylates and activates their restricted substrate, MEK1/2 (Mitogen-activated protein kinase kinase). MEK kinases in turn mediate the phosphorylation of threonine and tyrosine residues of ERK1/2 (Extracellular Signal-Regulated Kinase), their only substrates. This phosphorylation activates ERK1/2, which are protein-serine/threonine kinases. In contrast to RAF and

MEK1/2, which have narrow substrate specificity, ERK1/2 have dozens of substrates that are important for the regulation of cellular processes such as proliferation, differentiation, migration, and others (Karnoub and Weinberg 2008; Roskoski 2010).

RAF kinases

RAF comprises a family of three kinases, ARAF, BRAF and CRAF (CRAF also known as RAF-1), which are the primary kinases and key regulators of MAPK/ERK signalling pathway. All these three RAF kinases share three conserved regions (CR1, CR2, and CR3) and several regulatory phosphorylation sites. CR1 includes two RAS-binding sites, RAS-binding domain (RBD) and cysteine-rich domain (CRD), required for RAF membrane recruitment. CR2 contains a preserved Ser/Thr rich residues including important phosphorylating sites and CR3 includes the RAF kinase domain and a conserved serine residue that serves as a binding site for 14-3-3 (Figure 1-3) (Hindley and Kolch 2002; Leicht et al. 2007; Terrell and Morrison 2019).

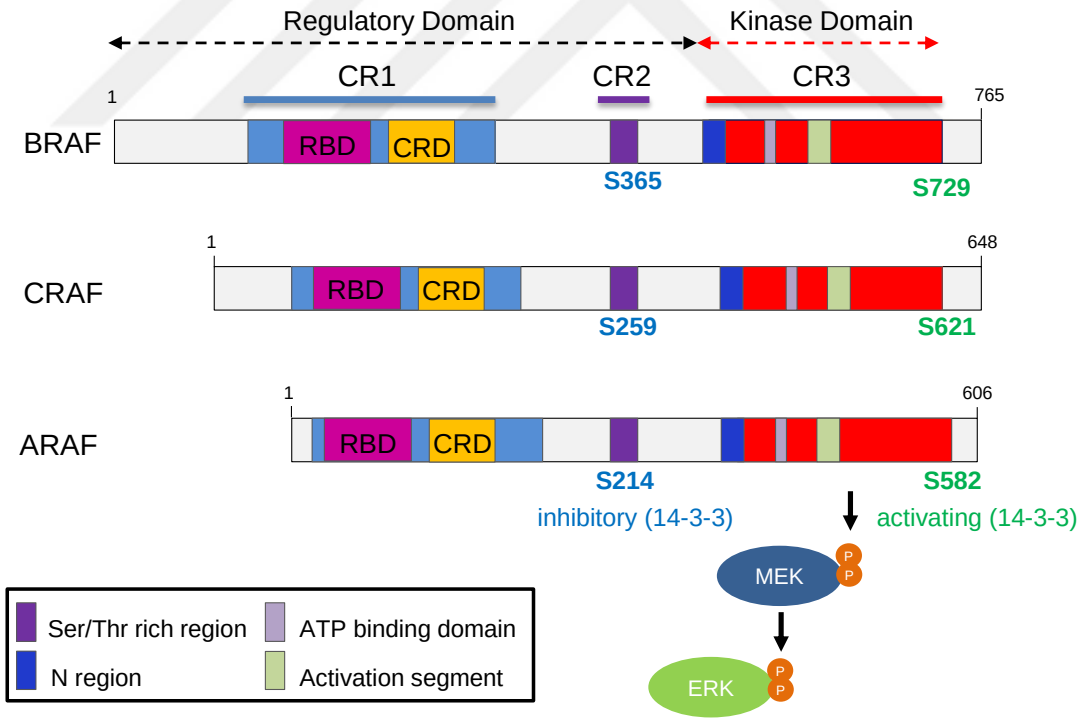

Figure 1-3. Structure of the RAF proteins

The RAF isoforms, ARAF, BRAF and CRAF, contain three conserved regions: CR1 (blue), CR2 (purple) and CR3 (red). CR1 contains a RAS-binding domain (RBD) and the cysteine-rich domain (CRD), while CR2 includes a Ser/Thr phosphorylation site. The 14-3-3 binding at this domain inhibits RAF (blue). CR3 (kinase domain) contains the activation segment, an ATP

binding domain and the N-region. At the C terminus, there is a secondary 14-3-3 binding site which activates dimerization (green). Adapted from (Terai and Matsuda 2006).

The RAF activation cycle is strikingly complex and involves a series of sequential processes that are still poorly understood despite of in-depth studies. Although there are some conflicting models, most of them agree that RAF activation includes RAS binding through RBD and CRD domains, plasma membrane recruitment, specific phosphorylation and dephosphorylation events, dimerization and other protein-protein interactions (McKay and Morrison 2007).

In agreement with the current model for RAF activation proposing that in normal cells and in the absence of upstream activity, RAF is maintained in the cytosol in an auto-inhibited inactive state by an interaction between the N-terminal region and the catalytic domain, which is in part mediated by a 14-3-3 dimer bound to two phosphorylated residues (S259 and S621 in CRAF, S365 and S729 in BRAF) (Morrison, 1997; Lavoie and Therrien 2015). This model has been confirmed with a recent paper, Park et al. (2019) reporting the auto-inhibited and active-state structures of full-length BRAF in complexes with MEK1 and a 14-3-3 dimer. Their Cryo-EM studies have shown that a dimeric 14-3-3 binds two phosphorylated serine residues on CRAF at Ser621 and on BRAF at Ser 729, and thereby stabilizes the side-to-side heterodimer or homodimer (Park et al. 2019).

Upon activation, RAS binding to the RBD of RAF recruits RAF to the plasma membrane which is generally appreciated to be an early step in RAF activation. Here, additional phosphorylation events and interactions facilitate activation of RAF catalytic function (Lavoie and Therrien 2015).

One of the earlier steps in RAF activation is the dephosphorylation of a conserved inhibitory site in the N-terminal regulatory domain (ARAF S214, BRAF S365, CRAF S259, hereby referred as ‘S259’). The activating mutations which are frequently found in RASopathies, cluster around this S259 14-3-3 binding site and highlight the importance of this regulatory step in RAF-ERK pathway activation (Molzan et al. 2010). Upon dephosphorylation of S259, 14-3-3 proteins are then displaced from this site, which destabilises the closed-conformation of RAF and allows the CRD (Cysteine-rich domain) to anchor RAF to the plasma membrane (Rommel et al. 1996; Jaumot and Hancock 2001; Dhillon et al. 2002). Re-orientation of 14-3-3 proteins to bind two phosphorylated ‘S621’ site at the carboxy-terminal tail,

mediates the RAF dimerization (Lavoie and Therrien 2015). The RAF kinases can form physiologically relevant homo- and hetero-dimers and their kinase activities are regulated by both negative and positive phosphorylation events (McKay and Morrison 2007; Taylor and Kornev 2011).

RAF proteins undergo multiple phosphorylation events by kinases during their activation cycle. Indeed, the aforementioned serine residues in the conserved 14-3-3 binding motifs at the N-terminus can be phosphorylated mainly by Protein Kinase A (PKA) (Dumaz and Marais 2003; Li et al. 2013) and AKT (Zimmermann and Moelling 1999; Guan et al. 2000) and at the C-terminus can be phosphorylated by AMP-activated protein kinase (AMPK) (Sprenkle et al. 1997) and PKA (Mischak et al. 1996). RAF proteins anchored to the membrane are in proximity to kinases that phosphorylate residues in the activation segment and the N-region (negative charge regulatory region) that promote their activation (Morrison and Cutler 1997; Lavoie and Therrien 2015). The activation segment of RAFs contains two conserved phosphorylation sites which are Thr452 and Thr455 for ARAF (Baljuls et al. 2008), Thr599 and Ser602 for BRAF (Zhang and Guan 2000; Chong et al. 2001) and Thr491 and Ser494 for CRAF (Kolch et al. 1993; Chong et al. 2001). With regards to N-region contains subtle sequence variations for phosphorylation among the three RAF isoforms, allowing them to have divergent regulation (Mason et al. 1999). In both ARAF and CRAF, the N-region contains ‘SSYY’ motif and requires phosphorylation of both serine and tyrosine residues by SRC or PAK for full kinase activation (Cleghon and Morrison 1994; Marais et al. 1995; Marais et al. 1997; Mason et al. 1999). In contrast, the N-region of BRAF includes the ‘SSDD’ motif, in which acidic aspartate residues ($DD^{448/9}$) provide a negative charge that promotes constitutive serine 445 phosphorylation by the CK2 kinase (Marais et al. 1997; Mason et al. 1999; Ritt et al. 2007). The combination of constitutive phosphorylation of S445 and acidic aspartate residues is thought to be responsible for BRAF elevated basal kinase activity compared to ARAF and CRAF (Mason et al. 1999).

Consequently, when RAF kinases are active, they can bind and subsequently phosphorylate its unique catalytic substrate MEK.

MEK kinases

The mitogen-activated protein kinase kinase (MAP2K), or MEK enzymes found in two different forms: MEK1 and MEK2. These kinases catalyse the phosphorylation of tyrosine and threonine residues of a specific tripeptide sequence (Thr-Glu-Tyr) of the extracellular signal-regulated protein kinase 1 (ERK1) and ERK2, as they called dual-specificity protein kinases (Savoia et al. 2019).

Similar to all other protein kinases, MEK1/2 have similar configuration consisting of N-terminal domain, catalytic (kinase domain) with an activation segment and C-terminal domains (Fischmann et al. 2009). MEK activation by RAF requires the phosphorylation of two serine residues (S218/S222 in MEK1 and S222/S226 in MEK2) in its activation segment (Alessi et al. 1994; Zheng and Guan 1994). However, the exact mechanism of MEK activation by RAF remains unclear. Some studies propose that in quiescent cells, MEK forms a heterodimer with BRAF in the cytosol and upon pathway activation this inactive complex recruits to the plasma membrane by active RAS, forming an active tetramer with another RAF-MEK complex (Haling et al. 2014). Here, RAF can phosphorylate MEK in this heterotetramer (two RAF, two MEK molecules) complex. Other studies suggest that MEK may be presented to active RAF by a scaffold protein kinase suppressor of RAS (KSR) (Brennan et al. 2011). According to this model, under quiescent conditions MEK forms a complex with KSR in the cytosol. KSR masks MEK activation sites ‘S218 and S222’ from RAF and thus prevents its access for phosphorylation (Brennan et al. 2011; McKay et al. 2011). In response to RAS activation, KSR-MEK complex is translocated from the cytosol to the plasma membrane. At the membrane, RAF dimerise with KSR-MEK complex, inducing conformational changes that expose the MEK activation segment, which in turn is phosphorylated by a different RAF dimer bound to RAS (Brennan et al. 2011; Dhawan et al. 2016).

Ultimately, active MEK kinases can phosphorylate and activate their only known physiological substrates, ERK kinases, which have dozens of cytosolic and nuclear substrates.

Extracellular signal-regulated kinases

Extracellular signal-regulated kinases 1 and 2 (ERK1/2), multifunctional serine/threonine kinases, ubiquitously expressed across all tissues, with particularly high levels in the brain, skeletal muscle, thymus, and heart (Boulton et al. 1990). The ERK1/2 are dually phosphorylated by MEK1/2 on a Thr-Glu-Tyr (TEY) sequence in the activation segment corresponding to Thr202 /Tyr204 in ERK1 and Thr183 /Tyr185 in ERK2 (Ahn et al. 1991; Payne et al. 1991). This phosphorylation causes dramatic conformational changes and stimulates a 1000-fold activation of intrinsic kinase activity (Zhang et al. 1994).

Upon activation, ERK1 and ERK2 can phosphorylate a plethora of cytosolic and nuclear substrates and phosphorylation of these substrates regulates the numerous biological functions (Eblen 2018). ERK1/2, phosphorylate downstream components on a consensus Pro-X-Ser/Thr-Pro motif where X is a neutral or basic amino acid (Alvarez et al. 1991).

In the nucleus, ERK1/2 modulate the activity of transcription factors, such as c-Fos, c-Myc, and c-Jun. In the cytoplasm, ERKs phosphorylate more than 50 substrates including cytoskeletal proteins, adherens junction components and ribosomal protein S6 kinases (RSKs) (Yoon and Seger 2006). RSKs are a family of ubiquitously expressed, serine-threonine kinases that also have nuclear and cystolic substrates and help enhancing the ERK signalling (Roux et al. 2003; Kidger and Cook 2018). Additionally, other important ERK targets are involved in cell cycle regulation, in apoptosis, and in several signalling pathways (Unal et al. 2017; Savoia et al. 2019).

In order to produce the correct biological response, ERK pathway activity is tightly regulated both spatially and temporally. The activation of ERK pathway is attenuated by negative feedback loops from ERK itself to upstream pathway components, such as RTKs, SOS, KSR, RAF and MEK (Corbalan-Garcia et al. 1996; Li et al. 2008; Lake et al. 2016). Phosphorylation of both CRAF and BRAF by ERK has been shown to disrupt RAS binding, plasma membrane localization and RAF dimerization and thus attenuating MEK phosphorylation and subsequent ERK activity (Rushworth et al. 2006; Ritt et al. 2010). In addition to immediate inhibitory phosphorylation, Dual-specificity phosphatases (DUSP) and Sprouty (SPRY) proteins are involved in transcriptional inhibition of the ERK signalling and perform a more delayed pathway inhibition (Huang and Tan 2012; Degirmenci et al. 2020). DUSPs

can inactivate ERKs by the direct cleaving of either one or both sites phospho-ERK 'pT-E-pY' motifs (Caunt et al. 2015) whereas SPRY proteins can inhibit the activity of ERK pathway at multiple levels upstream of ERK such as RTKs and SOS, through unclear mechanisms (Mason et al. 2006; Guy et al. 2009).

SHOC2 phosphatase complex

A phosphatase holoenzyme comprised of SHOC2 and the catalytic subunit of protein phosphatase 1 (PP1) functions as an effector of MRAS. This ternary holoenzyme complex (SHOC2 complex) has been identified as a key regulator of RAS/ERK pathway (Rodriguez-Viciana et al. 2006; Young et al. 2013; Young et al. 2018; Young and Rodriguez-Viciana 2018; Boned Del Rio et al. 2019; Jones et al. 2019).

The formation of SHOC2 complex is stimulated by activation of MRAS, and it leads to PP1-mediated specific dephosphorylation of the key inhibitory site in all RAF isoforms (S259 in CRAF, S365 in BRAF and S214 in ARAF) translocated to the plasma membrane by active RAS. This dephosphorylation event permits the homo- or heterodimerization and transactivation of RAF family members and subsequent downstream signalling to MEK and ERK (Figure 1-4).

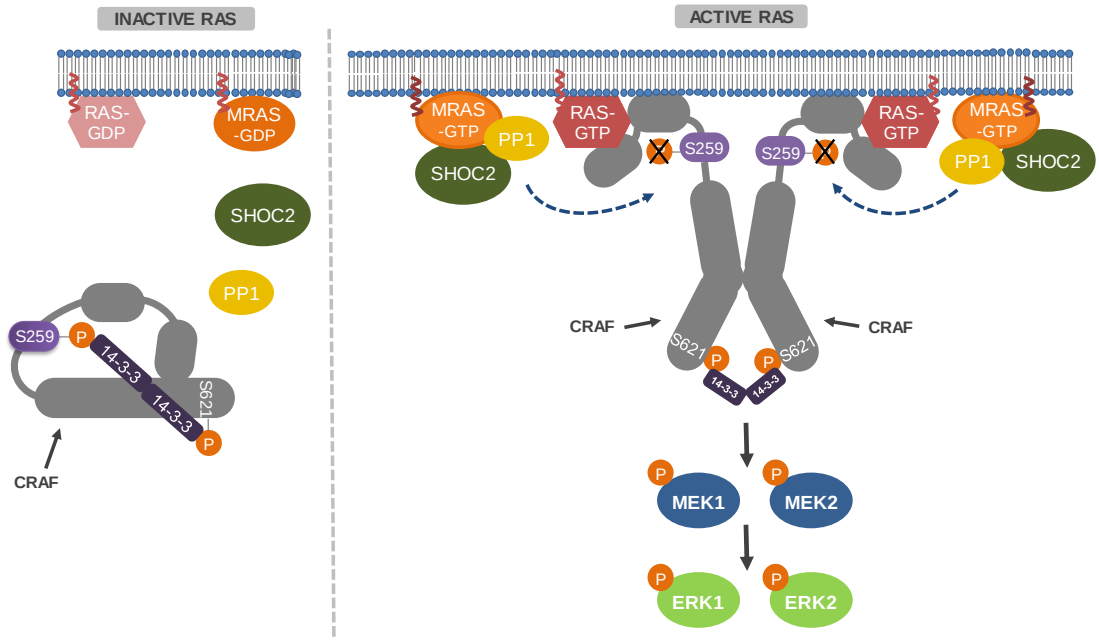

Figure 1-4. The SHOC2 phosphatase complex

RAF is kept in an auto-inhibited state in the cytosol. Upon activation, RAS recruits RAF to the plasma membrane, and MRAS promotes SHOC2-MRAS-PP1 complex formation. Subsequently, dephosphorylation of the conserved inhibitory site 'S259' by PP1 leads to the release of the 14-3-3 protein from this site. Then, phosphorylation steps occur, and the fully activated kinase can target MEK.

MRAS

MRAS (also known as RRAS3) is a member of the sub-family of RAS proteins and is the closest relative to the prototypical RAS oncoproteins. It shares many regulatory and effector interactions with other classical RAS proteins but it also has specific functions of its own in cellular processes such as differentiation, cytoskeletal remodelling and cell migration (Ohba et al. 2000; Young and Rodriguez-Viciana 2018).

Similar to the canonical RAS proteins, MRAS is activated by growth factors, cycling between an inactive GDP and active GTP form, with the same GAP/GEF specificity and it can bind directly to RAF isoforms via the RBD recruiting RAF to the plasma membrane (Ehrhardt et al. 2002; Rodriguez-Viciana et al. 2004). Besides, MRAS shares a similar HVR to KRAS4B but differs from HRAS and NRAS that are palmitoylated in their carboxy-terminal cysteines. MRAS cannot be palmitoylated as it lacks the essential cysteine residues and instead, like KRAS4B, it has a polybasic region. Both of them are similarly located in disordered membrane microdomains rather than organised lipid rafts which suggests they may signal in similar pathways and/or be similarly regulated (Ehrhardt et al. 2002).

PP1

Protein phosphatase 1 (PP1) is a ubiquitously expressed serine/threonine (S/T) phosphatase that has nearly 200 validated interacting proteins in vertebrates. Together with protein phosphatase 2A (PP2A), PP1 accounts for more than 90% of protein phosphatase activity in eukaryotes, and among them, the majority of S/T-linked phosphate ester bonds are hydrolysed by PP1 due to its wide substrate diversity (Heroes et al. 2013; Kolupaeva and Janssens 2013). In contrast to protein kinases, which can select substrates based on conserved amino acid sequences near a target phosphorylation site, PP1 exhibits limited recognition and dephosphorylation of phosphosites on its substrates (Bollen et al. 2010; Peti et al. 2013). For this

recognition, PP1 has to interact with regulatory proteins through multiple low-affinity interactions and form a holoenzyme in which the regulatory subunit defines substrate specificity, modulates the phosphatase activity and regulates the localization of PP1 (Virshup and Shenolikar 2009; Bollen et al. 2010).

SHOC2

SHOC2 (Soc-2 suppressor of clear homolog), also known as SUR-8 and SOC-2, is an evolutionarily conserved, 65 kDa ubiquitously expressed protein comprised almost entirely of leucine-rich repeats (LRRs). The LRR motifs consist of approximately 20-30 amino acids with a conserved 11-residue repeat sequence with the following consensus LxxLxLxxNxL where x can be any amino acids. The conserved leucine can be occupied by other hydrophobic amino acids such as isoleucine, valine and phenylalanine and asparagine can be replaced by a cysteine or threonine residues. LRR structures contain at least two or more repeats and form curved solenoid structures that are particularly suitable to mediate protein-protein interactions (Kobe and Deisenhofer 1994; Bella et al. 2008).

In *Caenorhabditis elegans,* where it was originally discovered in the late 1990s, SHOC2 acts as a positive modulator of the RAS/MAPK signalling cascade. Unlike RAF (*lin-45*), MEK (*mek-2*) or ERK (*mpk-1/sur-1*) genes (Wu et al. 1995; Lackner and Kim 1998; Hsu et al. 2002), SHOC2 (*sur-8*) in *C.elegans* was not essential for organ development and survival but its deletion strongly suppressed the phenotype of mutant RAS or high RTK (Fibroblast growth factor receptor - FGFR) signalling (Selfors et al. 1998; Sieburth et al. 1998; Motta et al. 2016). It was initially described to function as a scaffold protein, assembling RAS and RAF together into a functional complex (Li et al. 2000; Dai et al. 2006; Matsunaga-Udagawa et al. 2010; Yoshiki et al. 2010; Jang et al. 2014; Jang and Galperin 2016). However, our group has shown that SHOC2 has no direct interaction with classical RAS proteins (H, N and K) or RAF and instead it recognises both MRAS and PP1 as binding partners (Rodriguez-Viciana et al. 2006; Jeoung et al. 2013; Young et al. 2013; Young and Rodriguez-Viciana 2018).

The genetic screens in *C. elegans* pinpointed regions of SHOC2 as a critical area for MRAS and PP1 interaction. These original screens identified SHOC2^{D175N} point mutation as a loss-of-function mutant of SHOC2 and further validation analysis

highlighted that this mutation could uniquely disrupt SHOC2's interaction with either MRAS or PP1 whilst preserving interaction with other effectors, notably with the scaffold protein SCRIB (Rodriguez-Viciana et al. 2006). Therefore, this provides a unique SHOC2^{D175N} mutant tool to unravel the roles of SHOC2 *in vitro* and *in vivo* as part of the MRAS-SHOC2-PP1 holoenzyme complex or other complexes.

The crystal structure of the SHOC2 complex still remains unknown. However, SHOC2 itself is predicted to have a horse-shoe shaped structure similar to that of the PP2A subunit of the PP2 phosphatase (Young et al. 2018). Like the MRAS-SHOC2-PP1 phosphatase complex, PP2A is also a heterotrimeric holoenzyme that comprises the regulatory subunits 'A' and 'B' and a catalytic subunit 'C'. The 'A' subunit provides a similar horse-shoe shaped scaffold on which subunits 'B' and 'C' dock (Groves et al. 1999; Cho and Xu 2007). When forming the complex, the flexible structure and the ability to undergo various conformational changes of 'A' subunit allows it to bind diverse molecules (Seshacharyulu et al. 2013). It is anticipated that the flexible structure of SHOC2 may allow such an interaction and complex formation on binding active MRAS-GTP to permit PP1 binding to both components of the complex (Young et al. 2018).

The SHOC2 phosphatase holoenzyme complex is implicated in cancer and other diseases such as the RASopathies and thus exploring the undiscovered roles of this complex is important to find better ways to prevent and/or treat such diseases.

ERK pathway in cancer

The RAS/ERK pathway is frequently altered in human cancers, because of particularly prevalent RAS and RAF mutations (Fey et al. 2016). Oncogenic mutations in all RAS isoforms are found in about 30% of all human cancers with the highest incidence in pancreatic (~98%), colorectal (~52%), and lung (~32%) adenocarcinomas (Shin et al. 2020). KRAS is the most frequently mutated isoform present in 85% of all in human cancers compared to 11% for NRAS and 4% for HRAS according to the COSMIC dataset (Figure 1-5A) (Hobbs et al. 2016). RAS driver mutations are concentrated within three hotspots involving residues G12, G13, and Q61. In KRAS, G12 mutations accounts for 83% of all detected mutations, followed by G13 mutations (14%), and rare Q61 mutations (2%). In contrast, NRAS involves predominantly Q61 mutations, followed by G12 and G13. Lastly, HRAS exhibits an

intermediate pattern, with comparable mutation frequencies of G12, G13 and Q61(Figure 1-5B) (Hobbs et al. 2016). These mutations fix the RAS, in a constitutive active state due to a defect in cycling off to the inactive form. RAS proteins then become insensitive to GAPs thereby resulting in aberrant activation of RAS-effector signalling pathways that promote tumorigenesis (Lu et al. 2016; Shin et al. 2020).

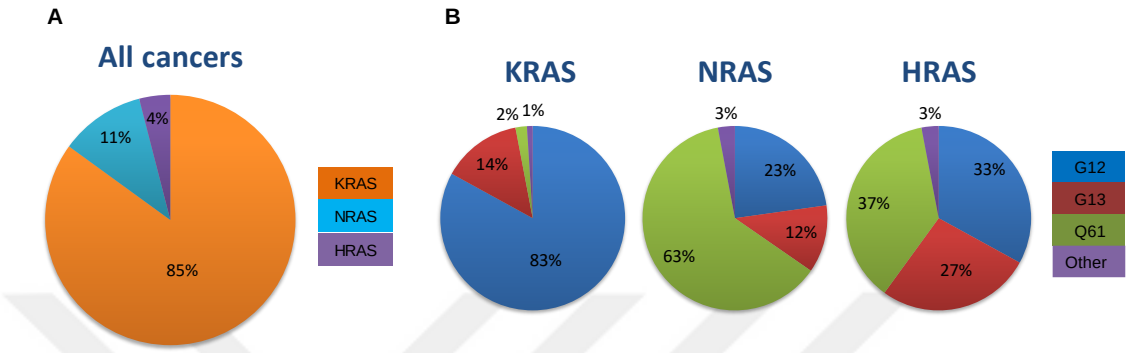

Figure 1-5. RAS mutations in cancer

A. Pie chart shows frequencies of H/N/KRAS mutations across all human cancers. RAS mutations occur in ~30% of all human cancers and KRAS is the predominant mutated isoform, accounting for 85% of the RAS mutations.
B. The oncogenic single base missense mutations in RAS isoforms are found predominantly at three residues: G12, G13 and Q61. Adapted from (Hobbs et al. 2016).

Upstream of RAS, aberrant expression and oncogenic mutations in RTKs such as EGFR and HER2/ErbB2, are also associated to a variety of human cancers (Lynch et al. 2004; Stephens et al. 2004; Hynes and Lane 2005; Nazarian et al. 2010). Classical EGFR activating mutations which are the single point mutation leucine-858 to arginine (L858R) in exon 21 and deletions in exon19 (dels746–750) represent the vast majority of EGFR mutations (Vyse and Huang 2019; Harrison et al. 2020). These mutations occur in the ATP-binding domain of the tyrosine kinase, leading to an increase of EGFR activity and enhance downstream RAS pathway activation by recruiting adaptor proteins like GRB2 and GEFs like SOS (Scaltriti and Baselga 2006; Yamaoka et al. 2018).

Downstream of RAS, mutations in RAF kinases can also cause aberrant activation of the ERK pathway, particularly BRAF is the most frequently mutated in 7% to 10% of all cancers (Bromberg-White et al. 2012). The higher frequency of BRAF mutations compared to ARAF and CRAF mutations associated to BRAF's higher basal kinase activity and its relatively more straightforward mechanism of activation as one single point mutation is sufficient to render BRAF constitutively

active. In contrast, other RAF isoforms may require multiple mutations or additional events to reach full activation (Desideri et al. 2015).

Cancer-related BRAF alterations can be categorized into three general functional classes based on how they trigger the pathway. Class I BRAF mutations which include BRAF V600 mutations (represent over 90% of BRAF alterations) activate RAF by mimicking phosphorylation of the activation loop (Degirmenci et al. 2020). BRAF V600E is the most common amino acid substitution, accounting for >90% of BRAF V600 mutations and it is common in melanoma (~50%), thyroid cancers (~40%), and colorectal adenocarcinomas (~10%) (Tan et al. 2008; Imperial et al. 2017). This mutation causes constitutive activation of the kinase, independent of upstream regulation or dimerization with other RAF molecules, as well as insensitivity to negative feedback mechanisms (Ascierto et al. 2012). Class II and III BRAF mutations are non-V600 BRAF mutations and found in only 5–16% of melanomas, but they are very common in non-small cell lung cancers (50–80%) and colorectal cancer (22-30%) (Jones et al. 2017; Noeparast et al. 2017; Dankner et al. 2018). Class II BRAF mutations are predominantly located in the activation segment (i.e. K601, L597) (Ikenoue et al. 2003; Andreadi et al. 2012) or P-loop (i.e. G464, G469) (Houben et al. 2004; Ikenoue et al. 2004) and they turn on RAF activity by destabilizing the auto-inhibitory status (Degirmenci et al. 2020). In contrast to Class I (high kinase activity) and Class II (high or intermediate kinase activity), Class III BRAF mutations have no or impaired kinase activity and thus, they cannot directly phosphorylate MEK (Wan et al. 2004). Instead, class III BRAF mutants, such as D594G and G466V, increase ERK signalling indirectly by amplifying signalling through transactivating CRAF with their enhanced dimerization affinity (Ikenoue et al. 2003; Noeparast et al. 2017).

Unlike BRAF, ARAF and CRAF mutations are exceptionally infrequent in human cancers. An activating ARAF S214A mutation has been identified in lung adenocarcinoma (Imielinski et al. 2014) and some mutations in CRAF, most frequently in S257 and S259 sites, have been reported in several tumor types, such as lung adenocarcinoma and colorectal cancer (Holderfield et al. 2014; Imielinski et al. 2014; Desideri et al. 2015). In addition, CRAF overexpression is present in bladder cancer, hepatocellular carcinoma and lung adenocarcinoma (Maurer et al. 2011).

MEK and ERK mutations are also very rare in cancer genomes. It has been reported that MEK mutations in cancer either turns on the kinase activity of MEK or

enhance MEK homodimerization (Yuan et al. 2018). These mutations have been found in melanoma, lung, ovarian and colorectal cancer (Nikolaev et al. 2011; Bromberg-White et al. 2012; Cancer Genome Atlas 2015; Maust et al. 2018; Savoia et al. 2019). With regard to ERK, a mutational hotspot has been identified on Dusp-mediated dephosphorylation site (Brenan et al. 2016). The ERK2 E322K mutant has been found at significant frequency in cervical and head and neck cancers (Arvind et al. 2005; Lawrence et al. 2014; Ojesina et al. 2014).

In clear contrast to H/K/N-RAS genes, mutations in MRAS is also extremely rare (COSMIC). Regarding the critical role of the RAF-ERK pathway in mediating RAS oncogenic properties, the lower affinity of MRAS for RAF and its notably weaker activation of the ERK pathway may account for this situation (Young et al. 2013; Young and Rodriguez-Viciana 2018). Yet still, MRAS is found amplified in 17% of lung squamous cell carcinomas; furthermore, it is also overexpressed in ovarian, cervical and head and neck squamous cell carcinoma (cBioportal).

With regards to the SHOC2, a recent study revealed that SHOC2 may have a crucial role in breast cancer as inactivation of SHOC2 significantly inhibited breast cancer cell proliferation and induced cell apoptosis (Geng et al. 2020). Additionally, SHOC2 was recently identified as one of five genes necessary for the viability of RAS mutant, but not RAS wild-type Acute Myeloid Leukaemia (AML) cell lines (Wang et al. 2017). Moreover, McDonald et al. (2017) reported a dependency of RAS oncogene signalling to SHOC2 when performing large-scale RNAi (McDonald et al. 2017). Similarly, SHOC2 and CRAF were identified in a synthetic lethal screen for genes whose knockdown sensitised resistant melanoma and colorectal BRAF V600E cell lines to the RAF inhibitor PLX4720 (Whittaker et al. 2015).

Our lab was the first to show that SHOC2 is essential for ERK pathway activation of RAS mutant cells (Rodriguez-Viciana et al. 2006) and SHOC2 appears to be selectively required for the tumorigenic properties of cells with oncogenic RAS. SHOC2 depletion has no effect on proliferation in 2D of non-transformed or tumour cells suggesting SHOC2 function is not required for ‘normal’ or anchorage-dependent proliferation. However, SHOC2 depletion in tumour cells with mutant RAS can inhibit loss of contact inhibition, anchorage-independent proliferation and tumour formation in xenograft assays (Young et al. 2013; Boned Del Rio et al. 2019; Jones et al. 2019). Lastly, our recent experimental work confirmed that Shoc2 is crucial for initial tumour

development in autochthonous KRAS-driven lung cancer mouse models (Jones et al. 2019).

Targeting hyperactive RAS/ERK pathway in cancer

Over the decades, oncogenic Ras proteins have been considered as 'undruggable' because of the lack of proper binding pocket for small molecule inhibitor binding and their high picomolar affinity with GTP, which is in stark contrast to ATP-competitive inhibitor success for kinase inhibitors, whose affinity for ATP is in a low nanomolar range (Cox et al. 2014). However, Ostrem et al. (2013) showed that KRAS G12C could be targeted by using a covalent small molecule which sequester KRAS G12C in its inactive state, by irreversible covalent occupancy of Cys12 (Ostrem et al. 2013). KRAS G12C inhibitors bind a novel pocket instead of the nucleotide-binding pocket, and they avoid the need to compete against the picomolar affinity of RAS for GTP. Moreover, other studies have shown that these inhibitors can stop signalling downstream of RAS through ERK and PI3K pathways as well as the growth of KRAS G12C cells but not any KRAS WT or KRAS G12S mutant cells (Lito et al. 2016). Although results from phase I trials are promising, KRAS G12C is only represented in a small subset of RAS mutant cancers with 11-16% of NSCLC and <4% of PDACs, so the challenge remains to drug the other RAS mutants (Hobbs et al. 2016; Degirmenci et al. 2020).

As the first kinase in RAS/RAF/MEK/ERK signalling cascade, RAF has been thought as a key target for drug development against cancers. Whereas significant clinical progress has been made for the treatment of BRAF V600E mutant tumours (particularly melanoma) with first-generation RAF inhibitors such as Vemurafenib and Dabrafenib, efforts to target RAS-driven or BRAF mutant RAS-dependent cancers have had less success (Tsai et al. 2008; Samatar and Poulikakos 2014). These inhibitors achieved high efficacy in the treatment of advance/metastatic BRAFV600E mutant melanoma although this efficacy was revoked by drug resistance (Lito et al. 2016; Sanchez et al. 2018). Mechanistically, upon inhibitor treatment cancer cells reactivate ERK pathway either upregulating the cellular level of active Ras, which leads to paradoxical ERK activation that triggers development of secondary malignancies, or alternative splicing of BRAF V600E to generate variants that enhance BRAF V600E homodimerization and decreases inhibitor affinity (Manousaridis et al. 2013a; Degirmenci et al. 2020). In order to overcome the drug

resistance of the first-generation RAF inhibitors, second-generation of RAF inhibitors or PanRAF inhibitors were developed. PanRAF inhibitors suppress C-terminal/N-terminal intramolecular interaction of RAF kinases and induce RAS-RAF and BRAF-CRAF dimerization (Jin et al. 2017).

MEK and ERK inhibitors have also been developed to block hyperactive RAS/ERK pathway in human cancers. FDA-approved two MEK inhibitors Trametinib and Cobimetinib have been using for the treatment of BRAF V600E melanoma as single agents (Flaherty et al. 2012) or in combination with RAF inhibitors (Robert et al. 2015). On the other hand, the development of ERK inhibitors has lagged far behind compared to RAF and MEK inhibitors, and the majority of them are still undergoing clinical trials. In contrast to RAF inhibitors, MEK and ERK inhibitors have no paradoxical effect, but they have limited therapeutic capacity due to considerable levels of toxicity in normal tissues (Caunt et al. 2015; Cheng and Tian 2017).

ERK pathway in development and tissue homeostasis (*in vivo* mouse models)

The MAPK/ERK pathway plays an important role throughout mammalian development, from embryogenesis to tissue-specific cellular homeostasis (Drosten and Barbacid 2020). Genetic and pharmacological perturbation of nodes of the RAS/RAF/MEK/ERK signalling axis is complicated by redundancy, feedback and cross-talk with other pathways (Scholl et al. 2007). Nevertheless, mouse models have highly improved our current understanding of the MAPK/ERK pathway in physiological and pathological contexts (Figure 1-6).

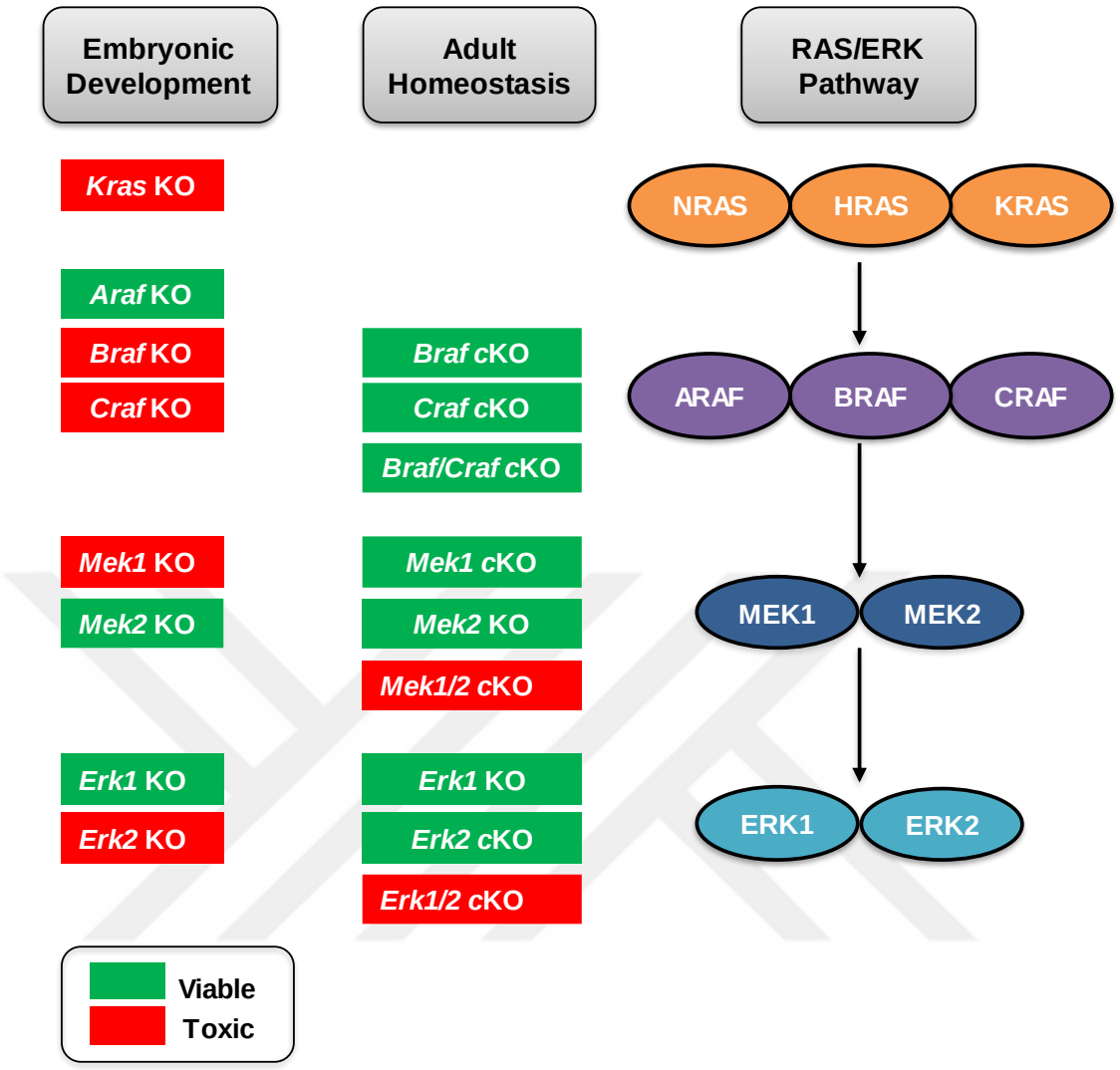

Figure 1-6. The RAS/ERK pathway in development and homeostasis using mouse models

Summary of the *in vivo* studies for the effects of germline gene knockouts in embryonic development and systemic elimination of the effectors in adult mice homeostasis. Red boxes show embryonic death while green boxes show survival beyond birth for embryonic development. For adult homeostasis, red boxes indicate high toxicity and rapid death, whereas green boxes show either none or acceptable toxicity. KO represents knockout, and cKO represents conditional knockout. Adapted from (Drosten and Barbacid 2020).

Genetic ablation of the RAS-MAPK/ERK components in mice shows that they have redundant and non-redundant functions in development. At the level of RAS no overt phenotype is reported in *HRas, NRas,* or both *HRas/NRas*-deficient mice, suggesting functional redundancy (Umanoff et al. 1995; Ise et al. 2000; Esteban et al. 2001). However, ablation of *KRas* results in death between embryonic day 12.5 and term of gestation, with fetal liver defects and anaemia (Johnson et al. 1997). At embryonic day 11.5, they demonstrate increased cell death of motoneurons in the

medulla and the cervical spinal cord, and at day E15.5 of gestation, ventricular walls are extremely thin. Uniquely among RAS isoforms this suggests that KRAS cannot be compensated for by other RAS isoforms (Koera et al. 1997).

Mras knockout mice were originally reported as phenotypically normal with a lack of detectable morphological defects (Nunez Rodriguez et al. 2006). However, subsequent studies showed that loss of Mras causes distention of the bladder and urinary retention in male mice only, which occurs in the absence of an obvious anatomical defect (Ehrhardt et al. 2015). Male mice are also phenotypically more aggressive and exhibit increased sexual behaviour (Boehme et al. 2015).

In the RAF tier, mice deficient in each RAF isoforms displays grossly different phenotypes. Although *ARaf* knockout mice are viable through embryogenesis, mice pups display severe neurological and gastrointestinal defects that lead to lethality between 7 and 21 days post-partum (Pritchard et al. 1996). By contrast, mice deficient for *BRaf* die in midgestation at E10.5-12.5 due to vascular rupture caused by abnormal patterns of endothelial cell apoptosis (Wojnowski et al. 1997) whereas *CRaf* knockout mice are embryonic lethal due to placental abnormalities, or die perinatally of lung and skin defects depending on the genetic background (Wojnowski et al. 1998). In addition, *CRaf* deficient embryos show increased apoptosis in embryonic tissues, especially fetal liver (Mikula et al. 2001). Intriguingly, lethality in *CRaf* knockout mice can be rescued by *knock-in* of a kinase-dead *CRaf* incapable of phosphorylating MEK (Huser et al. 2001). This would indicate that CRaf mediated MEK phosphorylation is not essential for normal mouse development. Although all of these studies have shown that germ line ablation of *CRaf* and *BRaf* kinase is embryonic lethal however, systemic deletion of individual RAF isoforms in adult mice is well tolerated (Blasco et al. 2011) but simultaneous deletion of all 3-RAF isoforms is lethal (Sanclemente et al. 2018).

Despite MEK1 and MEK2 (MAPKK), sharing 80% amino acid identity GEMM's have revealed that *Mek2* knockout mice are phenotypically normal, whereas *Mek1* null mice die at embryonic day 10.5 due to developmental defects and insufficient vascularization of the placenta (Giroux et al. 1999; Belanger et al. 2003; Bissonauth et al. 2006). However, Scholl et al. (2007) showed that no abnormal phenotype is observed by ablation of either protein alone in the epidermis due to redundancy, whereas combined *Mek1/2* deletion in the epidermis led to hypoproliferation, apoptosis, skin barrier defects, and death. Systemic deletion of either *Mek1* or *Mek2*

alone in adult mice is well tolerated but deletion of both *Mek1/2* is incompatible with adult life since *Mek1/2 knock-out* mice display a rapid deterioration of their health and die within ~ 2 weeks (Blasco et al. 2011).

Regarding ERK1 and ERK2 kinases, *Erk1* KO mice are viable, fertile, normal size and display no histological abnormalities, but they show abnormal proliferation and maturation of thymocytes (Pages et al. 1999; Nekrasova et al. 2005) and enhanced long-term memory potentiation (Mazzucchelli et al. 2002). On the other hand, *Erk2* null mice are embryonic lethal around E6.5 due to placental defects, despite expression of *Erk1* in early embryos (Hatano et al. 2003; Yao et al. 2003). Additionally, it has been shown that transgenic overexpression of *Erk1* rescues the placental and embryonic phenotypes of *Erk2*-deficient mice and *Erk1* and *Erk2* exert redundant functions during development (Fremin et al. 2015). Similar with *Mek* ablation, a single *Erk* allele is sufficient to maintain adult homeostasis however, systemic inactivation of both *Erk1/2* kinases is lethal (Blasco et al. 2011).

In the case of Shoc2, its constitutive deletion leads to embryonic lethality at E8.5 whereas endothelial-specific Shoc2 deletion causes a range of cardiac defects at E13.5 and subsequent death of the embryo at E15.5 (Yi et al. 2010). Those embryos are examined to address at which embryonic stage Shoc2 KO mice died, and they found that by E11.5, Shoc2 KO embryos are viable and overtly normal. Yet, at E12.5, they started to display some sporadic haemorrhaging in the surface, and at E13.5 some of the embryos died (2 out of 28), or the viable ones exhibited smaller body size. At E14.5 they had subcutaneous oedema in their dorsal body and fetal lung congestion, and finally, at E15.5 no viable Shoc2 KO embryos are obtained. Histological analysis on the E13.5 revealed that Shoc2 KO embryos exhibit a variety of cardiac defects and Shoc2 has shown to be required for normal development of heart valves (valvulogenesis). Importantly, they suggest Shoc2 may act in an ERK-independent pathway for its essential function in valvulogenesis since ERK activation has not appeared to be affected in mutant endothelial cells (Yi et al. 2010).

RASopathies

The RASopathies are a class of human genetic syndromes driven by germline mutations that cause hyperactivation of the RAS/MAPK pathway, affecting more than 1 in 1000 individuals (Dard et al. 2018). These syndromes include Noonan syndrome

(NS), Noonan syndrome with multiple lentigines (NSML or formerly called LEOPARD syndrome), neurofibromatosis type 1 (NF1), Costello syndrome, cardiofaciocutaneous (CFC) syndrome, neurofibromatosis type 1-like syndrome (NFLS or Legius syndrome) and capillary malformation-arteriovenous malformation syndrome (CM-AVM) (Cao et al. 2017; Simanshu et al. 2017).

Noonan syndrome is among the most common RASopathies, with an estimated incidence of 1 in 1000-2500 live births (Carcavilla et al. 2020). This genetic disorder caused by autosomal dominant inheritance and is characterized by a distinctive facial appearance, growth retardation, congenital heart disease mild to moderate learning disabilities, skeletal abnormalities and endocrine/metabolic imbalance (Tajan et al. 2018).

Gain-of-function mutations in NS patients are found to cluster at the S259 site in CRAF, including one mutation in the S259 position itself (S259F) (Pandit et al. 2007; Razzaque et al. 2007; Kobayashi et al. 2010) and are also found in all three members of the MRAS, SHOC2, PP1 complex (Komatsuzaki et al. 2010; Gripp et al. 2016; Higgins et al. 2017). Gain-of-function S2G mutation in SHOC2, are responsible for a subtype of NS, NS-like disorder with loose anagen hair (NS/LAH or formerly called Mazzanti syndrome), characterised by slow growth rate and short stature, loose anagen hair, congenital heart defects, skeletal anomalies and cognitive deficits (Cordeddu et al. 2009; Komatsuzaki et al. 2010). This mutation in *SHOC2* creates a myristoylation site at the amino terminus leading to constitute membrane localization and hyperactivation of MAPK signalling (Cordeddu et al. 2009; Simanshu et al. 2017).

In addition to S2G mutation, M173I (Hannig et al. 2014) and Q269_H270delinsHY (Motta et al. 2019) SHOC2 mutations have also been found in disorders that share certain features with NS and were revealed to have enhanced binding to MRAS and PP1 and increased signalling through the MAPK cascade (Young and Rodriguez-Viciana 2018; Motta et al. 2019). Taken together, these data underscore the important role of SHOC2 and RAF S259 dephosphorylation on ERK pathway activation.

The skin structure

The mammalian skin is the largest organ of the body and serves a main protective barrier between the body and the external environment against mechanical

pressure, physical damage, pathogen infection, water loss, and it has immunological functions that help the maintenance of body homeostasis (Cañedo-Dorantes and Cañedo-Ayala 2019). The multi-functionality of skin is supported by its organised structure. Its structure is composed of three layers, the epidermis (the outer layer), dermis (the middle layer) and subcutis or hypodermis (the innermost layer) (Figure 1-7A) (Sahle et al. 2015). The epidermis is a multi-layered epithelium extending from the basement membrane, which is rich in extracellular matrix, separating it from the dermis to the air. It is mainly populated by keratinocytes, along with melanocytes, and immune cells including αβ and γδ T cells and Langerhans cells which is a type of dendritic cell specialized in antigen presentation (Cruz et al. 2018). As the major structural element of the outer layer of the skin, keratinocytes function to synthesize keratin, a long, threadlike protein with a protective role (Kolarsick 2011). Depending on the maturation levels, keratinocytes create four major layers of epidermis: the stratum basale, the stratum spinosum, the stratum granulosum and the stratum corneum (Figure 1-7B) (Fuchs and Raghavan 2002).

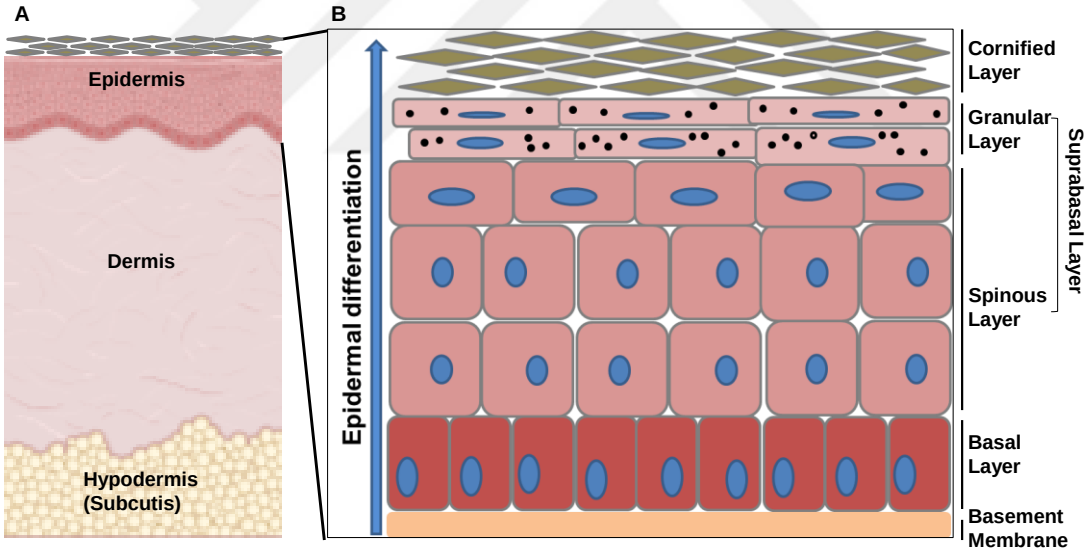

Figure 1-7. Schematic representation of the multiple layers in the skin and the epidermis

A. The skin is composed of three layers, the epidermis, dermis and hypodermis (Subcutis).
B. The stratified epidermis is separated from the underlying dermis by the basement membrane and it consists of basal, spinous, granular, and the cornified layers. Keratinocytes proliferate within the basal cell layer and they differentiate upwards through the other epidermal layers. Ultimately, the terminally differentiated keratinocytes shed their nuclei and form the cornified layer. The small black dots in the cells of the granular layer represent keratohyalin granules.

The stratum basale (basal layer), the closest to the dermis, contains a single layer of column-shaped keratinocytes that attach to the basement membrane. The basal layer is the major site of proliferation within the tissue as keratinocytes in this layer are mitotically active. Undifferentiated basal keratinocytes mainly express keratin 5 and 14 (K5 and K14). As soon as basal keratinocytes relocate to the upper layers of the epidermis, they stop proliferating and start the differentiation process (Proksch et al. 2008). The stratum spinosum (spinosum layer), consists of several layers of keratinocytes that differ in shape and structure depending on their location. For example, spinous cells close to the basal layer, are polyhedral in shape with a rounded nucleus, whereas cells of the upper spinous layers become flattered as they are moved upward through the epidermis. In this epidermal layer, K5/K14 are substituted by the early differentiation markers K1 and K10 (Chu 2008). The stratum granulosum (granular layer) is the most superficial layer of the epidermis, which is comprised of flattened cells holding abundant keratohyalin granules in their cytoplasm. The major components of these keratohyalin granules are profilaggrin (the precursor of the interfilamentous protein filaggrin), keratin filaments, and loricrin. Filaggrin aggregates the keratin filaments into tight bundles and together with loricrin, involucrin and small proline rich proteins (late differentiation markers) are all cross-linked to the plasma membrane to form cornified cell envelope. Then, a complex series of lipids covalently attached to cornified envelope to produce a complete barrier namely cornified layer (Candi et al. 2005). In the stratum corneum (cornified layer), granular keratinocytes undergo the final stage of differentiation which involves a programmed cell death known as cornification. During this process, granular keratinocytes lose their nucleus and almost all cellular contents except for keratin filaments within the filaggrin matrix, and they form stacked layers of dead, flattened cells referred to as corneocytes. The stratum corneum provides mechanical protection to the skin and a barrier to the water loss (Chu 2008).

In contrast to K5-K14 and K1-K10 keratin pairs which are typically related with different cell differentiation stages of keratinocytes, other keratins such as K6 and K16 are usually not expressed in healthy epidermis, however, their expression increases in pathological conditions such as hyperproliferation, inflammation and abnormal differentiation (Pasparakis et al. 2014; Zhang 2018). These keratins are constitutively expressed at low levels by proliferating keratinocytes in the outer root sheaths (ORS) of their hair follicles (Wojcik et al. 2001).

The epidermis continually renews itself throughout life to preserve the integrity of the epidermal barrier. If this self-renewal process is not tightly regulated, it can lead to disorders such as cancer, atopic dermatitis or psoriasis. Besides, too little proliferation may cause epidermal atrophy that is associated with skin fragility. Therefore, epidermal homeostasis depends on an exact balance between proliferation occurring in the basement membrane-proximal basal layer, and the programmed cell death, which takes place at the granular-to-cornified layer transition (Khavari and Rinn 2007).

The dermis is located below the epidermis and is a connective tissue that is composed of collagen and elastin, which allows for strength and flexibility of skin, respectively. The dermis also includes numerous distinct cells such as fibroblasts, endothelial cells, and immune cells such as mast cells, dendritic cells, T lymphocytes and macrophages. It also houses blood vessels and appendages such as hair follicles, and sebaceous glands. Hair follicles and sebaceous glands are linked to the epidermis but connect deep into the dermal layer (Matejuk 2018).

The hypodermis (subcutis), is the third and deepest layer which connects the skin to the underlying fibrous tissue of the muscles and bones. It consists of mainly adipose tissue which is vital in the production of Vitamin D and lipid storage. This layer also serves to absorb shock to underlying structures, shape the external features of the organism, and regulate temperature (Agarwal and Krishnamurthy 2020).

Hair Cycle

Hair, which is one of the distinguishing features of mammals, has many essential biologic functions, including thermoregulation, physical protection, sensory activity and distribution of sweat-gland products like pheromones (Schneider et al. 2009). Hair shafts are produced by thousands of hair follicles in mammalian skin, and these follicles are regenerating continuously throughout life (Abbasi and Biernaskie 2019). Hair follicles have highly organized tissue architecture with epidermal and dermal compartments. They are composed of an outer root sheath (ORS) that expresses epithelial keratins K6, K10 and K14, an inner root sheath (IRS) and the hair shaft (HS) which consists of hair-forming compartments medulla and cortex (Figure 1-8A). In addition to these major compartments, the upper segment of the hair

follicle includes the continuation of the outer root sheath toward the stratified epidermis and is also known as the infundibulum which expresses K6, K10 and K14 (Figure 1-8B) (Wagner et al. 2015).

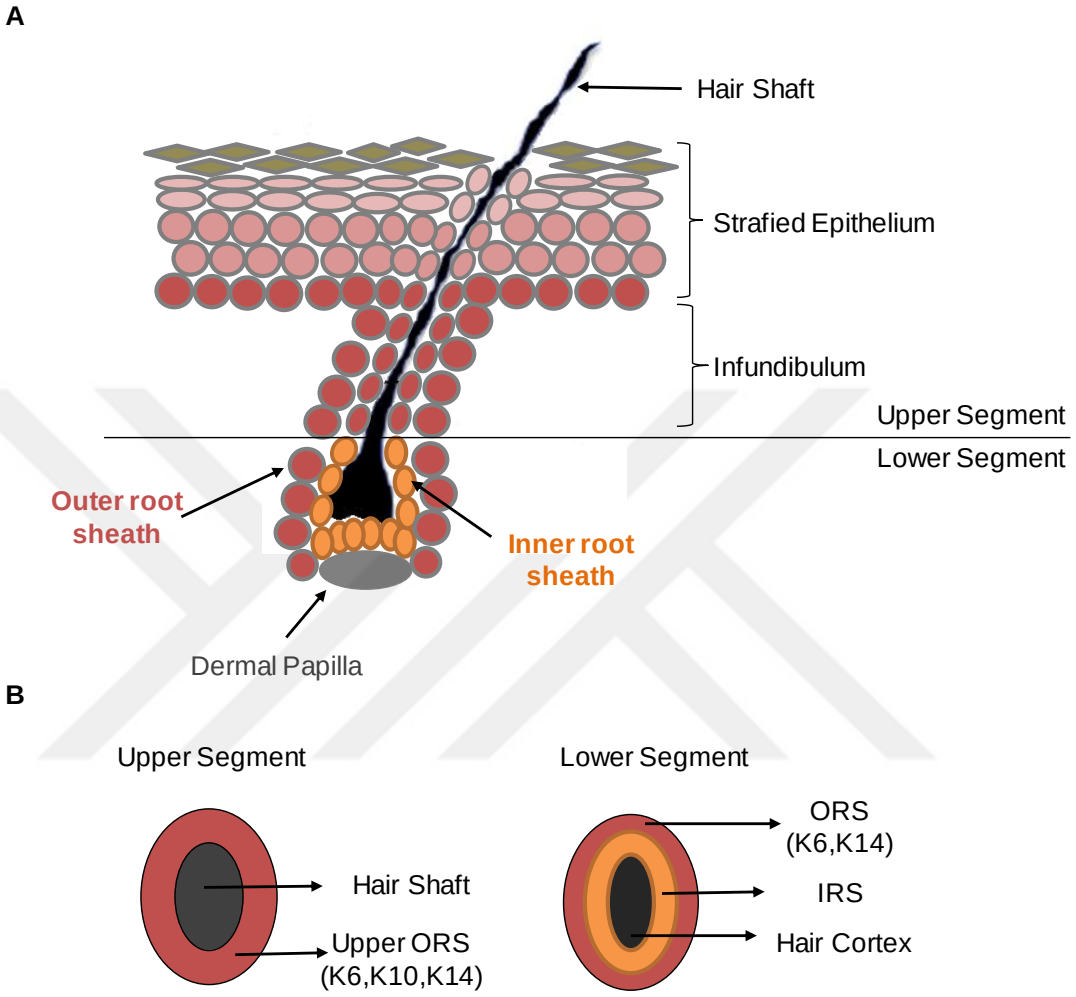

Figure 1-8. Schematic representation for compartments of hair follicle structure

A. Diagram demonstrates the hair follicle compartments, which is separated in upper and lower segment. Adapted from (Wagner et al. 2015).
B. Diagram demonstrates the cross-sections of the hair follicle to show upper and lower segment structures. The main components of the upper segment are hair shaft and outer root sheath (ORS) that contains K6, K10 and K14 expressed keratinocytes. Lower segment is mainly composed of ORS with K6 and K14, inner root sheath (IRS), and hair cortex. Adapted from (Wagner et al. 2015).

The hair follicle represents a unique, highly regenerative system which physiologically undergoes cycles of growth (anagen), apoptosis-mediated regression (catagen), and rest (telogen) numerous times in life. In mice, the first complete postnatal hair cycle (first anagen, first catagen, first telogen) is completed in the first 3-4 weeks after birth. The anagen phase of the first hair cycle starts after birth and

continues to postnatal day 17 (P17). After this active growth phase, the first catagen phase continues from P18–P20, and the first telogen phase follows from P21–P29 (Sugaya et al. 2015). In each cycle, a new hair shaft is generated, and the old hair is ultimately shed, mostly in an actively induced process called the exogen phase (Schneider et al. 2009).

During the anagen stage, hair follicles generate an entire hair shaft from tip to root. Stage-specific characteristics of anagen include thickening of the epidermal, dermal and adipose layers of the skin, increased size of hair follicles and extension of follicles deep into the hypodermis (Sato et al. 1999). During catagen, dynamic transition between anagen and telogen, each hair follicle regresses entirely in a process that includes apoptosis of epithelial cells in the bulb and outer root sheath (ORS) (Alonso and Fuchs 2006). At the telogen phase, hair follicles are in minimal size, lack of proliferative activity and quiescent. Histologically, hair follicles are typically confined to the upper layer of the dermis during this stage. Hairs in the telogen phase, are ultimately pushed out by the growing anagen hair shaft (Ballarò et al. 2005).

Various signalling molecules of several pathways including, Wnt pathway, fibroblast growth factor (FGF) and epidermal growth factor (EGF) are involved in different phases of hair growth (Stenn and Paus 2001). Among the diversity of growth factors expressed in association with the development of hair follicles, EGF and its receptor (EGFR) has an important role on skin and hair development as it will be further described in the following section.

EGFR/RAS/ERK pathway in the skin

The EGFR/RAS/ERK pathway has a well-described role in the skin and hair follicle development. Its function in the skin and its appendages, including hair follicles, is necessary for proper development and tissue homeostasis, and its deregulation rapidly results in defects in cellular proliferation and differentiation (Doma et al. 2013).

EGFR is mainly expressed in undifferentiated, proliferating keratinocytes in the basal and to a lesser extent, in the suprabasal layers of the epidermis and the outer layers of the hair follicles (Nanney et al. 1990; Kern et al. 2011). Activation of EGFR by its ligands such as EGF and TGFα has been shown to promote keratinocyte

proliferation, migration and survival (Fuchs 2009). The importance of EGFR signalling in epidermal development is highlighted in several *in vivo* studies. Systemic EGFR deletion in mice leads to embryonic lethality (Threadgill et al. 1995), yet certain strains of mutant mice, which can survive several weeks, demonstrate severe skin abnormalities including atrophic epidermis, low epidermal keratinocyte proliferation rates, failure to develop a hairy coat or progressive alopecia and aberrant hair follicle differentiation and inflammation (Miettinen et al. 1995; Sibilia and Wagner 1995; Threadgill et al. 1995). Similarly, severe alopecia was seen in transgenic mice where a dominant-negative EGFR mutant was expressed in the epidermis and hair follicles. Although paradoxically, in this case the interfollicular epidermis was found hyperplastic (Murillas et al. 1995). In addition, it was shown that EGFR signalling mediates the transition of anagen to catagen stage of hair growth cycle (Hansen et al. 1997) and in the context of *Egfr* deficiency, generally, hair follicles are unable to exit the anagen phase and to enter catagen, leading to progressive hair loss and inflammation (Doma et al. 2013). On the other hand, several animal models show that up-regulation of EGFR signalling, delays or blocks development of the hair follicles, at the final stage, reduces the hair diameter and increases proliferation in the basal layer (Moore et al. 1983; Mak and Chan 2003; Richardson et al. 2009).

Downstream of EGFR, expression of constitutively active RAS mutants in the basal layer of mouse epidermis has been shown to induce proliferation and inhibit differentiation (Khavari and Rinn 2007). In line with this, Drosten et al. (2013) showed that deletion of all three RAS isoforms (H/N/KRAS) from keratinocytes *in vitro* as well as specifically from the epidermis in mice, led to a dramatic decrease in proliferation, resulting in a substantially thinner epidermis and delayed appearance of differentiation markers (Drosten et al. 2013). Besides, as mentioned in the RASopathies section, germline activating mutations in the RAS/MAPK pathway, are frequently related with cutaneous, defects such as thickened palms and soles, progressive hair loss or poor hair growth and redundant skin and papilloma formation (Tidyman and Rauen 2009; Siegel et al. 2012).

With regard to RAF/MEK/ERK cascade in epidermal homeostasis, animal models show that that epidermis-restricted inducible activation of RAF or MEK results in massive cutaneous hyperplasia and reduced differentiation (Khavari and Rinn 2007). On the other hand, knockout of BRAF (Galabova-Kovacs et al. 2006) CRAF (Ehrenreiter et al. 2005), MEK1 or MEK2 (Scholl et al. 2007) ERK1 or ERK2 (Dumesic et al. 2009) has no effect on epidermal development and/or homeostasis. This may

result from functional redundancy within the pathway since simultaneous MEK1/MEK2, and ERK1/ERK2 ablation causes severe barrier function and inhibition of keratinocyte division, respectively (Scholl et al. 2007; Dumesic et al. 2009).

In the context of oncogenic RAS expression, CRAF and BRAF are essential for the development and progression of RAS-induced tumours. However, they perform different roles, with CRAF inhibiting keratinocyte differentiation (Ehrenreiter et al. 2009) and BRAF increasing proliferation through MEK/ERK activation (Kern et al. 2011).

Considering the key function of the EGFR/RAS/RAF/MEK/ERK pathway in the skin and its appendages, it is not surprising that cutaneous complications are the most frequent adverse side effects observed upon genetic and pharmacological EGFR/RAS/ERK pathway inhibition in both mouse models (Lichtenberger et al. 2013; Mascia et al. 2013; Raguz et al. 2016) and human patients (Flaherty et al. 2010; LoRusso et al. 2010; Gutzmer et al. 2011; Poulikakos and Solit 2011; Kim et al. 2013). Cancer patients receiving EGFR inhibitors usually develop acne-like rashes, xerosis (dry skin), folliculitis (inflamed hair follicles) and pruritus, with itching being a major symptom (Fischer et al. 2013; Guggina et al. 2017b). It has been reported that EGFR inhibitors induce the early inflammatory infiltrate of the skin rash which is dominated by numerous inflammatory cells such as dendritic cells, macrophages, granulocytes, mast cells, and T cells. Then, these inflammatory cells induce the expression of chemokines in epidermal keratinocytes and impair the formation of antimicrobial peptides and skin barrier proteins, leading to an increased permeability of skin and a defect in antimicrobial defence (Lichtenberger et al. 2013; Mascia et al. 2013). Similar to EGFR inhibitors, pruritus, skin rashes and xerosis are also seen in patients treated with MEK inhibitors such as selumetinib (Balagula et al. 2011) and trametinib (Infante et al. 2012) and RAF inhibitors such as vemurafenib and dabrafenib (Gençler and Gönül 2016). Inhibition of the ERK pathway in keratinocytes, either at the level of EGFR or at the level of MEK, can result in keratinocyte cell death, decreased cell migration, and inflammation, which leads to dermatologic toxicity (Cubero et al. 2018). The cutaneous side effect as well as malignant keratinocyte skin tumours such as keratoacanthomas and squamous cell carcinoma (Anforth et al. 2013; Ascierto et al. 2013), rely on paradoxical activation of ERK pathway via RAF inhibitors, thereby highlighting the significance of ERK pathway regulation for epidermal homeostasis.

Inflammation

Inflammation is a complex and vital component of the response to harmful physical, chemical or biological stimuli such as pathogens, damaged cells, or irritants. The inflammatory response can be acute or chronic. In acute inflammation, which is considered to be a short-term response, immune cells, primarily neutrophils, migrate to the site of injury where they defeat the cause of inflammation and repair the tissue. However, chronic inflammation is a sustained and dysregulated immune response which occurs either as a result of prolonged exposure to stimulation or an inappropriate reaction against self-molecules. This type of response results in tissue damage and fibrosis and frequently contributes to numerous chronic human diseases, including arthritis, asthma, atherosclerosis, autoimmune diseases, diabetes, and cancer (Germolec et al. 2018). During both acute and chronic inflammatory responses, a wide range of soluble factors including cytokines, chemokines and adhesion molecules are involved in leukocyte recruitment to the damaged area. Many of these soluble mediators regulate the activation of the resident cells such as fibroblasts, endothelial cells, macrophages, and mast cells as well as the newly recruited inflammatory cells like monocytes, lymphocytes, neutrophils, and eosinophils (Wright 1997).

The innate immune system is the first line of host defence against pathogens. The main purpose of the innate immune response is to immediately prevent the spread and movement of foreign pathogens throughout the body. However, some pathogens escape this first line of defence and the second line of defence, adaptive immune system, is then required to get involved. Adaptive immune responses are mainly dependant on the antigen-specific receptors expressed on the surfaces of B and T lymphocytes. The epithelial cell layers of skin, respiratory, gastrointestinal and urogenital tracts present a first physical barrier to pathogens. Mucus secretion and epithelial ciliary movement which permits to be continuously refreshed after it has been contaminated with inhaled or ingested particles are also part of this physical barrier (Chaplin 2010). Aforementioned tissue-resident and circulating innate immune cells remove foreign particles and host debris by phagocytosis, and they secrete signals like cytokines and chemokines for surrounding immune cells.

The granulocytes which include neutrophils, basophils and eosinophils are polymorphonuclear phagocytes. Neutrophils, the primary cellular mediators of the

innate immune system, are recruited from the blood to the inflammatory site by chemotaxis where they recognize and phagocytose invading pathogens via different cytotoxic mechanisms. Notably, the hallmarks of neutrophils, cytoplasmic granules, contain a variety of enzymes, peptides, and proteins and can also rapidly release reactive oxygen species which serve to destroy and digest organisms and foreign material following phagocytosis (Rosales et al. 2016). Basophils and eosinophils are crucial for the control of parasitic infections and allergic disorders as their granules contain mainly heparin and histamine. Likewise, mast cells also play essential roles in the induction of allergic immune responses due to their heparin, histamine and tryptase rich granules. Natural killer (NK) cells, also known as large granular lymphocytes, act as effectors of the innate immune system. NK cells recognize and destroy abnormal cells, such as cancer cells and infected cells, by exerting their cytolytic effects with perforin and granzymes. The mononuclear phagocytes group contains macrophages and dendritic cells. Macrophages, which present in all tissues, are also effector cells of the innate immune system that phagocytose dead cells, debris, tumour cells, and foreign materials. Furthermore, they secrete a wide range of cytokines and chemokines to attract other immune cells to the site of inflammation (Galli et al. 2011).

Dendritic cells act as a bridge between the innate and adaptive immune system as they present antigens to T and B lymphocytes via their major histocompatibility complex (MHC)-molecules. T cells are defined by their cell-surface expression of T cell receptor (TCR), which is crucial for their activation. T cells are divided into different groups based on lineage expressing markers and functional activities. They can express either CD8 glycoprotein on their surface and are called $CD8^+$ T cells (cytotoxic) which are activated by antigenic peptides presented by MHC class I molecules or CD4 glycoprotein and are then called $CD4^+$ helper T cells (TH) which are activated by MHC class II molecules. $CD8^+$ cytotoxic T cells act directly to damage target tissues, whereas $CD4^+$ helper T cells drive a specific immune attack by producing cytokines that can either be directly toxic or can help other immune cells to differentiate and perform their function. $CD4^+$ cells differentiate into different subsets: Th1 cells (pro-inflammatory), Th2 cells (anti-inflammatory), Th17 cells and regulatory T cells (Tregs) which are characterized by different cytokine profiles. In order to ensure tissue homeostasis, the majority of antigen-specific T cells die by apoptosis upon eliminating the foreign antigens. However, a small fraction of long-

lived memory cells remains that is poised to respond rapidly if the same antigen presents again (Golubovskaya and Wu 2016).

B cells are at the centre of the adaptive humoral immune system. When activated, B cells differentiate into plasma cells, which secrete large amounts of antigen-specific antibodies, or memory B cells, which can be re-activated upon second encounter with the same antigen. Both memory B cells and plasma cells are long-lived and play a significant role in the protection against re-exposure to pathogens (Lou et al. 2015).

Skin inflammation

The skin (epidermis and dermis) is home to a number of cell populations that can be resident, recruited, and recirculated. The resident cells of the skin include keratinocytes, fibroblasts, dermal and epidermal dendritic cells (Langerhans cells), T cells, macrophages, mast cells, eosinophils and endothelial cells of blood vessels. Recruited immune cells from the circulation into the skin, involves monocytes, granulocytes, B and T cells, and mast cells whereas the cells recirculating into the skin, those coming and going, include natural killer (NK) cells, T and B cells, and dendritic cells. These cells play a significant role to assure protection against pathogens but also contribute to the pathology of several inflammatory skin diseases (Pondeljak and Lugovic-Mihic 2020).

Keratinocytes have an essential role in maintaining the skin's physical barrier structure as well as in contributing to innate and adaptive immune responses. They are the major source of antimicrobial peptides (AMPs), small cationic innate immune mediators, acting as the first line of defence (Harder et al. 1997; Matejuk 2018). During skin infections, the expression of AMPs can be upregulated by some pro-inflammatory cytokines such as interleukin IL-17 and IL-22 (Liang et al. 2006). Those cytokines are generated by Th17 as well as $\gamma\delta$ T cells (Haas et al. 2012), and they increase AMP production by keratinocytes (Weaver et al. 2007). Therefore, they provide a significant link between keratinocytes and adaptive immune cells by regulating skin and mucosal immunity (Kolls et al. 2008; Nestle et al. 2009). In addition to AMPs, keratinocytes constitutively produce (at low levels) or are induced by numerous stimuli, such as UV radiation, microorganisms, allergens and trauma, to release various cytokines, including IL-1, IL-6, IL-10, IL-18 and granulocyte

macrophage-colony stimulating factor (GM-CSF) (Albanesi et al. 2005). Keratinocytes are also a significant source of chemokines such as CXCL9, CXCL10, CXCL11, and CCL20 thereby they communicate and cooperate with other cell types to modulate immune response. For instance, they can regulate the attracting of Langerhans cell precursors to the epidermis via the expression of CCL20 (Dieu-Nosjean et al. 2000).

Langerhans cells act as first-line fighters due to their localization, which is the outer part of the skin, epidermis, compared to dermal dendritic cells. In addition to their different anatomical locations, these different dendritic cell subsets have specific functional properties in the skin, but their main role is to provide immunosurveillance against pathogens by arranging efficient cytokine and chemokine network (Guttman-Yassky et al. 2007) and continually travel to the skin draining lymph nodes to initiate adaptive immune responses (Kissenpfennig et al. 2005; Nishibu et al. 2006). *In vivo* studies have shown that Langerhans cells are essential for capturing and processing protein antigens as well as inducing Th2 and Th17 cells in response to microbial antigens whereas dermal dendritic cells are responsible for the generation of Th1 cells (Igyarto et al. 2011). Macrophage and monocyte populations in the skin also support dendritic cells in surveillance functions. Resident skin macrophages carry out the early detection of antigen entering the body through the skin and can initiate an inflammatory response (Von Stebut 2007) besides circulating monocytes traffic through the skin and transport antigens to draining lymph nodes (Jakubzick et al. 2013). Furthermore, depending on their functions, monocytes and macrophages categorized as pro-inflammatory “M1” or anti-inflammatory/pro-repair “M2” monocytes/macrophages (Nguyen and Soulika 2019). M1 macrophages contribute to both acute and chronic inflammation in the skin by secreting inflammatory cytokines such as TNFα, IL-1β, and IL-6 (Mills 2015). However, M2 macrophages produce anti-inflammatory cytokines such as IL-10 and transforming growth factor-β (TGFβ), as well as vascular endothelial growth factor (VEGF) and accelerate tissue repair (Pasparakis et al. 2014).

In addition to dendritic cells and macrophages, mast cells and eosinophils are the other important skin-resident myeloid cells. Neutrophils are barely found in healthy skin; thereby, they are not called “skin-resident cells’ but their numbers are dramatically increased in inflammatory conditions and after a wound in the skin (Nguyen and Soulika 2019). Mast cells are commonly located in the upper dermal layer, where they can quickly respond to pathogens and injury. As mentioned before,

mast cells are known as typical allergy cells since they contain granules, including histamine, serotonin, and tryptase (Matejuk 2018). In allergic reactions, histamine, a short-lived vasoactive amine, causes an immediate increase in local blood flow and vascular permeability and tryptase effects on fibronectin by degrading extracellular matrix proteins allows immune cells such as neutrophils, monocytes and lymphocytes to migrate epidermis (Kaminska et al. 1999). Furthermore, mast cells produce numerous growth factors and cytokines such as TNFα, which is important for late-phase allergic reactions and neutrophil accumulation (Wershil et al. 1991) and IL-4 or IFN- γ which are essential for chronic skin inflammation such as psoriatic lesion and atopic dermatitis (Horsmanheimo et al. 1994; Ackermann et al. 1999). Eosinophils are other skin-resident cells which are traditionally known to induce host defence against parasitic infections (Jacobsen et al. 2012). In their large granules, they have highly toxic arginine-rich proteins which are able to mediate damage to tissues (Bochner and Gleich 2010). In response to a number of stimuli, eosinophils become activated and secrete these granule contents into the tissue (degranulation) that helps kill microbes or parasites as well as contributes to several inflammatory reactions, which may cause tissue damage. In addition to these cytotoxic granular proteins, like mast cells, eosinophils also release other inflammatory mediators such as chemokines and cytokines including IL-3, IL-5 and GM-CSF which are essential for trafficking, survival, activation, and degranulation of eosinophils (Akuthota and Weller 2012; Long et al. 2016).

As regards to lymphoid immune cells, the human skin surprisingly contains nearly 20 billion T cells which is approximately twice the number present in the entire blood volume (Clark et al. 2006). Both human and mouse skin include conventional $\alpha\beta$ T cells, and unconventional $\gamma\delta$ T cells along with natural killer T cells. Conventional $\alpha\beta$ T cells, which recognize peptide antigens complexed with the MHC macromolecules, are dominant in the human skin, whereas unconventional $\gamma\delta$ T cells, which recognize free soluble antigens and non-peptide antigens complexed with non-classical MHC-like molecules, are dominant in the mouse skin (Elbe et al. 1996; Mestas and Hughes 2004).

αβ T lymphocytes are found in the epidermis and dermis of both mice and human skin, and they are resident memory T cells which express cutaneous lymphocyte-associated antigen (CLA) (Bos and Kapsenberg 1993; Suwanpradid et al. 2017). $CD8^+$ resident memory T cells are shown to achieve highly effective protection against herpes simplex virus (HSV) infection through IFN-γ secretion

(Ariotti et al. 2014). $CD4^+$ resident memory T cells also compose a significant part of the skin-resident lymphocyte population, and it has been shown that those cells play a crucial role in the control of parasitic infection by IFNγ-mediated recruitment of circulating T cells to the skin (Glennie et al. 2015). Furthermore, immune responses in skin are efficiently controlled by $CD4^+$ regulatory cells T cells (Tregs) which are 5-10% of all human skin resident T cells (Vukmanovic-Stejic et al. 2008). Tregs mainly control the immune responses to self-antigens by suppressing the activation and production of cytokines as well as proliferation of other T cells (Sakaguchi 2005). They also induce anti-inflammatory functional profile in macrophages (Tiemessen et al. 2007) and together with LCs play a crucial role in dampening immune responses against pathogens (Gomez de Aguero et al. 2012). Other $CD4^+$ helper T cells including Th1, Th2 and Th17, provide an effective defence by producing numerous cytokines that in turn promote the release of IFNγ and antimicrobial peptides to protect skin against intracellular and extracellular pathogens (Nomura et al. 2014; Brockmann et al. 2017; Eyerich et al. 2017).

$\gamma\delta$ T cells that contain TCR with γ and δ chains, account for only a small percentage of all T cells in the epidermis (1–10%) and dermis (2–9%) of human skin (Vroom et al. 1991; Nestle et al. 2009). In contrast, more than 90% of the epidermal T cells (Bergstresser et al. 1985) and 50% of dermal T cells in mice are $\gamma\delta$ T cells (Sumaria et al. 2011). Mouse epidermal $\gamma\delta$ T cells are also known as dendritic epidermal T cells (DETCs), due to their morphology and location wherein immediate contact with neighbouring keratinocytes (Sulcova et al. 2015). They remain largely immobile and their dendritic morphology is also related to tight interaction with their ligand E-cadherin expressed on keratinocytes (Uchida et al. 2011). The DETCs $\gamma\delta$ TCR is not MHC-restricted and the entire repertoire of antigens recognized by DETCs remains unknown. However, the ligands for $\gamma\delta$ TCR appears to be constitutively expressed by keratinocytes (Chodaczek et al. 2012), or they can be antigens from damaged, stressed, or transformed keratinocytes, an interaction that seems essential for keratinocyte maintenance (Jameson et al. 2004). Therefore, the recognition and elimination of these keratinocytes reduces the risk of malignant transformation (Shimura et al. 2010). In addition, DETCs act as primary responders to wound repair due to their ability to produce keratinocyte growth factors such as KGF1, KGF2, and epidermal mitogens such as insulin-like growth factor (IGF) (Toulon et al. 2009). DETCs are also able to produce several AMPs allowing antimicrobial defence (Agerberth et al. 2000) as well as they, recognize and subsequently eliminate virus-

infected cells (Sciammas et al. 1994). Besides, DETCs negatively regulate inflammation induced by αβ T cells, thus contributing to local immune surveillance and immunoregulation (Girardi 2006).

Dermal γδ T cell subset is both phenotypically and functionally different from DETCs as they are round in morphology, and an important proportion are motile (Sumaria et al. 2011). Dermal γδ T cells can produce IL-17 when stimulated with IL-1β and IL-23, inducing several inflammatory cytokines (Sutton et al. 2009; Cai et al. 2011b). These cytokines cause the recruitment of more lymphocytes, neutrophils, and macrophages, forming a positive feedback loop that maintains cutaneous inflammation and induces epidermal hyperplasia. (Onishi and Gaffen 2010b; Cruz et al. 2018). Therefore, dermal γδ T cells are involved in innate pathogen defence through IL-17 (Tay et al. 2014). Recent *in vivo* studies have also revealed the importance of dermal γδ T cells in IL-23-induced psoriasiform lesions, in which they were the primary source of IL-17. It has been shown that neither αβ T cells nor DETCs, but dermal γδ T cells were essential for psoriasiform lesion development (Cai et al. 2011b; Gray et al. 2011; Pantelyushin et al. 2012).

Natural killer T cells (NKT) cells are considered to be particularly crucial in bridging innate and adaptive immunity. They are a subset of innate-like T cells that express an αβ T cell receptor recognizing glycolipids bound to the MHC-I like molecule, CD1d (Bendelac et al. 2007). Still, functionally they most closely resemble innate immune system cells, as they quickly evoke their effector functions following activation, and fail to develop immunological memory (Van Kaer et al. 2011). In the skin, NKT cells play a key role in antimicrobial immune responses by recognizing bacterial glycolipids (Kronenberg 2005) as well as they recognize self-derived glycolipids and activate keratinocytes thereby induce tissue pathology such as psoriatic lesions and allergic contact dermatitis (Bonish et al. 2000; Gober et al. 2008).

B cells are present in small numbers in normal skin under homeostatic conditions, but they are found in elevated levels in inflammatory skin conditions. B cells have been shown to exhibit both proinflammatory as well as suppressive roles in the pathophysiology of inflammatory skin disorders. They contribute to cutaneous inflammation via interactions with both innate immune cells and T lymphocytes (Egbuniwe et al. 2015). On the other hand, a population of regulatory B cells have been suggested to play suppressive function through the production of large amounts

of the regulatory cytokine IL-10 which inhibits proinflammatory cytokines in the cutaneous inflammatory conditions (Mauri and Bosma 2012).

Aims of the project

Despite the essential role of the ERK-MAPK pathway in RAS-driven cancers, current inhibitors targeting the RAF/MEK/ERK components have failed in the clinic primarily because on-target toxicity precludes a therapeutic index. Thus, finding new nodes to inhibit the ERK signalling pathway with better therapeutic margins is critical.

Our group has previously shown that SHOC2 is critical for ERK pathway activation by receptor tyrosine kinases and mutant RAS (Rodriguez-Viciana et al. 2006). On the other hand, SHOC2 appears to be selectively required for the tumorigenic properties of cells with oncogenic RAS (Young et al. 2013). Moreover, a recent study from our group has shown that Shoc2 inhibition delays tumour development and significantly prolongs survival in KRAS LUAD mouse models (Jones et al. 2019). Other studies also have reported a crucial role of Shoc2 in RAS-driven tumourigenesis (McDonald et al. 2017; Wang et al. 2017). In *C. elegans*, unlike RAF/MEK/ERK core components of the ERK pathway, Shoc2, is not essential for organ development, but loss of Shoc2 function strongly suppresses the mutant RAS phenotype (Selfors et al. 1998; Sieburth et al. 1998). Collectively, these observation suggests that SHOC2 has properties of an attractive therapeutic target for inhibition of the ERK-MAPK pathways in RAS driven tumours and that targeting the SHOC2 regulatory node may have lower toxicity, and thus provide better therapeutic margins than RAF/MEK/ERK core components

However, the effects of SHOC2 inhibition at the organismal level are still unknown and understanding the physiological role of SHOC2 in tissue homeostasis is crucial to validate SHOC2 as a good therapeutic target.

The aim of this research project is to use mouse models of conditional Shoc2 inactivation to systemically inhibit Shoc2 function in adult mice in order to study its role in normal tissue homeostasis, anticipate possible toxicities associated with systemic SHOC2 inhibition in the clinic and ultimately help validate SHOC2 as a therapeutic target for the many malignancies with upregulated RAS-ERK pathway activation.

Chapter 2 Materials and Methods

Materials and Reagents

Chemical compounds and reagents

All chemical reagents were of analytical grade and were purchased from Sigma-Aldrich, unless indicated otherwise.

Buffers

Buffers for Western blot

MOPS running buffer:

50 mM MOPS

50 mM Tris Base

0.2% SDS

1 mM EDTA

Transfer buffer:

25 mM Bicine

25 mM Bis-Tris

1 mM EDTA

10% Methanol (v/v) (freshly added)

Tween supplemented PBS (PBS-T):

1x PBS

0.1 % Tween-20 (v/v)

Blocking buffer:

5 % skimmed milk powder (w/v)

1x PBS-T

Wash buffer:

1x PBS-T

Ponceau Solution:

0.1% Ponceau S (w/v)

5% Acetic Acid (v/v)

Buffers for immunohistochemistry (IHC) and immunofluorescence (IF) stainings

1x PBS-T: 0.1 % Tween-20 (v/v) in PBS

Citrate buffer:

10 mM Sodium Citrate

pH 6

Hydrogen peroxide (H_2O_2) methanol blocking buffer:

3% H2O2

100% methanol

Normal serum blocking buffer:

2.5% Horse Serum (Vector ImmPRESS Kit)

Hematoxylin Counterstain Solution (Sigma, GHS132)

DPX mounting media (Sigma, 317616)

Buffers for flow cytometry experiments

RBC lysis buffer (Sigma, R7757)

FACS buffer:

1x PBS

2 mM EDTA

2 % Fetal Serum Albumin (FBS) (v/v)

Fixation Buffer:

1x PBS

16 % Paraformaldehyde (PFA)

Commercially available biological agents

The specific agonists used in this project were purchased from the following companies unless stated otherwise: Phorbol 12-myristate 13-acetate (PMA) (Sigma, P8139), Murine Macrophage Colony-Stimulating Factor (M-CSF) (Peprotech, AF-315-02), Granulocyte-Macrophage Colony-Stimulating Factor (GM-CSF) (Peprotech, 315-03), Lipopolysaccharide (LPS) (Sigma, L4391), Tamoxifen free base (Sigma), 4-OHT (Sigma).

Commercially prepared reagents

DAB (diaminobenzidine) chromogen component	Biolegend, SIG-31048
Protein Assay Dye Reagent Concentrate	Bio-Rad, 5000006
ECL Plus	Pierce, 32209
Luminata Forte	Merck, WBLUC0500

Cell culture reagents

DMEM (Dulbecco's Modified Eagle Medium)	Invitrogen
EMEM (Eagle’s Minimal Essential Medium)	Lonza
RPMI 1640	Invitrogen
FBS	Invitrogen

PenStrep (100x)	Sigma
PBS	Thermo Fisher
Keratinocyte-SFM (Serum Free Media)	Invitrogen
HEPES Buffer Solution	Invitrogen
Hank’s Balanced Salt Solution	Invitrogen
Fibronectin	Sigma
Collagen I	Life Technologies
DPBS (Dulbecco's Phosphate-Buffered Saline)	Invitrogen
Trypsin/EDTA	Thermo Fisher
DMSO	Sigma

List of antibodies

SHOC2 and MRAS antibodies were generated as described (Rodriguez-Viciana et al. 2006). BRAF P-S365 was generated by immunisation of rabbits with a phoshpo-peptide corresponding to the appropriate region of BRAF (Epitomics/Abcam). FOXP3 (clone 221D) antibody was a gift from Dr. G. Roncador, CNIO, Madrid, Spain.

Table 2-1. Primary antibodies for Western Blot experiments.

Antibody	Company	Catalogue number	Species
AKT (pan)	Cell Signaling Technology	2920	Mouse
AKT P-S473	Cell Signaling Technology	4060	Rabbit
β-Actin	Santa Cruz	sc-47778	Mouse
BRAF	Santa Cruz	sc-5284	Mouse
ERK 1/2	Cell Signaling Technology	9102	Rabbit
ERK 1/2 P-T202/Y204	Cell Signaling Technology	9101	Rabbit
FLAG	Sigma	F1365	Mouse
GAPDH	Genetex	GTX100118	Rabbit
MEK1	Santa Cruz	sc-6250	Mouse
MEK2	Santa Cruz	sc-13159	Mouse
MEK 1/2 P-S217/221	Cell Signaling Technology	9121 & 9154	Rabbit
MYC-TAG	Cell Signaling Technology	9B11	Mouse
PP1CA	Bethyl	A300-904A-T	Rabbit
RSK2	Santa Cruz	sc-9986	Mouse
RSK1 P-T359	Cell Signaling Technology	8753	Rabbit
SCRIB	Santa Cruz	sc-55543	Mouse
14-3-3 (pan)	Santa Cruz	sc-629	Rabbit

Table 2-2. Primary antibodies for immunohistochemistry and immunofluorescence.

Antibody	Company	Catalogue number	Species
B220	BD Bioscience	550286	Rat
CD3	Invitrogen	RM-9107-R7	Rabbit
CD4	Invitrogen	14-9766	Mouse
CD8	Invitrogen	14-0808	Mouse
CD45	Biolegend	103101	Rat
CD68	Dako	M0814	Mouse
F4/80	Bio-Rad	MCA497RT	Rat
GR-1	Biolegend	108401	Rat
K6	Biolegend	905702	Rabbit
K10	Biolegend	905403	Rabbit
K10	Biolegend	MMS-159S	Mouse
K14	Biolegend	905303	Rabbit
Ki67	Abcam	16667	Rabbit
Loricrin	Biolegend	905103	Rabbit

Table 2-3. Conjugated secondary antibodies.

Antibody	Company	Catalogue number
DyLight 488 Goat-anti-Rabbit-IgG	Bethyl	A120-101D2
Alexa Fluor 555 Donkey anti-Mouse IgG	Invitrogen	A31570
Donkey anti-Rabbit- IgG-HRP	GE Healthcare	NA934
Sheep anti-Mouse- IgG-HRP	GE Healthcare	NA931

Table 2-4. Conjugated primary antibody for flow cytometry analysis.

Antibody	Company	Catalogue number	Fluorophore
B220	Biolegend	103205	FITC
CD117 (c-kit)	BD Bioscience	566415	BB700
CD11b	Biolegend	101239	BUV661
CD11b	Biolegend	101211	APC
CD11c	Biolegend	117335	BV786
CD127 (IL-17Ra)	Biolegend	135013	PE-Cy7
CD135	Biolegend	135305	PE
CD150	Biolegend	115935	PE-Dazzle
CD16/32	Biolegend	101337	BV711
CD19	Biolegend	115527	AF700
CD24	BD Bioscience	612953	BUV496
CD3	BD Bioscience	741788	BUV737
CD3	Biolegend	100219	PE-CY7
CD34	Thermo Fisher Scientific	50-0341-82	AF 647
CD4	BD Bioscience	612952	BUV496
CD41	Biolegend	133915	PE-Cy7
CD45	BD Bioscience	748370	BUV805
CD45	BD Bioscience	612975	BUV661
CD48	Biolegend	103414	AF 488
CD68	BD Bioscience	566388	BV421
CD8	BD Bioscience	612898	BUV805
F4/80	Biolegend	123129	AF700
FcεRIα	Biolegend	134315	APC
FoxP3	Biolegend	126403	PE
gdTCR	BD Bioscience	745818	BB700
Lineage Cocktail	Biolegend	133311	BV421
Ly-6A/E (Sca-1)	Biolegend	108139	BV786
Ly6C	Biolegend	128035	BV605
Ly6G	BD Bioscience	612921	BUV563
MHC-II	Biolegend	107643	BV711
MHC-II	BD Bioscience	746197	BB700
NK1.1	BD Bioscience	564144	BUV395

Methods

Cell culture methods

L-929 fibrosarcoma cell line and generation of conditioned medium

Standard cell culture techniques were applied during the experiments. L-929 cells were kindly provided by Dr. York Posor. L-929 cells were cultured in DMEM, all supplemented with 10% fetal bovine serum (FBS) at 37°C and 5% CO2-humidified atmosphere for 12 days. For generating L929-conditioned medium, the supernatant was harvested after 12 days of incubation by pouring the contents of T175cm^2 flasks into reservoir of a 0.22 µm filter unit. Afterwards, supernatant was aliquoted into 50 ml tubes and stored at -80°C. L929-conditioned medium was used as a source of macrophage colony-stimulating factor (M-CSF) to get bone marrow-derived macrophages (BMMs).

Freezing and thawing of cell lines

The confluent cells (80-90%) were trypsinized and the cell pellet was obtained by centrifugation at 300 × g for 4 minutes at room temperature. After removing the supernatant, cell pellets were resuspended in FBS containing 10% DMSO (freezing medium). The cell suspension was then transferred into 2.0 ml cryogenic vials and initially frozen at -80 °C for at least 24 hours. Afterwards, cells were transferred to liquid nitrogen tank for long-term storage.

To thaw frozen cells, cryogenic vials were placed in a sterile 37°C water bath for about 45-60 seconds and then cells were immediately resuspended in pre-warmed medium. In order to eliminate possible toxic effects of DMSO, cells were centrifuged at 300 × g for 4 minutes at room temperature and re-suspended in fresh and warm medium.

Cell counting and assessment of viability

For seeding purposes and cell number determination, harvested cells were resuspended in complete growth medium, and 1 ml cell suspension was counted using Vi-Cell® automated cell counter (Cell Viability Analyser, Beckman Coulter), following the manufacturer‘s instructions. Cell concentration and viability were determined by the trypan blue dye exclusion method.

Isolation, preparation, immortalization and culture of primary murine keratinocytes

The preparation and culturing of primary murine keratinocytes (PMKs) from the tails of adult mice was performed according to previously published protocols (Li et al. 2017). Shortly, 6-15 weeks of age mice were sacrificed, and the tails were cut off at their proximal ends of the body. The tails of adult mice were sterilized in 70% ethanol for 3 minutes. Afterwards, the tail skin was peeled off the bone and cut into 2-3 cm long pieces. The skin pieces, then carefully flattened and placed onto 0.25% Trypsin in HBSS without calcium and magnesium solution with the dermis facing down and incubated at 4 °C refrigerator overnight. The next day, the dermis was dragged away from the epidermis and the epidermis was minced in Keratinocyte-SFM (Serum Free Media) using a crosswise action of 2 scalpels. The suspension was centrifuged at 150 × g 4 °C for 5 minutes and was passed through 70-µm nylon cell strainer. To ensure that the maximum number of cells were harvested, the initial tube was rinsed with fresh Keratinocyte-SFM and rinsed it through the same filter into the same tube. PMKs were then seeded on 12-well or 6-well pre-coated collagen-fibronectin plates. The growth medium was changed the following day to eliminate dead cells. Then, in order to maintain PMKs in culture long enough to be able to perform experiments, they were immortalized by retroviral expression of Simian Virus 40 (SV40) large T-antigen. After 5-8h incubation at 37 °C, viral supernatant was replaced for fresh growth medium. Transduced cells were selected the following day with 2.5 µg/ml puromycin (Sigma-Aldrich). The growth medium was changed every other day for 5 to 7 days before use in experiments or freezing.

Isolation, preparation and culture of murine bone marrow derived macrophages

Bone marrow-derived macrophages (BMMs) were obtained from the femur and tibia bones of adult mice according to established protocols (Liu and Quan 2015). Briefly, 6-8 weeks old mice were euthanized and abdomen area and skin of hindlimbs were sterilized with 70% ethanol. The abdominal cavity was opened, and the surface muscles were removed. Afterwards, the hind leg was cut off above the pelvic-hip joint to release the whole leg (femur and tibia) while keeping the femur intact. The tibia was then cut at the knee and the ankle joints and both tibias and femurs were collected in sterile PBS. The muscles and residue tissues surrounding the femur and tibia were removed with sterile forceps and scissors. Both ends of tibias and femurs were cut off and bone marrow flushed with a 26-gauge needle and syringe containing complete RPMI (RPMI 1640 with 1x Pen/Strep, 1x sodium pyruvate, 1x L-glutamine, 10% FBS). The suspension was centrifuged at 450 × g 4 °C for 5 minutes and re-suspended in complete RPMI then filtered through 40-µm cell strainer. Afterwards, cells were seeded into non-tissue culture treated 15 cm plates with complete RPMI supplemented with 10% L929-conditioned medium. Cells were treated with 1 µM 4-OHT (Sigma) overnight to induce Cre-recombination for Shoc2 deletion. The following day, the medium was exchanged completely and replaced with complete RPMI supplemented with 20% L929-conditioned medium. All non-adherent cells were retained and placed back into the plates. The medium supplemented with 10% L929-conditioned medium was changed every other day for 7-days. After 7-days in presence of L929-conditioned medium, supernatant was removed, and plates were washed with sterile PBS. Next, cells were detached using pre-warmed PBS containing 2 mM EDTA solution at 37°C for 5-10 minutes. Detached cells then were centrifuged at 300 × g for 5 minutes at room temperature. Finally, cells were re-suspended in complete RPMI without L929-conditioned medium and seeded 24-well or 12-well plates for the experiments.

Cell proliferation assays

Immortalized murine keratinocytes were seeded in 24-well plates and imaged on the IncuCyte (Essen BioScience). Pictures were automatically taken every 2 hours (Four different images per well). Confluence was quantified over time as an average

of the 4-pictures and used to generate growth curves (%Confluence). Growth medium was replaced every other day.

Biochemical methods

Cell lysis and determination of protein content by Bradford Assay

To prepare cell lysates, plates were placed on to ice and washed with ice cold PBS. Afterwards, cells were lysed with an appropriate amount of (70-200 µl) ice cold PBS-E lysis buffer (PBS/1% Triton-X- 100/1 mM EDTA/Protease Inhibitors (Roche)/Phosphatase Inhibitors/1 mM DTT (dithiothreitol). The plates placed on a rocker at 4°C for 10 minutes. Crude homogenates were then centrifuged for 10 minutes at 4°C, 13,000 rpm to pellet insoluble material. Then the supernatant (soluble protein fractions) transferred into a fresh pre-chilled 1.5 ml Eppendorf tubes. Protein concentrations were measured by Bradford Protein Assay Reagent (5x, Bio-Rad, 5000006). Briefly, Bradford reagent was diluted 1 part to 4 parts ddH_2O and 1 ml was added to 1.5 ml tubes. A BSA (Bovine Serum Albumin, Sigma-Aldrich) standard (0-12 µg/ml) was prepared by adding appropriate volumes of 1 mg/ml BSA stock to the Bradford reagent. Appropriate volumes of cleared total cell lysate or purified protein were added to tubes containing Bradford reagent in order that the colour change in the reagent was within the range of the standard. 200 µl of each sample was loaded in duplicate into a clear flat bottom 96 well polystyrene plate including a blank (Bradford reagent only). A plate reader was used to measure absorbance at 495 nm and from this a standard curve was prepared that could be used to calculate the concentration of the samples being tested. The obtained measurements were correlated to the one with the lowest concentration for equal loading (relative quantification). Finally, 20 µl of lysate supernatant was transferred to another tube containing 60 µl of 4X NuPAGE LDS Sample Buffer (Invitrogen). The mixtures were vortexed well and quickly spanned before being heated at 70°C for 10 minutes to denature proteins. Lysates were stored at -20°C.

Western blot

Western blot was performed by heating samples to 70°C for 10 minutes and loaded onto 4-12% NuPAGE Bis-Tris gels (Invitrogen) along with Pre-stained Protein

Standards (Bio-Rad). Gels were run at 180 V for 1h using MOPS running buffer (50 mM MOPS, 50 mM Tris base, 0.2% SDS, 1 mM EDTA). The transfer was set up using Nitrocellulose (for fluorescent imaging using the Li-COR system) and run at 15 V for 13h at 4°C in Transfer Buffer (25 mM Bicine, 25 mM Bis-Tris, 1 mM EDTA, 10% Methanol). Nitrocellulose membranes were stained with Ponceau Solution (0.1% Ponceau S, 5% Acetic Acid) and rinsed with PBS-T (PBS, 0.1% Tween 20). Membranes were scanned using a standard document scanner and incubated with blocking buffer (PBS-T/5% non-fat milk powder) with gentle agitation for 1h at RT. Membranes were incubated in primary antibody (Table 2.1) diluted in 3% BSA/PBS-T/Azide overnight at 4°C. Membranes were washed 3 x 5 minutes with PBS-T followed by 1h incubation with a species-specific secondary antibody diluted in blocking buffer. Membranes were washed 3 x 5 minutes with PBS-T and signal was visualised by either chemiluminescence or by using the Li-COR scanner.

Mostly, secondary antibodies conjugated to IRDyes (680 and 700) were used and an Odyssey CLx scanner was used to image the membranes. The two main advantages of this system are that two species of primary antibody can be imaged at the same time (e.g. a phospho-specific and an antibody recognising total protein) and the sensitivity of the system means that the signals can be accurately quantified. Image analysis was performed using ImageStudio Lite software (Li-COR).

For chemiluminescent signal where secondary antibodies conjugated to HRP were used, membranes were incubated with LumiGLO substrate for one minute and placed inside a film cassette within a protective plastic sheet. X-Ray film was exposed to the membranes for various lengths of time and developed using a film developer. Films were scanned to generate a digital image and where used, densitometry analysis was performed using ImageJ software. Briefly, relevant protein bands were scanned on X-ray films and bands of interests were selected, the software calculated the intensity of the plotting area of each band.

Immunoprecipitation (IP)/Pulldown

Flag-Tag and Myc-Tag immunoprecipitation experiments were performed as previously described (Young et al. 2018). The selected tissues processed and lysed as described in section ‘Necropsy, tissue preparation and fixation of tissues for histology’. The lysates were transferred to eppendorf tubes on ice containing 10 µl

packed Flag-M2 (Sigma) and Myc-9B11 (Cell Signalling) beads. Lysates were incubated with beads for 1-3h rotating at 4°C. Tubes were briefly spun to bring down the beads and placed on ice, followed by aspiration of the lysate. Beads were washed to remove proteins that had bound non-specifically; 1 ml cold PBS-E lysis buffer (without inhibitors or DTT) was added to each tube, which was vortexed to re-suspend the beads and spun briefly. The wash was aspirated, and the step was carried out a further two times. After the final wash, the residual buffer was removed with a 25 G needle attached to the aspirator. 20 µl of 2X LDS was added to the beads at RT and tubes were vortexed to resuspend the beads. Lysates and beads in sample buffer were stored at -20°C. Samples were then analysed by Western blot.

Animal studies

Mouse breeding and colony maintenance

All the mice used in this project were maintained at the Charles River UK. Experimental animals were transferred to the animal research facility of UCL and were maintained in individually ventilated cages (IVCs) with suitable bedding according to institutional guidelines. All in vivo experiments were conducted under an appropriate UK project license in accordance with the regulations of UK home office for animal welfare according to ASPA (animal (scientific procedure) Act 1986).

Generation of Shoc2 KO and Shoc2^{D175N} KI mouse models

Shoc2 mice were generated by Taconic Artemis. Shoc2 KO model was generated by the insertion of LoxP sites into exon 4 of endogenous Shoc2. For the generation of the Shoc2^{D175N} knock-in (KI) mouse model, we employed a ‘minigene’ strategy where the wild-type Shoc2 allele is expressed in a cDNA configuration with a Flag-tag at the N- terminus under the control of the endogenous promoter. The wild type Shoc2 cDNA sequence is deleted after Cre-mediated recombination and replaced by the mutant Shoc2^{D175N} allele containing a Myc-tag. Both models are on a pure C57BL/6 background.

Cre induction by tamoxifen for Shoc2 KO and KI mice

The animals were acclimatized for 7 days before the start of experiments and had free access to a standard diet and water during this period and during the following treatment period. The mice were weighed at the start of experiments, and three times a week during treatment.

Tamoxifen free base (Sigma) was dissolved in corn oil (Sigma) to a final concentration of 20 mg/ml. The mixture was rotated in the dark at room temperature until the tamoxifen was completely dissolved. Single-use aliquots (500µl) were prepared and stored for five days at -20 ^{o}C.

Adult *Shoc2$^{fl/fl}$ KO/KI Rosa26-CreER^{T2}* and *Shoc2$^{+/+}$ KO/KI Rosa26-CreER^{T2}* mice (6-12 weeks old) were exposed to tamoxifen by oral gavage or intraperitoneal injection in order to induce Cre recombinase activity. The oral gavage technique was used to deliver the tamoxifen for initial experiments. Mice were subject to 80 mg/kg tamoxifen for 10-days in 2, 5 day treatment windows with a week break in between. For following experiments, the mice to be injected were weighed in a sterile cabinet and tamoxifen delivered by the intraperitoneal (IP) injection using 25xG needles (Terumo® Neolus) in volumes up to 100µl/25 g of animal, on five consecutive days. The dosage of tamoxifen administered in adult mice was determined based on the universal protocol published from Jackson Lab. It states that 2 mg of tamoxifen for 5 consecutive days is sufficient to drive Cre activation in adult mice.

Genotyping

All mice were ear sampled at 2-3 weeks of age for genotyping. Ear biopsies were lysed in alkaline lysis buffer (25 mM NaOH/ 0.2 mM disodium EDTA, pH 8) at 95 °C for 45-60 minutes and consequently neutralised with neutralization buffer (40 mM Tris HCl, pH 4.5). Samples were preserved at -20 °C until use. PCR mix was prepared with Dream Taq and appropriate sets of primers:

SHOC2 conditional KO forward	AAACCAGAATGATAGCCAAGCT
SHOC2 conditional KO reverse	TTGATAATCCTGCATTAATGGG

SHOC2 conditional KI D175N forward	CCATGGACTACAAGGACGACG
SHOC2 conditional KI D175N reverse	TGATTGTGAGCTACATCCAGGG
SHOC2 WT forward	AGTGAAGCTTGAGTCACCATGAG
SHOC2 WT reverse	GCCGTTTGATGGTATTGTCG
CreER^{T2} forward	GAATGTGCCTGGCTAGAGATC
CreER^{T2} reverse	GCAGATTCATCATGCGGA

PCR products were run in a 2% agarose gel at 220V for 20 minutes. Gels were visualized with GBox Syngene.

Timed matings

A single male mouse was mated with one or two females, which were plug checked daily. The embryonic days were counted starting as E0.5 on the day the vaginal plug was detected. The embryos were taken from the mothers at E8.5 and lysed and genotyped as described above.

Necropsy, tissue preparation and fixation of tissues for histology

Experimental mice were weighed and euthanized by carbon dioxide inhalation followed by cervical dislocation. Selected organs, including pancreas, liver, heart, colon, kidney, spleen, skeletal muscle, lung, white adipose tissue and thymus were removed quickly with sterile instruments and frozen on dry ice. The tissue samples were excised and fragmented using a scalpel (10–100 mg tissue portions were taken). After the addition of ice-cold PBS-E lysis buffer (PBS/1% Triton-X- 100/1 mM EDTA/Protease Inhibitors (Roche)/Phosphatase Inhibitors/1 mM DTT (dithiothreitol) the samples mixed by rotation at 4°C for ten minutes. Crude homogenates were then centrifuged for 30 minutes at 4°C, 13,000 rpm to pellet insoluble material. Soluble supernatant transferred into a fresh 2 ml Eppendorf tube. 20 µl of lysate supernatant was transferred to another tube containing 60 µl of 4X NuPAGE LDS Sample Buffer (Invitrogen). The rest of the supernatant was stored at -80°C.

For histology, in addition to organs listed above, skin, bladder and prostate tissues were also resected. Tissues were processed for microscopic evaluation were fixed in 10% neutral-buffered formalin (Sigma) o/n. Formalin was replaced with 70% ethanol to avoid over-fixation before embedding.

Sampling mouse serum

Animals were anesthetized with isoflurane administration and the skin was depilated by shaving to take images. The whole blood collected via cardiac puncture using a 26G needle. For serum samples, the blood was allowed to clot for 30–60 minutes at 37°C and centrifuged at 5000g for 10 minutes at 4°C. Serum samples were stored at -80°C until analysis. Clinical chemistry tests for serum samples were performed by MRC Harwell as a paid service.

Blood smear preparation

In order to collect the blood sample, each mouse was placed in a restraint chamber. The blood sample was obtained from each mouse by tail vein collection, in which the tail was wiped with ethanol swab and was punctured with a sterile needle about two-thirds down the tail, from the tail root. A small drop of blood was placed on a clean glass microscope slide, and a thin smear was immediately made and allowed to air dry. After enough blood was collected, the tail was compressed with the wet paper towel until bleeding stopped. All smears were stained with Wright-Giemsa stain by Ms. Adriana Resende Alves (UCL, Core Facility Pathology Service) as a paid service.

Ex vivo studies

Histology

All major organ systems and any grossly abnormal tissues were fixed in 10% neutral phosphate-buffered formalin. Formalin-fixed tissues were trimmed. All tissues were paraffin embedded and sectioned at 4–5 µm thickness. Samples were mounted

on slides and stained with hematoxylin and eosin (H&E). Tissue embedding and sectioning were performed by Ms. Adriana Resende Alves (UCL, Core Facility Pathology Service) as a paid service. Slides were scanned using a Hamamatsu Nanozoomer S210 whole slide scanner, and resulting digital images were visualized at 1680 × 1050 pixel resolution with NDP.view software. Alternatively, tissue sections were examined with an Evos FL Auto G25 microscope.

Immunohistochemistry

The formalin-fixed paraffin-embedded skin and spleen sections were stained following routine immunostaining protocols. In brief, sections were deparaffinized with xylene (Sigma), and rehydrated through incubation in aqueous solutions of decreasing ethanol concentration (5 minutes in 100% ethanol, 5 minutes in 80% ethanol, 5 minutes in 70% ethanol). Antigen retrieval was performed by heating sodium citrate buffer (pH 6.0) for 10-15 minutes in an antigen retriever (2100 Antigen Retriever, BioVendor), followed by cooling of the slides for 20 minutes at room temperature. Endogenous peroxidases were quenched by incubating the slides in 3% hydrogen peroxide (Sigma) for 10 minutes. The sections were then washed with PBS-T for 10 minutes. Slides were blocked in 2.5% horse serum (Vector ImmPRESS Kit) for 20 minutes at room temperature. Next, primary antibodies were applied for 60 minutes at room temperature (Table 2-2). After rinsing the slides in PBS-T, they were incubated in secondary antibody goat anti-rabbit IgG or rabbit anti-rat IgG (Vector ImmPRESS Kit) for 30 minutes at room temperature. After washing with PBS-T for 15 minutes colour development was managed by performing diaminobenzidine tetrahydrochloride (DAB) component with stabilizer solution (Biolegend) for one to five minutes, depending on the primary antibody. After rinsed in deionized water, the sections were counterstained with haematoxylin solution (Sigma), dehydrated through ethanol and xylene, and cover-slipped using DPX mounting medium (Sigma). Alternatively, traditional immunohistochemistry was performed on automated BOND-III (Leica Microsystems) according to a protocol previously described (Marafioti et al. 2004).

Immunofluorescence (IF)

The deparaffinization/rehydration, antigen retrieval and the blocking steps were performed to formalin-fixed paraffin-embedded skin sections as described in the section above. Then, slides were incubated with primary antibodies (Table 2-2) diluted in 5% BSA in PBS at 4 °C overnight. After extensive washing with PBS-T, slides were incubated with corresponding fluorescently labelled secondary antibodies (Table 2-3) diluted in 5% BSA in PBS at room temperature in the dark for 1 hour. After incubation, slides were then washed with PBS-T for 15 minutes after the washes, nuclei were counterstained with Hoechst (Sigma) at a concentration of 1 µg/ml in PBS for 10 minutes and subsequently washed twice for 1 minute each with PBS. Then, slides were mounted with a drop of mounting media (Dako) and pictures were obtained using a Zeiss AxioImager A1.

Dermatitis scoring criteria

The dermatitis severity was recorded according to established protocol with slight modifications (Taraborrelli et al. 2018). Briefly, the severity of dermatitis for Shoc2 KO/KI mice and WT controls was determined macroscopically based on two main clinical criteria in a blinded manner. Each region of the body, including back, head (face), throat and flank, affected by lesions, was given a score of 1 and the sum of these provided information of how expanded the lesions were. The other criteria was the characteristics of the lesion that was evaluated and graded from 1 to 3, as follows: punctuated small crusts, coalescent crusts, and ulceration, respectively. The sum of both criteria represented the total severity score of the lesions (Table 2.5). When any of those two main criteria reached score 2, the monitoring was increased to twice a day, and if the conditions deteriorated and proceeded to score 3, mice were euthanized immediately.

Table 2-5. Dermatitis severity scoring system to show affected regions (A) and character of lesion (B).

A

Score	Regions affected
0	None
1	Back
1	Head (Face)
1	Throat
1	Flank
4	**SUM**

B

Score	Character of Lesion
0	No lesions
1	Punctuated small crust
2	Coalescent multiple crusts
3	Ulceration

Epidermal thickness quantification

The epidermal thickness was quantified in three different positions and for at least 10 different measurements per mouse. Quantification was performed using ImageJ Software.

Scratching behaviour measurement

Scratching behaviour was quantified for 2 minutes during which time the number of scratches were counted. A total of 5 Shoc2 KO, 5 Shoc2 KI and 5 WT control male mice were used. One scratch was defined as the animal raising a hind limb from the cage floor, scratching with the limb and then returning the limb to the cage floor. This was repeated 3 times for each mouse analysed.

Lymph node size determination

The lymph node size was examined from the areas of digital images with 1680 × 1050 pixel resolution and a magnification of × 1.25 which obtained from NDP. view software. Quantification was performed using ImageJ Software.

Determination of water intake and urine volume

The average water intake per mouse was determined by weighing water bottles of group-housed mice (aged matched 5 mice per cage) before and after five days of housing. The mouse whole bladder was isolated to measure full bladder volumes. A sterile 5 ml syringe is passed directly into the bladder to collect the urine sample**.**

Flow Cytometry

Tissues used for characterisation of cell populations by flow cytometry included two femurs and tibias for bone marrow populations, spleen, skin and both sides of inguinal, brachial and axillary lymph nodes from individual experimental mice. The tissues were removed from mice and collected in DMEM/0% FBS. Mice spleens and lymph nodes were mechanically dissociated with the top of a syringe piston. Single-cell suspension was prepared by pressing the tissues through a 70µm cell strainer with a 2 ml syringe plunger. Cells from spleen and lymph nodes were washed with 10 ml DMEM/0% FBS. Red blood cell (RBC) lysis was performed on spleen suspension, as follows: cell suspension was centrifuged at 400g for 5 minutes at 4°C and the supernatant discarded. Splenic pellets were resuspended in 3 ml of the RBC lysis buffer (Sigma) and then washed with 10 ml DMEM/0% at 400g for 1-3 minutes at 4°C. RBC lysis was not required for lymph node cell suspensions.

For purification of bone marrow populations, tibias and femurs were harvested from euthanized mice and crushed using mortar and pestle in a small volume of FACS buffer (2% FBS +2mM EDTA in PBS). The resulting mixture was filtered with 40µm cell strainer (BD Falcon) and the suspension was cleared of RBCs using 4 ml of the RBC lysis buffer (Sigma). Next, cells were resuspended in ice cold FACS buffer.

The throat skin (between 50 and 100 ug) of mice was pulled off and chopped in 890 ul of RPMI /0% FBS in a 2 ml Eppendorf tube. Then, 100 ul Liberase (5 mg/ml) and 10 ul DNAse (7.5 mg/ml) were added to each tube and vortex-mixed vigorously. Skin samples were subsequently incubated for 30 minutes at 37ºC in a water bath and vortex-mixed every 10 minutes. Next, digestion was stopped by adding 1 ml of RPMI /10% FBS/1X Glutamine with 5 mM EDTA to each tube. After that, skin samples were disaggregated with the top of a syringe piston through a 70 um cell strainer into

a 60 mm dish with a complete RPMI and 5 mM EDTA solution. Samples were then centrifuged at 400g for 5 minutes at 4°C and the supernatant discarded. Pellet was resuspended in 1 ml of complete RPMI with 10 ul DNAse (7.5 mg/ml) and incubated 5 minutes on ice. Next, cell suspension was centrifuged at 400g for 5 minutes at 4°C. The supernatant discarded and the pellet was resuspend in 200 ul of FACS buffer.

Samples of cell suspensions were then transferred to the wells of a 96-well round-bottomed plate and blocked with anti-CD16/32 at 4°C for 15 minutes. Samples were then stained for various markers in the dark for 30 min on ice (Table 2.6). Cells were then washed, fixed and permeabilized on ice before flow cytometry quantification beads were added to the samples before the analysis. The analysis was performed using the FlowJo program. Flow cytometry immunophenotyping experiments were performed by Cristobal Costoya from Sergio Quezada lab.

Statistical analysis

Graphics and statistical analyses were performed using the GraphPad Prism 8 (GraphPad Software) and the Microsoft Excel. Statistical analyses were performed by unpaired Student's t test. All results are presented as mean ± Standard Error of Mean (SEM), unless stated otherwise. Statistical significance in survival curves was determined using a log-rank test. For all tests, p value> 0.05 was not considered significant (NS), whereas differences were considered statistically significant when p-values were below 0.05 (*), 0.01 (**), 0.001 (***) or 0.0001 (****) respectively. In all cases comparisons were made between the indicated *knock-out/knock-in* mice and the respective wild type littermate controls.

Chapter 3 Generation of Shoc2 Knock-Out and Knock-In Mouse Models

Introductory statement

Shoc2 ablation has been shown previously to be embryonic lethal at E8.5 and conditional knockout of Shoc2 in murine endothelial tissues leads to embryonic lethality at E13.5 due to a range of cardiac defects (Yi et al. 2010). Shoc2 was shown to be required for normal development of heart valves (valvulogenesis) and for endothelial-mesenchymal transformation, which is a critical step in endocardial cushion formation (Yi et al. 2010). However, the effects of Shoc2 ablation in adult mice has not been addressed. In order to address Shoc2's physiological role at the organismal level, we have generated genetically engineered modified mouse models (GEMMs) of Shoc2 inactivation.

Generation of Shoc2 Knock-Out and Knock-In Mouse Models

In order to investigate Shoc2 function at the organismal level and characterize its role in normal tissue homeostasis, the lab has generated two GEMMs where Shoc2 expression can be conditionally inactivated a conditional *knock-out* (cKO) and a conditional *knock-in* (cKI) model. The first model contains a *Shoc2* gene, where exon 4 is flanked by LoxP sites: upon Cre-mediated recombination exon 4 is deleted and this prevents expression of Shoc2, rendering the model a KO (Figure 3-1A). The second mouse model contains a conditional D175N KI mutation in Shoc2. A 'minigene' strategy was used to generate a conditional KI (cKI) mouse where the wild-type *Shoc2* allele is expressed in a cDNA configuration with a Flag-tag at the N-terminus under the control of the endogenous promoter. The wild type *Shoc2* cDNA sequence is deleted after Cre-mediated recombination and replaced by the mutant *Shoc2*^{D175N} allele containing a Myc-tag (Figure 3-1B). This 'double tag' strategy enables us to monitor recombination (and subsequent expression of *Shoc2*^{D175N}) by measuring loss-of-signal with a Flag antibody and gain-of-signal with a Myc-tag antibody. Crucially, this D175N substitution disrupts the formation of the SHOC2-MRAS-PP1 complex but preserves other scaffold functions of SHOC2, such as the interaction with SCRIB (Rodriguez-Viciana et al. 2006; Young et al. 2013; Young et al. 2018). Consequently, this second KI model enables us not only attribute effects to SHOC2 but specifically to its function as part of a phosphatase complex with MRAS and PP1, more closely mimicking pharmacological inhibition of this complex in the

clinic and providing a stronger rationale for drug development targeted against this complex.

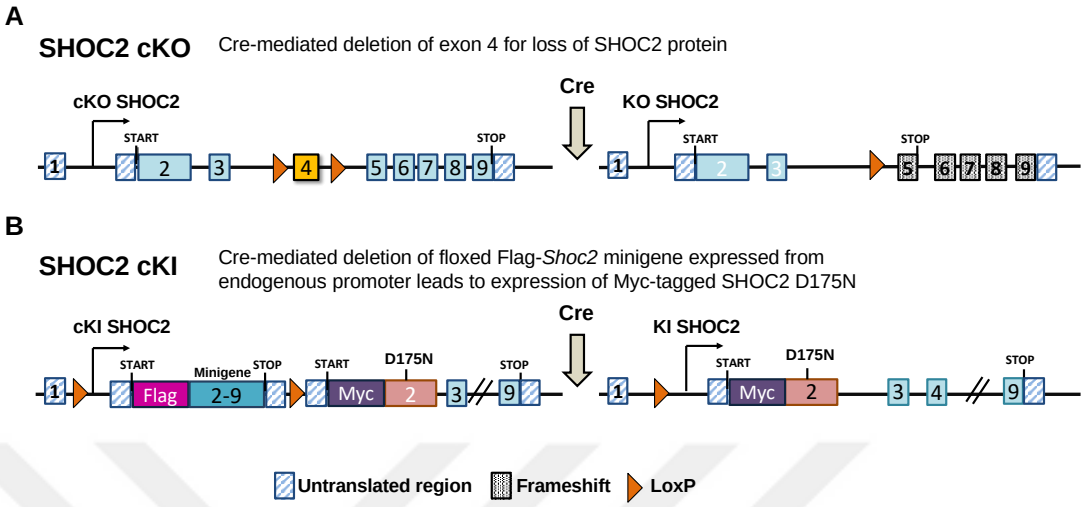

Figure 3-1. Schematic of targeting strategy used to generate Shoc2 cKO and cKI mouse models

A. Shoc2 cKO mouse model
B. Shoc2^{D175N} cKI mouse model

Effect of germline deletion of Shoc2 in mice

To assess the effect of constitutive Shoc2 inactivation and its role during development using both KO and KI strategies, Shoc2 cKO/cKI mice were crossed with a transgenic line that uses the CMV promoter to drive ubiquitous expression of the Cre recombinase (CMV-Cre transgenic mice) (Schwenk et al. 1995). After this cross, constitutive Shoc2 KO/Cre$^{WT/WT}$ or Shoc2 KI/Cre$^{WT/WT}$ heterozygous mice were intercrossed (Figure 3-2A).

Genotyping of new-born litters demonstrated an increased frequency of WT and Shoc2 KO or KI heterozygous mice over the expected frequencies with heterozygous mice being overtly normal. In contrast, viable homozygous Shoc2 KO or KI mice were not identified (Figure 3-2B). Therefore, these observations indicate that Shoc2 KO and KI homozygous mice are dying during embryonic development. Yi et al., (2010) showed that *Shoc2* null mice are embryonic lethal at embryonic day 8.5. To confirm this observation on the KO model and assess whether inactivation by KI had a similar effect, the time matings were set up and embryos dissected at E8.5 from pregnant females. This analysis revealed only one homozygous embryo

remained viable at E8.5 for each genotype. Therefore, consistent with previously published data, we observed that constitutive deletion of Shoc2 in mice results in early embryonic lethality at E8.5 and furthermore, we show for the first time that similarly, Shoc2 KI mice for the D175N mutation also undergo embryonic lethality at the same stage of embryogenesis (Figure 3-2C).

A

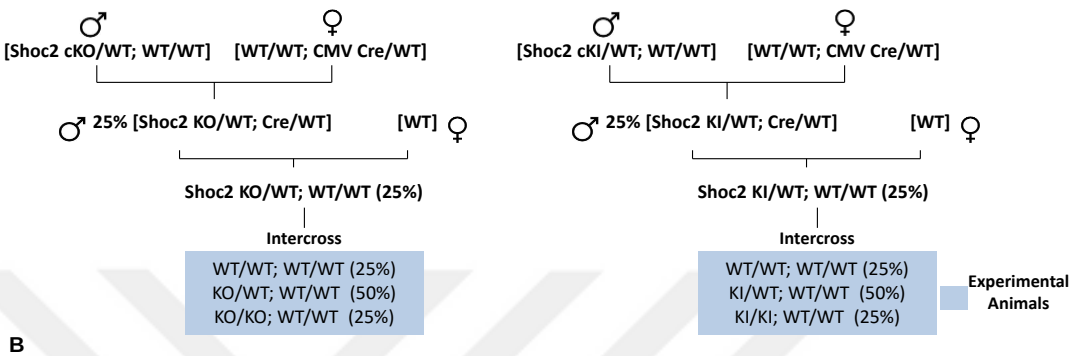

B

KO: Shoc2$^{KO/WT}$ x Shoc2$^{KO/WT}$ D175N KI : Shoc2$^{KI/WT}$ x Shoc2$^{KI/WT}$

Animals obtained

Genotype	Expected	Observed	Genotype	Expected	Observed
Shoc2 $^{KO/KO}$	14 (25%)	**0**	Shoc2 $^{KI/KI}$	20 (25%)	**0**
Shoc2 $^{KO/WT}$	28 (50%)	38 (67.9%)	Shoc2 $^{KI/WT}$	40 (50%)	43 (53.7%)
Shoc2 $^{WT/WT}$	14 (25%)	18 (32.1%)	Shoc2 $^{WT/WT}$	20 (25%)	37 (46.3%)
Total	**56**	**56**	**Total**	**80**	**80**

C

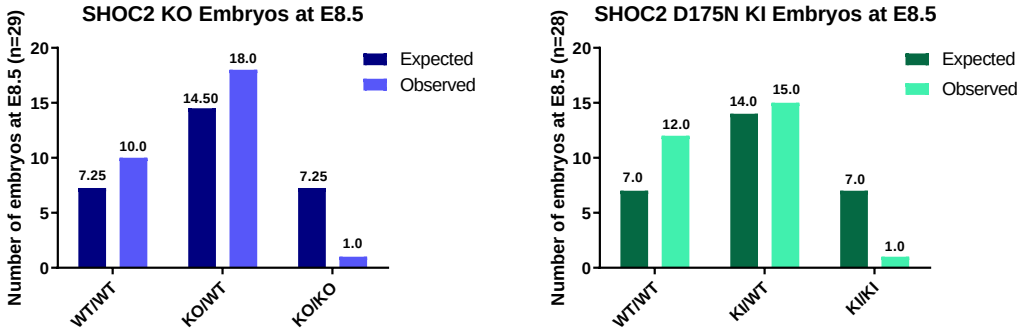

Figure 3-2. Constitutive Shoc2 inactivation using both KO and KI approaches is embryonic lethal

A. Outline of the breeding strategy used to generate experimental cohorts of mice and expected genetic ratios of offspring.
B. Quantification of genotypes of animals obtained after intercrossing Shoc2 KO-KI/ Cre$^{WT/WT}$ heterozygous mice. Experimental homozygous animals were not born at the expected Mendelian ratio consistent with embryonic lethality. Percentage of expected and observed embryos are shown in brackets. KO (n= 56) and KI (n=80).

C. Graph showing expected versus observed E8.5 embryos from breedings of heterozygous Shoc2 KO and KI lines based on normal Mendelian inheritance. KO (n= 29) and KI (n=28).

Generation of *Shoc2$^{fl/fl}$ Rosa26-CreER^{T2}* mouse model of systemic Shoc2 inactivation in adult mice

In order to bypass the embryonic impact observed in constitutive Shoc2 *knock-out* and *knock-in* mice and more accurately mimic potential SHOC2 therapeutic inhibition in the clinic, we generated tamoxifen-inducible Cre mice that are homozygous for floxed Shoc2. In this way, Shoc2 can be silenced at a chosen time point after major developmental processes have taken place. To this end, we crossed *Shoc2$^{fl/fl}$* cKO and cKI mice with *Rosa26-CreER^{T2}* mice to generate *Shoc2$^{fl/fl}$ KO/KI Rosa26-CreER^{T2}* mice, which carry an inducible ubiquitously expressed CreER^{T2} recombinase (Figure 3-3A). CreER^{T2} is currently the most successful CreER version, which utilizes a mutated estrogen receptor (ER) fused to Cre as a transgene (CreER). It only becomes activated and then translocates into the nucleus upon binding of the active tamoxifen metabolite 4-hydroxytamoxifen (4-OHT) (Zhong et al. 2015). The efficiency of deletion of this strain is reported to vary between different organs but usually exceeds 70%, except for the brain. In the brain, deletion efficiency is lower since tamoxifen crosses the blood/brain barrier rather inefficiently (Blasco et al. 2011). Tamoxifen-mediated Cre recombination of the floxed *Shoc2* gene (Figure 3-3B) led to Shoc2 inactivation in different organs that will be shown in the following sections.

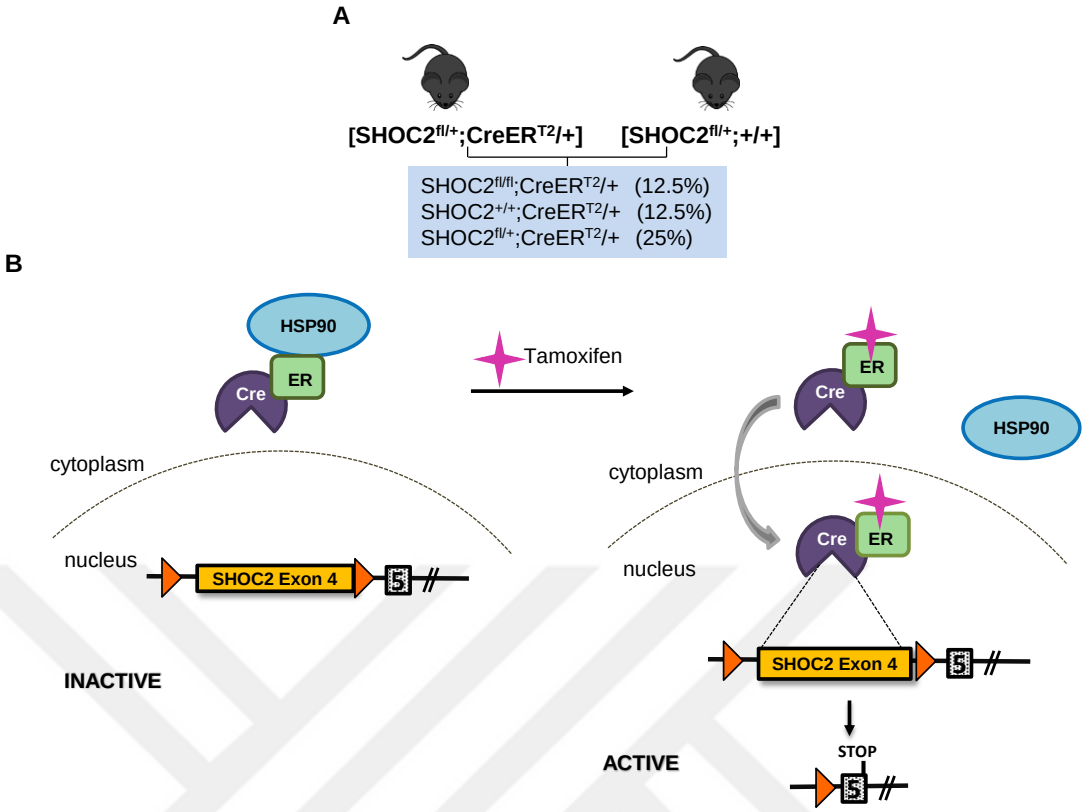

Figure 3-3. *Rosa26-CreER^{T2}* mouse model of systemic Shoc2 inactivation in adult mice

A. Outline of the breeding strategy used to generate experimental cohorts of mice and expected genetic ratios of offspring.
B. Schematic representation of the tamoxifen-regulated gene expression in the CreER^{T2} system. In the absence of tamoxifen, CreER is sequestered in the cytoplasm by HSP90. In the presence of tamoxifen, HSP90 dissociates from CreER and it is translocated to the nucleus where it recognizes loxP sequences (orange triangles) and cleaves the Exon 4 of Shoc2.

Validation of Shoc2 deletion with *Rosa26-CreER^{T2}* model

In order to examine the recombination efficiency at the protein level, 6 weeks old *Shoc2$^{fl/fl}$ cKO Rosa26-CreER^{T2}* (cKO) and control Shoc2$^{+/+}$ *Rosa26*-CreER^{T2} (WT) mice were treated with tamoxifen by oral gavage for 5-consecutive days. After one-week gap, a second tamoxifen treatment was administered for another 5-consecutive days (Figure 3-4A). To compare one-week versus two-weeks tamoxifen treatment, 8 weeks (for one-week tamoxifen-treated mice) and 6 weeks (for two weeks tamoxifen-treated mice) after the last tamoxifen administration, mice were sacrificed and different organs such as brain, pancreas, liver, heart, colon, kidney, spleen, skeletal muscle, lung, thymus and lymph nodes were harvested (Figure 3-4B). As determined

by western blot quantification, two weeks-tamoxifen treated mice were found to have higher recombination efficiency compared to one-week- treated ones across different organs. Notably, in liver, recombination stimulated by two weeks of tamoxifen was approximately 10-fold higher than that of one-week treatment (Figure 3-4C). We observed a similar increase in lung, about 7-fold higher in mice treated with tamoxifen twice. Although Shoc2 expression was lower in kidney, 2 weeks tamoxifen treatment still increased recombination efficiency (about 2.5-fold). In other tissues such as pancreas, colon, spleen and skeletal muscle, loss of Shoc2 expression was about 90% in both conditions (Figure 3-4C). Regardless of one or two-week of treatment with tamoxifen, there was no recombination in the brain likely due to the blood/brain barrier. As a result, two-weeks tamoxifen administration was found more effective compared to one-week treatment (Figure 3-4D). Besides, in order to validate the recombination efficiency at the DNA level, 6 weeks old adult *Shoc2*$^{+/+}$ (WT/WT), *Shoc2*$^{fl/fl}$ cKO (cKO/cKO), and *Shoc2*$^{fl/+}$ cKO (cKO/WT) mice with *Rosa26-CreER*^{T2} were subjected to PCR genotyping for detection of Shoc2 WT and KO alleles after Cre recombinase activity. Ear notches were lysed before and 6 weeks after the second tamoxifen treatment. The different allele combinations were shown in Figure 3-4E.

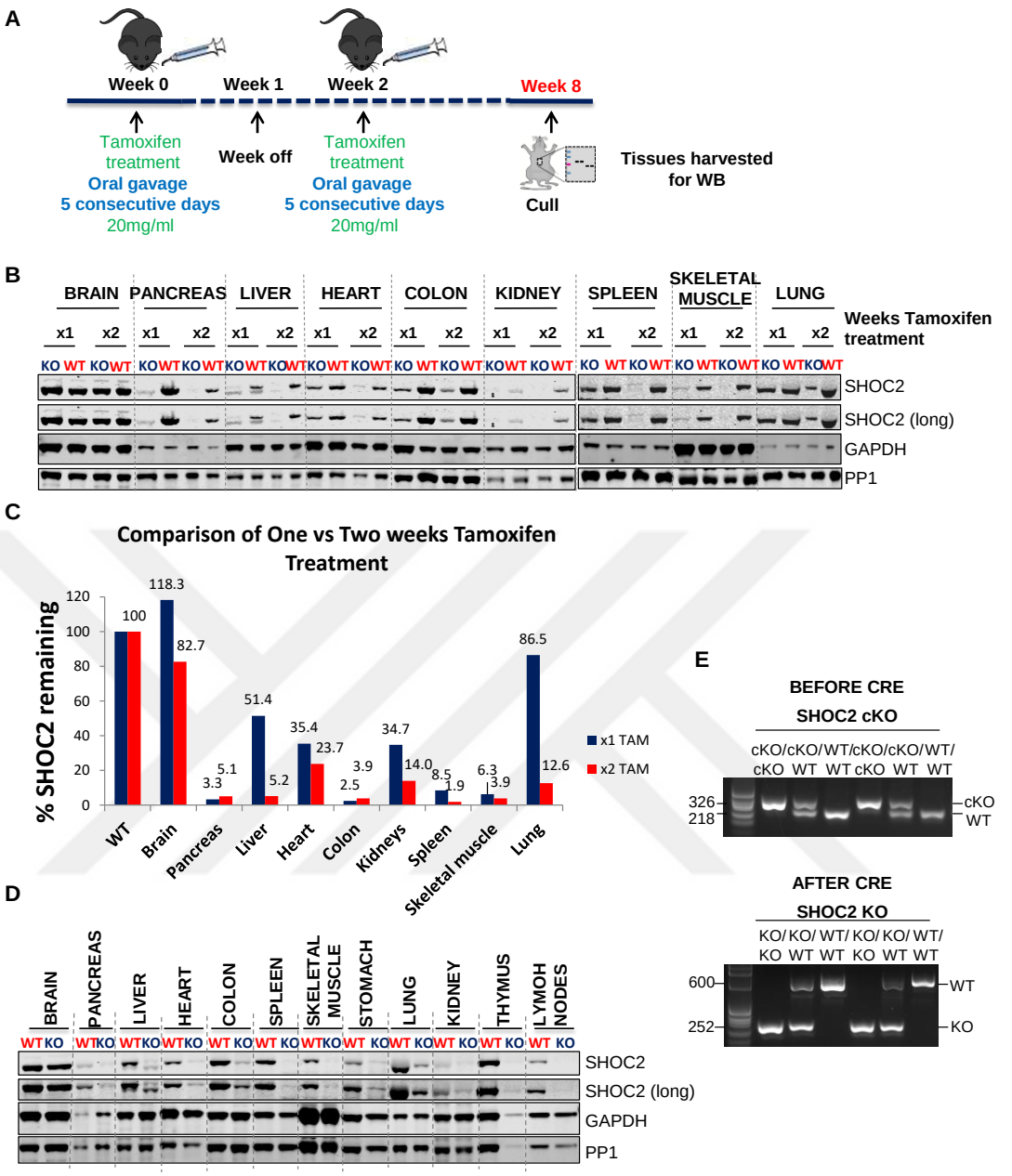

Figure 3-4. Efficient systemic Shoc2 deletion in adult mice upon tamoxifen treatment with *Rosa26-CreER^{T2}* KO model

A. Schematic layout of tamoxifen treatment by oral gavage to induce systemic Shoc2 inactivation in adult mice.
B. Comparison of one-week vs two-weeks tamoxifen treatment by oral gavage. Lysates from indicated tissues were analysed by Western Blot (n=1 for each genotype and n=2 independent experiments).
C. Quantification of Shoc2 levels relative to GAPDH loading control of (B) using Odyssey CLx Imaging system (LI-COR). Protein levels of WT mice were set to 100%.
D. Western blot of two-weeks tamoxifen treatment across different organs Blot (n=1 for each genotype and n=2 independent experiments).
E. PCR genotyping of DNA isolated from the ear notch of mice with the indicated genotypes. cKO: conditional Shoc2 knock-out allele, WT: wild-type allele, KO: constitutive Shoc2 knock-out allele (n=2 for each genotype).

Comparison of oral gavage and intraperitoneal injection

In rodents, there are several methods of tamoxifen administration, including oral gavage, intraperitoneal injection (IP), or as a supplement in drinking water or chow. The administration of tamoxifen in chow might be convenient because it reduces stress and avoids adverse effects in mice; however, mice may suffer a temporary loss of weight immediately after starting the new diet (Whitfield et al. 2015). Several studies have shown that dietary tamoxifen can be unsuitable for studies requiring acute activation of modified ligand-binding domain of the estrogen receptor (ER^{TAM}) proteins (Wilson et al. 2014) and besides, mice can unexpectedly die after switching to a tamoxifen-containing diet (Chiang et al. 2010). On the other hand, oral gavage is a highly accurate and reliable technique, but this method can be technically challenging due to the fact that the restraining and intensive handling of mice can result in increased stress levels (Diogo et al. 2015). In our experimental system, we have administered tamoxifen in two weeks with a week break in between by oral gavage (3 weeks in total). Therefore, in order to reduce treatment duration and overcome the technical challenge of oral gavage, we decided to compare the effect of tamoxifen on recombination efficiency when administered to mice by IP injection versus oral gavage.

To test whether IP injection of tamoxifen is as effective as oral gavage, mice were injected either with 20 mg/ml tamoxifen for one day, for five consecutive days, or fed with tamoxifen by oral gavage for two weeks (one week on, one week off, one week on). Three weeks after the last IP injection and one week after the second oral gavage treatment, brain, spleen, colon, liver and lungs were collected from the experimental mice. Western blot quantification showed that mice treated for one day with IP had very low recombination efficiency in all organs. Mice treated for five consecutive days by IP and the ones treated for two weeks with oral gavage had very similar rates of recombination. In the lung, the two weeks of oral gavage treatment showed results which were two-fold higher than in the mice treated for five consecutive days by IP, whereas in the colon, lung and spleen both methods were equally effective. Interestingly, about 55% recombination was seen in the brains of the mice treated by IP injection for five consecutive days (Figure 3-5A and B). Because of the efficient recombination results and shorter treatment period (5 days

with IP injection instead of 10 days of treatment by oral gavage), the IP injection method was used for further experiments (Figure 3-5C).

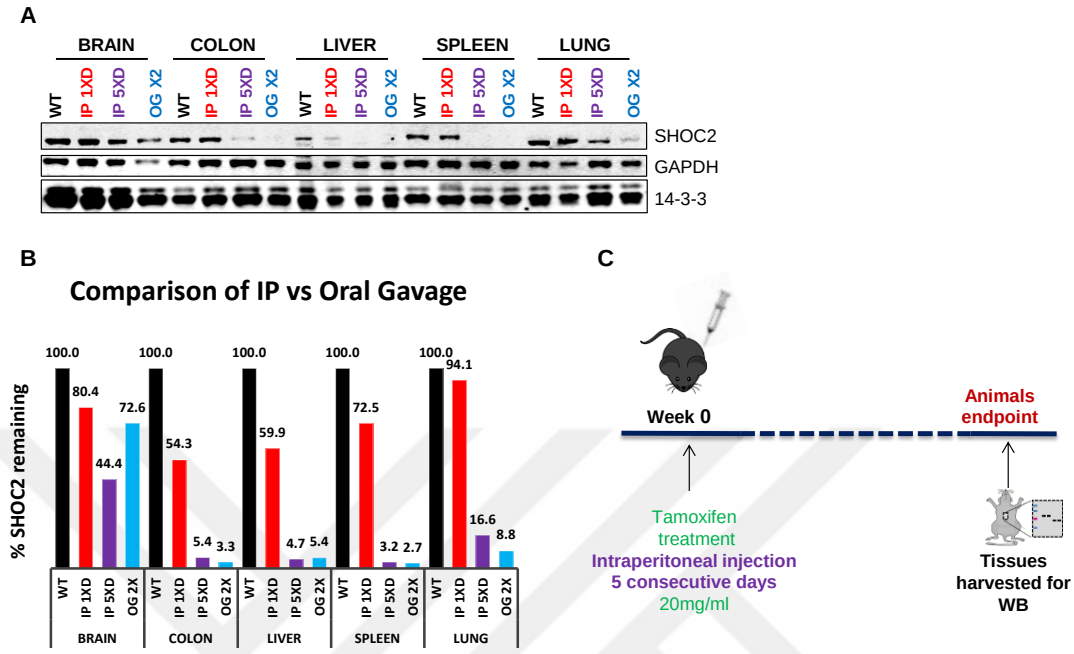

Figure 3-5. 5 days IP injection has similar recombination efficiency to 2 weeks oral gavage

A. Lysates of the brain, colon, liver, spleen and lung. One day IP (IP 1XD) group had very low recombination efficiency. 5 days IP injection (IP 5XD) and 2 weeks oral gavage groups (OG 2X) had similar rates of recombination (n=1 for each genotype and n=2 independent experiments).
B. Quantification of Shoc2 levels relative to GAPDH loading control of (A) using Odyssey CLx Imaging system (LI-COR). Protein levels of WT mice were set to 100%.
C. Schematic layout of tamoxifen treatment by IP injection to induce systemic Shoc2 inactivation in adult mice.

Investigation of recombination efficiency at different time-points

To determine the time course of Shoc2 protein loss after tamoxifen treatment and assess whether this loss is sustained over time *Shoc2*$^{fl/fl}$ *KO Rosa26-CreER*^{T2} (KO) and *Shoc2*$^{+/+}$ *Rosa26-CreER*^{T2} (WT) mice were sacrificed at different time points post-injection and loss of Shoc2 protein was tested on several tissues by western blot. Firstly, 6-12 weeks old Shoc2 KO and WT mice were sacrificed at 1 week after the last tamoxifen treatment. Colon, liver, spleen and pancreas tissues were harvested to analyse for Shoc2 expression by western blotting of whole tissue extracts (Figure 3-6A). As a result, more than 90% recombination was detected in all

tissues from different mice (Figure 3-6B). Interestingly, ERK phosphorylation was observed only in liver and pancreas tissues but Shoc2 ablation had no effect (Figure 3-6A). Secondly, the loss of Shoc2 expression was assessed in different organs over 15 weeks post-tamoxifen treatment. The same tissues as above were harvested from Shoc2 KO and WT mice and efficient Shoc2 deletion was observed in all the different tissues (Figure 3-6C and D).

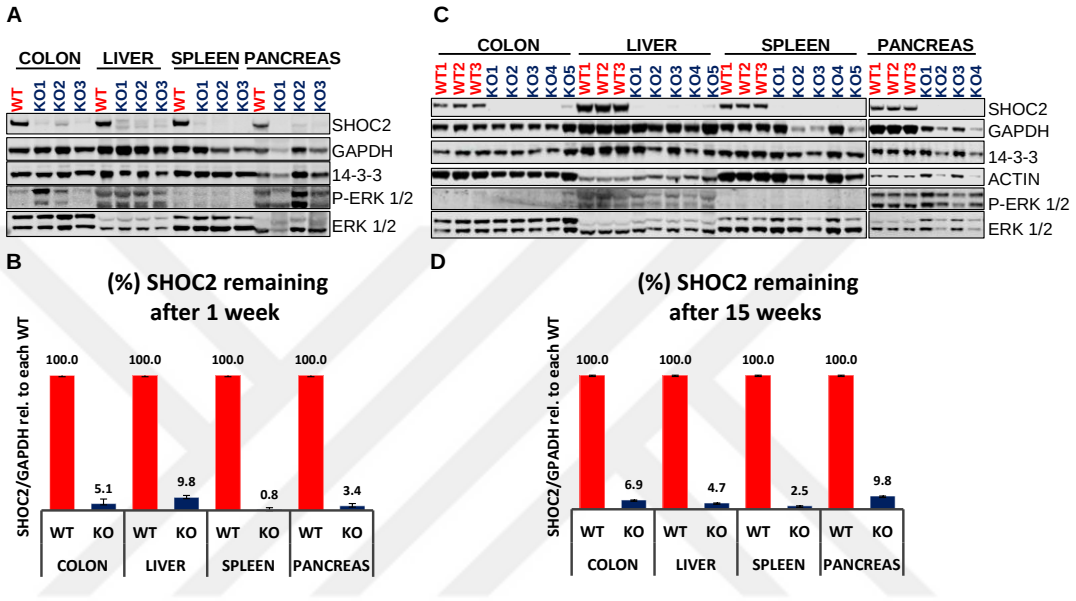

Figure 3-6. Loss of Shoc2 proteins is maintained over time after 1-week IP treatment

A. Western blot of whole tissue extracts at 1 week post-tamoxifen treatment. Colon, liver, spleen and pancreas lysates were analysed by Western blotting at 1 week post-tamoxifen treatment. WT (n=1) and KO (n=3).
B. Quantification of (A) using Odyssey CLx Imaging system (LI-COR). Protein levels of control mice were set to 100%. Each column of organs represents the mean of 3 different KO mice. Error bars correspond to standard deviation.
C. Western blot of whole tissue extracts 15 weeks post-tamoxifen treatment as in A. Colon, pancreas, spleen, liver and lung tissues were analysed as in A from mice at 15 weeks post-tamoxifen treatment. WT (n=3) and KO (n=5). Strong reduction is still observed in Shoc2 KO mice after the last tamoxifen treatment.
D. Quantification of (C) using Odyssey CLx Imaging system (LI-COR) as in B.

Validation of Shoc2 inactivation in Shoc2^{D175N} KI model

As mentioned earlier, in the Shoc2 knock-in mouse model, the wild-type Flag-tag *Shoc2* sequence is deleted after Cre-mediated recombination and replaced by the mutant *Shoc2*^{D175N} allele containing a Myc-tag. Therefore, a concomitant increase in the Myc signal and a decrease in the Flag signal by western blot is the readout for efficient recombination in the Shoc2^{D175N} KI model (Figure 3-7A and B).

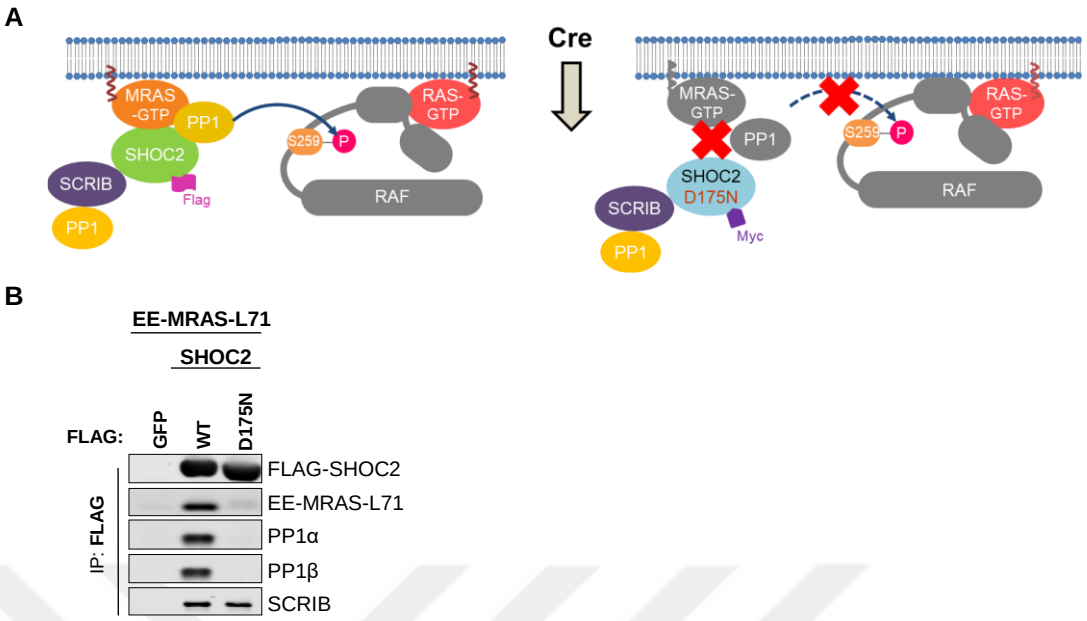

Figure 3-7. Illustration for the Shoc2^{D175N} KI mouse model

A. Schematic illustrations demonstrating recombination in the Shoc2^{D175N} KI mouse model.
B. Shoc2^{D175N} mutation, although defective for PP1 and MRAS binding, can still interact with SCRIB. Flag immunoprecipitations (IPs) were performed and immunoblotted using Odyssey CLx Imaging system (LI-COR).

In order to examine the recombination efficiency at the protein level, 6-12 weeks old *Shoc2$^{fl/fl}$ cKI Rosa26-CreER^{T2}* (cKI) mice treated with tamoxifen by intraperitoneal injection for 5-consecutive days. *Shoc2$^{fl/fl}$ cKI Rosa26-CreER^{T2}* mice that had not been treated with tamoxifen (NT) were used as control animals. All experimental mice were sacrificed 4 weeks later to extract the following tissues: brain, colon, liver, pancreas and spleen to analyse for Shoc2 expression by western blotting (Figure 3-8A). However, western blot analysis revealed that although Myc-Shoc2 D175N can be detected, expression levels of Flag-Shoc2 was still high in all tissues showing that recombination efficiency by intraperitoneal injection for 5-consecutive days is not as efficient in the KI (Figure 3-8B) as in the KO model shown (Figure 3-5B).

To increase recombination efficiency, we then treated Shoc2 KI mice with tamoxifen by intraperitoneal injection for 2 weeks with a week break in between (one week ON-OFF-ON). Mice were sacrificed 15 weeks post-tamoxifen and it was observed that 2 weeks treatment led to efficient loss of Flag and concomitantly gain of Myc in all the tissues tested (Figure 3-8C and D). In order to confirm that efficient recombination is still seen at later time points, we sacrificed a cohort of Shoc2 KI and

control mice over 35 weeks post-tamoxifen treatment. A significant decrease in Flag as well as a notable increase in Myc expression, demonstrating that the recombination was highly efficient in the Shoc2^{D175N} KI mouse model even after 35 weeks post-tamoxifen treatment (Figure 3-8E and F). We also validated *Shoc2 KI Rosa26-CreER^{T2}* mouse model at the DNA level. To this end, 6-12 weeks old *Shoc2$^{+/+}$* (WT/WT), *Shoc2$^{fl/fl}$* cKI (cKI/cKI), and *Shoc2$^{fl/+}$* cKI (cKI/WT) mice with *Rosa26-CreER^{T2}* were subjected to PCR genotyping for detection of Shoc2 WT and KI alleles after tamoxifen treatment. Ear notches were lysed before and 6 weeks after the second tamoxifen treatment. The different allele combinations are shown in Figure 3-8G.

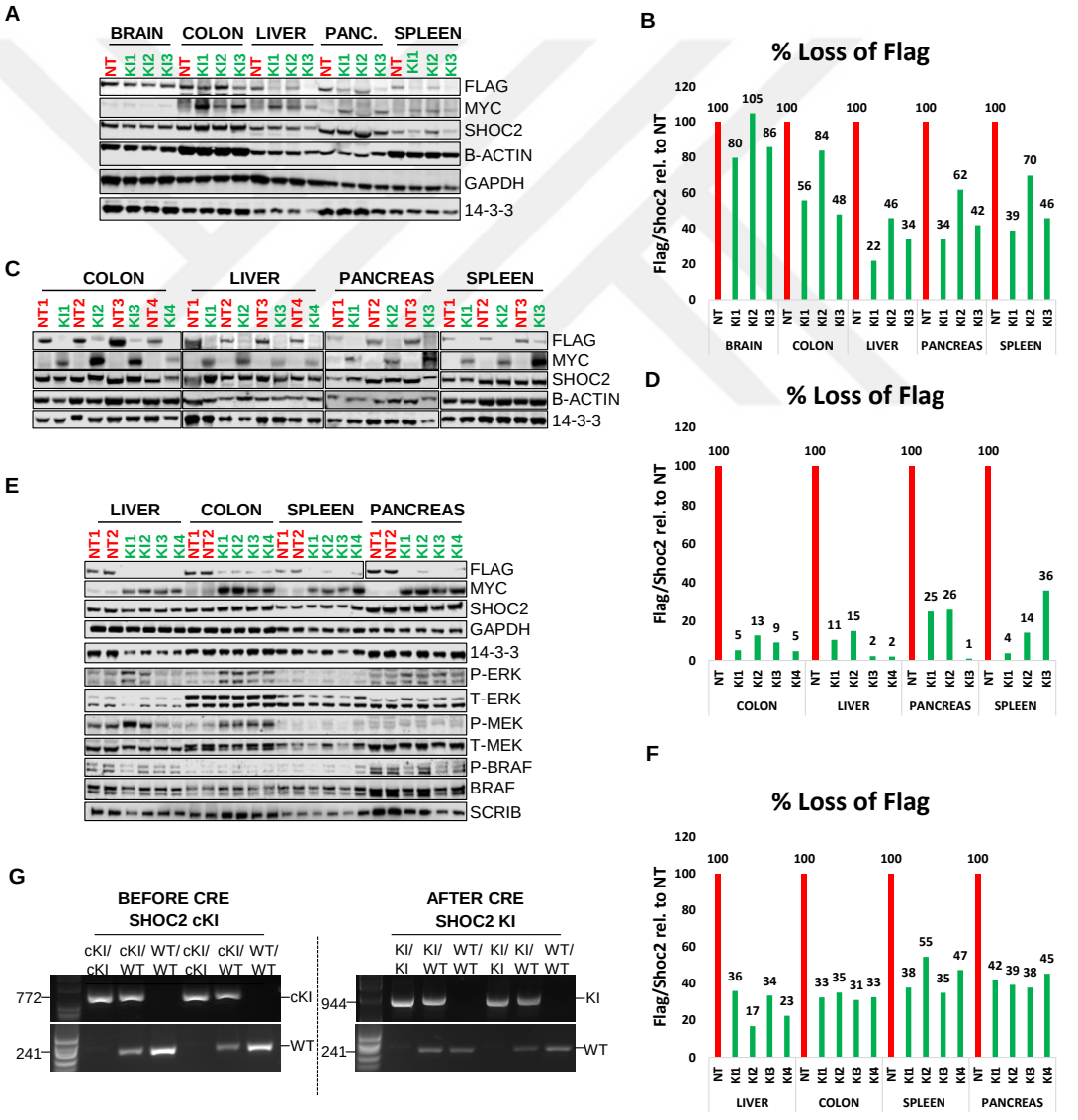

Figure 3-8. Recombination efficiency in *Rosa26-CreER^{T2}* Shoc2^{D175N} KI mouse model

A. Western blot of whole tissue extracts from *Shoc2$^{fl/fl}$ cKI Rosa26-CreER^{T2}* mice treated with tamoxifen by intraperitoneal injection for 5-consecutive days (n=3). Non-tamoxifen treated *Shoc2$^{fl/fl}$ cKI Rosa26-CreER^{T2}* mice (NT) used as control (n=1). 4 weeks post-tamoxifen treatment, brain, colon, liver pancreas and spleen tissues were analysed. Recombination efficiency is monitored by measuring loss of signal with a Flag antibody and gain of signal with a Myc-tag antibody.
B. Quantification of (A) using Odyssey CLx Imaging system (LI-COR). Flag protein expression levels of non-treated *Shoc2$^{fl/fl}$ cKI Rosa26-CreER^{T2}* mice (NT) were set to 100%.
C. Western blot of whole tissue extracts from KI mice treated with tamoxifen by intraperitoneal injection for 2 weeks and a week break in between (n=4 for colon and liver and n=3 for pancreas and spleen). Non-tamoxifen treated *Shoc2$^{fl/fl}$ KI Rosa26-CreER^{T2}* mice (NT) used as control (n=4 for colon and liver and n=3 for pancreas and spleen). 15 weeks post-tamoxifen treatment colon, pancreas, spleen and liver tissues were analysed as in (A).
D. Quantification of (C) using Odyssey CLx Imaging system (LI-COR) as in (B).
E. Western blot of whole tissue extracts 35 weeks post-tamoxifen treatment. Colon, pancreas, spleen and liver tissues were analysed (n=4 for each genotype) as in (A).
F. Quantification of (E) using Odyssey CLx Imaging system (LI-COR) as in (B).
G. PCR genotyping of DNA isolated from the ear notch of mice with the indicated genotypes. cKI: conditional Shoc2 knock-in allele, WT: wild-type allele, KI: constitutive Shoc2 knock-in allele (n=2 for each genotype).

Conclusions

Taken together, these observations show that constitutive deficiency of Shoc2 in mice results in embryonic lethality demonstrates the importance of Shoc2 in embryonic development. Furthermore, we show for the first time that inactivation of Shoc2 by the D175N mutation also results in embryonic lethality at the same stage of embryogenesis of E8.5. This D175N substitution in Shoc2 disrupts the formation of the SHOC2-MRAS-PP1 complex but preserves other scaffold functions of Shoc2 such as the ability to interact with the polarity proteins SCRIB (Young et al. 2013). Thus, embryonic lethality upon Shoc2 inhibition at E8.5 is dependent on its RAF phosphatase function.

In order to overcome embryonic lethality and precisely manipulate the timing of recombination to study Shoc2 function during adulthood, we generated tamoxifen-inducible *Rosa26-CreER^{T2} Shoc2 KO and Shoc2^{D175N} KI* mouse models. In this chapter, we have tested different methods and time points used to deliver tamoxifen and five days of consecutive injections of tamoxifen was found the most effective way to induce recombination in different tissues of Shoc2 KO mice whereas for ten days in two, five day treatment windows with a week break in between for Shoc2 KI mice. As a result, we have observed good recombination across the breath of tissues tested.

Chapter 4 Characterisation of Systemic Shoc2 Inactivation in Adult Mice

Introductory statement

In Chapter 3 we have shown that *in vivo* Shoc2 ablation leads to embryonic lethality by E8.5 when using either KO or KI Shoc2^{D175N} mouse models. Furthermore, it was also shown that systemic Shoc2 inactivation in adult mice mediated by *CreER^{T2}* recombinase upon tamoxifen administration is highly efficient. After validation of the recombination efficiency of both *Shoc2$^{fl/fl}$ Rosa26-CreER^{T2}* KO and KI mouse models, we have monitored those experimental mice for the development of macroscopic phenotypes with the aim to address Shoc2's function in normal tissue homeostasis in adult mice.

Survival analysis of Shoc2 KO and KI mice

To determine the role of Shoc2 in homeostasis, *Shoc2$^{fl/fl}$ Rosa26-CreER^{T2}* KO and KI mice were monitored for macroscopic phenotypic changes upon aging for up to 35 weeks after tamoxifen treatment. *Shoc2$^{+/+}$ Rosa26-CreER^{T2}* littermate mice (WT) and *Shoc2$^{fl/fl}$ cKI Rosa26-CreER^{T2}* mice that had not been treated with tamoxifen (NT) were used as control.

Homozygous Shoc2 KO mice began to show signs of malaise ~4-5 weeks post-tamoxifen treatment, with ruffled coats and patchy alopecia especially around the eyes (periocular alopecia) and on the throat areas which exacerbated over time (Figure 4-1A). They also developed skin lesions (Figure 4-1A) that progressed in severity over time and that will be discussed in detail in the following chapter. Some male KO animals, but interesting not females, also developed enlarged abdominal area (Figure 4-1C).

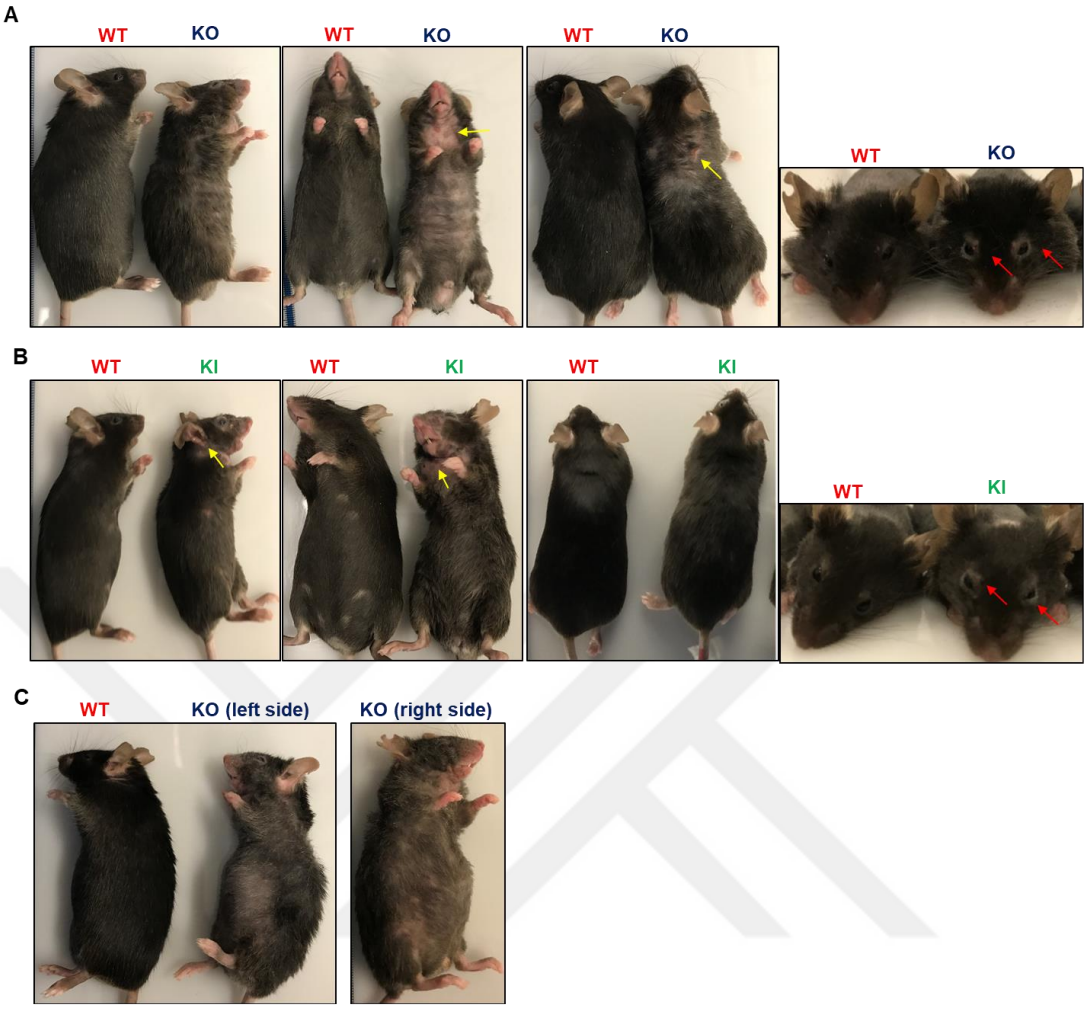

Figure 4-1. Shoc2 KO and KI mice develop ruffled coats and skin lesions

A. Representative images of littermate mice with (KO) or without (WT) Shoc2 inactivation at 13 weeks post-tamoxifen treatment to illustrate signs of poor body condition. WT mice have thick, shiny and black fur in the flanks, dorsal and ventral areas. In contrast, Shoc2 KO mice have sparse and scruffy coats and trunk hair turned greyish. Yellow arrows indicate skin lesions and red arrow heads show periocular alopecia.
B. Representative images of Shoc2 KI and WT mice at 20 weeks post-tamoxifen treatment as in (A).
C. Representative images of Shoc2 KO male mice at 17 weeks post-tamoxifen treatment to show enlarged abdominal area.

As these phenotypes worsened with time, Shoc2 KO mice had to be euthanized because of severe skin dermatitis, weight loss exceeding 15% of total body weight or due to a swollen abdominal area (males only) (Figure 4-2A), with the earliest at 9 weeks and the latest at 21 weeks post-tamoxifen treatment. Shoc2 KO heterozygous did not show any phenotype and were indistinguishable from wild type animals in terms of overt phenotypes or survival.

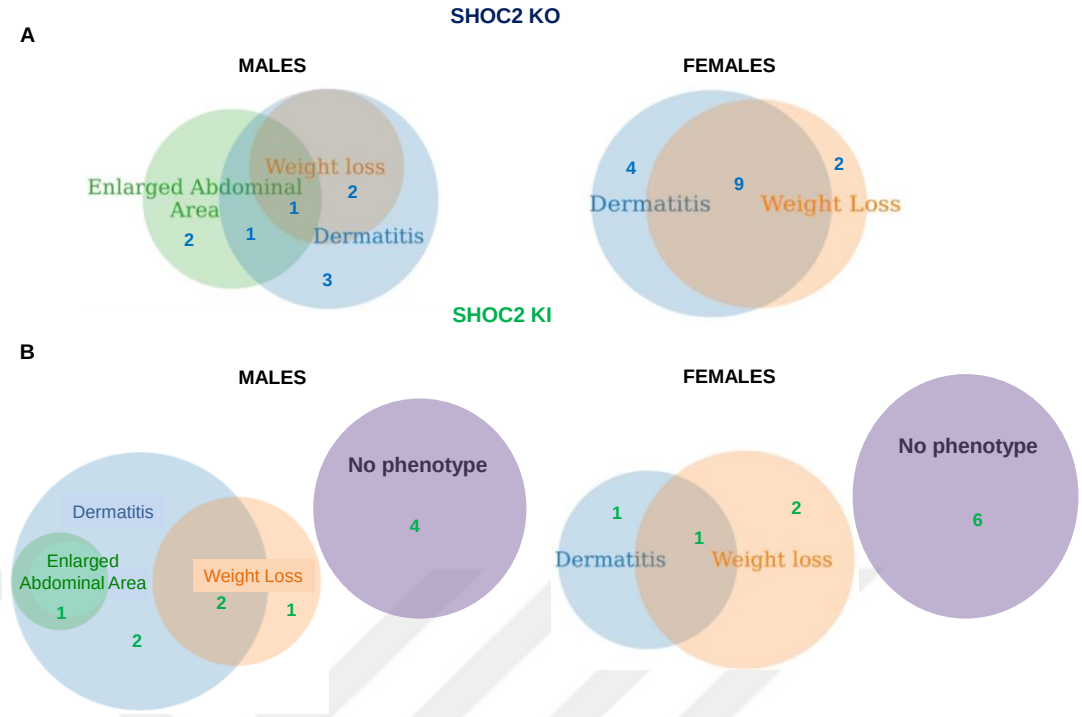

Figure 4-2. Cause of death in male and female Shoc2 KO and KI mice

A. Proportional Venn diagram for cause of death in Shoc2 KO males (n=9) and females (n=15). Venn Diagram drawn using Meta-Chart Venn Diagram Maker (https://www.meta-chart.com/venn#/display).
B. Proportional Venn diagram for cause of death in Shoc2 KI males (n=6) and females (n=4) as in (A). High number of censored subjects were not included the diagram for Shoc2 KI male (n=4) and female (n=6) mice as no obvious maladies were seen in their life span.

Kaplan-Meier survival curves showed the median lifespan of Shoc2 KO homozygous mice to be 15 weeks post-tamoxifen treatment (Figure 4-3A). When results were analysed based on gender, female KO mice had a small but significant decrease in median survival compared to KO males (13 and 17 weeks, respectively) (Figure 4-3B).

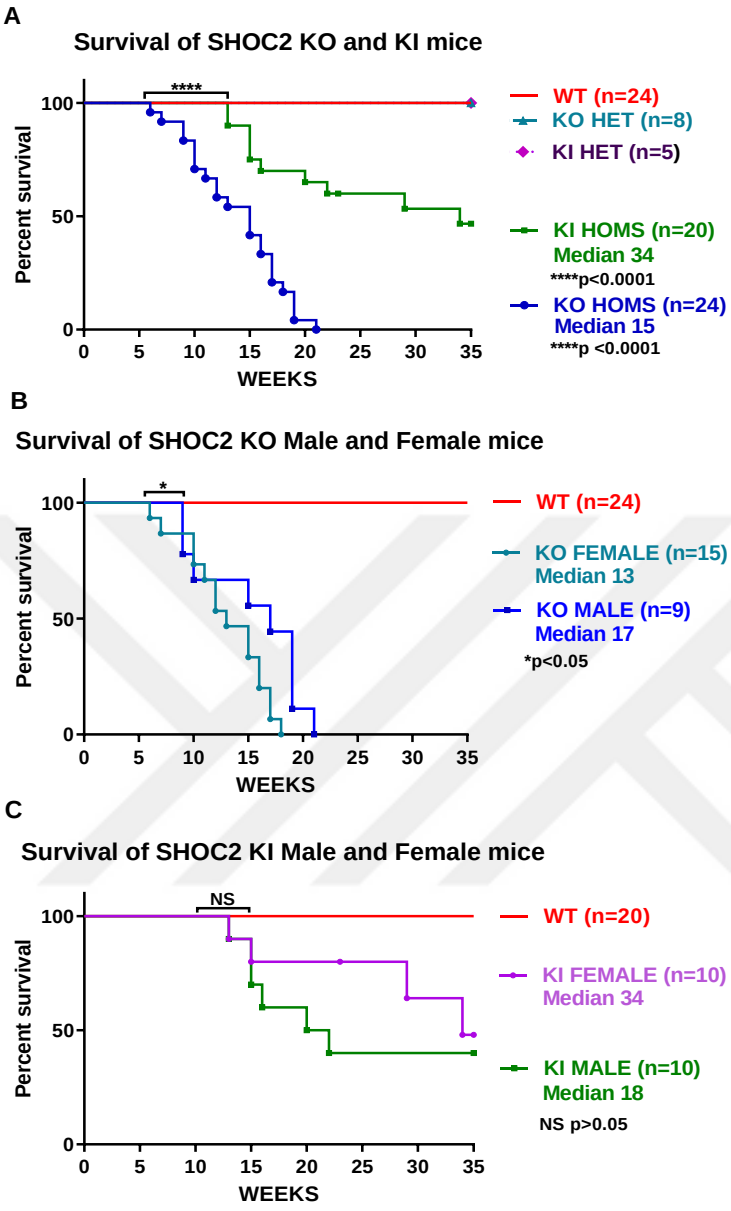

Figure 4-3. Kaplan-Meier survival curves of Shoc2 KO and KI mice

A. The survival rate of the Shoc2 KO HOM (n=24) and Shoc2 KI HOM (n=20) mice was significantly lower than that of the WT (n=24) controls or HET (n=8 or n=5) mice.
B. Breakdown by gender for Shoc2 KO HOM mice: males (n=9) and females (n=15).
C. Breakdown by gender for Shoc2 KI HOM mice: males (n=10) and females (n=10).Significance is determined using the Kaplan-Meier log rank test ****p<0.0001, *p<0.05. NS: Not Significant.

Shoc2 KI homozygous mice show extended survival compared to their KO counterparts although they did have significantly decreased survival compared to WT or heterozygous KI littermate mice (median survival of 34 weeks, Figure 4-3A). No differences in survival by gender within Shoc2 KI mice were apparent (Figure 4-3C). Some mice developed skin lesions that appeared at later time points and progressed in severity more slowly compared KO mice (Figure 4-1B) and had to be euthanized because of this and/or weight loss exceeding 15% (Figure 4-2B). However, a significant number mice (n=10) were still alive without overt phenotypes, except for periocular alopecia, after 35 weeks post-tamoxifen treatment (Figure 4-2B). Thus, inactivation of Shoc2 in the KI model by expression of a point mutant that selectively

disrupts the ability of Shoc2 to form a phosphatase complex with MRAS and PP1, leads to a milder and less penetrant phenotype that complete loss of Shoc2 protein using the KO model.

Blood chemistry analysis of Shoc2 mice

Serum biochemical assessment helps to predict pathological processes in vital internal organs of the body such as the liver, muscle, heart, pancreas and kidney (Stockham and Scott, 2013). In order to shed light on any alterations caused by systemic Shoc2 deletion on metabolism and organ functions, blood of WT or KO mice was collected by cardiac puncture at morbidity (mean survival of 15 weeks) and biochemical parameters in serum analysed. The blood test on the biochemistry profile included a series of biomarkers for liver function such as aspartate aminotransferase (AST), alanine aminotransferase (ALT), alkaline phosphatase (ALP) and bilirubin; triglycerides, free fatty acids, glycerol, low-density lipoprotein (LDL), high-density lipoprotein (HDL) and total cholesterol for lipid levels, urea, creatinine and creatine kinase (CK) for kidney functions, sodium, potassium, calcium, chloride, inorganic phosphorus, magnesium and iron for electrolytes as well as glucose, fructose, total protein and albumin as additional metabolic markers.

Most of the serum chemistry parameters were unaffected suggesting Shoc2 inactivation does not cause major and/or clear alterations in liver or kidney function (Table 4.1). However, albumin, total cholesterol, HDL, glucose, fructose and ALP levels were significantly decreased in Shoc2 KO mice compared to wild type controls (Figure 4-4). While the significance of these changes is unclear, they are consistent with the weight loss that was observed in the Shoc2 KO mice at the time of analysis and thus may be the reflection of weight loss caused by other abnormalities (see later) i.e. consequence rather than cause.

Table 4-1. Serum Biochemical Analysis

Measured parameter	WT (n=11)	Shoc2 KO (n=11)	p-value
Sodium (mmol/l)	158,27±13,99	156,91±1,45	NS
Potassium (mmol/l)	4,52±0,26	4,76±0,48	NS
Chloride (mmol/l)	119,09±10,52	117,45±0,99	NS
Urea (mmol/l)	10,27±1,71	10,17±0,80	NS
Creatinine (µmol/l)	11,15±0,87	11,37±0,92	NS
Calcium (mmol/l)	2,46±0,25	2,40±0,06	NS
Inorganic Phosphorus (mmol/l)	2,13±0,22	2,73±0,24	NS
ALP (U/l)	85,91±10,10	50,09±5,47	0,0054
ALT (U/l)	39,00±4,51	43,64±12,79	NS
AST (U/l)	147,27±33,95	145,00±33,67	NS
Total Protein (g/l)	49,77±0,90	51,12±1,42	NS
Albumin (g/l)	25,89±0,52	17,06±0,66	<0,0001
Total Cholesterol (mmol/l)	2,57±0,18	1,59±0,11	0,0002
HDL (mmol/l)	1,79±0,14	0,93±0,05	<0,0001
LDL (mmol/l)	0,74±0,07	0,70±0,08	NS
Glucose (mmol/l)	19,19±1,55	12,68±1,62	0,0088
Triglycerides (mmol/l)	1,22±0,14	1,0±0,14	NS
Glycerol (µmol/l)	285,10±25,73	228,78±25,22	NS
Free Fatty Acids (mmol/l)	0,59±0,05	0,48±0,05	NS
Total Billirubin (µmol/l)	2,05±0,27	1,64±0,36	NS
LDH (U/l)	630,64±154,17	823,00±184,78	NS
Iron (µmol/l)	21,45±1,26	22,03±3,91	NS
Amylase (U/l)	644,00±36,63	486,09±81,73	NS
CK (U/l)	960,45±541,46	196,00±55,15	NS
Fructose (µmol/l)	209,55±6,58	131,78±106,50	<0,0001
Magnesium (mmol/l)	1,03±0,04	1,04±0,07	NS

ALP, alkaline phosphatase; ALT, alanine aminotransferase; AST, aspartate aminotransferase; HDL, high-density lipoprotein; LDL, low-density lipoprotein; LDH, lactate dehydrogenase; CK, creatine kinase. Blood from WT (n=11) and KO (n=11) mice is collected at morbidity (mean survival of 15 weeks). Data are presented as mean values ± SEM. Significance is determined using an unpaired student's t-test. NS=p>0.05.

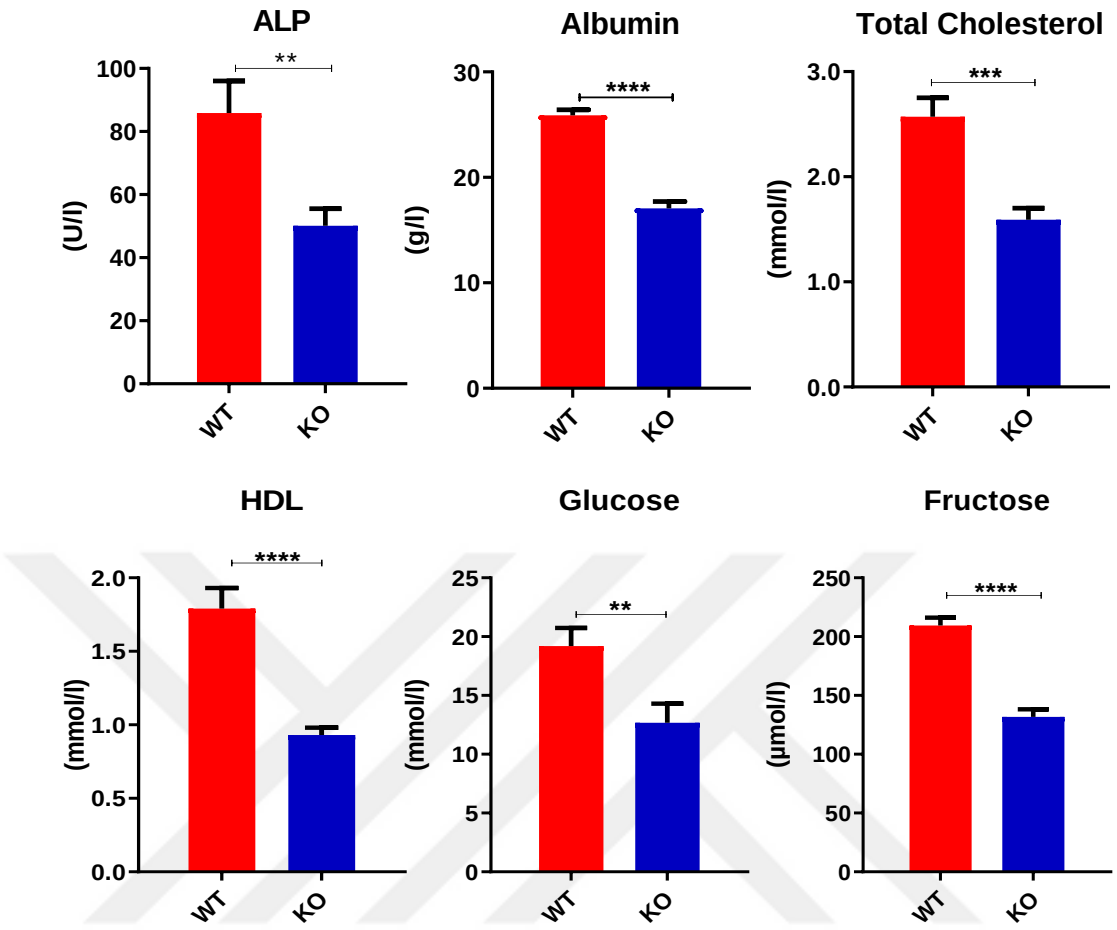

Figure 4-4. Decreased serum chemistry values in Shoc2 KO mice

Significant decrease was observed in ALP, albumin, total cholesterol, HDL, glucose and fructose levels. Blood from WT (n=11) and KO (n=11) mice is collected at morbidity (mean survival of 15 weeks). Data are presented as mean values ± SEM. Significance is determined using an unpaired student's t-test **p<0.01, ***p<0.001 or ****p< 0.0001 (n=11 for each genotype).

Histopathology of Shoc2 KO and KI mice

As mentioned in Chapter 3, Shoc2 KO and KI mice developed skin lesions starting at ~4 weeks post-tamoxifen treatment that progressively increased in severity and were the main cause of euthanasia. This include alopecia around the eyes and throat areas, and skin lesions on the back, head (face), throat, and flanks of the mice (Figure 4-5A). Lesions varied in severity and included punctuated small crusts, coalescent crusts, and ulceration (Figure 4-5B). To characterize and quantify the severity of the dermatitis upon Shoc2 inactivation, a clinical skin dermatitis severity scoring system that is described in detail in the Methods section (Table 2-5) was

used (Figure 4-5C). This scoring system shows that skin lesions in KI mice are considerably less severe than in KO mice. Notably, the overall disease score was significantly higher in male compared to female mice in KO but not in KI model (Figure 4-5D). Shoc2 KO mice also developed pruritus and displayed consistent and severe scratching of their throat areas (Figure 4-5E). Considering that all the skin regions affected are accessible anatomical regions and thus prone to scratching, this observation suggests that pruritus and scratching is an important factor in the initiation and/or progression of skin lesions in Shoc2 KO mice. A detailed histological characterization of the skin will be covered in Chapter 5.

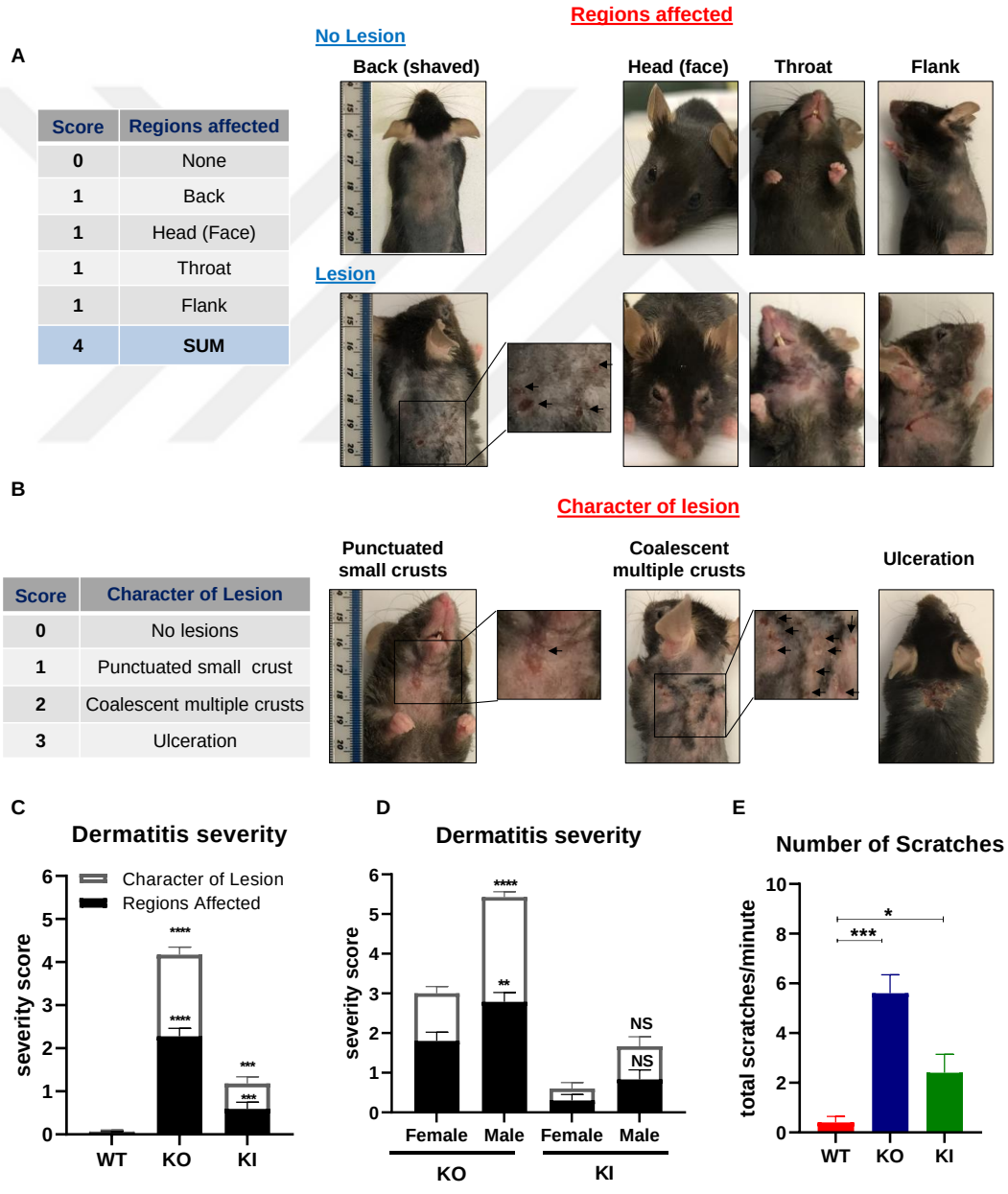

Figure 4-5. Shoc2 inactivation in adult mice leads to skin dermatitis with pruritus

A. Dermatitis severity scoring system for affected regions (left) and representative images of mice to illustrate locations of skin lesions (right). Inset shows higher magnification of indicated area and arrows indicate skin lesions.
B. Dermatitis severity scoring system for character of lesion (left) and representative images (right). Insets show higher magnification of indicated areas and arrows show skin lesions.
C. Severity score of dermatitis was assessed at morbidity in mice of the indicated genotypes (~15 weeks Post-Tam. for Shoc2 KO, n=24; ~34 weeks Post-Tam for Shoc2 KI, n=20). Data are presented as mean values ± SEM. Significance is determined using an unpaired student's t-test ***p<0.001 or ****p< 0.0001.
D. Severity score by gender at morbidity as in (C). Shoc2 KO: Females (n=15) and Males (n=9); Shoc2 KI: Females (n=10) and Males (n=10). Data are presented as mean values ± SEM. Significance is determined using an unpaired student's t-test. **p<0.01, ****p< 0.0001 or NS: Not Significant.
E. Spontaneous scratching was counted in mice at 6 weeks post-tamoxifen treatment for 2 min (n=5 for each genotype). Data are presented as mean values ± SEM. Significance is determined using an unpaired student's t-test *p<0.05 or ***p<0.001.

To identify possible additional pathological conditions, organs of Shoc2 KO and KI mice were examined histologically at morbidity. No obvious macroscopic and microscopic abnormalities were observed in skeletal muscle, colon, lung, liver, heart, pancreas and thymus from Shoc2 KO (Figure 4-6A) and KI (Figure 4-6B) male or female mice, that were undistinguishable from organs of WT animals.

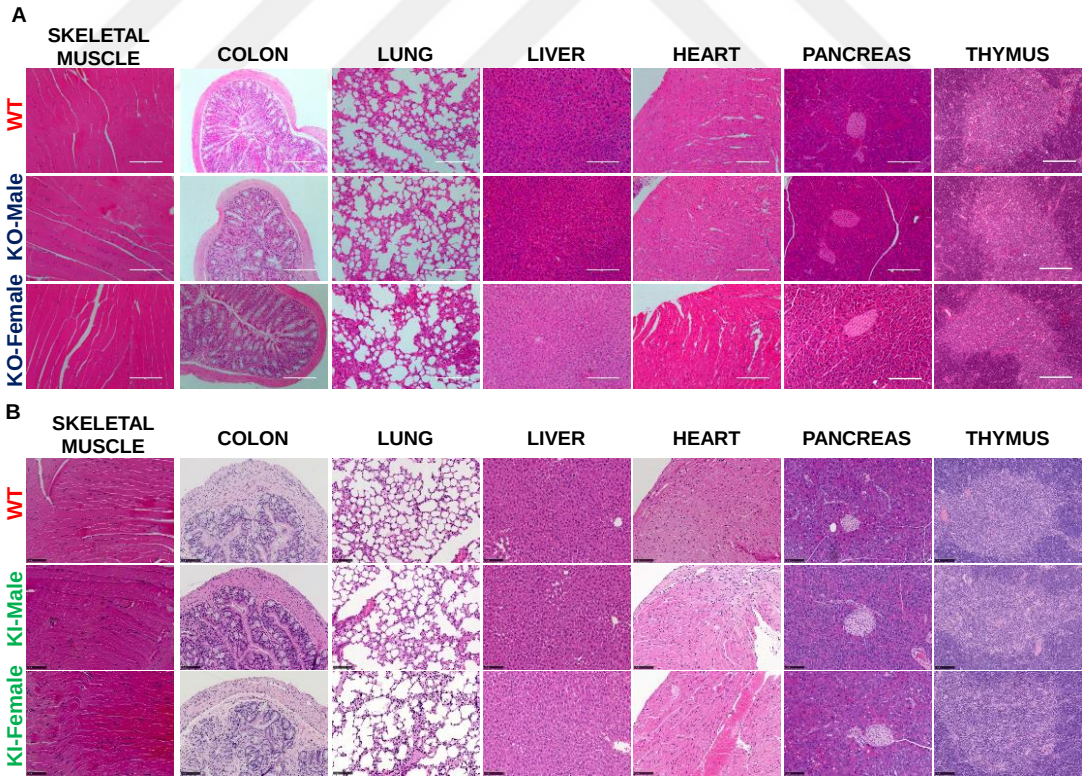

Figure 4-6. Major organs from Shoc2 KO and KI mice with no difference by histological analysis relative to wild type controls

A. Representative H&E stained sections were generated from the indicated organs of Shoc2 KO and WT mice (n=4 for each genotype). Scale bar=200 µm.
B. Representative H&E stained sections of Shoc2 KI and WT mice as in (A) (n=4 for each genotype). Scale bar=100 µm.

On the other hand, post-mortem studies revealed that Shoc2 KO and KI mice have enlarged secondary lymphoid organs, namely spleen (Figure 4-7A and B) and lymph nodes. Splenomegaly was most dramatic in KO mice but also significant in KI mice. No significant difference was observed between the spleen weights of WT and Shoc2 KO/KI heterozygous mice. In contrast to skin severity, no difference in splenomegaly by gender was detected, as both sexes in KO and KI homozygous mice had similarly enlarged spleens (Figure 4-7C). Despite the striking increase in spleen size, H&E staining revealed no obvious histological abnormalities (Figure 4-7D).

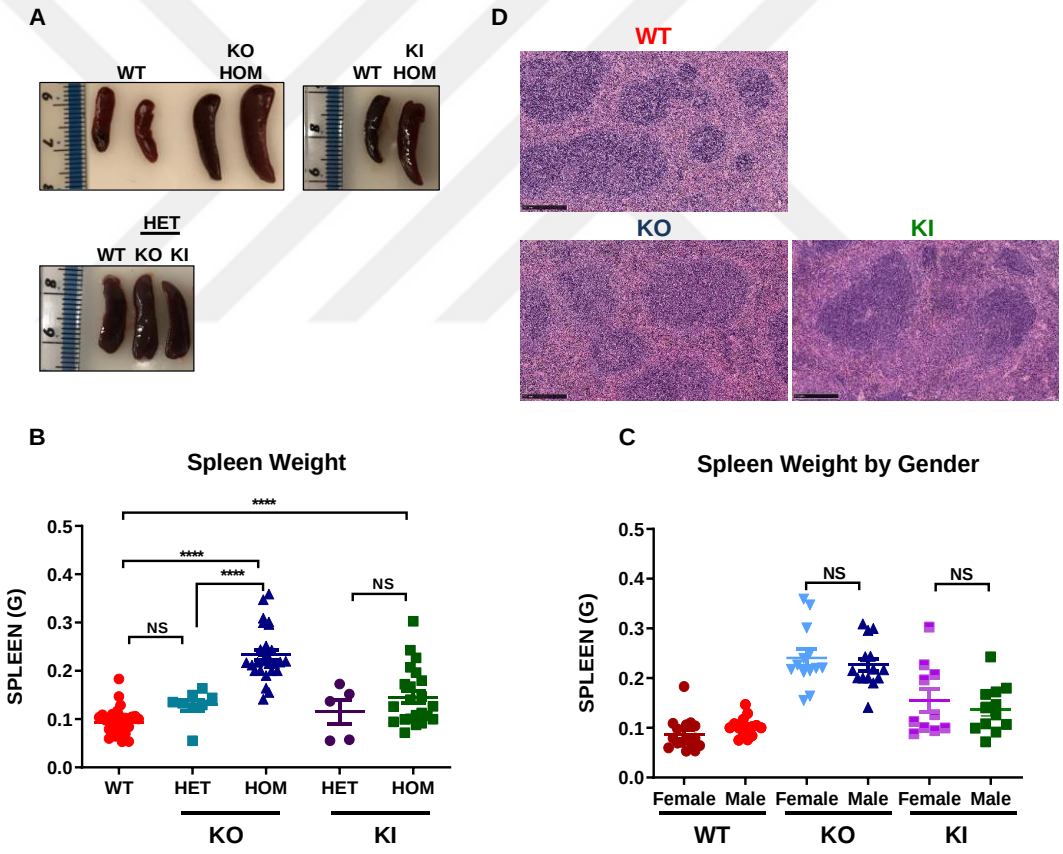

Figure 4-7. Shoc2 KO and KI mice develop splenomegaly

A. Representative images of spleens from WT, Shoc2 KO/KI homozygous (HOM) and heterozygous (HET) mice to illustrate splenomegaly.
B. Quantification of Shoc2 KO/KI HOM and Shoc2 HET spleen weights compared to that of WT mice. WT (n=31), Shoc2 KO HET (n=8), Shoc2 KO HOM (n=27), Shoc2 KI HET (n=5) and Shoc2 KI HOM (n=22). Data are presented as mean values ± SEM. Significance is determined using an unpaired student's t-test ****p<0.0001 or NS: Not Significant.

C. Quantification of spleen weight by gender as in (B). Females: WT (n=16), Shoc2 KO (n=13) and Shoc2 KI (n=10). Males: WT (n=15), Shoc2 KO (n=14), and Shoc2 KI (n=12). Data are presented as mean values ± SEM. Significance is determined using an unpaired student's t-test NS: Not Significant.
D. Representative H&E staining of Shoc2 KO, KI and WT mice spleen sections (n=4 for each genotype). Scale bar=250 μm.

In addition to spleen, Shoc2 KO and KI mice also had enlarged lymph nodes upon necropsy at morbidity compared with their control counterparts (Figure 4-8A and B). Inguinal lymph nodes weight increased to almost three fold in Shoc2 KO mice and two fold in KI mice compared to WT mice (Figure 4-8C). A similar pattern was observed for submandibular lymph nodes of Shoc2 KO mice (Figure 4-8D). Quantification of the submandibular lymph nodes also revealed a statistically significant increase in the total area by measuring overall lymph node area using ImageJ (Figure 4-8E). Despite, severely inflamed submandibular lymph nodes in some Shoc2 KO mice, H&E staining of salivary glands revealed no obvious histological abnormalities in sublingual, submandibular or parotid glands (Figure 4-8F).

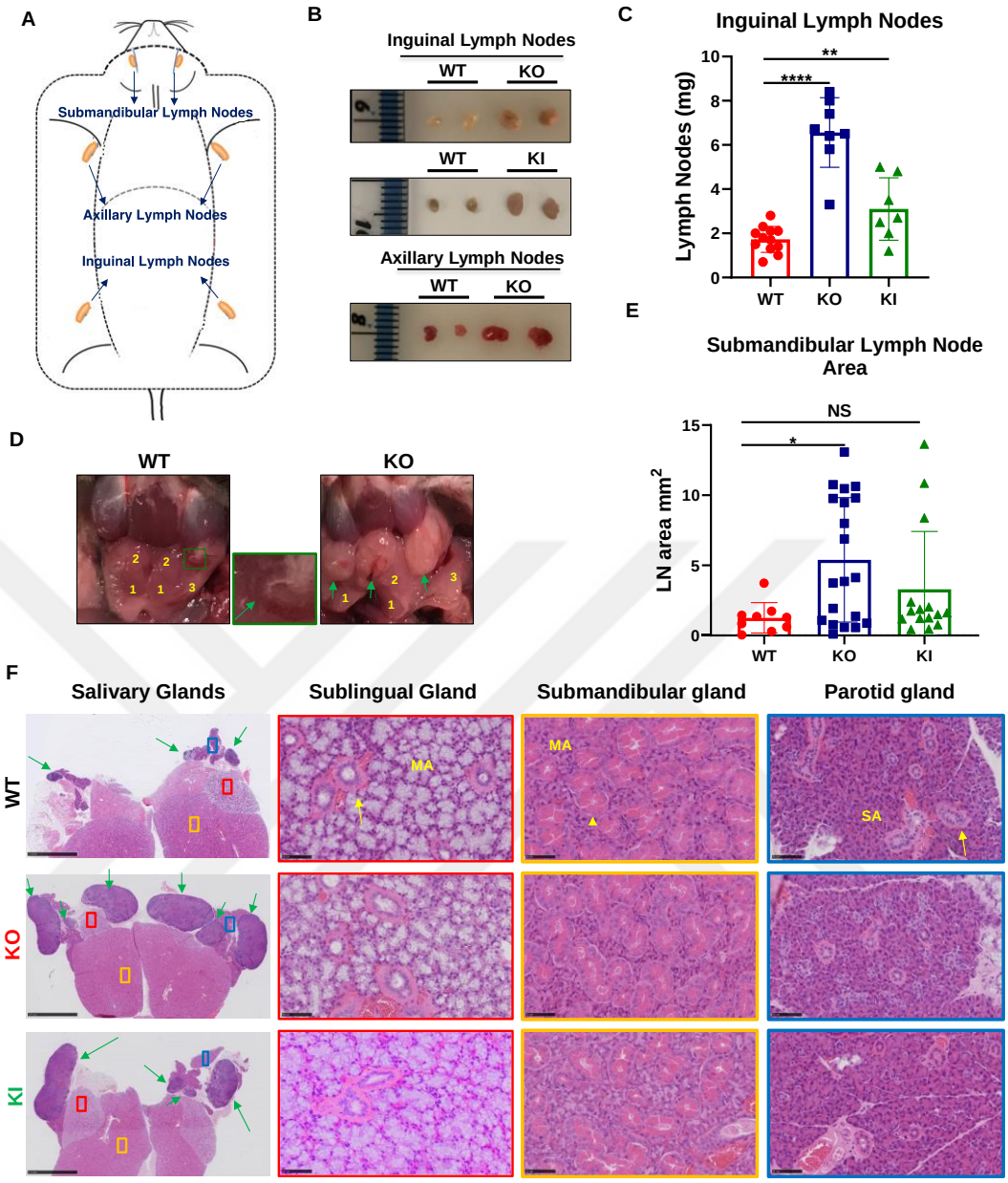

Figure 4-8. Shoc2 KO and KI mice exhibit lymphadenopathy

A. Diagram to illustrate dissected lymph nodes.
B. Representative images of inguinal and axillary lymph nodes from mice with the indicated genotypes at morbidity.
C. Quantification of enlarged inguinal lymph nodes from Shoc2 KO (n=4) and KI (n=4) mice (WT: n=6 mice). Data are presented as means ± SEM. Significance is determined using an unpaired student's t-test **p<0.01 or ****p<0.0001.
D. Representative images of submandibular lymph nodes and salivary glands from WT and Shoc2 KO mice. Arrows indicates lymph nodes and inset shows higher magnification image of lymph node from WT mouse. Salivary glands: 1 indicates submandibular glands, 2 indicates sublingual glands and 3 indicates parotid gland.
E. Quantification of submandibular lymph nodes from Shoc2 KO (n=5), KI (n=4) and WT (n=4) mice. Data are presented as mean values ± SEM. Significance is determined using an unpaired student's t-test *p<0.05 or NS: Not Significant. 2-6 submandibular lymph nodes were analysed per mouse.

F. Representative H&E sections of submandibular lymph nodes and salivary glands from WT, KO and KI mice (n=4 mice per genotype). Green arrows indicate lymph nodes, red, orange and blue squares represent higher magnification of indicated areas in salivary glands. Yellow arrows indicate excretory ducts, arrowhead indicates secretory granular ducts, MA represents mucous acini and SA represents serous acini. Scale bar=2.5 mm. Insets show the higher magnification of indicated areas. Scale bar=50 µm.

Immunophenotyping of spleen and lymph nodes

In order to characterize the immune cell sub-populations in the enlarged spleen of Shoc2 KO mice, single cell preparations of spleens were generated from mice at morbidity and analysed by flow cytometry with a panel of antibodies that allowed to distinguish lymphoid and myeloid compartments (Figure 4-9A and B). A significant accumulation of granulocytes ($CD11b^+/Ly6G^+$) and inflammatory macrophages ($CD11b^+/Ly6C^+/CD68^+$) were observed in the spleen of Shoc2 KO mice at morbidity. In contrast, a significant decrease in the effector ($CD3^+/CD4^+/FOXP3^-$) and cytotoxic ($CD3^+/CD8^+$) T cells and B cells ($CD19^+/MHC\text{-}II^+$) was observed in Shoc2 KO spleens (Figure 4-9C).

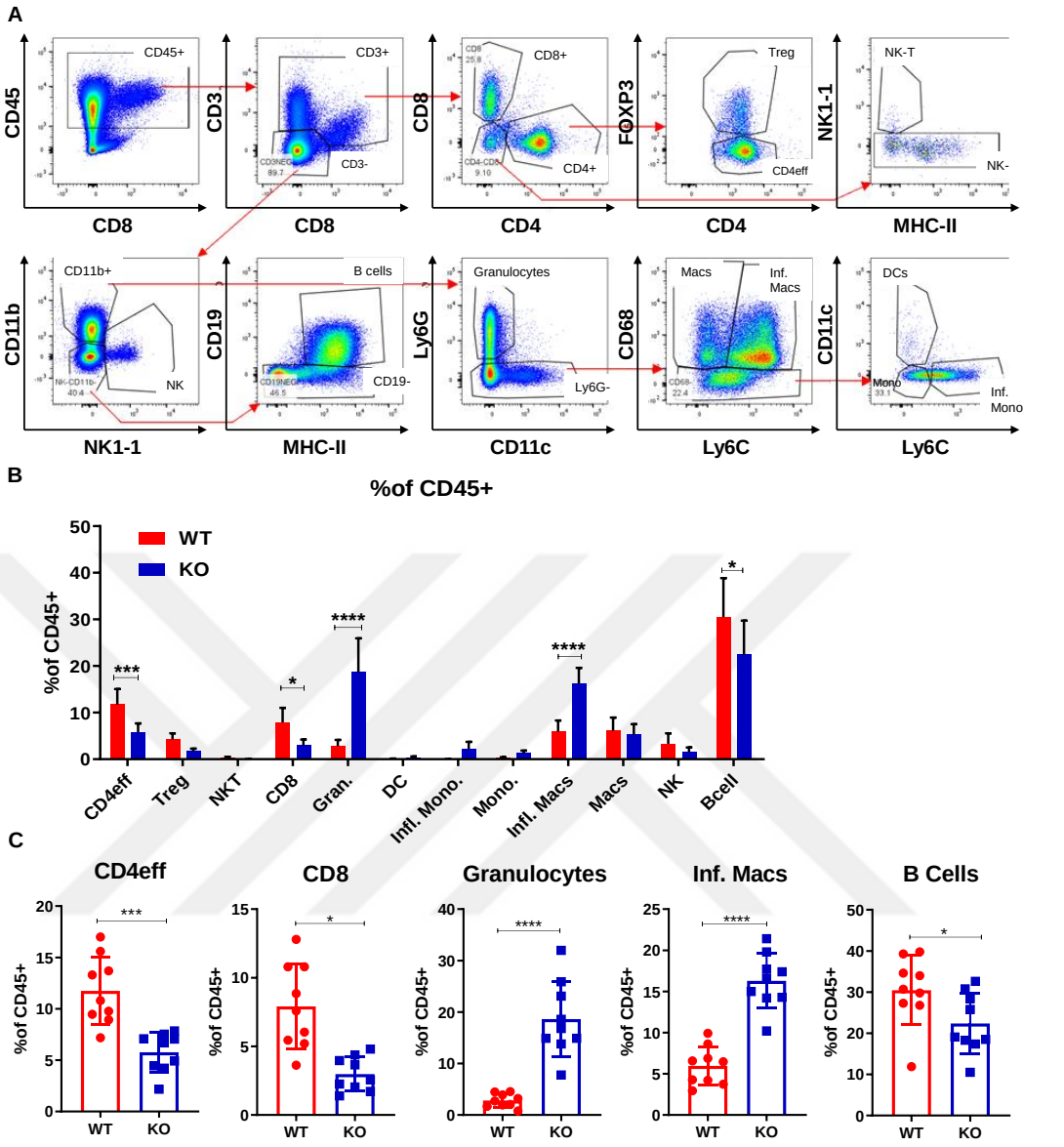

Figure 4-9. Shoc2 deletion leads to expansion of the myeloid compartment including inflammatory macrophages and granulocytes in the spleen

A. The representative gating strategy for Shoc2 KO and WT spleens.
B. Quantification of immune cell types as a percentage of CD45$^+$ cells of Shoc2 KO and WT spleens (n=9 for each genotype). Data are presented as mean values ± SEM. Significance is determined using an unpaired student's t-test. *p< 0.05, ***p< 0.001 or ****p< 0.0001. CD4eff: CD4$^+$ Effector cells (CD3$^+$/CD4$^+$/FOXP3$^-$), Treg: Regulatory T cells (CD3$^+$/CD4$^+$/FOXP3$^+$), NKT: Natural Killer T cells (CD3$^+$/CD4$^-$/CD8$^-$/NK1.1$^+$), Gran: Granulocytes (CD11b$^+$/Ly6G$^+$), DC: Dendritic cells (CD68$^-$/CD11c$^+$), Mono.: Monocytes (CD11b$^+$/Ly6G$^-$/ CD11c$^-$/Ly6C$^{lo/-}$), Infl. Mono.: Inflammatory monocytes (CD11b$^+$/Ly6G$^-$/CD11c$^-$/Ly6C^{hi}), Macs:Macrophages (CD11b$^+$/Ly6G$^-$/ CD68$^+$/Ly6C$^{lo/-}$) Infl. Macs.: Inflammatory macrophages (CD11b$^+$/Ly6G$^-$/ CD68$^+$/Ly6C$^+$).
C. Quantification of significant immune cell types as a percentage of CD45$^+$ cells of Shoc2 KO and WT spleens (n=9 for each genotype). Data are presented as means ± SEM. Significance is determined using an unpaired student's t-test. *p< 0.05, ***p< 0.001 or ****p< 0.0001. This figure was generated with the help of Jake Henry from Sergio Quezada lab.

For further validation, we performed immunohistochemistry staining of Shoc2 KO and WT spleens and observed that KO spleens had an increased granulocyte (GR-1$^+$) and macrophage (F4/80$^+$) infiltration but slightly fewer T (CD3$^+$) and B cells (B220$^+$) consistent with observation obtained by flow cytometry (Figure 4-10).

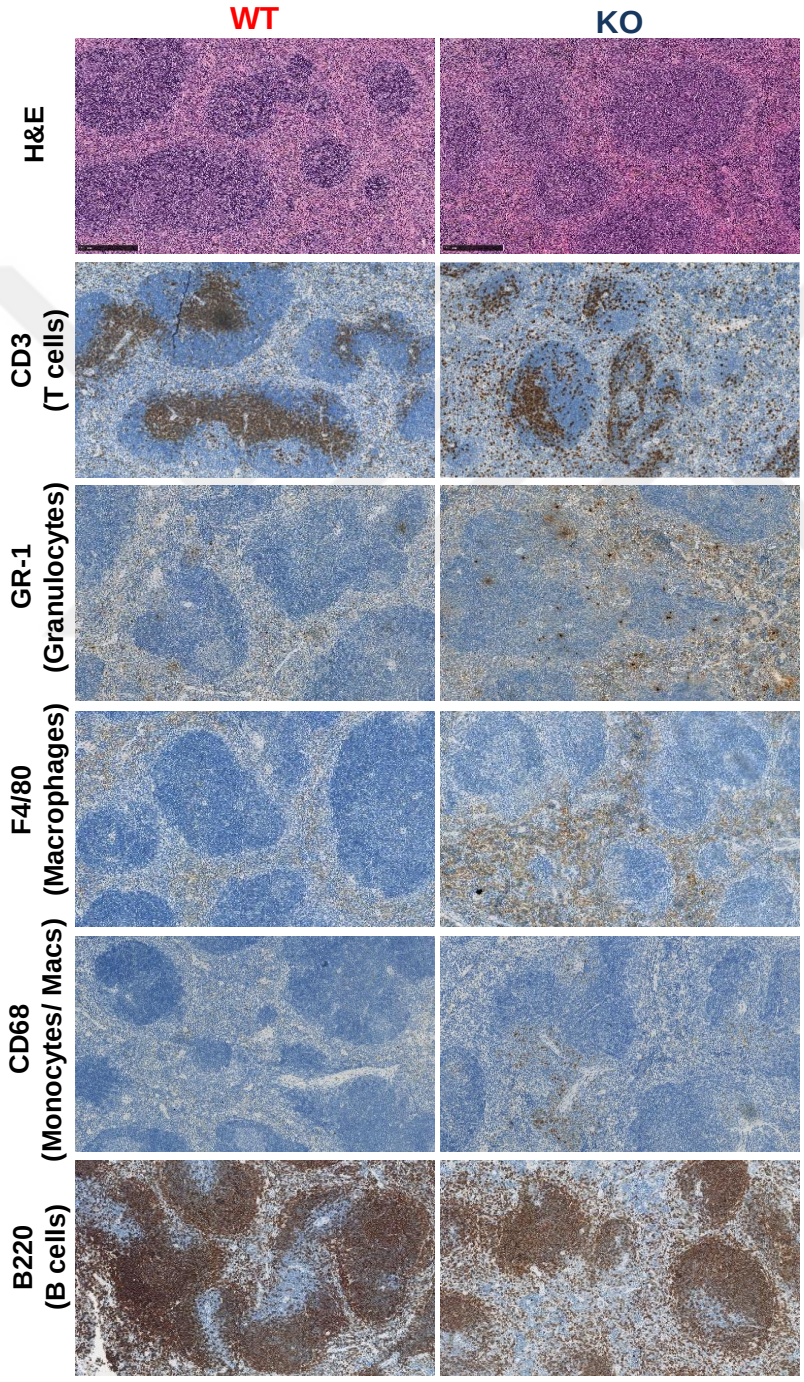

Figure 4-10. IHC analysis confirms the increase in granulocytes and macrophages in the spleen section of Shoc2 KO mice

Representative immunohistochemical staining of Shoc2 KO and WT mice spleen sections with the indicated antibodies. Positive immunoreactivity is indicated by the brown color, with a blue hematoxylin counterstain (n=3 for each genotype, at morbidity). Scale bar=250 μm. This figure was generated with the help of Ayse Akarca from Teresa Marafioti lab.

The expansion of myeloid compartment in the spleen may alter circulating white blood cells (WBC) in the blood. To determine the effect of Shoc2 in blood,

Wright-Giemsa staining was applied onto air dried blood of Shoc2 KO and KI mice compared to age- and sex-matched WT controls (8 weeks Post-Tam.). Increased number of WBCs was observed in the blood smears of Shoc2 KO and KI mice (Figure 4-11).

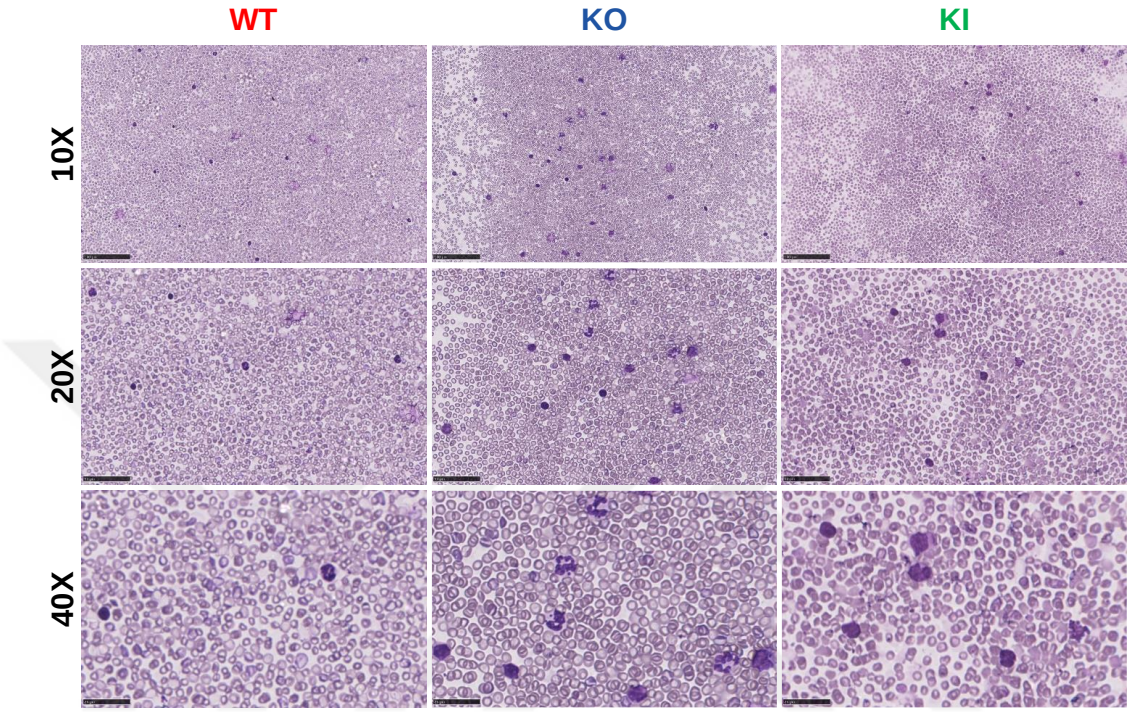

Figure 4-11. Whole blood analysis confirms alterations in the immune appearance of Shoc2 KO mice.

A. Representative Wright-Giemsa stained peripheral blood smear of Shoc2 KO, KI and WT mice (8 weeks Post-Tam, n=6 for each genotype). Scale bar 10x=250 μm, 20x= 100 μm, 40x= 50 μm.

The previous experiment was performed on spleen samples collected from KO mice at morbidity (15 weeks post-tamoxifen treatment). Next, we performed an experiment to compare immune populations in spleens, lymph nodes and bone marrow from KO and KI mice at an earlier and fixed endpoint of 8 weeks post-tamoxifen. A slightly different gating strategy was used (Figure 4-12).

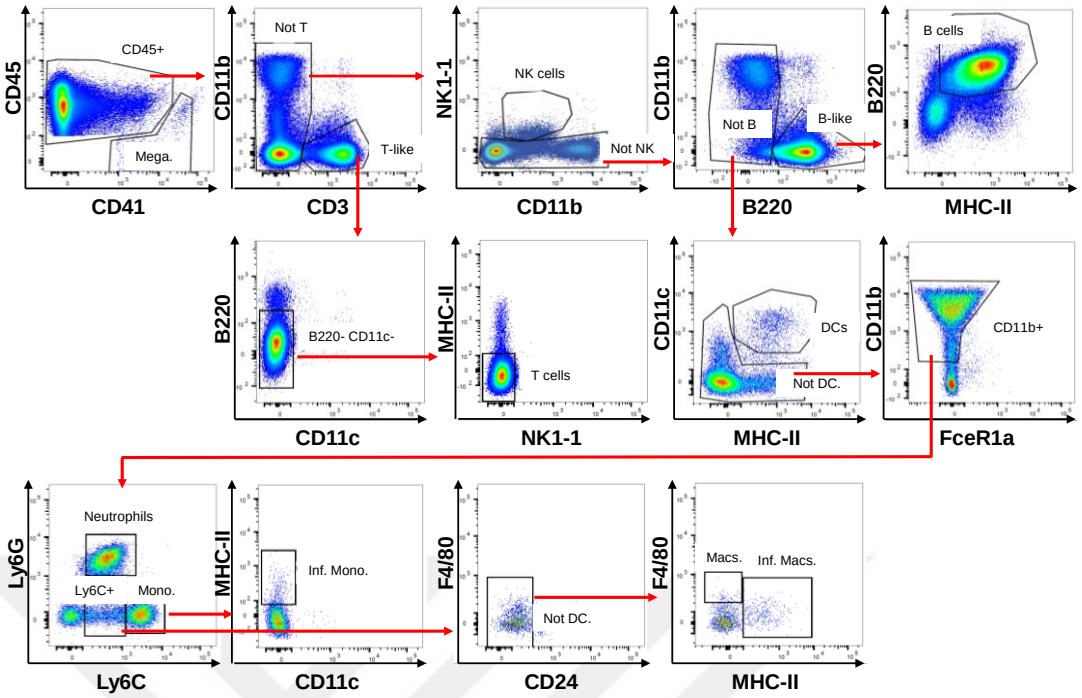

Figure 4-12. Gating strategy for flow cytometry analysis of spleen and lymph nodes of Shoc2 KO and KI mice

Immune cell subtypes characterization strategy by flow cytometry. Mega: Megakaryocytes, NK: Natural Killer cells, DC: Dendritic cells, Infl. Mono.: Inflammatory monocytes, Infl. Macs.: Inflammatory macrophages. This figure was generated with the help of Cristobal Costoya from Sergio Quezada lab.

In line with the previous results, flow cytometric analysis revealed an increase in neutrophils ($CD11b^{+}/Ly6G^{hi}/Ly6C^{lo}$), inflammatory monocytes ($CD11b^{+}/Ly6C^{hi}/MHC\text{-}II^{+}$) and inflammatory macrophages ($CD11b^{+}/F4/80^{+}/MHC\text{-}II^{+}$) whereas there were reduced T ($CD3^{+}$) and B ($B220^{+}$) cell proportions in Shoc2 KO spleens. No differences were reported in the other cellular populations analysed, such as monocytes ($CD11b^{+}/Ly6C^{hi}$), macrophages ($CD11b^{+}/Ly6C^{lo}/F4/80^{+}$), dendritic cells ($CD11c^{+}/MHC\text{-}II^{+}$) and natural killer cells ($CD3^{-}/NK1.1^{+}$) (Figure 4-13A). An increase in neutrophils, inflammatory macrophages and inflammatory monocytes was also detected in the lymph nodes of the same mice (Figure 4-13B). Interestingly, although the numbers did not achieve significance, a clear tendency for increased numbers of neutrophils, inflammatory macrophages and inflammatory monocytes could be observed in KI mice, consistent with a milder and/or slower response in the KI model (Figure 4-13A).

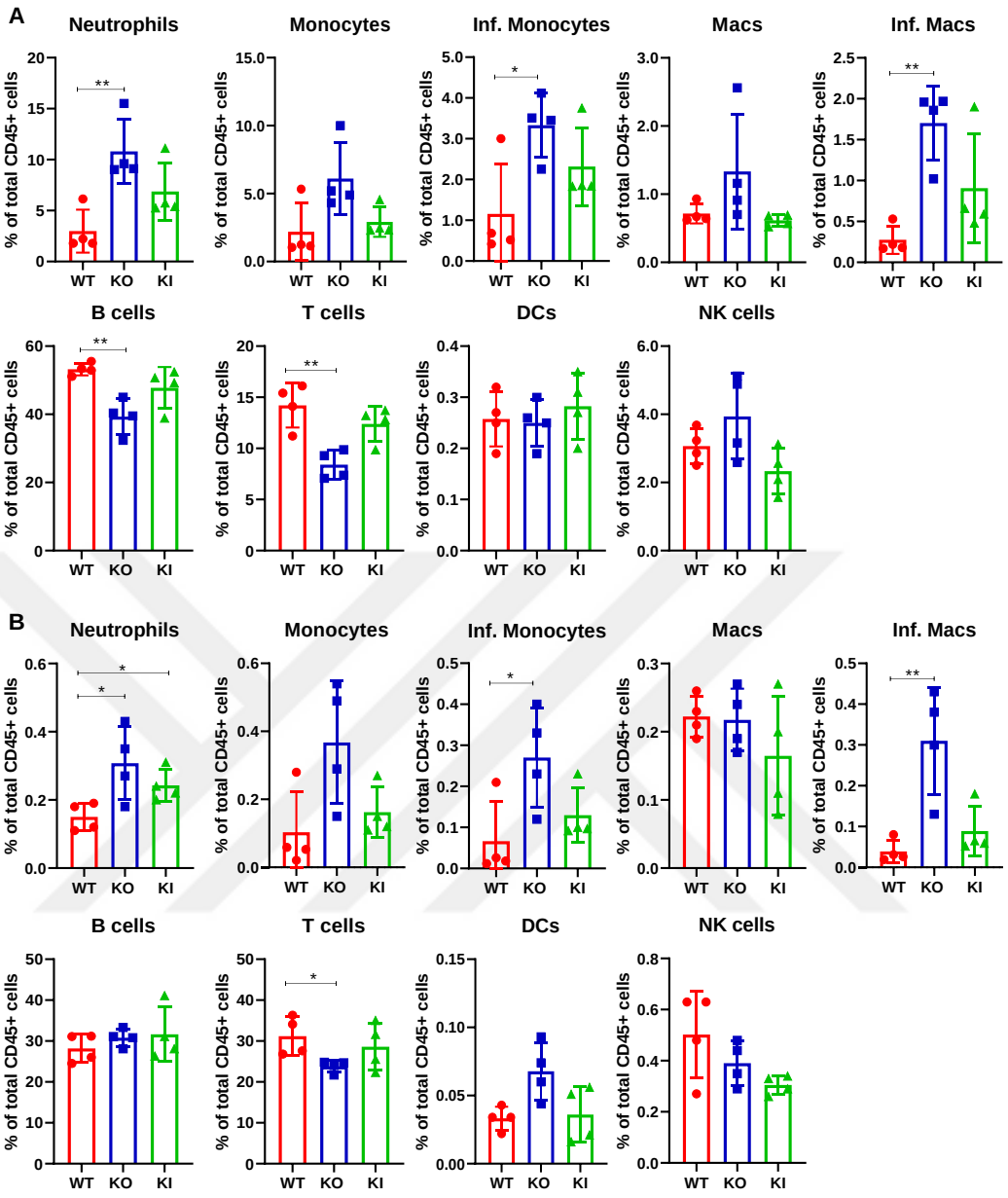

Figure 4-13. Shoc2 inactivation leads to expansion of the myeloid compartment in the spleen and lymph nodes of Shoc2 KO mice

A. Quantification of immune cell types as a percentage of CD45⁺ cells in spleen of Shoc2 KO, KI and WT mice (n=4 for each genotype). Data are presented as mean values ± SEM. Significance is determined using an unpaired student's t-test. *p< 0.05 or **p< 0.01. NK cells: Natural killer cells, DC: Dendritic cells, Infl. Mono.: Inflammatory monocytes, Infl. Macs.: Inflammatory macrophages.

B. As above (A) but using pooled inguinal, axillary and brachial lymph nodes from the same mice as in A. This figure was generated with the help of Cristobal Costoya from Sergio Quezada lab.

Role of Shoc2 in haematopoiesis

Considering the known role of the RAS-MAPK pathway in proliferation and differentiation, the systemic increase (seen in spleen, blood and lymph nodes) of cell types of the myeloid lineage (particularly neutrophils) that is observed upon Shoc2 ablation, could be related to a role of Shoc2 in regulating the balance between proliferation and differentiation and/or lineage commitment during haematopoiesis. To address this possibility an immunophenotyping panel was used to identify the stem and progenitor cell compartments in the bone marrow of Shoc2 KO, KI and WT mice.

Hematopoietic stem cells (HSCs) and their downstream progeny, multipotent progenitors (MPPs), (Figure 4-14A) are known to cycle rapidly to expand the system and generate common myeloid progenitors (CMPs) and common lymphoid progenitors (CLPs) that then further produce downstream cell types of the myeloid and lymphoid lineages respectively (Spangrude et al. 1988; Morrison et al. 1997) (Figure 4-14B).

A

*KLS: **Lin⁻ Sca1⁺cKit⁺**

HSC (LT-HSC)	KLS CD34- CD48- CD150+ CD135-	Long-term self-renewal Multipotent
MPP1 (ST-HSC)	KLS CD34+ CD48- CD150+ CD135-	Short-term self-renewal Multipotent
MPP2	KLS CD34+ CD48+ CD150+ CD135-	Multipotent
MPP3	KLS CD34+ CD48+ CD150- CD135-	Myeloid bias
MPP4	KLS CD34+ CD48+ CD150- CD135+	Lympoid bias

B

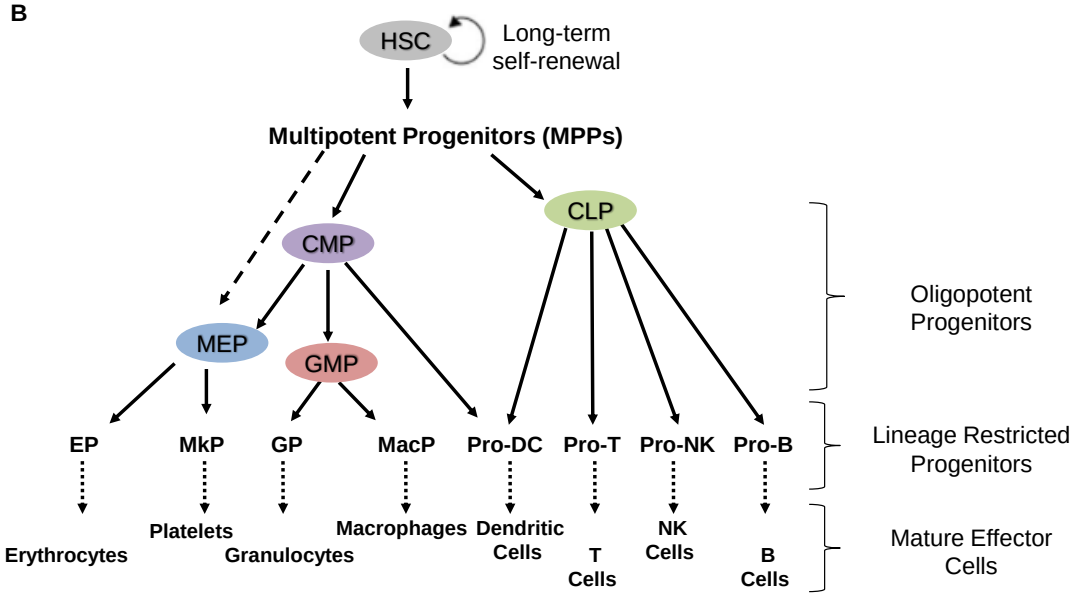

Figure 4-14. Cell surface markers for identification of hematopoietic stem cells (HSCs) and multipotent progenitors (MPPs) and hierarchy of haematopoiesis

A. FACS strategies for detection of HSCs and MPPs and functional differences among different subtypes of MPPs. MPP subsets are able to generate cells of both the myeloid and the lymphoid lineages, and also, they can be divided into MPP1-MPP4 which characterized by increasing proliferation rate but decreasing self-renewal potential along with more pronounced lineage bias (Zhang and Hsu 2017). Adapted from (Zhang and Hsu 2017).
B. Schematic for hierarchy of hematopoiesis. HSC: hematopoietic stem cell, CLP: common lymphoid progenitor, CMP: common myeloid progenitor, GMP: granulocyte/macrophage progenitor, MEP: megakaryocyte/erythrocyte progenitor, EP: erythrocyte progenitor, MkP: megakaryocyte progenitor, GP: granulocyte progenitor, MacP: macrophage progenitor, DC: Dendritic cells. Adapted from (Chotinantakul and Leeanansaksiri 2012).

The KLS fraction (Lineage$^-$/Sca1$^+$/c-Kit$^+$) was gated into long-term (LT-HSCs), short-term hematopoietic stem cells (ST-HSCs or MPP1), and MPPs (MPP2, MPP3 and MPP4) according to surface expression of CD34, CD48, CD135 and CD150 (Figure 4-15A). Interestingly, Shoc2 KO mice showed increased numbers of all stem and progenitor populations except for MPP4, which have lymphoid bias (Oguro et al. 2013; Cabezas-Wallscheid et al. 2014; Pietras et al. 2015) (Figure 4-15B). A significant increase in LT-HSCs and ST-HSCs and decrease in MPP4 was also observed in the bone marrow of Shoc2 KI mice compared to WT controls (Figure 4-15B).

Next, the Lineage$^-$/Sca1$^-$/c-Kit$^+$ fraction was gated to distinguish common myeloid progenitors (CMPs; CD16-32$^-$/CD34$^+$), granulocyte/monocyte progenitors (GMPs; CD16-32$^+$/CD34$^+$) and megakaryocyte/erythroid progenitors (MEPs; CD16-32$^-$/CD34$^-$). Lineage$^-$/Sca1^{lo}/c-Kit^{lo} fraction was then gated for common lymphoid precursors (CLPs; CD127$^+$). Notably, numbers of CMP and GMP, but not CLP or MEP were significantly higher in Shoc2 KO mice compared to WT controls (Figure 4-15C).

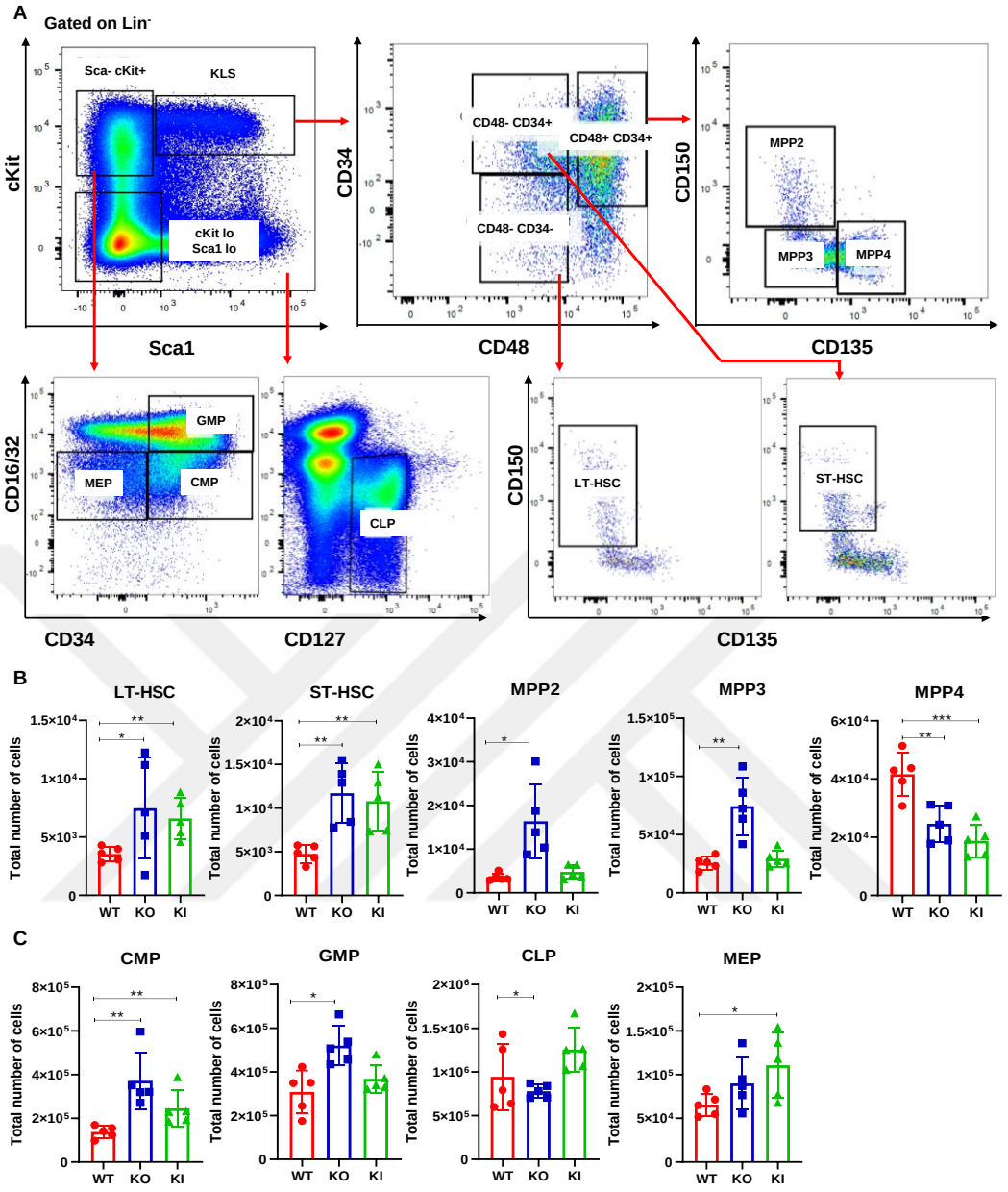

Figure 4-15. Shoc2 deletion causes an expansion of myeloid progenitors in the bone marrow

A. Representative gating strategy for Shoc2 KO, KI and WT bone marrows.
B. Quantification of the total number of HSCs and MPPs of Shoc2 KO, KI and WT bone marrows (n=5 for each genotype). Data are presented as mean values ± SEM. Significance is determined using an unpaired student's t-test. *p< 0.05, **p< 0.01 or ***p<0.001. LT-HSC: long-term hematopoietic stem cell, ST-HSC: short-term hematopoietic stem cell, MPP2-4: Multipotent progenitors 2-4, CMP: common myeloid progenitor, GMP: granulocyte/macrophage progenitor, CLP: common lymphoid progenitor, MEP: megakaryocyte/erythrocyte progenitor (n=2 independent experiments). This figure was generated with the help of Cristobal Costoya from Sergio Quezada lab.

Collectively, these results indicate that systemic Shoc2 deletion led to an expansion of myeloid compartment.

Bone marrow-derived macrophages as an *in vitro* model to study the role of Shoc2 in cell signalling

In order to study the role of Shoc2 in a more tractable model *in vitro*, primary bone marrow-derived macrophages (BMMs) was chosen as a cell model where the effect of Shoc2 inactivation in differentiation and cell signalling could be studied. In the presence of the lineage-specific growth factor, macrophage colony-stimulating factor (M-CSF), monocyte/macrophage progenitors present in the bone marrow will proliferate and differentiate into a homogenous population of mature BMMs (Mossadegh-Keller et al. 2013).

Bone marrow cells from *Shoc2*$^{fl/fl}$ *Rosa26-CreER*^{T2} were isolated and cultured with or without an initial one day treatment of 4-hydroxy-tamoxifen (4-OHT) to induce Shoc2 recombination *in vitro*. Seven days later, cells were seeded for experiments and stimulated with different agonists such as M-CSF, granulocyte/macrophage colony-stimulating factor (GM-CSF), lipopolysaccharide (LPS) and phorbol myristate acetate (PMA) for indicated time points of between 2 and 60 minutes to determine the response of the ERK-pathway to agonist stimulation overtime.

Upon M-CSF, which is known to stimulate type III tyrosine kinase transmembrane receptor: macrophage colony stimulating factor receptor (M-CSFR) (Hamilton 2008), ERK activation was impaired in the absence of Shoc2. The MEK, ERK and RSK phosphorylation was impaired at 5 and 10 minutes of M-CSF treatment in 4-OHT treated Shoc2 KO cells compared to control cells (non-treated with 4-OHT) (Figure 4-16A and B). In contrast, no effect was seen on AKT S473 phosphorylation in the absence of Shoc2 (Figure 4-16A and B).

GM-CSF signalling is mediated via a variety of kinase cascades including MAPK/ERK, JAK/STAT, PKC, and PI3K (de Groot et al. 1998; Wheadon et al. 1999). Upon GM-CSF treatment, MEK, ERK and RSK phosphorylation are impaired at the 5 and 10 minutes, in the absence of Shoc2 while minimum differences were seen between them by 20 minutes. Similar to M-CSF treatment, AKT phosphorylation by GM-CSF was not affected in Shoc2 KO cells (Figure 4-16C and D).

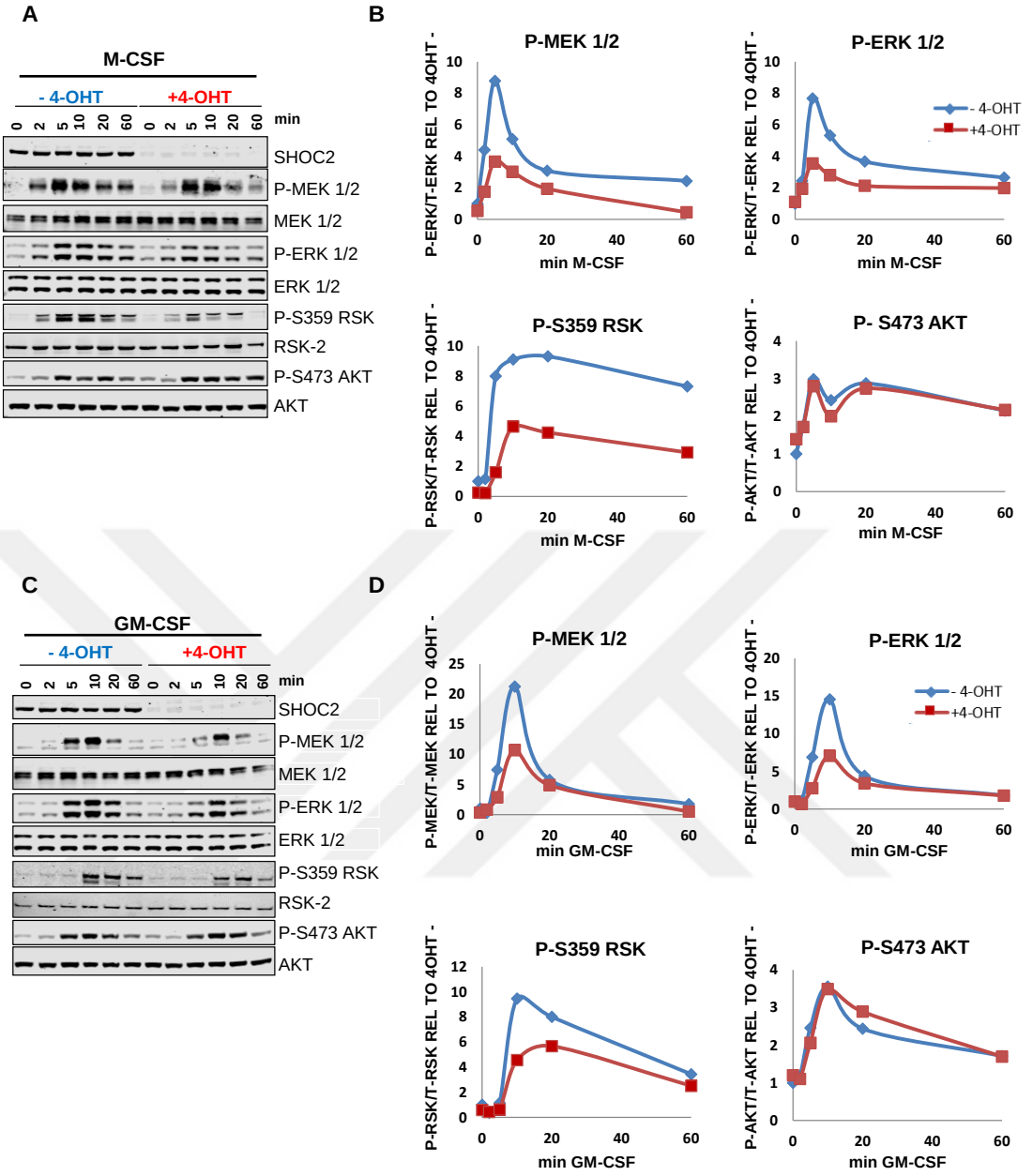

Figure 4-16. Shoc2 deletion impairs ERK but not AKT pathway activation by M-CSF and GM-CSF

A. Shoc2 is required for ERK pathway activation on M-CSF treatment in bone marrow derived macrophages. 4-OHT treated Shoc2 KO (+4-OHT) and untreated control (-4-OHT) BMMs were stimulated with 10 ng/ml of M-CSF for indicated time points and lysates probed with the indicated antibodies.
B. Quantification of P-MEK, P-ERK, P-RSK and P-AKT in (A), relative to control condition (0'mins of -4-OHT) using Odyssey CLx Imaging system (LI-COR).
C. As (A) with 10 ng/ml of GM-CSF stimulation.
D. As (B) with 10 ng/ml of GM-CSF stimulation.

We next determined the effect of Shoc2 ablation on signalling responses to LPS. LPS is the major component of the outer membrane of gram-negative bacteria

and it has been previously described to induce ERK pathway activation in BMMs (Valledor et al. 2000). Our data shows that in contrast to M-CSF and GM-SCF which induced a peak of ERK activity at 5 minutes and 10 minutes of stimulation respectively, LPS induced ERK activation was slower which started to be detected at 10 minutes and peaked at 20 minutes of LPS treatment. Importantly, ERK and AKT activation by LPS was completely unaffected in 4-OHT treated Shoc2 KO cells (Figure 4-17A and B).

Lastly, we stimulated BMMs with the activating agent PMA. PMA is a potent protein kinase C (PKC) activator, which drives RAS- and RAF- dependent activation of the ERK pathway (Downward et al. 1990a; Lee et al. 2002). Our time-course analysis shows that PMA induces ERK pathway activation within 5 minutes of the treatment and the response of the ERK pathway to PMA-stimulation is strongly reduced on Shoc2 inhibition. No effect of PMA on AKT phosphorylation was observed (Figure 4-17C and D).

In summary, Shoc2 is required for ERK-MAPK, but not AKT, pathway activation in an agonist-dependent manner. Our results show that activation by M-CSF and GM-CSF is only partially impaired in the absence of Shoc2, whereas LPS response is completely unaffected, is consisted with previous observations from the lab showing the existence of SHOC2-dependent and independent mechanism of ERK pathway activation (Boned Del Rio et al. 2019) that differentially contribute in a context and agonist-dependent manner.

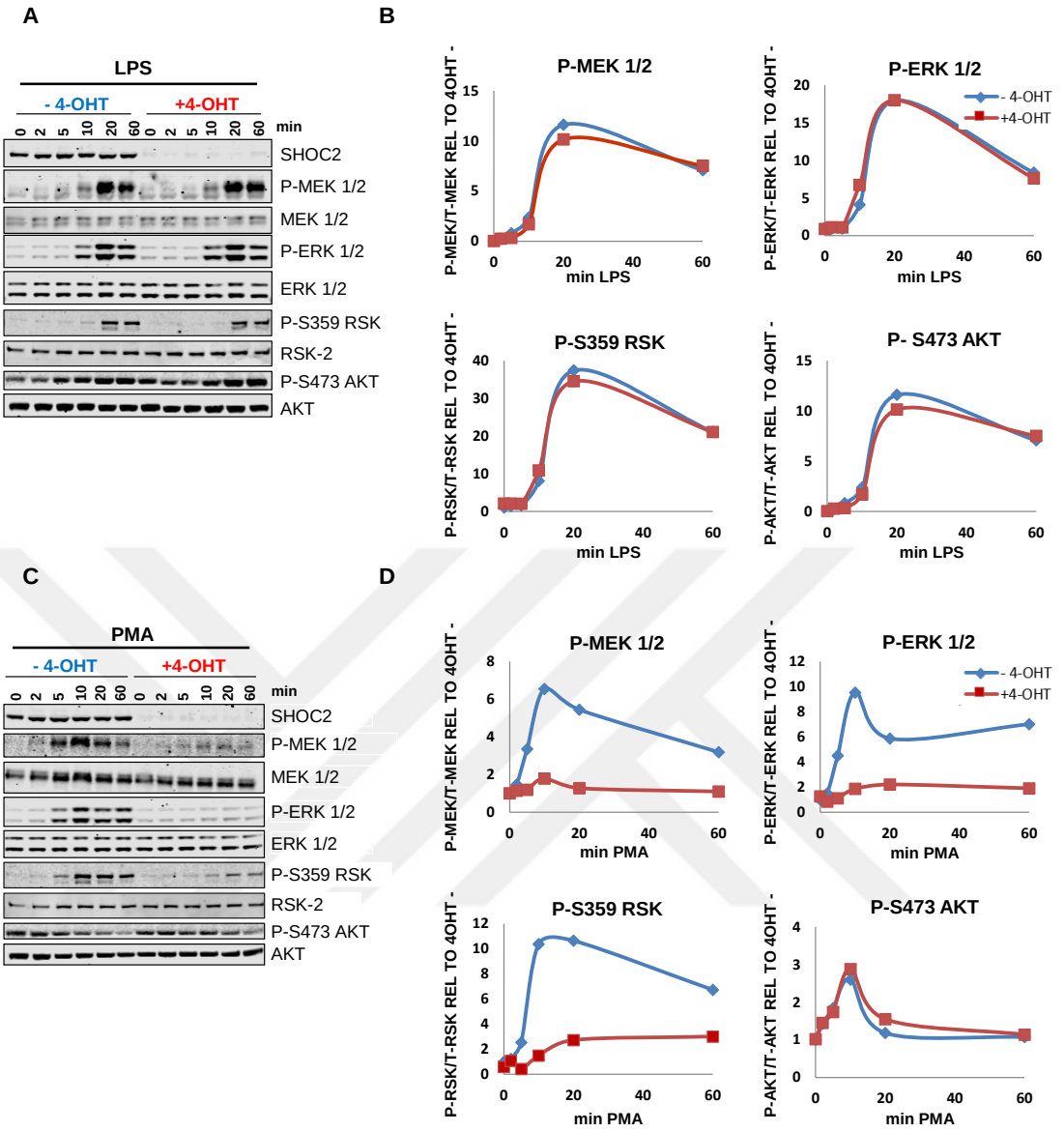

Figure 4-17. Shoc2 deletion impairs ERK pathway activation by PMA but not LPS

A. Shoc2 is not required for ERK pathway activation on LPS treatment in bone marrow derived macrophages. 4-OHT treated Shoc2 KO (+4-OHT) and untreated control (-4-OHT) BMMs were stimulated with 100 ng/ml of LPS for indicated time points and lysates probed with the indicated antibodies.
B. Quantification of P-MEK, P-ERK, P-RSK and P-AKT in (A), relative to unstimulated -4-OHT control condition (0'mins of -4-OHT) using Odyssey CLx Imaging system (LI-COR).
C. BMMs were stimulated with 100 ng/ml of PMA and lysates probed with the indicated antibodies.
D. Quantification of (C) as in B.

Effect of Shoc2 elimination in urinary bladder function

During mice dissections we noted that Shoc2 KO mice that presented enlarged abdominal areas (Figure 4-1C) invariably had grossly enlarged and distended bladders full of urine. This was specific to Shoc2 KO males as bladders from Shoc2 KO females were normal and similar in volume to WT female bladders (Figure 4-18A). Of note also, this phenotype was observed with partial penetrance with 7 out of 17 (~41.2%) of KO male mice showing no phenotype. No enlarged bladders were observed from Shoc2 KI male or female mice (data not shown).

Bladder capacity ranges from 0.12-0.15 ml in mice (Reis et al. 2011). Post-mortem urinary bladder volumes were significantly higher in Shoc2 KO males 6-19 weeks post-tamoxifen treatment compared to WT males (Figure 4-18B). The protein concentration was significantly higher in urine from Shoc2 KO males at morbidity (Figure 4-18C). The higher protein concentration may have been due to decreased water consumption. However, when water consumption was measured 10 weeks post-tamoxifen treatment for 5 days, no differences in water intake between Shoc2 KO and WT males was observed (Figure 4-18D).

To identify any possibly morphological bladder abnormalities that may account for the observed distended bladder phenotype, H&E-stained sections of bladders from WT and Shoc2 KO mice were studied by pathologists. No significant histological differences were observed with bladders from Shoc2 KO males showing normal, compact organization of smooth muscle and epithelium (urothelium) layers (Figure 4-18E).

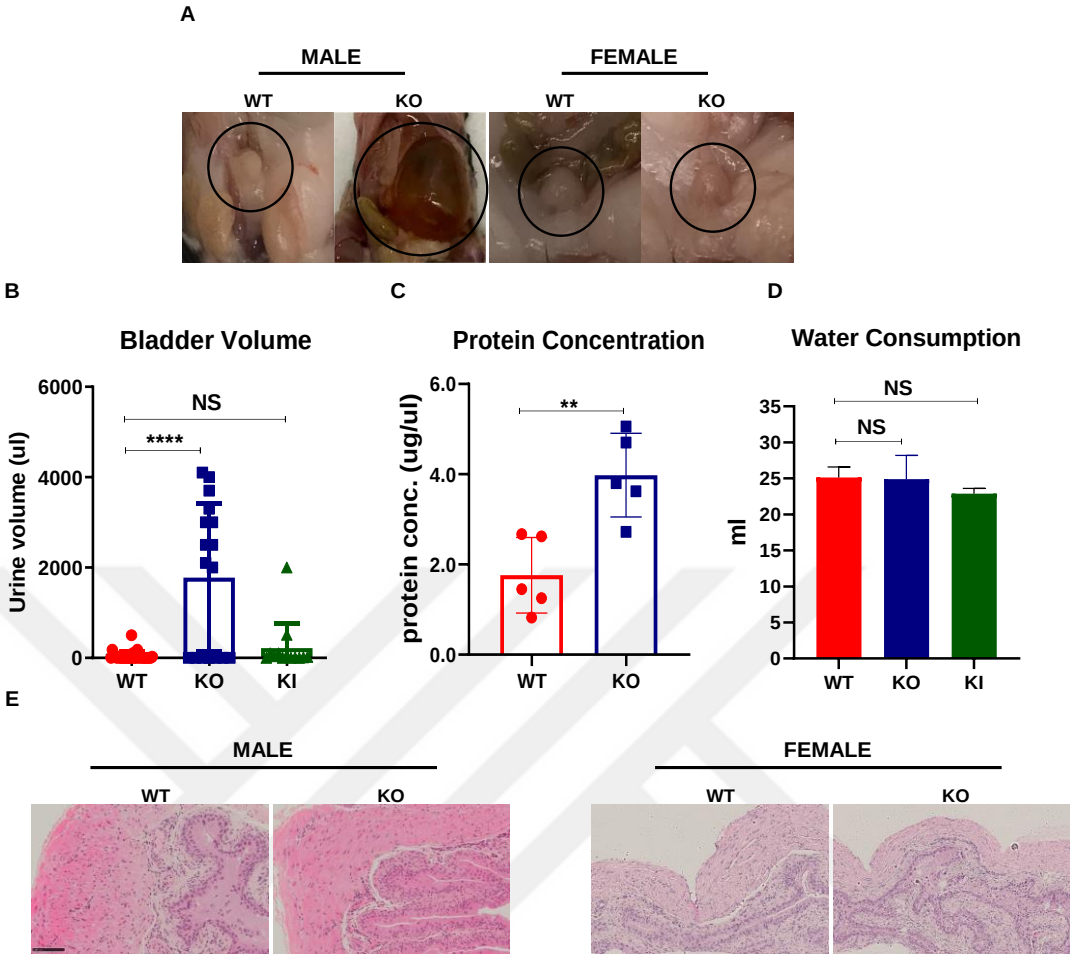

Figure 4-18. Male, but not female Shoc2 KO mice developed enlarged bladder

A. Representative images of Shoc2 KO male with enlarged bladder full of urine.
B. Quantification of urine volume in Shoc2 KO, KI and WT male mice at morbidity (KO and WT: n=17; KI: n=13). Data are presented as mean values ± SEM. Significance is determined using an unpaired student's t-test. ****p< 0.0001 or NS: Not Significant.
C. The protein concentration of urine samples is elevated in Shoc2 KO male mice at morbidity (n=5 for each genotype). Data are presented as mean values ± SEM. Significance is determined using an unpaired student's t-test. **p< 0.01 or NS: Not Significant.
D. Quantification of water intake of Shoc2 KO, KI and WT male mice at 10 weeks post-tamoxifen treatment (n=5 for each genotype). Data are presented as mean values ± SEM. Significance is determined using an unpaired student's t-test. NS: Not Significant.
E. Representative H&E stained histological sections of Shoc2 KO male and female bladders at morbidity. Scale bar=100μm.

Next, we speculated that urine retention in male Shoc2 KO mice could be the consequence of an anatomical obstruction related to a male-specific organ such as an enlarged prostate. In order to examine prostate glands, the prostate was dissected together with the urethra, bladder and seminal vesicles (Figure 4-19A). However, neither macroscopic nor histological examination revealed any obvious abnormality in the prostate glands of affected Shoc2 KO male mice (Figure 4-19B). In addition,

when compared to WT controls, no histological abnormalities were noted in the kidneys of KO mice (Figure 4-19C). In summary, Shoc2 KO, but not KI mice, develop enlarged and distended bladders that are full or urine without any apparent anatomical obstruction

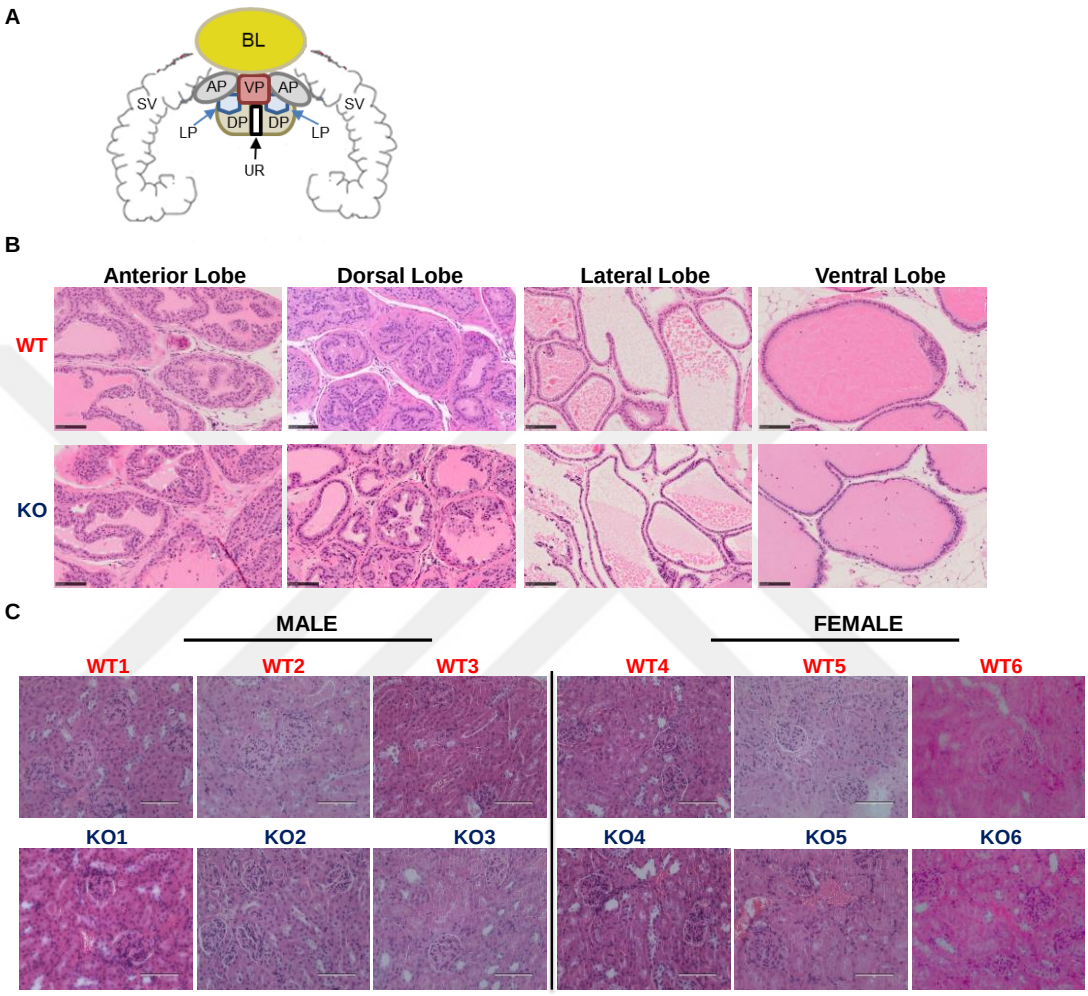

Figure 4-19. Histological analysis revealed no structural abnormalities in the prostate and kidney tissues of Shoc2 KO mice

A. Diagram of the mouse urogenital region and prostate anatomy. Bladder (BL), seminal vesicles (SV), anterior prostate (AP), ventral prostate (VP), lateral prostate (LP), dorsal prostate (DP) and urethra (UR).
B. Representative H&E images of anterior, dorsal, lateral and ventral lobes of prostate from adult WT and Shoc2 KO mice (n=4 for each genotype). Scale bar=100µm.
C. Representative H&E images of kidney from male and female WT and Shoc2 KO mice (n=6 for each genotype). Scale bar=100µm.

Conclusions

Systemic inactivation of Shoc2 by *CreER*^{T2}-mediated recombination in adult mice decreases viability for both Shoc2 KO and KI mice (median survival of ~15 and ~34 weeks, respectively). Post-mortem studies revealed no gross abnormalities or detectable histological alterations in major organs including lung, heart, liver, kidney, colon, pancreas, skeletal muscle and thymus. However, several phenotypes develop after sustained Shoc2 deletion. The main phenotype for both Shoc2 KO and KI mice is skin dermatitis accompanied by pruritus. This skin dermatitis is progressively increased in severity and is the primary cause of euthanasia. The comprehensive histological characterization of the skin will be discussed in detail in the following chapter. Shoc2 KO and KI mice also develop splenomegaly and lymphadenopathy. Characterization of the immune cell sub-populations in spleen and lymph nodes of Shoc2 KO mice showed expansion of the myeloid compartment with a significant accumulation of neutrophils. We also identified a sexually dimorphic role of Shoc2 in urinary bladder function with the male, but not female KO mice developing enlarged urinary bladders without obvious anatomical obstruction.

Chapter 5 Physiological role of Shoc2 in skin homeostasis

Introductory statement

The EGFR-RAS-ERK pathway has a well-described role in skin homeostasis (Doma et al. 2013). Its function in the skin and its appendages is necessary for proper development and tissue homeostasis, and its deregulation rapidly results in defects in cellular proliferation and differentiation. The consequences can be the development of lesions, structural and functional defects of its appendages such as hair follicles (Schneider et al. 2009). Considering the role of SHOC2 within the EGFR-RAS-ERK pathway and the observation that Shoc2 inactivation results in dermatitis, we thus, aimed to explore the role of Shoc2 in skin homeostasis.

Validation of Shoc2 inactivation in adult mouse skin

In order to confirm Shoc2 inactivation in adult mouse skin, 6-12 weeks old *Shoc2$^{fl/fl}$ KO/KI Rosa26-CreER^{T2}* mice were subjected to 5-days 80 mg/kg tamoxifen treatment by intraperitoneal injection and skin samples harvested 4 weeks later to determine Shoc2, Flag and Myc protein levels. *Shoc2$^{fl/fl}$ cKI Rosa26-CreER^{T2}* mice that had not been treated with tamoxifen (NT) were used as control animals (Figure 5.1A). High level of deletion was observed in KO mice (Figure 5.1B) and efficient loss of Flag and concomitantly gain of Myc was detected in KI mice skin.

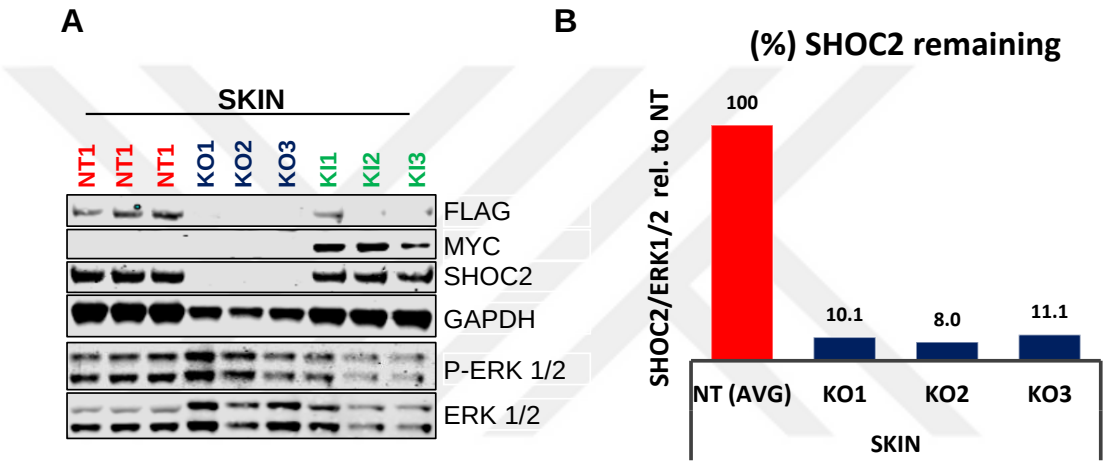

Figure 5-1. Shoc2 inactivation in adult mouse skin

A. Western blots of skin lysates from Shoc2 KO and KI mice (n=3 for each genotype).
B. Quantification of Shoc2 levels relative to ERK 1/2 loading control of (A) using Odyssey CLx Imaging system (LI-COR). The average protein levels of non-treated *Shoc2$^{fl/fl}$ cKI Rosa26-CreER^{T2}* control mice (NT) were set to 100%.

Histological analysis of Shoc2 ablation in adult mice skin

To characterize the histopathology of skin alterations observed upon Shoc2 ablation, regions of skin with lesions (in upper back area) as well as without lesions (non-lesional skin in lower back area) (Figure 5-2A) were analysed by H&E staining. Lesional skin (Figure 5-2B) contained multiple alterations including increased number of hair follicles in the hypodermis (Figure 5-2C), epidermal thickening (acanthosis) (Figure 5-2D), thickening of the stratum corneum (hyperkeratosis) (Figure 5-2E), and immune cell infiltration in dermis (Figure 5-2F).

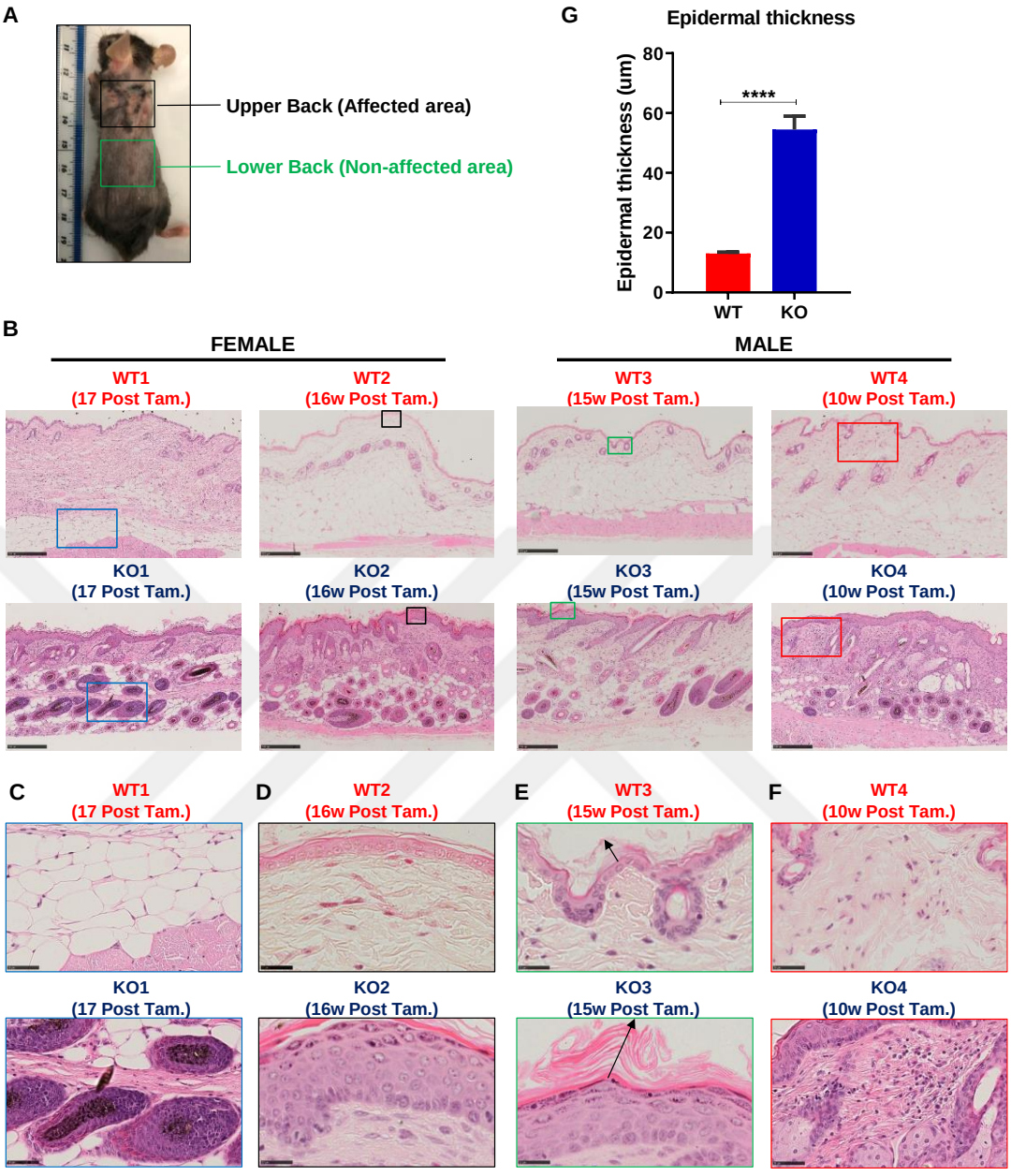

Figure 5-2. Ablation of Shoc2 causes skin alterations

A. Representative image showing skin regions used for analysis containing affected and non-affected areas in Shoc2 KO mice.
B. Representative H&E images (10x) from upper back (affected) area of WT and Shoc2 KO mice (2 males and 2 females each) (n=7 mice per genotype). Scale bar=250 μm.
C. 40x magnification of indicated blue square in (B) to highlight increased hair follicles in the hypodermis of Shoc2 KO skin (n=7 mice per genotype). Scale bar=50 μm.
D. 80x magnification of indicated black square in (B) to highlight thicker epidermis (acanthosis) of Shoc2 KO skin (n=7 mice per genotype). Scale bar=25 μm.
E. 80x magnification of indicated green square in (B) to highlight hyperkeratosis (arrow) in Shoc2 KO skin (n=7 mice per genotype). Scale bar=25 μm.
F. 40x magnification of indicated red square in (B) to highlight immune infiltration in the dermis of Shoc2 KO skin (n=7 mice per genotype). Scale bar=50 μm.

G. Epidermal thickness quantification of affected skin sections from Shoc2 KO and WT mice at morbidity (n=7 for each genotype). The epidermal thickness was quantified in three different positions and for at least 10 different measurements per mouse. Data are presented as mean ± SEM. Significance is determined using an unpaired t test ****p< 0.0001.

Similar although less severe alterations were found in non-lesional areas of Shoc2 KO skin (Figure 5-3A). For instance, hair follicles in the hypodermis were observed in some but not all animals and immune cell infiltration was observed at lower levels compared to lesional areas of Shoc2 KO mice (Figure 5-3B). This also correlated with low epidermal thickening in non-lesional skin of Shoc2 KO mice (Figure 5-3C).

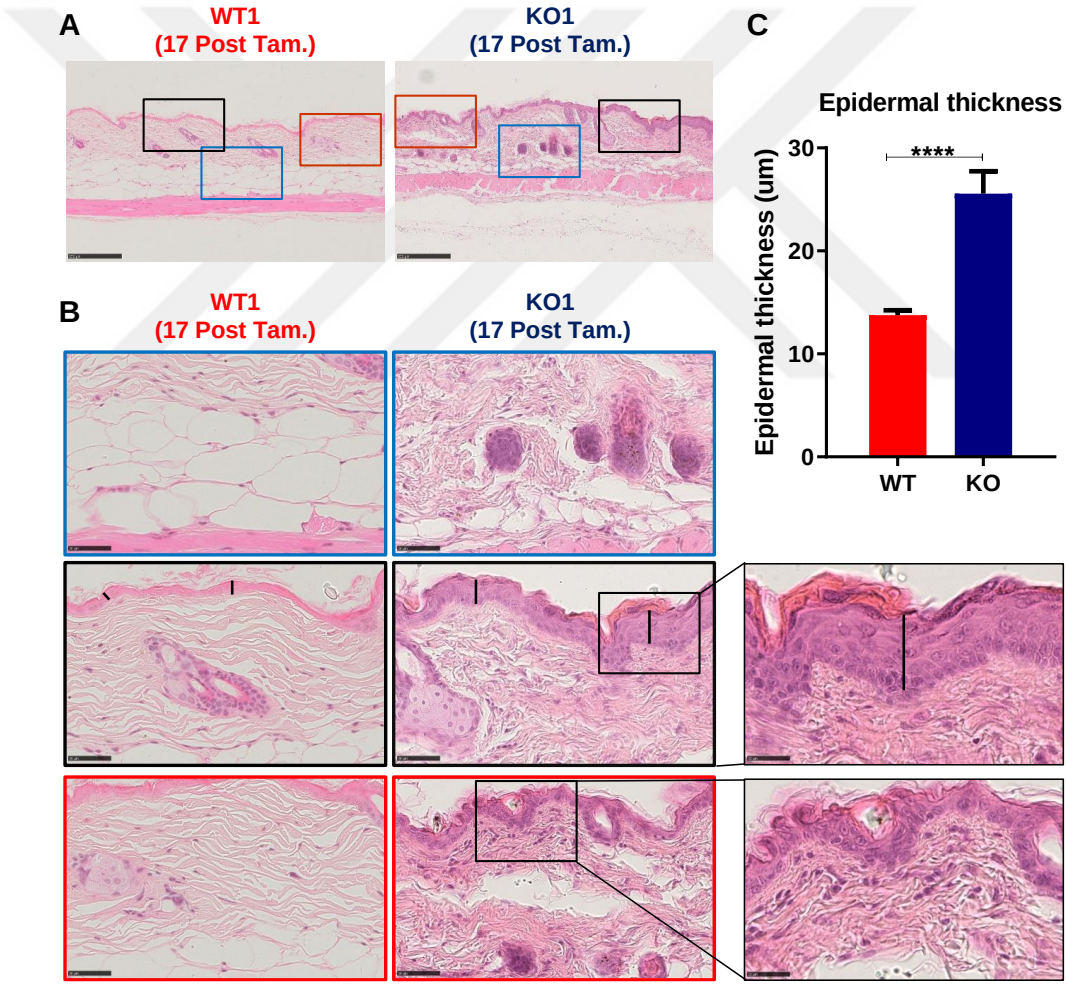

Figure 5-3. Shoc2 ablation leads to less dramatic skin alterations in non-affected areas

A. Representative H&E images (10x) from lower back (non-affected) area of WT and Shoc2 KO mice (n=7 mice per genotype). Scale bar=250 µm.
B. Representative 40x magnification of indicated blue square in (A) to highlight increased hair follicles in the hypodermis, black square in (A) to highlight thicker epidermis (black bar) and red square in (A) to highlight immune infiltration in the dermis of Shoc2 KO

skin (n=7 mice per genotype). Scale bar=50 μm. Insets show the higher magnification of indicated areas. Scale bar=25 μm.

C. Epidermal thickness quantification of non-affected skin sections from Shoc2 KO and WT mice (n=7 for each genotype). The epidermal thickness was quantified in three different positions and for at least 10 different measurements per mouse. Data are presented as mean ± SEM. Significance is determined using an unpaired t test ****p< 0.0001.

Characterization of epidermis from Shoc2 KO mice skin by immunohistochemistry

To further characterize the epidermal phenotype, skin sections were stained with a panel of well-established keratinocyte markers of the different layers of the epidermis (Figure 5-4A) and the main components of the hair follicles (Figure 5-4B). As shown in Figure 5-4C, Shoc2 KO mice displayed significant alterations in the expression of these markers. Keratin 14 (K14), which is normally expressed in the basal layer of the epidermis and hair follicles of mice, was detected throughout all epidermal layers in Shoc2 KO skin, consistent with epidermal hyperplasia and defective differentiation. Keratin 10 (K10) expression is normally restricted to the spinous layer (as a part of suprabasal layer) but was also found expanded in Shoc2 KO mice epidermis. Staining of Keratin 6, which is usually expressed in hyperproliferative keratinocytes was also significantly higher in Shoc2 KO epidermis compared to WT mice. Lastly, the expression of Loricrin, a marker of terminally differentiated cells in the stratum corneum was also significantly increased in the epidermis of Shoc2 KO mice (Figure 5-4C).

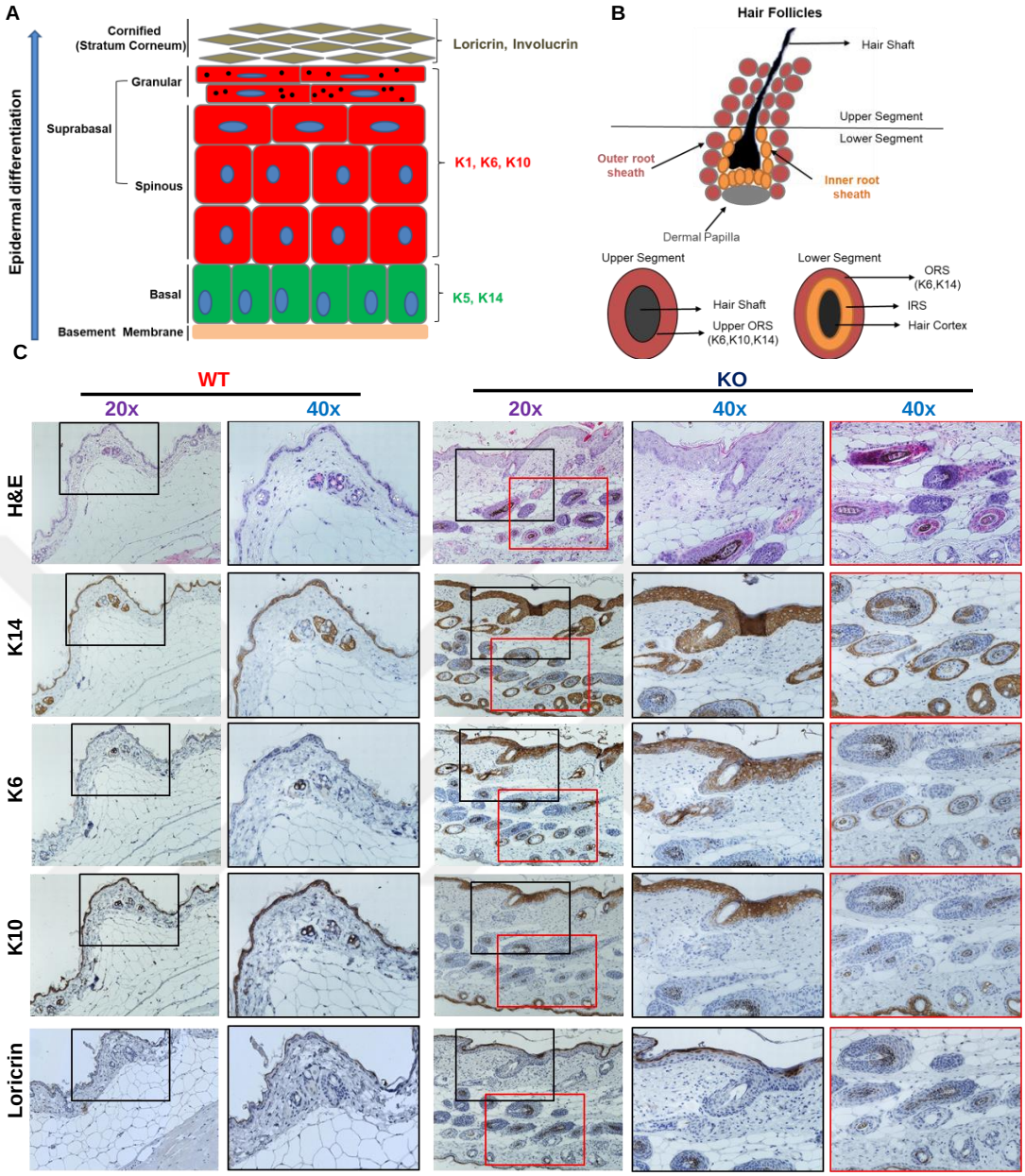

Figure 5-4. Immunohistochemical staining reveals expansion of basal, suprabasal and cornified layers in epidermis and root sheaths in hair follicles of Shoc2 KO mice

A. Schematic illustration of mouse skin epidermis.
B. Schematic illustration of the hair follicle compartments, which is separated in upper and lower segment.
C. Immunohistochemical staining of Shoc2 KO and WT mice dorsal skin sections with the indicated antibodies. Black square represents higher magnification of indicated area to show expansion of epidermal layers and red square shows higher magnification of increased number of hair follicles in KO hypodermis (n=4 for each genotype). Scale bars 20x=100 µm and 40x=50 µm.

This keratinocyte marker expression pattern was similarly observed when immunofluorescence was used as a detection method, with Shoc2 KO skin from both

male and female mice displaying a clear expansion of basal, suprabasal and cornified layers of epidermis (Figure 5-5). These results thus indicate that acute Shoc2 ablation in adult mice leads to increased proliferation and defective differentiation of keratinocytes in the skin epidermal layer.

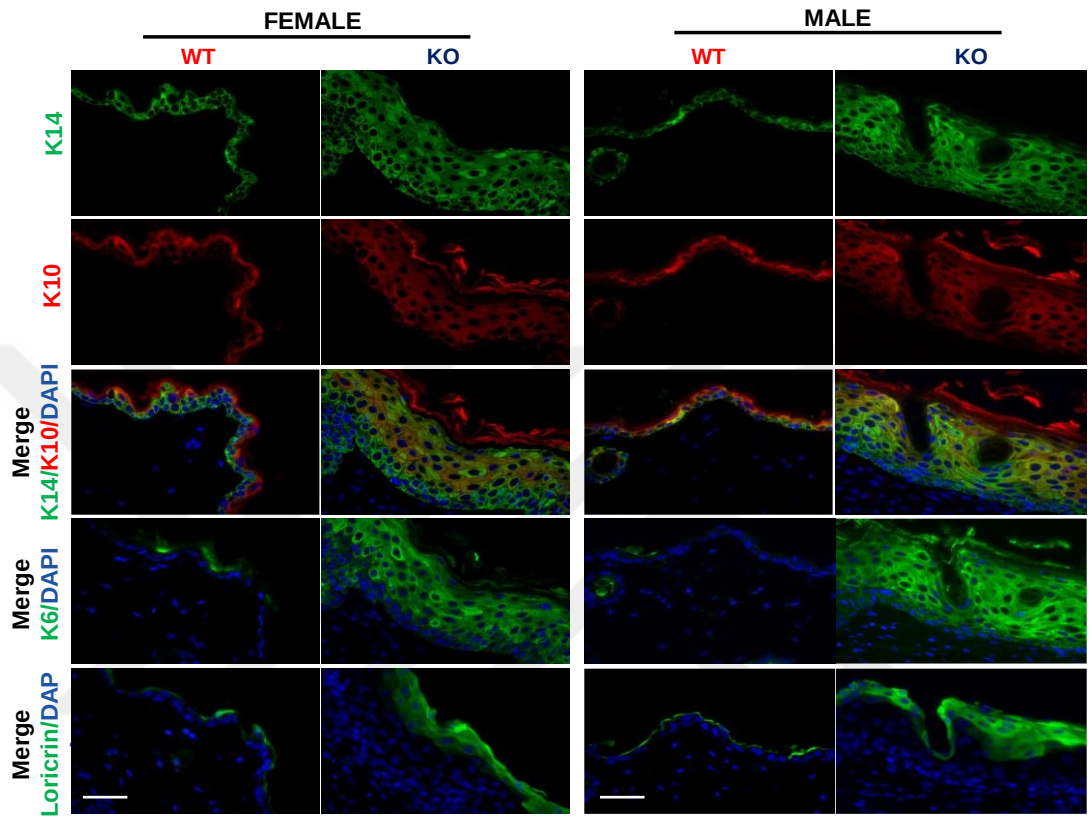

Figure 5-5. Immunofluorescence staining reveals expansion of basal, suprabasal and cornified layers in epidermis of Shoc2 KO mice

Immunofluorescence staining of Shoc2 KO and WT female and male mice dorsal skin sections with the indicated antibodies. Nuclei were stained with DAPI (blue) (n=4 for each genotype). Scale bars=50 μm.

A striking feature of the skin of Shoc2 KO mice was a dramatic increase in the number and size of hair follicles in the subdermal adipose layer (hypodermis) (Figure 5-2B and 4C). As mentioned in the introduction chapter, hair follicles undergo cycles of growth (anagen), apoptosis-mediated regression (catagen), and rest (telogen) numerous times in life (Figure 5-6). In skin samples of age- and gender-matched WT mice hair follicles of were typically in the telogen phase and confined to the dermis. In contrast, hair follicles in Shoc2 KO mice appeared locked in the anagen phase (Figure 5-2B and 4C). In order to investigate whether an aberrant anagen-phase hair follicles has an effect on hair growth, age-matched Shoc2 KO and WT male mice

were depilated and monitored for 28 days. No significant differences were found in hair regeneration Shoc2 KO and WT mice (Figure 5-7) showing that the increase in hair follicles in anagen-phase in Shoc2 KO does not necessarily correlate with increased hair growth.

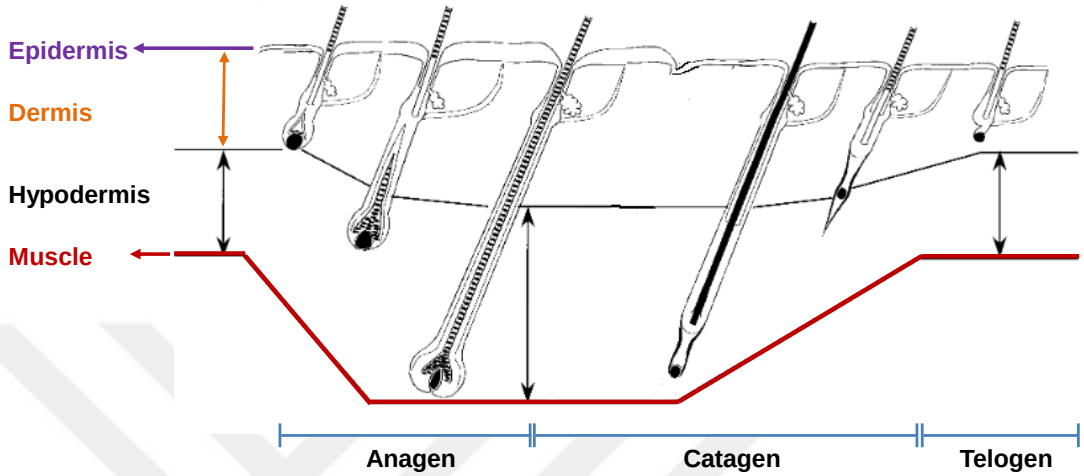

Figure 5-6. The hair growth cycle

Schematic representation of the hair cycle within the different layers of the skin. Arrows between muscle and the border dermis/hypodermis indicate the hair cycle-associated changes in the thickness of the hypodermis. Adapted from (Muller-Rover et al. 2001).

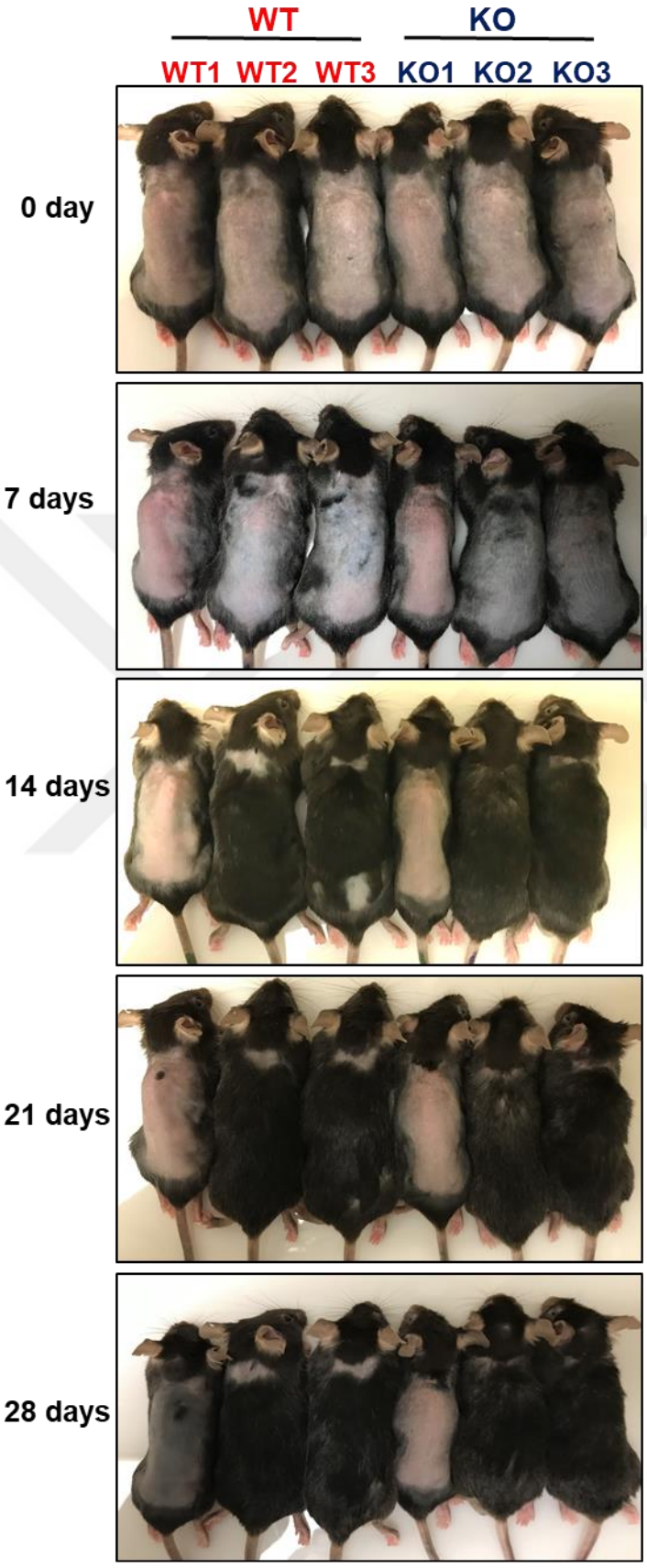

Figure 5-7. Shoc2 ablation has no significant effect on hair growth in adult mice

The back skin of 6 weeks old male mice was shaved 1 week after the last tamoxifen treatment and photographed at 0, 7, 14, 21, and 28 days (n=3 for each genotype and n=3 independent experiments).

Skin Immunophenotyping by immunohistochemistry

As shown above, H&E staining of Shoc2 KO mice suggested that the observed skin alterations were accompanied by a significant increase in immune cell infiltration. This was confirmed by immunohistochemical (IHC) staining with a CD45 immune cell marker (Figure 5-8). To further characterize the nature of this immune response, additional immune markers including F4/80 (macrophages), GR1 (granulocytes), B220 (B cells) and CD3 (T cells) were used on IHC in a collaboration with Professor Teresa Marafioti and Ayse Akarca from her team. As shown in Figure 5-8, the skin of Shoc2 KO mice collected at morbidity had a clear increase in staining of CD3-positive T cells within the dermis and to a lesser degree in the epidermis. F4/80- and GR1-positive myeloid cells were also increased in the dermis of Shoc2 KO skin (Figure 5-8). However, no difference was detected in B cells between the skin of Shoc2 KO mice and the age- and gender-matched WT control mice (Figure 5-8).

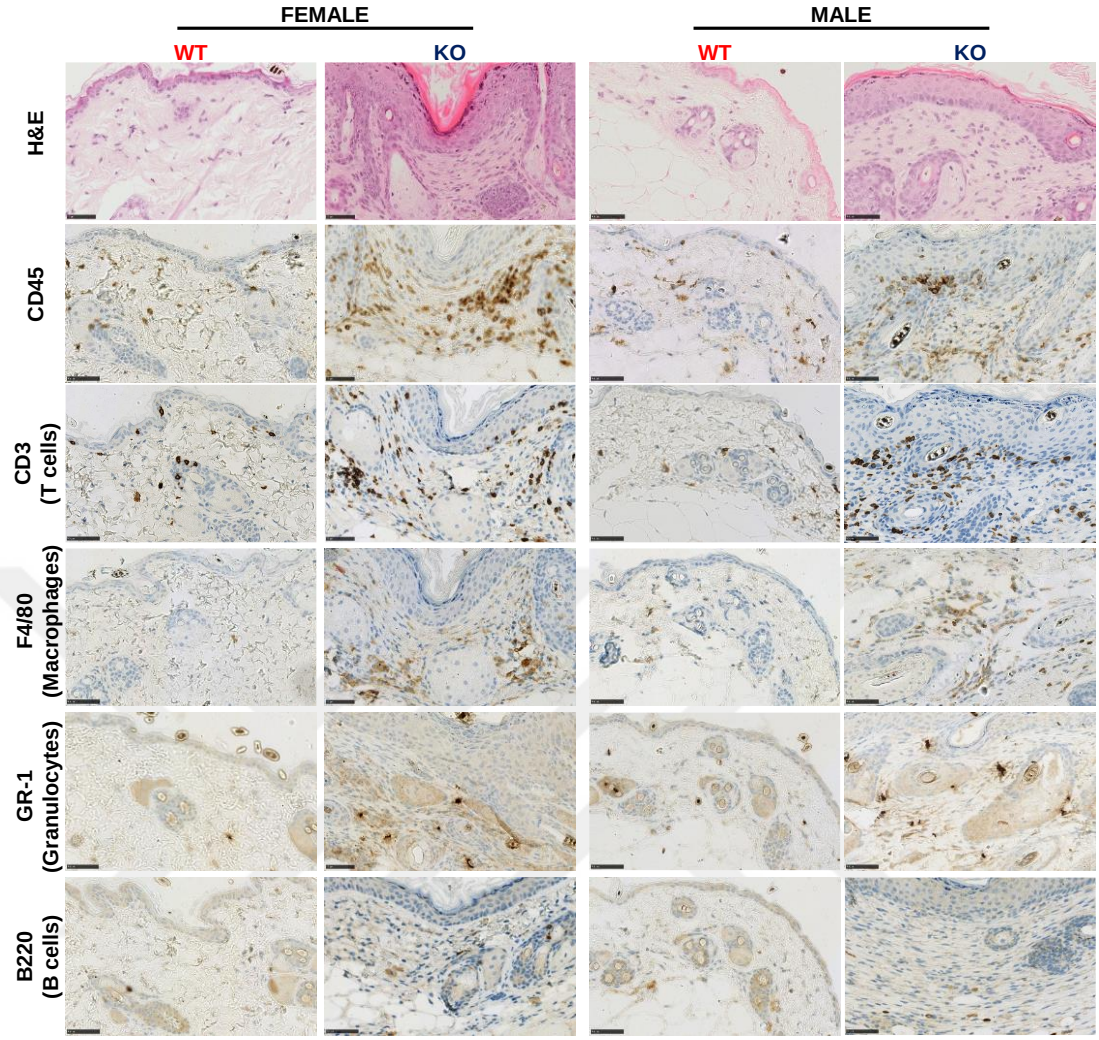

Figure 5-8. Immunohistochemical staining reveals Shoc2 deletion leads to skin inflammation in adult mice

Representative immunohistochemical staining of Shoc2 KO and WT skin sections with the indicated antibodies. Positive immunoreactivity is indicated by the brown colour, with a blue hematoxylin counterstain (n=3 for each genotype). Scale bar=50 μm. This figure was generated with the help of Ayse Akarca from Teresa Marafioti lab.

Skin Immunophenotyping by flow cytometry

To further characterise the immune cell sub-populations that infiltrate the skin of Shoc2 KO mice, flow cytometry experiments were performed using a panel of markers for the myeloid and lymphoid compartments. To this end, 10-12 weeks old male Shoc2 KO and littermate control WT mice were sacrificed at 4 weeks and 10 weeks post-tamoxifen treatment and throat skin samples as well as spleens were processed to obtain single cell suspensions. To minimize self-inflicted wounds

caused by scratching, nails were trimmed weekly for the first 4 weeks. Shoc2 KO mice displayed bald throats and macroscopic skin lesions 10 weeks post tamoxifen treatment, but not after 4 weeks (Figure 5-9A).

In line with the IHC results, flow cytometry analysis (Figure 5-9B) revealed a significant increase in CD45$^+$ cells in the skin of Shoc2 KO mice compared to WT control littermates 10 weeks but not 4 weeks post-tamoxifen treatment (Figure 5-9C).

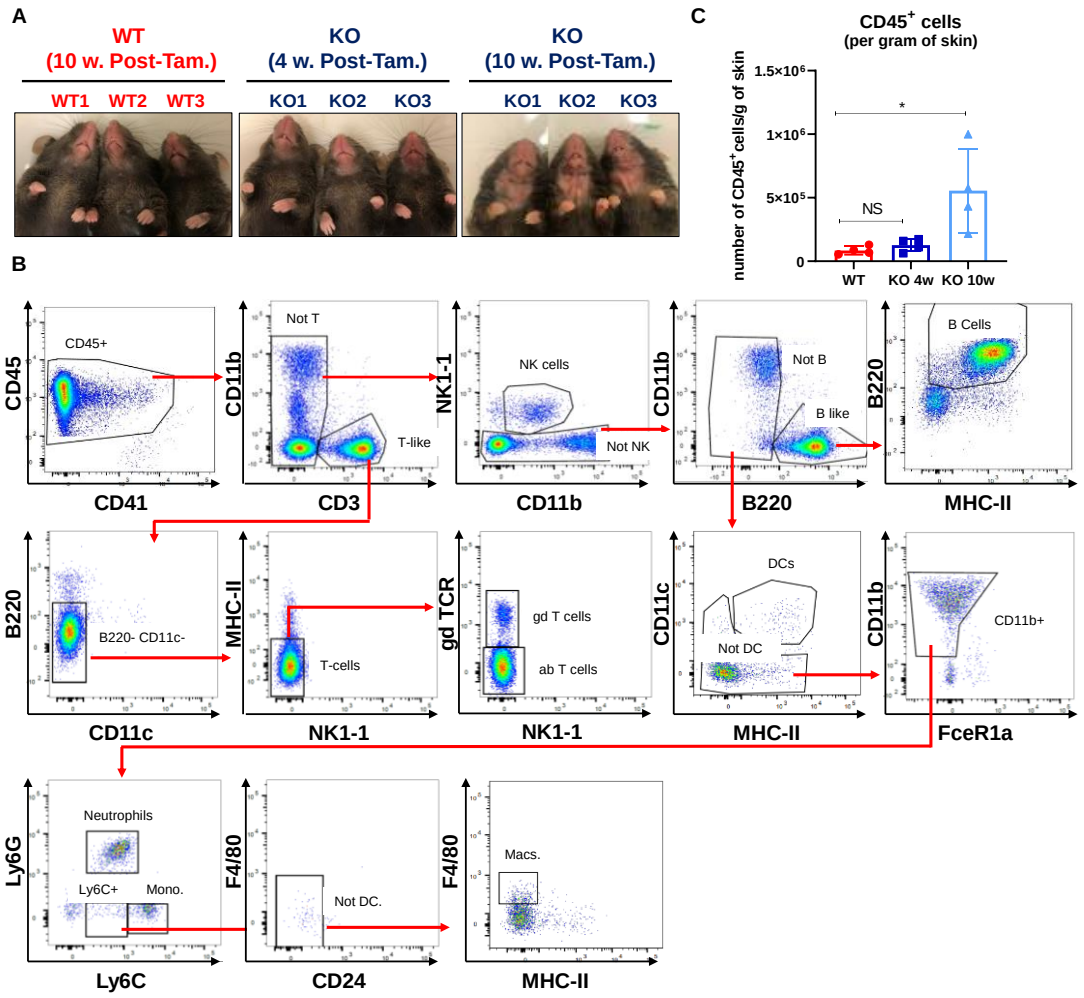

Figure 5-9. Flow cytometry analysis of skin from WT and Shoc2 KO mice at 4 weeks and 10 weeks post-tamoxifen treatment

A. Representative images of the throat area of mice used for analysis.
B. Gating strategy used for flow cytometry. This figure was generated with the help of Cristobal Costoya from Sergio Quezada lab.
C. Quantification of CD45$^+$ cells normalized to weight of skin tissue (n=4 for each genotype). Results are expressed as mean values ± SEM. Significance is determined using an unpaired student's t-test. *p< 0.05 or NS: Not Significant.

No significant differences were observed in αβ T cells ($CD3^+/\gamma\delta$ TCR^-) neutrophils ($CD11b^+/Ly6G^{hi}/Ly6C^{lo}$), DC ($CD11c^+$/MHC II^+) NK ($CD3^-/NK1.1^+$) and B cells ($B220^+$) between WT and Shoc2 KO skin at either 4 or 10 weeks post-tamoxifen treatment (Figure 5-10A). On the other hand, a significant increase in macrophages ($CD11b^+/Ly6C^{lo}/F4/80^+$) and in monocytes ($CD11b^+/Ly6C^{hi}$) was observed at 10 weeks post-tamoxifen treatment. Strikingly, a significant accumulation of γδ T cells ($CD3^+/\gamma\delta$ TCR^+) was detected in the skin of Shoc2 KO mice at 4 and 10 weeks post-tamoxifen treatment (Figure 5-10A). Therefore, despite the fact that increased recruitment of immune $CD45^+$ cells to the skin was only apparent at 10 weeks, an increase in γδ T cells as a percentage of $CD45^+$ cells was the first change detected in Shoc2 KO skin as early as 4 weeks.

When the same analysis was performed on the spleen of the same mice, not only monocyte/macrophages (both at 4 and 10 weeks) but also neutrophils (10 weeks) increased in the spleen. In addition, a small but significant increase in γδ T cells was also detected at 4 weeks in the spleens of Shoc2 KO mice (Figure 5-10B). Thus, the earliest changes detected in immune cell populations upon Shoc2 ablation were an increase in γδ T cells in both skin and spleen (but much more prominent in the skin) together with an increase in monocytes/macrophages which was accompanied at 10 weeks by an increase in neutrophils specifically in the spleen (Figure 5-10B).

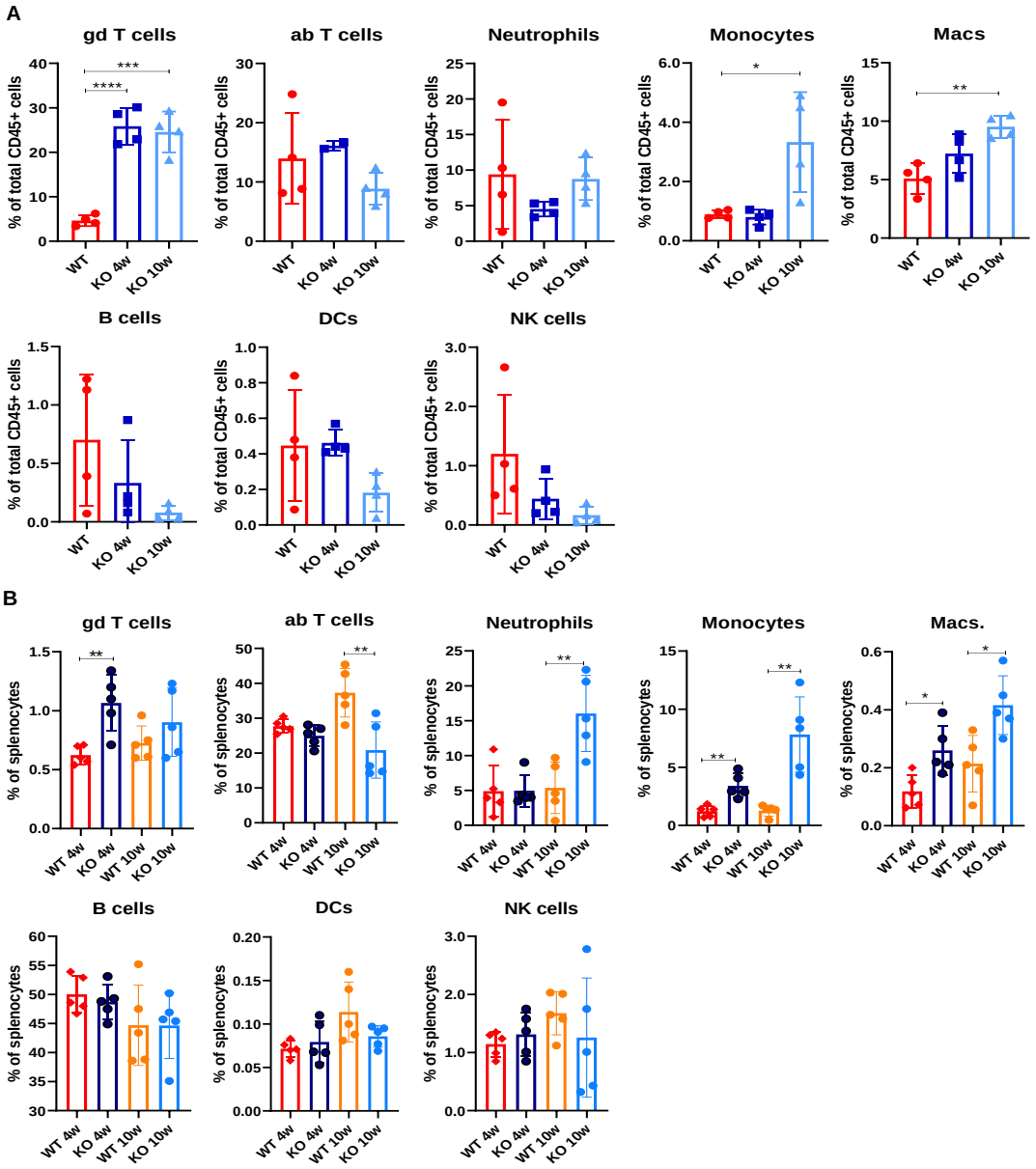

Figure 5-10. Flow cytometry analysis reveals Shoc2 deletion leads to skin inflammation starting as early as 4 weeks post-tamoxifen treatment

A. Quantification of immune cell types as a percentage of CD45⁺ cells of 4 and 10 weeks post-tamoxifen treated Shoc2 KO and WT skin (n=4 for each genotype). Results are expressed as mean values ± SEM. Significance is determined using an unpaired student's t-test. *p< 0.05, **p< 0.01, ***p< 0.001 or ****p< 0.0001. NK cells: Natural killer cells, DC: Dendritic cells, Macs.: Macrophages.

B. Quantification of immune cell types of 4 and 10 weeks post-tamoxifen treated Shoc2 KO and WT spleen (n=5 for each genotype). Results are expressed as mean values ± SEM. Significance is determined using an unpaired student's t-test. *p< 0.05, **p< 0.01. This figure was generated with the help of Cristobal Costoya from Sergio Quezada lab.

Effect of ex vivo Shoc2 ablation in murine keratinocytes

RAS/RAF/MEK/ERK signalling is known to be required for proliferation of murine keratinocytes *in vitro* (Drosten et al. 2013). As previously described, one of the critical skin alterations of Shoc2 KO mice is epidermal hyperplasia. Here, we sought to examine the effect of Shoc2 deletion in epidermal keratinocytes in cultured primary murine keratinocytes *in vitro*.

In order to explore the functions of Shoc2 in keratinocytes, we prepared primary keratinocyte cultures from the tails of adult *Shoc2*$^{fl/fl}$ *Rosa26-CreER*^{T2} (cKO) mice according to previously published protocols (Li et al. 2017). Despite several attempts, we failed to maintain the primary keratinocytes in culture long enough to be able to perform experiments. It was also observed that keratinocytes were sensitive to 4-OHT treatment with even WT cells being affected, although *Shoc2*$^{fl/fl}$ KO cells in particular never recovered. In order to overcome these issues, keratinocytes were immortalized by retroviral expression of Simian Virus 40 (SV40) large T-antigen (Figure 5-11A).

In order to optimize the minimal exposure time of 4-OHT treatment to induce Shoc2 deletion and get an indication of the time course of associated loss of Shoc2 protein, immortalized keratinocytes were treated with 4-OHT for 1 day or 2 days and lysed 4 or 5 days later (Figure 5-11B). Shoc2 deletion was confirmed by western blot with more than 90% recombination observed in all conditions (Figure 5-11C and D). Because of the efficient recombination and shorter treatment period, 1 day 4-OHT treatment and 4 days incubation after the removal of 4-OHT was used as a starting point for further experiments.

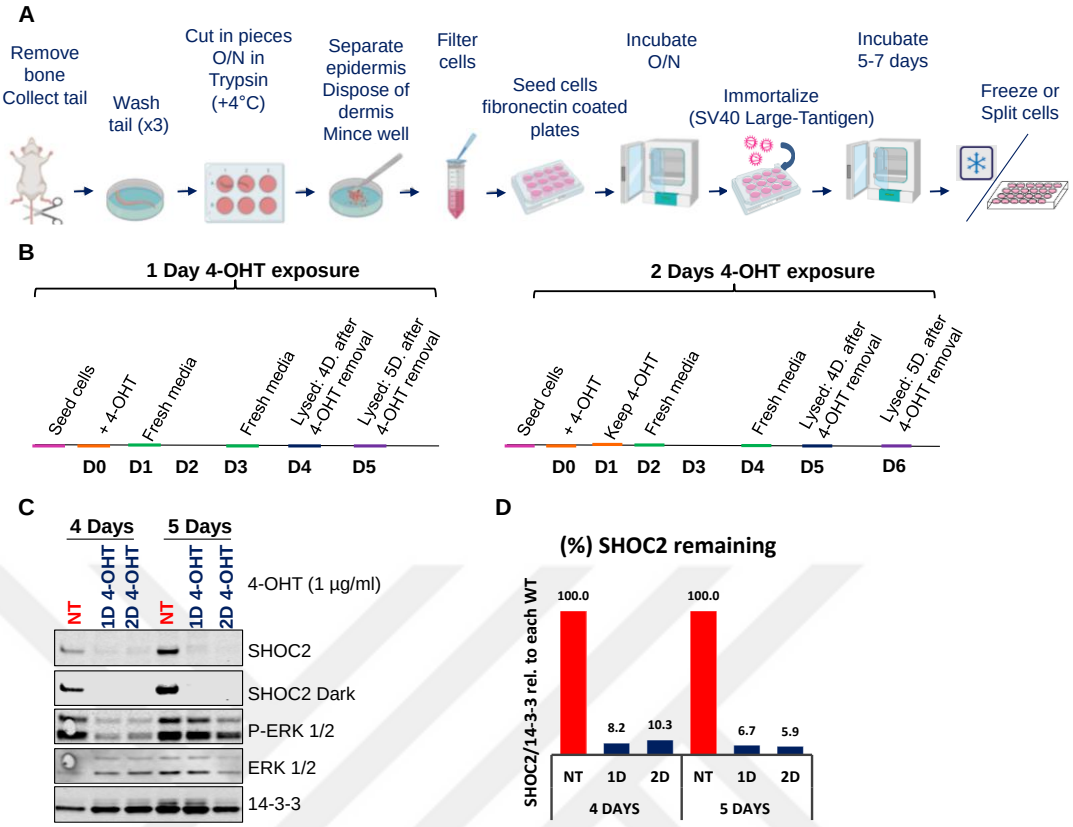

Figure 5-11. Shoc2 inactivation *in vitro* in immortalized epidermal keratinocytes from the tail of adult mice

A. Schematic protocol of the generation of immortalized epidermal keratinocytes from the tail of 6-12 weeks old Shoc2 cKO mice.
B. Schematic layout of tamoxifen treatment to induce Shoc2 deletion in immortalized epidermal keratinocytes.
C. Western blot of lysates of keratinocytes in B.
D. Quantification of Shoc2 levels relative to 14-3-3- loading control of (C) using Odyssey CLx Imaging system (LI-COR). Protein levels of each non-treated cells were set to 100%. NT: Non Treated, 1D: 1 day of 4-OHT treatment and 2D: 2 days of 4-OHT treatment.

Next, we examined the role of acute Shoc2 inactivation on the proliferation of immortalized keratinocytes by performing Incucyte growth curves. Immortalized keratinocytes were seeded sparsely and images captured at regular intervals to plot confluence over time. Shoc2 ablation by 4-OHT treatment led to slower proliferation of Shoc2 KO keratinocytes compared to untreated cells (Figure 5-12A). While non-treated keratinocytes reached ~85% confluence after 3 days in culture, Shoc2 KO cells were only ~45% confluent (Figure 5-12B). Thus, Shoc2 is required for efficient proliferation of murine keratinocytes.

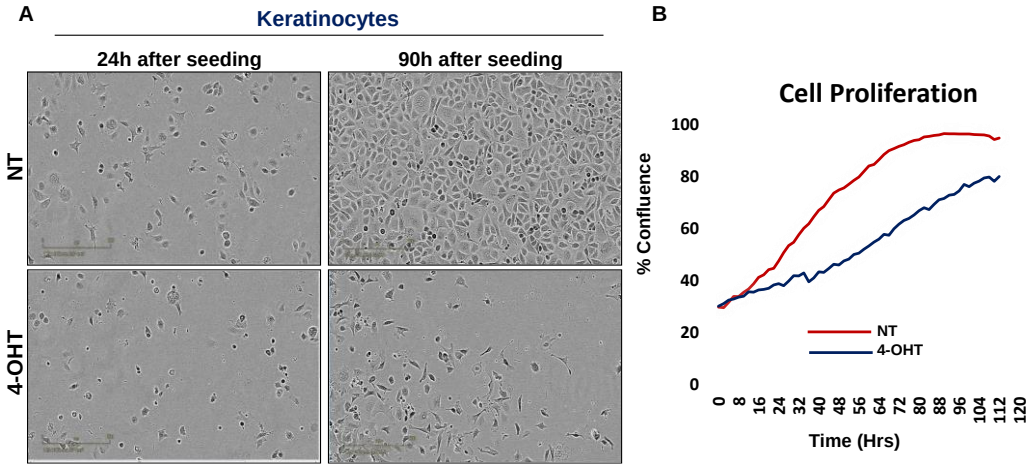

Figure 5-12. Shoc2 inactivation decreases cell proliferation of immortalized epidermal keratinocytes

A. Phase contrast images of immortalized non-treated (NT) parental and 4-OHT treated (1 day) Shoc2 KO epidermal keratinocytes after 24 and 96 hours of seeding. Scale bar is 300µm.
B. Incucyte growth curves were generated using the IncuCyte Live Cell imaging system.

A time course of EGF stimulation was performed in immortalized keratinocytes (Figure 5-13A). EGF induces ERK pathway activation with a peak at 5 minutes of the treatment and the response of the ERK pathway to EGF-stimulation is reduced on Shoc2 inhibition (Figure 5-13B).

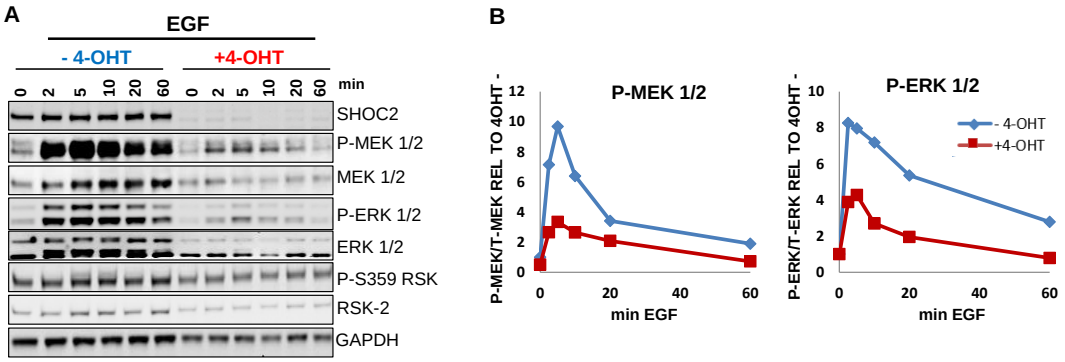

Figure 5-13. Shoc2 deletion reduces ERK pathway activation by EGF in immortalized murine keratinocytes

A. Shoc2 is required for ERK pathway activation on EGF treatment in immortalized murine keratinocytes. 4-OHT treated Shoc2 KO (+4-OHT) and untreated control (-4-OHT) keratinocytes were stimulated with 25 ng/ml of EGF for indicated time points and lysates probed with the indicated antibodies.
B. Quantification of P-MEK and P-ERK in (A), relative to control condition (0'mins of -4-OHT) using Odyssey CLx Imaging system (LI-COR).

Conclusions

The results presented in this study show that systemic inactivation of Shoc2 in adult mice results in skin dermatitis as well as a range of histopathological alterations that include epidermal hyperproliferation with hyperkeratosis, an increased number of hair follicles that fail to enter catagen and remain in aberrant anagen and a robust inflammatory cell infiltration. Immunophenotyping analysis of skin indicates that the inflammation is mostly attributed to increased numbers of $\gamma\delta$ T cells, a project that is currently under study in the laboratory.

In this chapter, we have also described the generation of a cellular model of acute Shoc2 inactivation in immortalized keratinocytes. Preliminary studies show that Shoc2 is required for efficient ERK pathway activation downstream of EGF as well as for efficient keratinocyte proliferation *in vitro*. Due to time constraints, only a limited analysis of this cell model was performed. However, these cells are currently being used by others lab members and will no doubt provide a useful model to further study the effects of Shoc2 inactivation at the biochemical and cellular level using genomics and proteomics approaches.

Strikingly, although *in vitro* proliferation assays show that keratinocytes display defective proliferation in the absence of Shoc2, Shoc2 ablation *in vivo* leads to epidermal hyperplasia, with increased proliferation and defective differentiation of keratinocytes in the skin. These results strongly suggest that the epidermal hyperproliferation observed *in vivo* is not a keratinocyte autonomous effect but rather is likely a consequence of inflammation driven by immune cells, with $\gamma\delta$ T cells likely playing a role. Future studies should address this possibility and extend this observations to the KI mouse model.

Chapter 6 Time-course study in adult *Shoc2*$^{fl/fl}$ *Rosa26-CreER*^{T2} mice

Introductory statement

As described in previous chapters, Shoc2 inactivation leads to several phenotypic changes in adult mice that include skin alterations, splenomegaly and enlarged bladders (in male mice only) and reduces median lifespan of Shoc2 KO mice to ~15 weeks. In this chapter, we aimed to track their rate of appearance of these phenotypes and measure their development over time, with a particular emphasis on skin alterations. To this end, Shoc2 KO, KI and WT mice were culled at different times of post-tamoxifen treatment and phenotypic differences investigated by histopathology and immunohistochemical analyses.

Periocular alopecia is the first phenotype developed

To monitor the rate of development of macroscopic fur and skin abnormalities, photographs of Shoc2 KO, KI and WT mice were taken weekly after tamoxifen treatment. The first phenotype to become apparent macroscopically in KO and KI mice was the loss of hair in a ring around the eyes (periocular alopecia). In KO mice, periocular alopecia could be observed starting at week 2, whereas in KI mice it was apparent at 3-4 weeks post-tamoxifen. This phenotype progressively got worse, and was accompanied by skin dermatitis around the eyes at later times (Figure 6-1).

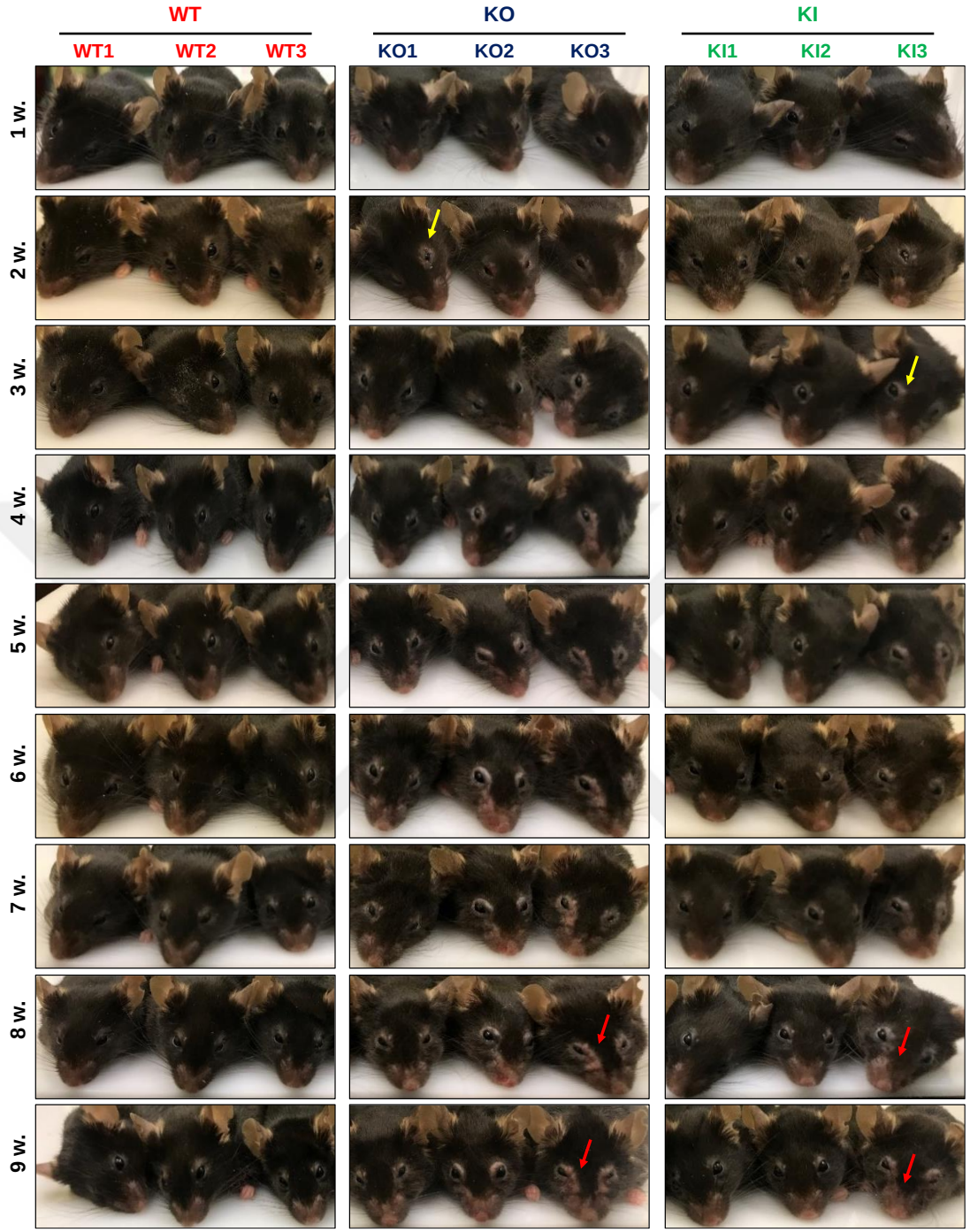

Figure 6-1. First characteristic phenotype of Shoc2 inactivation is periocular alopecia

Representative images of WT, KO and KI mice from 1 week to 9 weeks post-tamoxifen treatment to show characteristic progressive periocular alopecia (n=5 for each genotype and n=3 independent experiments). Yellow arrows indicate starting of periocular alopecia and red arrows show skin dermatitis around the eyes.

Periocular alopecia was followed by progressive alopecia in the throat area which began ~3-4 weeks post-tamoxifen for Shoc2 KO mice and ~8-9 weeks post-tamoxifen for Shoc2 KI mice, and that precede the development of skin lesions.

Mild skin lesions on the throat could be observed at ~4 weeks post-tamoxifen treatment in some but not all Shoc2 KO mice (i.e. 2/5 of KO mice) but after 6-7 weeks post-tamoxifen most mice had mild or moderate skin lesions (Figure 6-2). Alopecia and lesions on the throat area of Shoc2 KI mice emerged later and with lower penetrance (1/5 of KI mice had mild lesions at 9 weeks).

Figure 6-2. Following characteristic phenotype of Shoc2 inactivation is loss of fur and onset of dermatitis in the throat

Representative images of WT, KO and KI mice from 1 week to 9 weeks post-tamoxifen treatment to show loss of fur from throat and onset of skin dermatitis (n=5 for each genotype and n=3 independent experiments).

At later time points, starting from ~9-10 weeks post-tamoxifen treatment, Shoc2 KO mice developed mild skin lesions on their backs. Over time, lesions

progressed and became more severe, developing into crusty and/or ulcerated skin lesions (Figure 6-3A). As seen with the throat area, skin lesion on the back of Shoc2 KI mice developed later and were less severe, although no lesions were observed at ~10 weeks post-tamoxifen, dermatitis was observed in some mice at ~20 (Figure 6-3B).

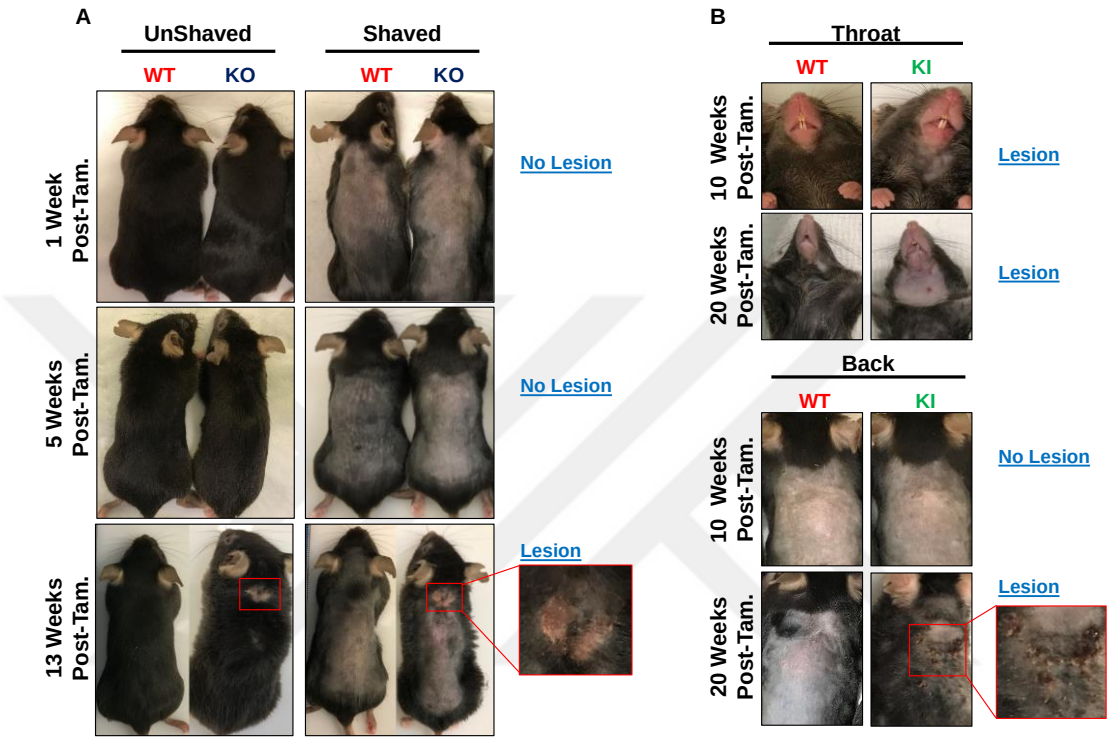

Figure 6-3. Dermatitis develops in the back skin of Shoc2 KO and KI mice at later time points

A. Representative images of age and gender matched WT and KO mice at 1, 5 and 13 weeks post-tamoxifen treatment to show dermatitis in the back skin. Inset shows higher magnification image of lesions (n=3 or 4 independent experiments).
B. Representative images of WT and KI age and gender matched littermate mice at 10 and 20 weeks post-tamoxifen treatment to show skin dermatitis in the throat and back skin. Inset shows higher magnification image of lesions (n=3 or 4 independent experiments).

Histological analysis of skin alterations caused by Shoc2 ablation

As discussed previously, Shoc2 inactivation leads to skin alterations that include increased number of hair follicles in the hypodermis, epidermal thickening (acanthosis), and immune cell infiltration in the dermis. In order to assess their rate of appearance, we culled Shoc2 KO, KI and WT mice starting from 1 week to 10 weeks post-tamoxifen treatment. Histological analyses revealed that the first

alteration observed in Shoc2 KO skin phenotypes was increased hypodermal hair follicles in the throat skin (Figure 6-4). As early as 1 week post-tamoxifen treatment, hair follicles from Shoc2 KO mice accumulate with variable severity in the adipose tissue and appear locked in the anagen phase. In contrast, follicles from aged-matched control WT mice were in the telogen phase. Of note, an aberrant number of hair follicles in the adipose tissue was observed in the absence of any apparent skin lesions on the throat at these times.

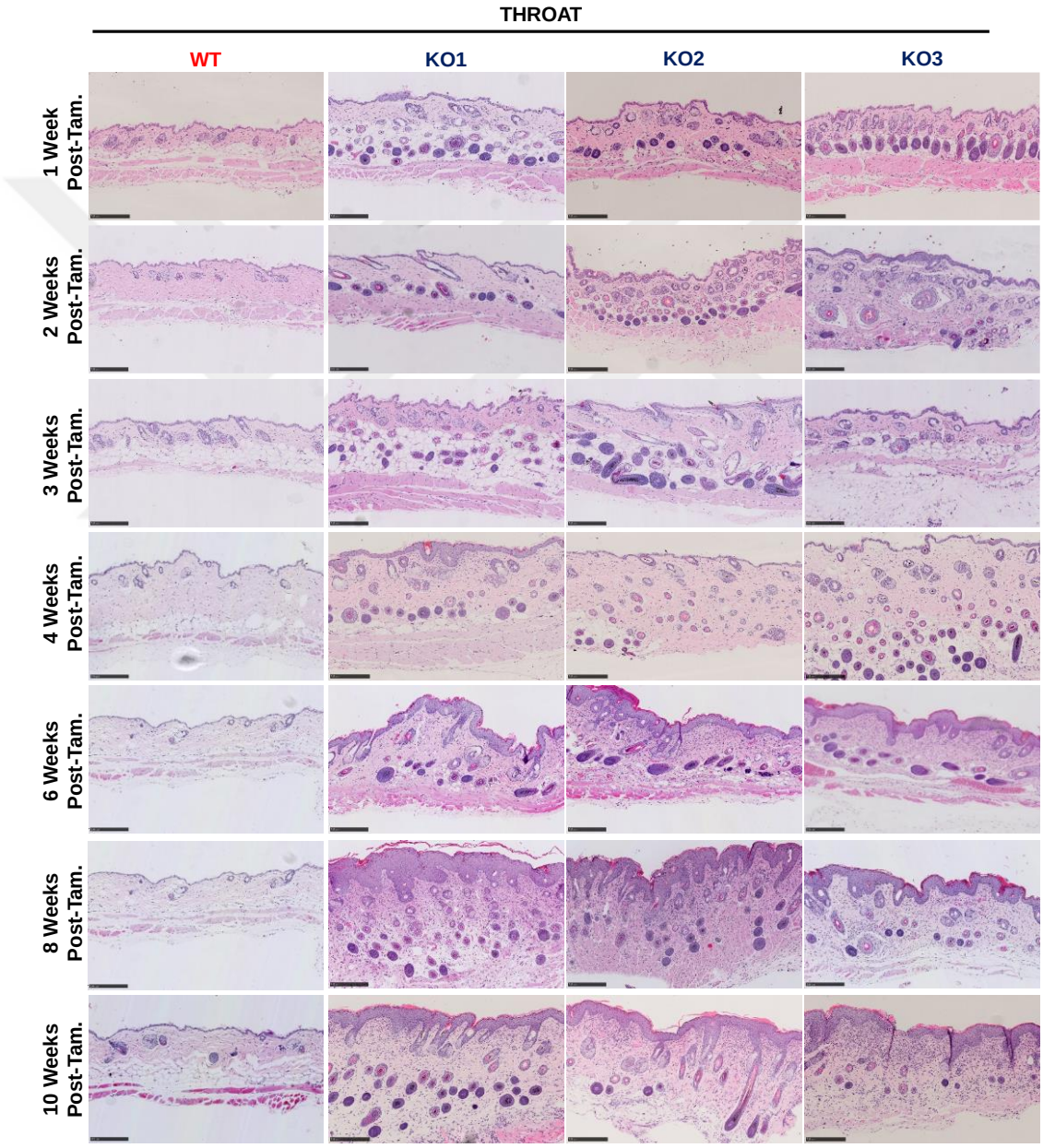

Figure 6-4. Increased hypodermal hair follicles on throat skin is the first microscopic alteration detected upon Shoc2 ablation

Representative H&E images from skin throat of WT and Shoc2 KO mice 1 to 9 weeks post-tamoxifen treatment (n=3 for each genotype). Scale bar=250 µm.

When samples of back skin were analysed, increased hair follicles in the hypodermis were not detected after 1 week (in contrast with skin samples from the throat area from the same mice) but were prominent after 5 weeks (Figure 6.5A), at a time where no skin lesions on the back could be observed. Thus, our observations indicate that abnormalities in hair follicles growth precede dermatitis and skin lesions and that they appear earlier on the throat area. A similar scenario was observed in skin from KI mice, although again with a delayed time course relative to KO mice, with increased hair follicle numbers in the hypodermis seen after 4 weeks in skin from the throat but not the back where alterations were nevertheless observed at ~10 week in some mice (Figure 6-5B).

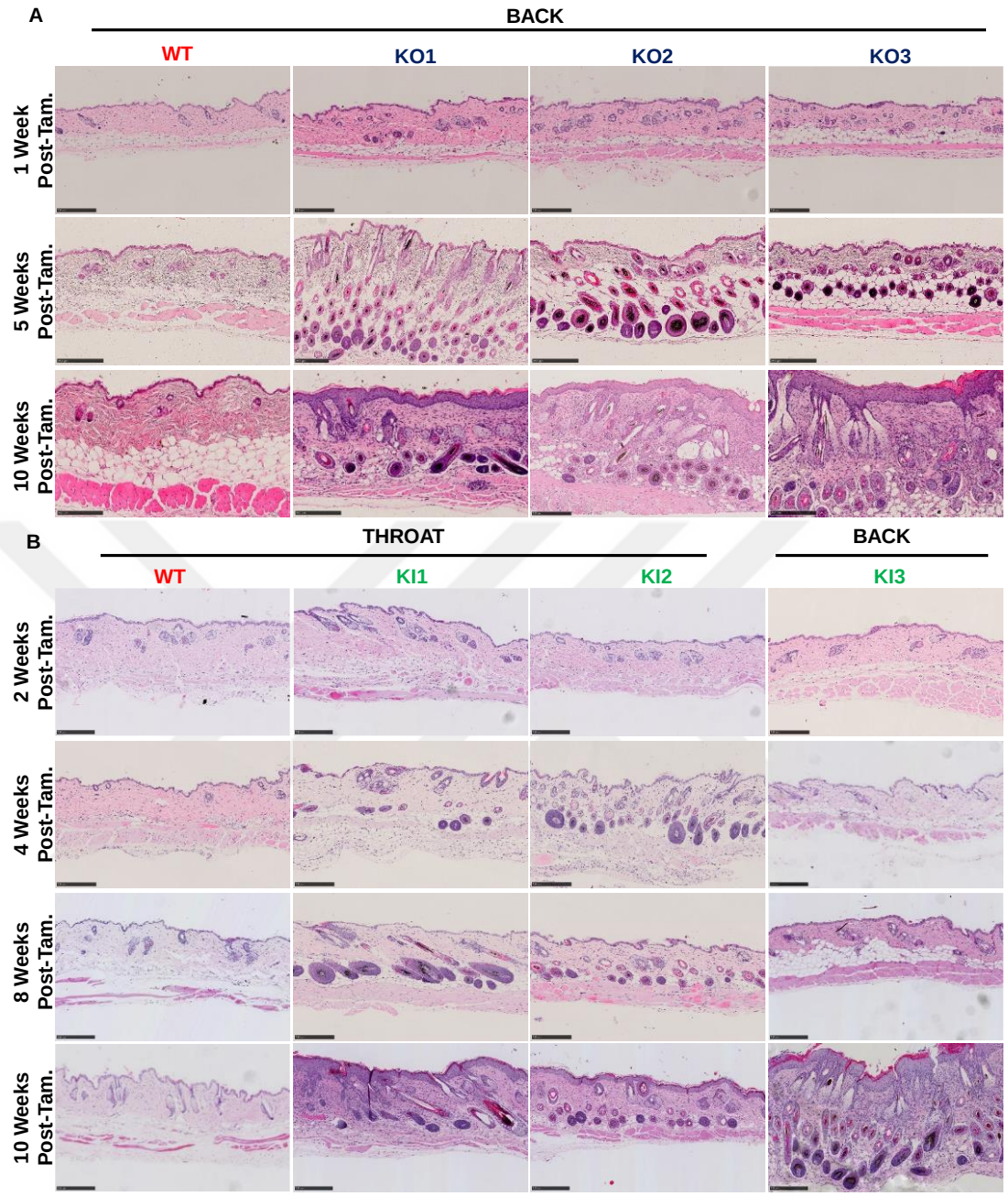

Figure 6-5. Increased hypodermal hair follicles are observed at later times in the back skin relative to the throat area for Shoc2 KO and KI mice,

A. Representative H&E images from back of WT and KO mice at 1, 5 and 10 weeks post-tamoxifen treatment to highlight increased hair follicles in the hypodermis of Shoc2 KO skin (n=3 for each genotype). Scale bar= 250 μm.
B. As above (A) but in the throat and back skin of Shoc2 KI mice (n=3 for each genotype). Scale bar= 250 μm.

Histologic examination of adult Shoc2 KO and KI skin revealed also marked epidermal thickening accompanied by hyperkeratosis. The time-course study revealed that the thicker epidermis in Shoc2 KO mice throat skin began to appear at

2 weeks post-tamoxifen treatment and increased gradually over time (Figure 6-6A and B). On the other hand, epidermal hyperplasia was milder and developed more slowly in KI mice (Figure 6-6A and B).

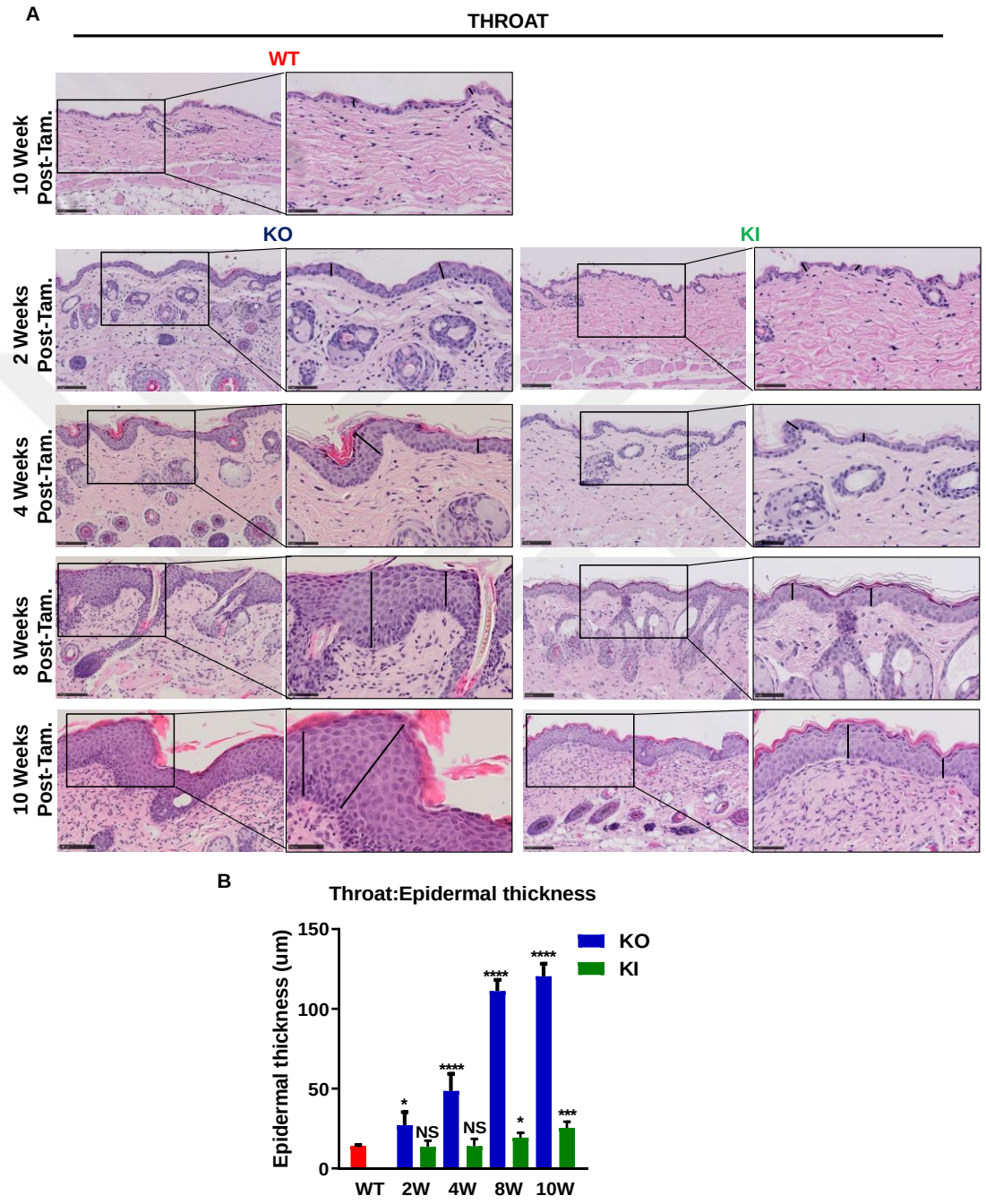

Figure 6-6. Epidermal thickening in Shoc2 KO and KI throat skin

A. Representative H&E images from throat skin of WT (10 weeks Post-Tam) and Shoc2 KO and KI mice (2, 4, 8 and 10 weeks Post-Tam.) to show epidermal thickness. Black bars indicate epidermal thickness (n=3 for each genotype). Scale bar=100 μm and inset= 50 μm.

B. Epidermal thickness quantification of throat skin sections from Shoc2 KO, KI and WT mice (n=3 for each genotype). Results are expressed as mean values ± SEM. Significance is determined using an unpaired student's t-test. *p< 0.05, ***p< 0.001 ****p< 0.0001 or NS: Not Significant.

In terms of back skin, epidermal thickening was clearly detectable 8 weeks post-tamoxifen treatment for Shoc2 KO mice and with less severity and lower penetrance in KI mice (Figure 6-7A and B).

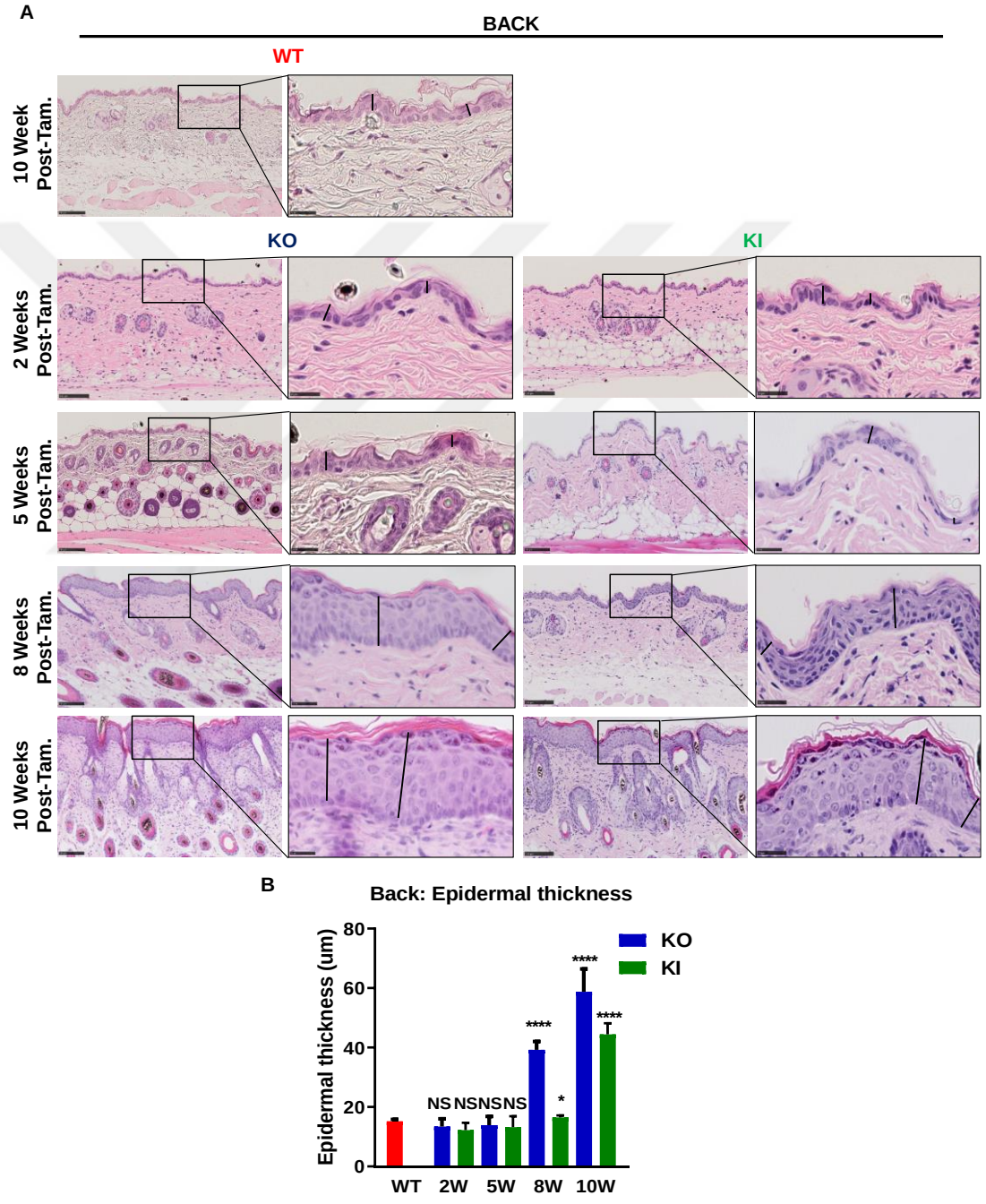

Figure 6-7. Epidermal thickening in Shoc2 KO and KI back skin

A. Representative H&E images from back skin of WT (10 weeks Post-Tam.) and Shoc2 KO and KI mice (2, 5, 8 and 10 weeks Post-Tam.) to show epidermal thickness. Black bars indicate epidermal thickness (n=3 for each genotype). Scale bar=100 μm and inset= 50 μm.
B. Epidermal thickness quantification of back skin sections from Shoc2 KO, KI and WT mice (n=3 for each genotype). Results are expressed as mean values ± SEM. Significance is determined using an unpaired student's t-test. *p< 0.05, ****p< 0.0001 or NS: Not Significant.

One of the critical histological observations of Shoc2 KO skin was immune cell infiltration in the dermis. To analyse the rate of infiltration of different immune cell populations, a similar staining panel as used in Figure 5-8 was used for IHC on throat skin samples of mice 2,4,6 and 10 weeks post-tamoxifen treatment. In addition to CD45 (common leukocyte), F4/80 (macrophages), GR1 (granulocytes), and CD3 (T cells) markers, toluidine blue staining was used for mast cells and Keratin 6 (K6) as a marker of keratinocyte activation (Figure 6-8). Two weeks post-tamoxifen a modest but significant increase in CD45 and CD3-positive cells could be observed within the dermis, and to a lesser degree in the epidermis, that increased over time and was very prominent by 4-6 weeks. This was parallel by $K6^+$ staining (keratinocyte activation) which could also be faintly detected at 2 weeks and increased prominently over time (Figure 6-8). In clear contrast, no significant increase in $GR1^+$ neutrophils, $F4/80^+$ macrophages or toluidine $blue^+$ mast cells could be detected at 2 weeks. However, increased numbers of all three cell types (neutrophils, macrophages and mast cells) could be detected from 4-6 weeks onwards. Thus, it appears that the first cells to be recruited to the skin upon Shoc2 ablation are T cells, which are then followed by the other cell types.

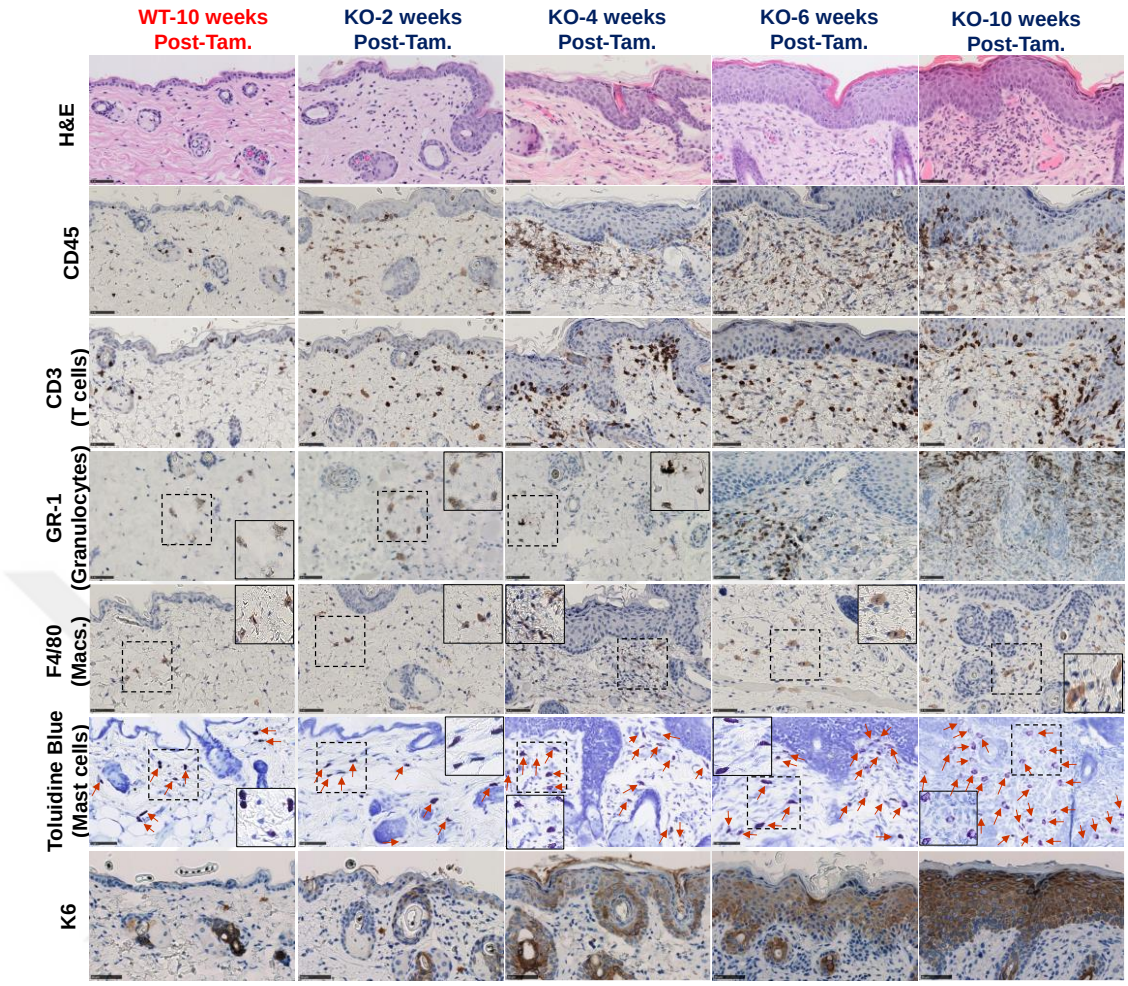

Figure 6-8. T cells are the first immune cells recruited to the skin upon Shoc2 ablation

Representative immunohistochemical staining of WT (10 weeks Post-Tam) and Shoc2 KO (2, 4, 6 and 10 weeks Post-Tam.) throat skin sections. Positive immunoreactivity is indicated by the brown color, with a blue hematoxylin counterstain. Toluidine blue staining used for mast cells (purple). Red arrows show mast cells (n=3 for each genotype). Scale bar=50 μm and inset=25 μm. This figure was generated with the help of Ayse Akarca from Teresa Marafioti lab.

We further characterised T-cell subpopulations by triple immunohistochemical staining with CD4, CD8 and FOXP3 markers for Shoc2 KO and WT throat skin at mice 2,4,6 and 10 weeks post-tamoxifen treatment and dorsal skin at morbidity (15 weeks post-tamoxifen treatment). Regulatory T cells (Tregs) were defined as $CD4^+/FOXP3^+$ cells, with CD4 (brown/orange signal) and FOXP3 (blue signal), and cytotoxic T cells were defined as $CD8^+$ cells with red/pink signal. Intriguingly, $CD3^+$ staining was consistently higher than $CD4^+$, $CD8^+$ and $CD4^+/FOXP3^+$ cells in the same selected area (Figure 6-9). This would be consistent with $TCR^+ \gamma\delta$ T cells being the $CD3^+$ cells involved as suggested by our immunophenotyping of skin by FACs (Figure

5-10A). Unfortunately however, we were unable to get staining of γδ T cells by IHC to work.

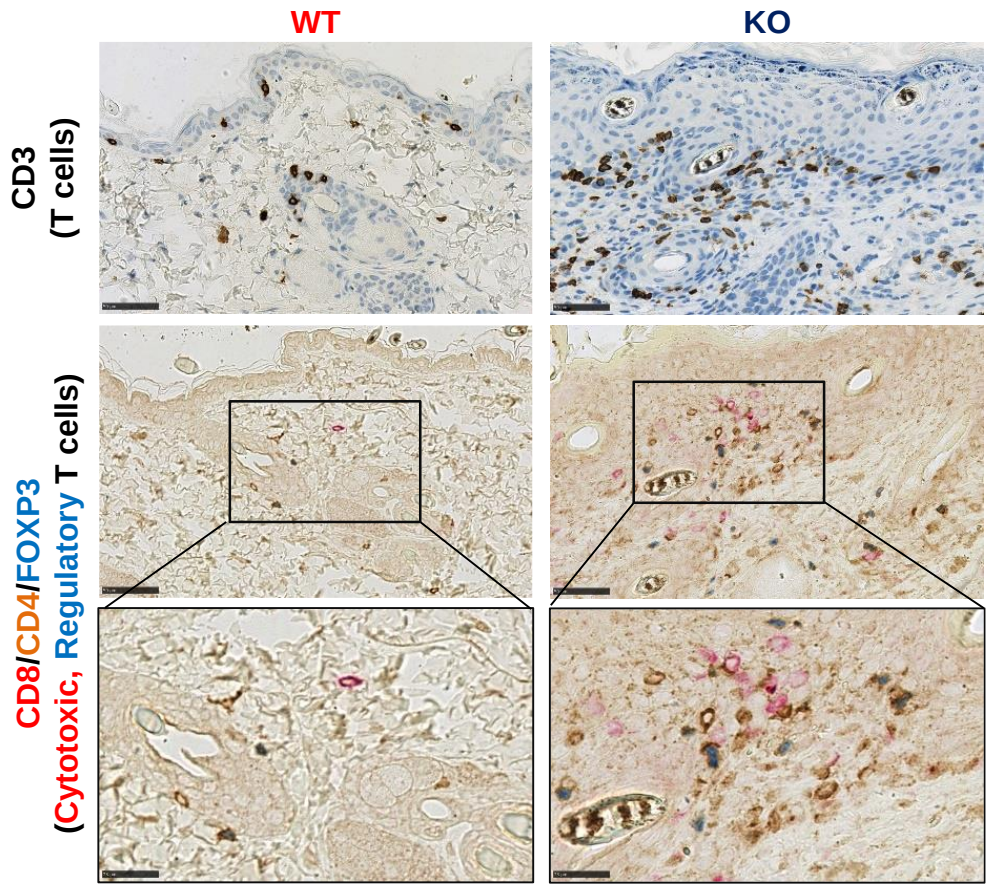

Figure 6-9. Immunohistochemical analysis reveals a high discrepancy between CD3⁺ and CD4⁺, CD8⁺ and CD4⁺/FOXP3⁺ staining in the WT and Shoc2 KO dorsal skin

Triple immunostaining for FOXP3 (blue), CD8 (red) and CD4 (brown) in the dorsal skin of WT and Shoc2 KO mice (n=3 for each genotype) at morbidity. Insets show higher magnification of indicated areas. Scale bar 50 μm and 25 μm (inset). Staining was performed by Ayse Akarca from Teresa Marafioti lab.

Using immunohistochemical sections from 2,4,6 and 10 weeks post-tamoxifen treatment and at morbidity, we counted the numbers of $CD8^+$ and $CD4^+/FOXP3^+$ double positive T lymphocytes and revealed a small but significant increase in cytotoxic T cells that became very prominent at morbidity. A more striking progressive increase in regulatory T cells in Shoc2 KO mice skin was also seen starting at 2 weeks post-tamoxifen treatment (Figure 6-10A and B). It is worth noting that the increase in CD3 cells seen by IHC contrasts with the previous FACs observation (Figure 5-10A) that showed a selective increase in γδ but not αβ T cells. The reason for this discrepancy is not clear but may be related to different experimental conditions (e.g.

antibodies used and method of cell isolation) and should be investigated in future experiments.

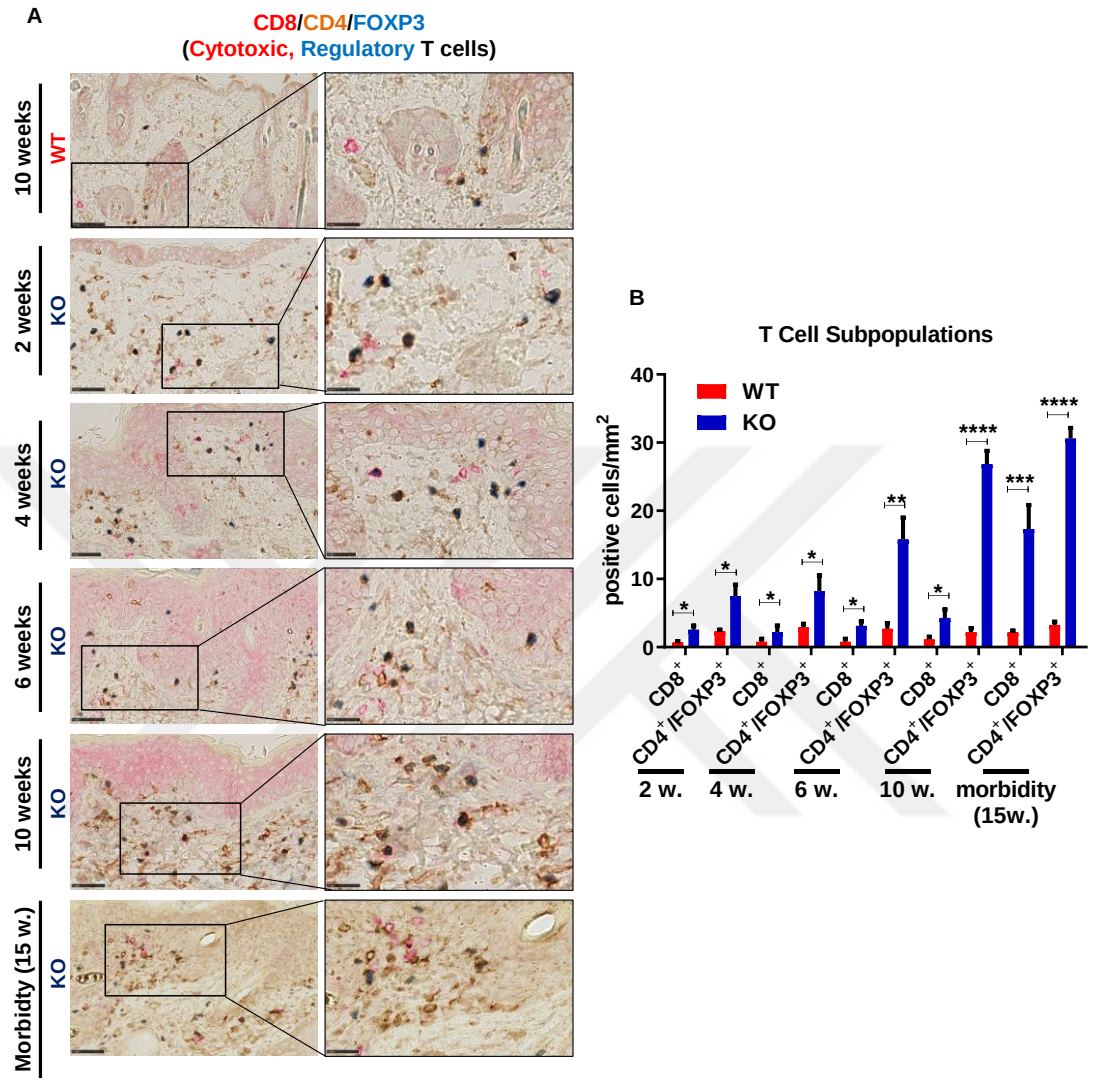

Figure 6-10. Immunohistochemical staining reveals Shoc2 deletion leads to increase in Tregs and cytotoxic T cells

A. Triple immunostaining for FOXP3 (blue), CD8 (red) and CD4 (brown) in the throat skin of WT at 10 weeks and Shoc2 KO mice at 2,4,6 and 10 weeks post-tamoxifen treatment as well as dorsal skin of WT and Shoc2 KO mice at morbidity (n=3 for each genotype). Insets show higher magnification of indicated areas. Scale bar=50 μm and 25 μm (inset). Staining was performed by Ayse Akarca from Teresa Marafioti lab.
B. Quantification of the infiltrating $CD8^+$ (cytotoxic) and $CD4^+/FOXP3^+$ (Tregs) T cells. Data are presented as mean values ± SEM of positive cells/mm^2. Significance is determined using an unpaired student's t-test NS: Not Significant.

Time-course study for skin dermatitis, splenomegaly and enlarged bladder phenotypes

As our Shoc2 KO mice developed pleiotropic phenotypic changes that in addition to skin abnormalities also consist of splenomegaly and lymphadenopathy as well as enlarged bladders of males, we aimed to examine the rate of onset of these phenotypic changes. To this end, we sacrificed Shoc2 KO, KI and WT control mice on different time points. At these time points, from 1 week to 10 weeks post-tamoxifen treatment, we quantified the severity of skin dermatitis, and upon necropsy, we measured the spleen weight and urine volume of bladders of male mice to see whether one phenotype precedes the others. The skin dermatitis severity scoring system revealed that Shoc2 KO mice developed significant macroscopic skin lesions starting at 4 weeks post-tamoxifen treatment that progressed in severity over time (Figure 6-11A). However, Shoc2 KI mice showed no skin phenotypes until 8 weeks post-tamoxifen treatment but began to develop minor skin lesions after this point and slightly increased in severity at 9 and 10 weeks post-tamoxifen treatment, but importantly this increase was not statistically significant. The only significant increase in skin dermatitis score for Shoc2 KI mice was reported at morbidity (mean survival=34 weeks post-tamoxifen treatment) (Figure 6-11A).

In contrast to skin severity, no significant difference in splenomegaly was detected until 5 weeks post-tamoxifen treatment for Shoc2 KO mice. With regard to Shoc2 KI mice, there was no significant increase in spleen weights at the latest time point of this experiment (10 weeks post-tamoxifen treatment) and only in independent cohorts at morbidity (mean survival=34 weeks post-tamoxifen treatment) was a significant increase detected (Figure 6-11B). Collectively, these findings indicate that skin dermatitis precedes splenomegaly suggesting splenomegaly and lymphadenopathy could be secondary to the progressively more severe skin inflammation that develops in Shoc2 KO mice (see final discussion).

Another phenotype of Shoc2 inactivation identified in this study is a male-specific urinary bladder enlargement that is observed with incomplete penetrance. Although not achieving statistical significance, a tendency for progressively more enlarged bladders was observed at 5 and 10 weeks but was highly significant at morbidity (mean survival=15 weeks post-tamoxifen treatment) (Figure 6-11C). Thus,

bladder enlargement, like splenomegaly appear to develop with a delayed rate relative to dermatitis, i.e. after longer periods of sustained Shoc2 inactivation.

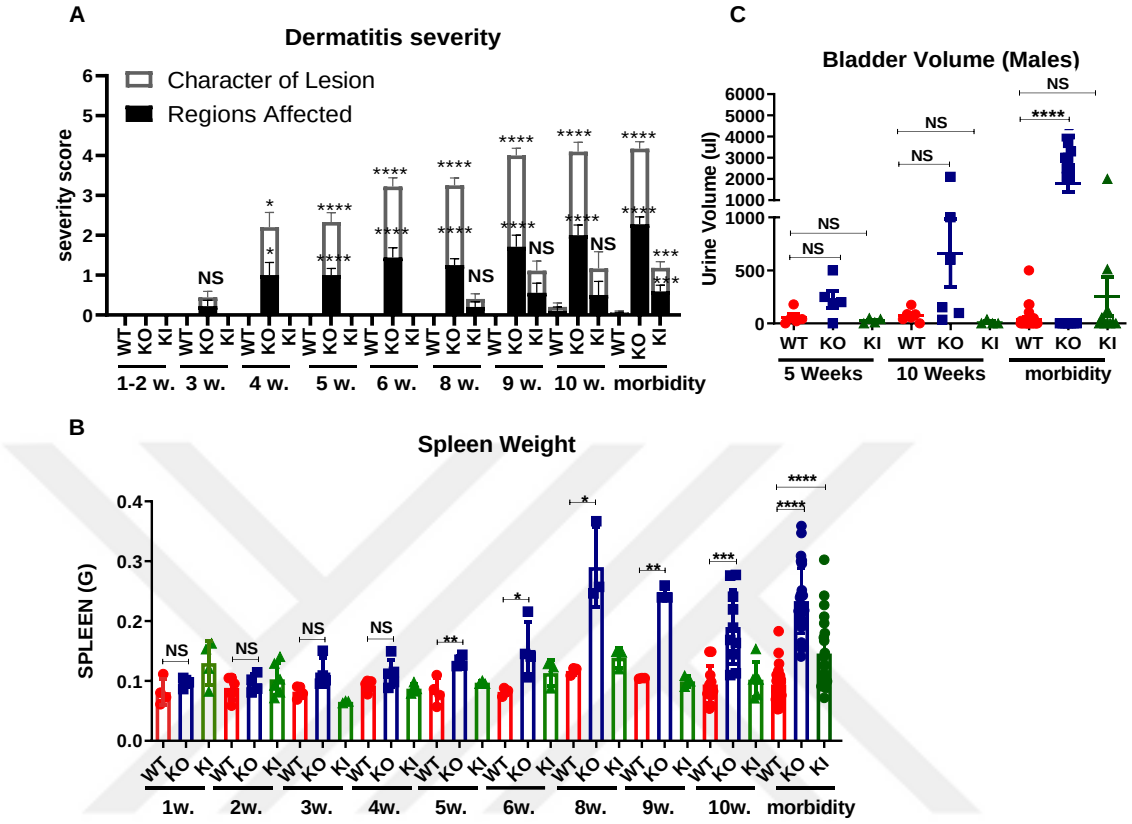

Figure 6-11. Time-course study for Shoc2 inactivation associated phenotypes reveals that skin dermatitis precedes splenomegaly and bladder enlargement

A. Severity score of dermatitis was assessed from 1 week to 10 weeks post-tamoxifen treatment as well as at morbidity (~15 weeks Post-Tam. for Shoc2 KO and ~34 weeks for Shoc2 KI) in mice of the indicated genotypes. Data are presented as mean values ± SEM. Significance is determined using an unpaired student's t-test *p< 0.05, ****p< 0.0001 or NS: Not Significant. 1-9 weeks Post-Tam.: (n=3-6 for each genotype), 10 weeks Post-Tam.: WT and KO (n=10) KI (n=6), Morbidity: WT and KO (n=24) KI, (n=22).
B. Quantification of Shoc2 KO and KI spleen weights compared to that of WT mice from 1 week to 10 weeks post-tamoxifen treatment. Data are represented as means ± SEM. Significance is determined using an unpaired student's t-test *p< 0.05, **p<0.01, ***p<0.001. 1-9 weeks Post-Tam.: (n=3-6 for each genotype), 10 weeks Post-Tam.: WT and KO (n=10) KI (n=6), Morbidity: WT and KO (n=24) KI, (n=22).
C. Quantification of urine volume in Shoc2 KO, KI and WT male mice. Data are presented as mean ± SEM. Significance is determined using an unpaired student's t-test ****p< 0.0001 or NS: Not Significant. 5 and 10 weeks Post-Tam: (n=5-6 for each genotype), Morbidity: WT and KO (n=17) KI, (n=13).

Conclusions

The work presented in this chapter shows that periocular alopecia is the first characteristic sign observed macroscopically after Shoc2 inactivation (~2 weeks Post-Tam. in Shoc2 KO and ~3-4 weeks in KI mice respectively) followed by thinning and loss of fur from the throat area (~3-4 weeks for Shoc2 KO and ~8-9 weeks for Shoc2 KI). Skin lesions appeared first in the face and/or throat regions and later in the back skin for both Shoc2 KO and KI mice. On the other hand, increased hypodermal hair follicles can be detected as early as 1 week post-tamoxifen treatment and is the earliest phenotype identified upon Shoc2 inactivation. Inflammation and epidermal hyperproliferation can be observed starting at 2 weeks in the throat area, with T cells (likely $\gamma\delta$ T cells) being the first immune cells recruited, followed by granulocytes, macrophages and mast cells. Splenomegaly becomes significant after the onset of dermatitis, suggesting a systemic inflammatory phenotype could be the result of to the severe skin inflammation observed after sustained Shoc2 inactivation.

Chapter 7 Discussions and Future Perspectives

Discussion and future perspectives

The results presented in this research project, contribute to characterising the function of Shoc2 at the organismal level and understanding its role in tissue homeostasis by analysing phenotypic changes associated with systemic genetic Shoc2 inactivation in mice.

Role of Shoc2 in development

The physiological importance of Shoc2 in development has been underlined by a previous report (Yi et al. 2010) showing that constitutive *Shoc2* deletion leads to embryonic lethality at E8.5 whereas endothelial-specific Shoc2 deletion cause a range of cardiac defects at E13.5 and subsequent death of the embryo at E15.5. This study reveals that *Shoc2* deficiency in endothelial cells leads to defects in the development of heart valves (valvulogenesis) and endothelial-mesenchymal transformation, which is a critical step in endocardial cushion formation. Intriguingly because ERK activation did not appear to be affected in Shoc2-deficient endothelial cells, Yi et al. (2010) suggest Shoc2 may act in an ERK-independent pathway for its essential function in valvulogenesis (Yi et al. 2010). Interestingly, *BRaf* KO mice have a similar time point of embryonic lethality that is associated with disrupted vasculature, as well as showing sporadic haemorrhaging and subcutaneous oedema, due to incomplete formation of an endothelial layer lining the vessels. Because Shoc2 function is required for BRAF activation (by dephosphorylation of the S365 inhibitory site) it is tempting to speculate that embryonic death due to defective vasculature upon Shoc2 deletion might occur due to subsequent inactivation of BRAF (Wojnowski et al. 1997; Yi et al. 2010).

In our study, we have further confirmed that Shoc2 deficiency results in embryonic lethality. After examining a progeny of more than 50 mice from Shoc2 heterozygous mouse intercrosses, not a single mouse with homozygous Shoc2 deletion was born. Furthermore, we show for the first time that inactivation of Shoc2 by the D175N mutation also results in embryonic lethality at the same stage of embryogenesis of E8.5 (Figure 3-2B and C). This D175N substitution in Shoc2 disrupts the formation of the SHOC2-MRAS-PP1 complex but preserves other scaffold functions of Shoc2 such as the ability to interact with the polarity proteins

SCRIB (Young et al. 2013). This suggests that, embryonic lethality upon Shoc2 inhibition at E8.5 is dependent on its RAF phosphatase function, which is essential for ERK pathway activation and would be consistent with ERK pathway dependant function of Shoc2 being important during embryogenesis. Further studies are required to establish the exact cause of death of the embryos and the importance of Shoc2 for embryonic development and the signalling mechanisms which is involved.

Role of Shoc2 in tissue homeostasis in adult mice

There is no previous report of systemic Shoc2 inactivation in adult mice; however as mentioned in the introduction, a wide array of findings exists in the literature about depletion of the other key components of the RAS-ERK pathway. Upon complete elimination of RAF, MEK or ERK function by systemic genetic inhibition of the A, B and C*Raf, Mek1 and 2* or *Erk1 and 2* paralogues, mice die within 2-3 weeks from multiple organ failure (Blasco et al. 2011; Sanclemente et al. 2018). In clear contrast, the results presented in this thesis show that after efficient elimination of Shoc2 in all tissues (except brain), mice survive considerably longer, with a median lifespan of ~15 weeks and 34 weeks for Shoc2 KO and KI mice, respectively (Figure 4-3A). Thus, our results suggest that systemic Shoc2 inactivation is tolerated considerably better than the RAF, MEK or ERK nodes of the ERK-MAPK pathway. This is despite the fact that uniquely among the many components of the ERK-MAPK pathway, including RTKs, SOS, RAS, RAF, MEK and ERK nodes, SHOC2 does not have any paralogues. In addition, the milder toxicity of Shoc2 inactivation in mice is consistent with genetics studies in *C.elegans*. In contrast to RAF (Lin-45), MEK and ERK (Sur-1), SHOC2 (Sur-8) was not an essential gene for organ development or viability although it was necessary for RAS oncogenic phenotypes (Selfors et al. 1998; Sieburth et al. 1998).

A recent study from the lab helps explain why Shoc2 inactivation has no effect of on ERK phosphorylation on tissue lysates (Figure 3-6A-C and Figure 3-8E) and is tolerated better than RAF, MEK or ERK nodes of the pathway, which are essential core components absolutely required for pathway activation and for viability (Boned Del Rio et al. 2019). There appears to be redundancy at the level of the Shoc2 node, where Shoc2 can play a key contribution to RAF and ERK pathway activation in some contexts (e.g. downstream of EGFR activation), but not in other contexts where RAF and ERK activity can be activated independently of SHOC2 (Boned Del Rio et al.

2019).This redundancy and selective context-dependent contribution of Shoc2 to ERK-pathway signalling likely helps explain why Shoc2 deletion is better tolerated in adult mice than core, non-redundant, ERK-pathway nodes.

Our lab has also shown that Shoc2 is critical for tumour development in autochthonous KRAS-driven lung cancer mouse models. Shoc2 inactivation using either Shoc2 KO or KI^{D175N} approaches, inhibits overall tumour burden, delays tumour progression, and significantly increases overall survival in both the $Kras^{G12D}$ (K model) or the more severe KP (with a $Trp53^{R172H}$ allele) mouse models (Jones et al. 2019). Taken together, these observations of a dependency of oncogenic RAS on SHOC2 function, together with our data highlighting that Shoc2 inhibition in adult mice is tolerated better than targeting other nodes of the ERK pathway, suggests SHOC2 inhibition in the clinic could provide better therapeutic margins than current therapies that target RAF, MEK or ERK nodes of the pathway.

However, pleiotropic phenotypes do emerge after sustained Shoc2 ablation. One of the major findings presented in this study is that systemic Shoc2 inactivation in adult mice causes skin dermatitis (Figure 4-5) which progresses in severity until mice need to be euthanized (according to the terms of the lab's PPL licence) and is the main cause of death for Shoc2 mice. In line with this dermatitis phenotype, Shoc2 ablation causes several alterations in the skin and its appendages such as hair follicles. In addition, Shoc2 inactivation leads to enlarged urinary bladders in male, but not female mice.

Role of Shoc2 in hair follicle cycle

The earliest phenotype observed upon Shoc2 inactivation is a sharp increase in the number of hair follicles in the subdermal adipose layer (hypodermis). The hair follicles appear to remain in an aberrant anagen phase unable to enter the catagen phase.

The EGFR signalling pathway plays a crucial role in hair follicle homeostasis and both hyperactivation and inactivation of the pathway can impair the hair growth cycle (Kern et al. 2011; Doma et al. 2013). Importantly, animal models show that EGFR signalling regulates the transition of anagen to catagen stage of hair growth cycle (Hansen et al. 1997; Schneider et al. 2008). Loss of EGFR activity causes a disordered arrangement of hair follicles and blocks exit from anagen and entry to

catagen (Murillas et al. 1995; Lichtenberger et al. 2013; Mascia et al. 2013; Bichsel et al. 2016) eventually leading to progressive hair degeneration and alopecia as well as inflammation (Doma et al. 2013). Considering the known key role of Shoc2 in ERK pathway activation by EGF, all these observations taken together strongly suggest that Shoc2 is a key component downstream of the EGFR pathway in regulating the hair growth cycle, particularly the anagen-to-catagen transition.

Furthermore, gain-of-function S2G mutation in SHOC2 in humans cause a subtype of Noonan syndrome (Noonan Syndrome with Loose Anagen Hair) that is characterized for its unique hair phenotype (Cordeddu et al. 2009; Dhurat and Deshpande 2010; Komatsuzaki et al. 2010; Kane et al. 2017). Hairs are predominantly in the anagen phase and are easily pluckable, sparse, and slow growing with distorted and misshapen bulbs, ruffled cuticles, and absent inner and outer root sheaths (Dhurat and Deshpande 2010). Therefore, Shoc2 loss-of-function in mice and gain-of-function in humans cause defects in the hair cycle underscoring a key role for Shoc2 in the regulation of the anagen to catagen transition of the hair cycle.

Because aberrant numbers of hair follicles is the first phenotype to appear upon Shoc2 ablation, preceding skin inflammation, it is possible that it could be a driver of the inflammatory response in the skin, for example leading to a stress response in epithelial keratinocytes. Murillas et al. (1995) described transgenic mice expressing an EGFR dominant-negative mutant in the basal layer of the epidermis and outer root sheath of hair follicles with striking alterations in the development of hair follicles, which fail to enter into catagen stage, in a phenotype reminiscent of that observed upon Shoc2 deletion. The skin in these mice also shows strong infiltration with inflammatory elements (Murillas et al. 1995). However, inflammation was seen after hair follicles underwent necrosis (with mice developing alopecia) which is not seen in Shoc2 mice. Furthermore, Lichtenberger et al. (2013) reported that mice lacking epidermal EGFR display hair follicle degeneration and skin inflammation. Yet, skin inflammation was still seen in a hairless (hr/hr) background indicating that skin inflammation is not induced by hair follicle degeneration (Lichtenberger et al. 2013). Thus, the role of defects on hair growth upon Shoc2 inactivation in driving the skin inflammatory response (see also below) remains unclear and needs further investigation.

Role of Shoc2 in bladder function

In this study, we also discovered a sexually dimorphic role of Shoc2 in urinary function, with male, but not female KO mice developing severely distended bladders full of urine. No significant histopathological change such as epithelial hyperplasia or tumour formation were detected in bladder and urethra of Shoc2 KO mice. In addition, no renal damage is obvious in mice with enlarged bladders. Urethral obstruction is known as the most common cause of bladder distention in humans (Docherty et al. 2006). This obstruction can be caused by anatomic abnormalities such as prostate enlargement (Dmochowski 2005). However, the prostate glands of Shoc2 KO mice were of normal size and appearance without any obvious histological abnormalities. Furthermore, affected mice appeared able to urinate normally and water consumption was unaltered. Thus, urethral or prostate obstruction appear unlikely to be responsible.

On the other hand, non-obstructive causes of urinary retention include neural problems interfering with signalling between the brain and bladder and a weakened bladder muscle. Insufficient contraction of the bladder detrusor muscle can lead to, some or all of the urine remaining in the bladder (Yoshimura and Chancellor 2004). Intriguingly, Estrada et al. (2006) demonstrated that inhibition of EGFR pathway by EGFR inhibitors attenuates smooth muscle proliferation resulting from sustained distension of the urinary bladder (Estrada et al. 2006). Thus, defective EGFR signalling in smooth muscle cells in the absence of Shoc2 may play a role that needs further investigation.

Strikingly, mice deficient for M-Ras, another subunit of SHOC2 holoenzyme complex, also develop urinary retention and enlarged bladders uniquely in males in the absence of obvious anatomical outlet obstruction, a phenotype that exacerbates with age (Ehrhardt et al. 2015). Ehrhardt et al. (2015) suggest that M-Ras may regulate bladder control in male mice by regulating expression of muscarinic receptors M2R and M3R which play an important role in the control of micturition by mediating the cholinergic contractile stimuli of the detrusor muscle (Ehrhardt et al. 2015). Studies have shown that muscarinic receptors, particularly M3R, is critical for voiding in male mice (Matsui et al. 2000; Matsui et al. 2002), whereas its contribution to female micturition is small, as it is mediated by purinergic signalling instead (Matsui et al. 2002; Burnstock 2014).

Ehrhardt et al. (2015) showed that M-Ras KO mice had elevated M2R expression but impaired upregulation of M3R expression that is seen with age, leading to lower ratios of M3R/M2R expression that correlated with the bladder abnormalities (Ehrhardt et al. 2015). Although further studies are required to better understand the role of Shoc2 and M-Ras in the urinary system, the similar phenotype in M-Ras and Shoc2 deficient mouse models strongly suggest that their function within the MRAS-SHOC2-PP1 holoenzyme complex is responsible for the abnormalities observed and highlight a role for this phosphatase complex in bladder function that remains to be clarified.

Shoc2 inactivation leads to skin inflammation

One of the main findings presented in this research project is that systemic Shoc2 inactivation in adult mice leads to skin dermatitis. Mice first develop periocular alopecia which is followed by progressive alopecia in the throat area. Subsequently, skin lesions develop on the throat, then around the eyes and back areas. These all areas which are accessible and prone to scratching and Shoc2 KO (and KI mice to a lesser degree) could be observed to frequently scratch themselves around the eyes and throat areas, likely due to pruritus. In line with this possibility, recent results from the lab show that serum IgE levels are found elevated in Shoc2 KO mice (data not shown). Histologic examination of Shoc2 KO and KI mice skin lesions revealed marked keratinocyte proliferation with defective differentiation leading to epidermal thickening accompanied by hyperkeratosis. The skin also developed an extensive dermal and epidermal inflammatory infiltrate containing a variety of immune cells. With all of these alterations, Shoc2 KO/KI mice are sharing pathological features associated with human chronic inflammatory skin syndromes such as Atopic Dermatitis (AD) and psoriasis (Brunner et al. 2017; Dainichi et al. 2018).

AD is a common chronic inflammatory skin disorder with underlying impaired barrier function and is accompanied by intense pruritus and related with T-helper type 2 mediated inflammation (Brunner et al. 2017; Dainichi et al. 2018; Kim et al. 2019) AD skin lesions exhibit distinct features including epidermal hyperplasia with hyperkeratosis, diminished terminal differentiation of keratinocytes and accumulation of extensive inflammatory T cells and mast cells in lesions (Hamid et al. 1994; Bieber 2008; Jin et al. 2009). In addition, mouse models of AD (Chan et al. 2001; Zheng et al. 2009) and most of the patients with AD present elevated serum IgE levels (Leung

et al. 2004; Jin et al. 2009). Mechanistically, AD is thought to initiate with barrier dysfunction due to impaired terminal differentiation of keratinocytes which allows increased penetration of cutaneous antigens and becomes chronic with the help of constant itching and a type 2 inflammation loop via IL-4 and IL-13 (Horimukai et al. 2014; Dainichi et al. 2018).

Psoriasis is another prevalent chronic inflammatory skin disease that is characterized by thickened epidermis with hyperkeratosis and parakeratosis (retention of nuclei within corneocytes) due to enhanced proliferation and diminished differentiation of keratinocytes. Furthermore, accumulation of neutrophils and a dense immune cell infiltration which predominantly consists of T cells, monocytes/macrophages and dendritic cell in epidermis and dermis, is another typical feature of psoriatic skin lesions (Wolk et al. 2009; Sabat et al. 2019). T helper-17 (Th17) cytokines such as IL-17 and IL-22 are regarded to be the main player of the disease. Activation of the IL-23/IL-17 axis in the skin defines psoriatic inflammation (van der Fits et al. 2009; Wohn et al. 2013) and this activation is believed to initiated by the activation of skin-resident DCs which produce IL-23, driving Th17 cells to produce IL-17 and IL-22. Then, IL-17 activates epidermal keratinocytes to produce proinflammatory cytokines and chemokines which mostly attract neutrophil recruitment and thus propagate psoriatic inflammation (Type 17 inflammatory loop) (Dainichi et al. 2018; Sabat et al. 2019).

Similar to both AD (Guttman-Yassky et al. 2009; Suarez-Farinas et al. 2011) and psoriatic skin lesions (Wolk et al. 2009; Eberle et al. 2016), ablation of Shoc2 results in an expansion of both the basal and suprabasal layers of the epidermis with highly increased expression of K14 and K10, respectively, as well as hyperproliferation marker K6; but differently also enhances the final stages of terminal differentiation with more extensive loricrin expression (Figure 5-4 and 5). Although most of the studies show that both AD and psoriatic skin have diminished expression of skin barrier proteins including loricrin (Guttman-Yassky et al. 2009; Wolk et al. 2009; Eberle et al. 2016; Kim et al. 2019), other shows that similar to our results, loricrin expression is significantly increased in both AD (Jensen et al. 2004) and psoriasis (Ha et al. 2014).

Immunophenotyping of skin by FACS reveals that the earliest difference detected in Shoc2 KO mice is a strong increase in $\gamma\delta$ T cells that appear to be the first immune cells recruited. Immunohistochemical staining also shows an increase in

$CD3^+$ T cells in Shoc2 KO skin, starting at 2 weeks post-tamoxifen treatment that precedes the increase in granulocytes ($GR\text{-}1^+$) and macrophages ($F4/80^+$). In line with the over-scratching phenotype of Shoc2 KO mice, mast cells are also found elevated in those mice. Unfortunately, the expansion of γδ T cells could not be confirmed by IHC due to technical issues but, the discrepancy between high $CD3^+$ T cells and low αβ T cells consistent with increased levels of γδ T cells in Shoc2 KO mice skin. Future studies with frozen cryosection immunofluorescence staining for γδ T cells may validate the increase of this population in Shoc2 KO mice skin.

γδ T cells are important players of both innate and adaptive immune systems by serving as the guardians of the skin, lung, reproductive tract, and intestine epithelium against trauma, infection, and other forms of damage. In the epidermal skin, γδ T cells exhibit dendritic morphology (DETCs) and upon damage/stress signals of local keratinocytes they produce growth factors to initiate wound healing and also trigger macrophage recruitment to assist in inflammation (Fay et al. 2016). Dermal γδ T cells (round in morphology) are mainly responsible for pathogenic inflammatory responses via secreting several inflammatory chemokines and cytokines, particularly IL-17 (O'Brien and Born 2015).

Previous studies have shown γδ T cells have a key role in psoriasis, through IL-17 production (Mabuchi et al. 2011; Sumaria et al. 2011; Sandrock et al. 2018). IL-23 drives IL-17 synthesis from dermal γδ T cells which are the main IL-17-producing lymphocyte subset within the skin during psoriasis, and this further expands the Th17 pool (Cai et al. 2011a). IL-17 leads to the recruitment of more neutrophils, lymphocytes, and myeloid cells creating a positive feedback loop that maintains cutaneous inflammation and causes epidermal hyperplasia (Onishi and Gaffen 2010a; Cruz et al. 2018). On the other hand, IL-17-producing γδ T cells also appear to be involved in the regulation of IgE production, which indicates they might also play an important role in AD (Kamijo et al. 2020). Future studies, for instance using *Tcrd*$^{-/-}$ mice (Sandrock et al. 2018) should address the role of γδ T cells and IL-17 in driving the skin inflammation seen upon Shoc2 ablation. Similarly, genetic or pharmacological inhibition with neutralizing antibodies could be used to assess the contribution of Th2 cytokines such as IL-4 and IL-13. Regardless, the increased pruritus and elevated serum IgE levels observed in Shoc2 KO mice are consistent with sustained Shoc2 inactivation leading to an atopic dermatitis-like inflammatory syndrome.

Importantly, mouse models with disruption of components of EGFR/RAS/RAF/MEK/ERK signalling pathway also develop dermatitis with striking similarities (Murillas et al. 1995; Hobbs et al. 2004; Mukhopadhyay et al. 2011; Lichtenberger et al. 2013; Raguz et al. 2016). For instance, Raguz et al. (2016) show that epidermis restricted BRAF/CRAF KO mice exhibit a skin disease similar to human AD which starts with a barrier defect accompanied by the reduced expression of tight junction proteins and then progresses with the increased expression of Th2-type cytokines and chemokines produced by keratinocytes as well as mast cell infiltration (Raguz et al. 2016). In addition, Yang et al. (2010) showed that mice lacking *FGFR1* and *FGFR2* receptors in keratinocytes develop an AD-like skin phenotype. Interestingly, as observed in Shoc2 KO mice, an increase in the number of γδ T cells was also seen in *FGFR 1/2* KO mice prior to the development of the phenotype (Yang et al. 2010).

Pharmacological inhibition of EGFR/RAS/RAF/MEK/ERK pathway also causes cutaneous complications. Increased pruritus as well as acneiform eruptions (rashes) and xerosis are the most frequent side effects observed in patients treated with EGFR inhibitors (Fischer et al. 2013; Guggina et al. 2017a). Such manifestations can be seen also in patients treated with RAF (Anforth et al. 2012; Mandala et al. 2013) and MEK inhibitors (Manousaridis et al. 2013b; Russo et al. 2018).

In summary, our observation that cutaneous toxicities seen upon Shoc2 inactivation are very similar to those seen upon genetic and/or pharmacological inhibition of the EGFR/RAS/MAPK pathway is entirely in line with Shoc2's role as a key player required for efficient ERK-MAPK activation downstream of EGFR and with a key role of the EGFR/RAS/MAPK pathway in skin homeostasis (Doma et al. 2013).

Based on all the skin alterations observed upon Shoc2 inactivation in adult mice, we hypothesised that systemic ablation of Shoc2 leads to inflammatory skin disease with similarities to both atopic dermatitis and psoriasis (Figure 7-1). We speculate that Shoc2 inactivation and the subsequent inhibition of the ERK-MAPK pathway lead to a damage/stress response in keratinocytes then release signals that remain to be identified. Cytokines, chemokines and/or other molecules secreted by keratinocytes would then recruits γδ T cells that secrete IL-17 which stimulates keratinocyte proliferation (epidermal hyperplasia) and recruits other immune cells such as granulocytes (neutrophils), macrophages and mast cells. We speculate that independently, Shoc2 ablation sets in motion a Th2-type response by a mechanism

that remains to be identified. These inflammatory loops would also elicit pruritus and an itch/scratch cycle that likely also play an important contribution to inflammation (Figure 7-1).

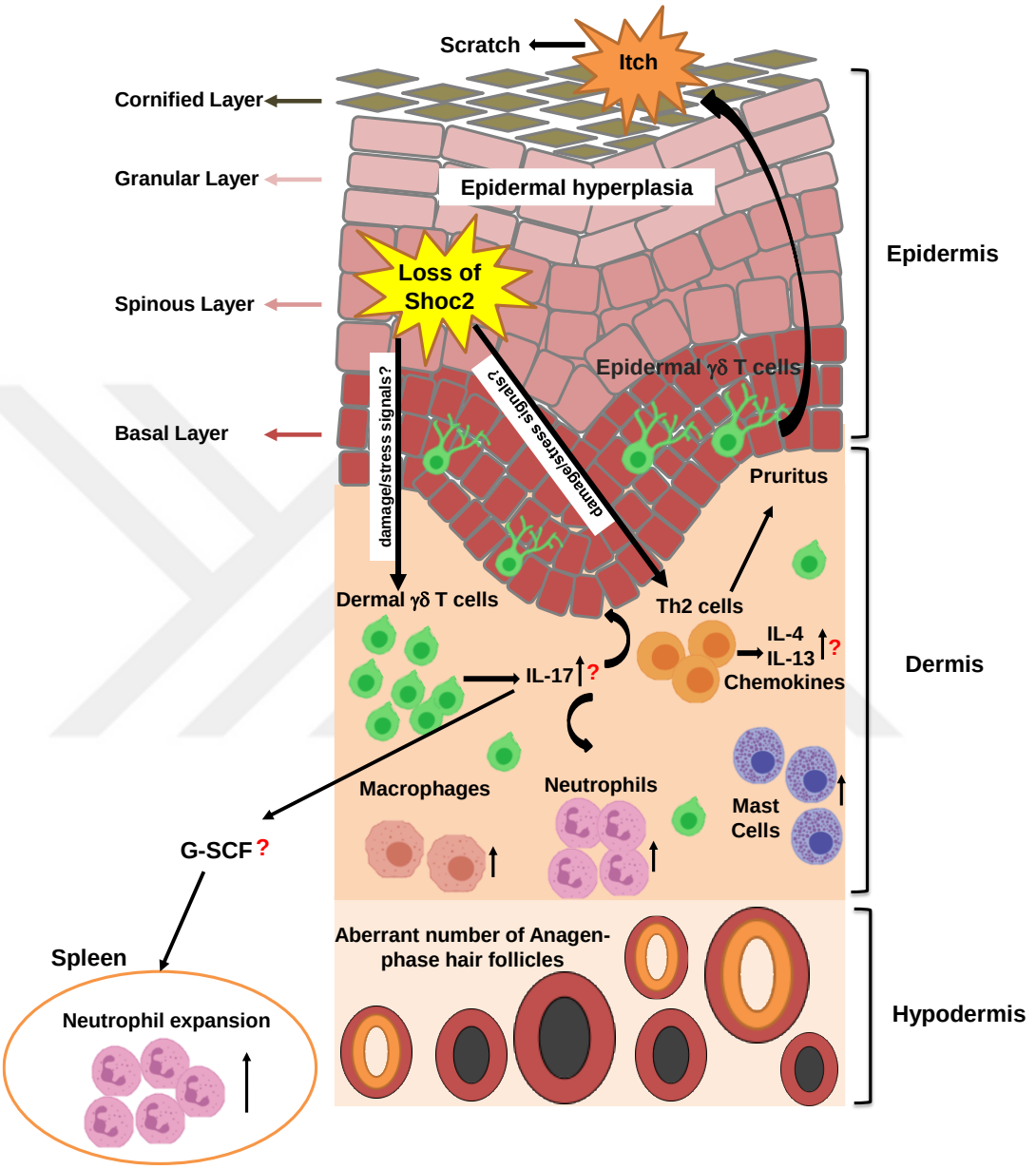

Figure 7-1. Model for Shoc2 inactivation caused skin dermatitis

This model depicts the alterations in the skin caused by systemic Shoc2 inactivation. Shoc2 ablation causes inflammatory skin disease akin to AD and psoriasis. Upon Shoc2 inactivation, an increased number of hair follicles, which remain in the anagen phase, accumulate in the hypodermis. Whether this contributes to the inflammatory response remains to be addressed. The Shoc2 inactivation in keratinocytes (in skin and/or hair follicles) lead to the release of a damage/stress signal from keratinocytes that leads to expansion of γδ T cells that secrete IL-17. Enhanced IL-17 stimulates epidermal hyperplasia and promotes the recruitment of other immune cells such as neutrophils, macrophages, and mast cells. The scratching response to pruritus contributes to irritation and inflammation. In addition, Shoc2 inactivation caused skin

dermatitis may also drive systemic inflammation with splenomegaly via a γδ T cells/IL-17/G-CSF axis leading to neutrophil expansion in the spleen of Shoc2 KO mice.

At the systemic level, we observed splenomegaly and lymphadenopathy with a significant accumulation of neutrophils, inflammatory monocytes and macrophages (Figure 4-13A and B). Besides, increased number of leukocytes have been found in the blood of Shoc2 KO mice. This systemic phenotype recapitulates the one observed in epidermis restricted BRAF/CRAF KO mice which presented with enlarged spleens and lymph nodes that could largely be attributed to increased numbers of macrophages and granulocytes. This study suggests that even though BRAF/CRAF deletion is only in the skin, systemic effect is consequence of chronic skin inflammation (Raguz et al. 2016). In addition, mice lacking epidermal EGFR progressively develop skin dermatitis accompanied by pruritus, after the first week of age and later they exhibit splenomegaly and lymphadenopathy with aging (Mascia et al. 2013). Coffelt et al. (2015) showed a clear link between γδ T cell and increased neutrophil recruitment, in a phenomenon reminiscent of that observed upon Shoc2 inactivation. In this study, they indicate that in the context of breast cancer, mammary tumours induce IL-1β production which activates γδ T cells to produce IL-17. Increased systemic IL-17 levels cause upregulation of granulocyte colony-stimulating factor (G-CSF), which subsequently causes neutrophil expansion (Coffelt et al. 2015). Therefore, future experiments should measure levels of IL-17 and G-CSF to address the role of γδ T cells in the splenomegaly observed in Shoc2 KO mice (Figure 7-1).

The time-course study shows that skin inflammation upon Shoc2 ablation precedes splenomegaly and, our results are also consistent with a model where the AD-like skin dermatitis is caused by Shoc2 inactivation eventually leads to a systemic inflammatory response. However, additional studies are required to understand the role of Shoc2 in immune cell function that needs to be further explored mechanistically.

To this end, Shoc2-keratinocyte-specific-deficient mice (*K14CreER^{T2} Shoc2$^{flox/flox}$*) may be used in the future, to see whether inactivation of Shoc2 in the skin alone may cause a similar systemic inflammatory phenotype. Therefore, this new mouse model may provide a better understanding of the mechanisms behind inflammatory skin disease and systemic inflammatory response.

In addition, RNAseq and scRNA-seq experiments could be performed to further characterize at the transcriptional level the nature of the inflammatory

response in different cell populations. Also, immunophenotyping experiments should be performed where the production of Type-1, -2, -17, and -22 cytokines are measured.

Disrupted barrier function is a hallmark of AD with impaired expression of tight junction proteins and adherens junction proteins such as E-cadherin (Goleva et al. 2019). A recent study reported that M-Ras-Shoc2 complex control cell migration by modulating turnover of E-cadherin and cell–cell adhesion through ERK signalling cascade (Kota et al. 2019). Therefore, future research should address whether Shoc2 has an implication in skin barrier integrity likely via regulation of E-cadherin and tight junction proteins.

Altogether these results establish the importance of SHOC2 in fundamental physiological processes to show the possible toxicities when using a future inhibitor against the SHOC2 phosphatase complex. Data from our group (Jones et al. 2019) suggests that the NSCLC KRAS-mutant tumours are likely to respond to a SHOC2 targeted therapy, if not as monotherapy at least as combination therapy with MEK inhibitors. In addition, recent research by Sulahian et al. (2019) in which a study is made for novel targets to sensitize MEK inhibitors underlined the therapeutic advantage of Shoc2 depletion (Sulahian et al. 2019). Given the fact that a majority of the current ERK pathway inhibitors have failed in the clinic against RAS-driven cancers, primarily because of unacceptable toxicities that constrained therapeutic index, a future SHOC2 inhibitor is predicted to be better tolerated and thus potentially provide improved therapeutic margins over current ERK pathway inhibitors. However, this study also indicates that sustained inhibition may lead to toxicities and underscore the importance of optimizing treatment windows as well as close monitoring of particularly sensitive tissues such as the skin. A better understanding of the molecular mechanisms involved in the initiation and/or progression of skin dermatitis caused by Shoc2 ablation However, future research is now needed to decipher how Shoc2 is relevant to initiation and/or progression skin dermatitis, which is the major phenotype caused by Shoc2 ablation.

Better understanding of molecular mechanism of toxicities could have therapeutic implications in using current biologicals used for treatment of AD or psoriasis to treat toxicities. AD and psoriasis share many clinical characteristics and as mentioned earlier both diseases result in chronic, systemic inflammation with increased circulating populations of leukocytes, lymphocytes, cytokines, and

chemokines (predominantly Th2 pathways in AD and Th17 pathways in psoriasis). Previous therapeutic options for AD and psoriasis, were limited to topical and non-targeted systemic treatments, such as emollients, corticosteroids, cyclosporin (suppresses T-cell activation) (Chovatiya and Silverberg 2019). However, over recent years, a new generation of biologic treatments for psoriasis and AD has emerged, including monoclonal antibodies targeting IL-17, IL-12/IL-23 and TNFα for psoriasis and IL-31, IL-4 and IL-13 for AD. These treatment approaches highlight that blocking cytokines uniquely expressed in the disease is crucial to stop a vicious circle (Sugaya et al. 2015; Brunner et al. 2017).

Our Shoc2 KI model selectively disrupts the ability of SHOC2 to form a phosphatase complex with MRAS and PP1 and more closely mimics the effects of pharmacological inhibition of the phosphatase activity of the SHOC2 complex in the clinic. Importantly, Shoc2 KI mice exhibited milder toxicity, delayed emergence and lower penetrance of the phenotypes observed in Shoc2 KO mice which have complete loss-of-function. This suggests that scaffold-type functions of Shoc2 separate to its RAF phosphatase function contribute to tissue homeostasis in ways that remain to be defined.

Serine/threonine (S/T) phosphatases have long been thought undruggable due to the misconception that phosphatases are less specific and less tightly regulated than kinases. This general notion was completely based on studies using their isolated catalytic domains. However, now it is clear that the specificity of the phosphatases is given by a broad range of regulatory protein partners that bind to the catalytic subunit to form highly specific holoenzyme complexes (Fahs et al. 2016).

PP1 is known to interact with over 200 regulatory proteins, which means PP1c is the catalytic subunit of more than hundreds of holophosphatase complexes and thus, catalytic inhibitors of PP1c such as calyculin-A (Cohen 2002) and cyanobacterial toxin microcystin (MacKintosh et al. 1995) are highly toxic. For that reason, research efforts targeting the catalytic subunits of PP1 had been abandoned (Cohen 2002). However, recent studies have highlighted the possibility of inhibition of PP1 holophosphatases by targeting regulatory subunits (Carrara et al. 2017; Bertolotti 2018). For instance, Guanabenz and Sephin1 directly bind to the regulatory PPP1R15A subunit and they induce conformational change which impairs the formation of the PP1-PPP1R15A complex and thus prevents substrate (eukaryotic translation initiation factor 2, eIF2α) dephosphorylation (Harding et al. 2009). Another

inhibitor is, Raphin1, which binds the other regulatory subunit PPP1R15B with 30-fold higher affinity than the PPP1R15A subunit and also inhibits eIF2α dephosphorylation (Krzyzosiak et al. 2018). Therefore, these research efforts provide a strong evidence that PP1 holoenzymes are indeed druggable suggesting that allosteric phosphatase inhibitor targeting SHOC2 could also be possible.

On the other hand, our KO model would mimic Shoc2 inhibition using a PROTAC/degrader strategy. As a new and promising technology PROTAC (PROteolysis TArgeting Chimera) modulates protein function by degrading target proteins instead of inhibiting them. In addition, PROTACs have higher chance to affect the non-enzymatic functions of proteins, facilitating the control of protein functions that are not easily achieved by traditional small molecule inhibitors (Sun et al. 2019; Burslem and Crews 2020). This strategy uses the ubiquitin-protease system to target a specific protein such as transcription factors, enzymes, and regulatory proteins and induce its degradation in the cell by taking advantage of the cell's own protein destruction mechanism (Sakamoto et al. 2001; Zou et al. 2019). Therefore, SHOC2 could be inhibited in the clinic also with a PROTAC, in addition to a phosphatase inhibitor.

To conclude, the study in this thesis addresses, for the first time, the role of Shoc2 in tissue homeostasis using mouse models of acute systemic Shoc2 inhibition. This study shows that future SHOC2 targeted therapies may be tolerated better compared to inhibition of other core components of ERK-pathway and thus, help validate SHOC2 as a therapeutic target for RAS-driven cancers. However, this study also indicates that sustained inhibition may lead to toxicities, particularly in the skin. Future studies understanding the molecular mechanism involved may allow for adjuvant treatments to minimize these toxicities. Furthermore, this study identifies phenotypes and sensitive tissues that should be closely monitored during future clinical trials with SHOC2 inhibitors.

References

Abbasi S, Biernaskie J. 2019. Injury modifies the fate of hair follicle dermal stem cell progeny in a hair cycle-dependent manner. *Exp Dermatol* **28**: 419-424.

Ackermann L, Harvima IT, Pelkonen J, Ritamaki-Salo V, Naukkarinen A, Harvima RJ, Horsmanheimo M. 1999. Mast cells in psoriatic skin are strongly positive for interferon-gamma. *Br J Dermatol* **140**: 624-633.

Agarwal S, Krishnamurthy K. 2020. Histology, Skin. in *StatPearls*, Treasure Island (FL).

Agerberth B, Charo J, Werr J, Olsson B, Idali F, Lindbom L, Kiessling R, Jornvall H, Wigzell H, Gudmundsson GH. 2000. The human antimicrobial and chemotactic peptides LL-37 and alpha-defensins are expressed by specific lymphocyte and monocyte populations. *Blood* **96**: 3086-3093.

Ahmadian MR, Stege P, Scheffzek K, Wittinghofer A. 1997. Confirmation of the arginine-finger hypothesis for the GAP-stimulated GTP-hydrolysis reaction of Ras. *Nat Struct Biol* **4**: 686-689.

Ahn NG, Seger R, Bratlien RL, Diltz CD, Tonks NK, Krebs EG. 1991. Multiple components in an epidermal growth factor-stimulated protein kinase cascade. In vitro activation of a myelin basic protein/microtubule-associated protein 2 kinase. *J Biol Chem* **266**: 4220-4227.

Akuthota P, Weller PF. 2012. Eosinophils and disease pathogenesis. *Semin Hematol* **49**: 113-119.

Albanesi C, Scarponi C, Giustizieri ML, Girolomoni G. 2005. Keratinocytes in inflammatory skin diseases. *Curr Drug Targets Inflamm Allergy* **4**: 329-334.

Alessi DR, Saito Y, Campbell DG, Cohen P, Sithanandam G, Rapp U, Ashworth A, Marshall CJ, Cowley S. 1994. Identification of the sites in MAP kinase kinase-1 phosphorylated by p74raf-1. *EMBO J* **13**: 1610-1619.

Alonso L, Fuchs E. 2006. The hair cycle. *Journal of Cell Science* **119**: 391-393.

Alvarez E, Northwood IC, Gonzalez FA, Latour DA, Seth A, Abate C, Curran T, Davis RJ. 1991. Pro-Leu-Ser/Thr-Pro is a consensus primary sequence for substrate protein phosphorylation. Characterization of the phosphorylation of c-myc and c-jun proteins by an epidermal growth factor receptor threonine 669 protein kinase. *J Biol Chem* **266**: 15277-15285.

Andreadi C, Cheung LK, Giblett S, Patel B, Jin H, Mercer K, Kamata T, Lee P, Williams A, McMahon M et al. 2012. The intermediate-activity (L597V)BRAF mutant acts as an epistatic modifier of oncogenic RAS by enhancing signaling through the RAF/MEK/ERK pathway. *Genes Dev* **26**: 1945-1958.

Anforth R, Fernandez-Penas P, Long GV. 2013. Cutaneous toxicities of RAF inhibitors. *Lancet Oncol* **14**: e11-18.

Anforth RM, Blumetti TC, Kefford RF, Sharma R, Scolyer RA, Kossard S, Long GV, Fernandez-Penas P. 2012. Cutaneous manifestations of dabrafenib (GSK2118436): a selective inhibitor of mutant BRAF in patients with metastatic melanoma. *Br J Dermatol* **167**: 1153-1160.

Ariotti S, Hogenbirk MA, Dijkgraaf FE, Visser LL, Hoekstra ME, Song JY, Jacobs H, Haanen JB, Schumacher TN. 2014. T cell memory. Skin-resident memory CD8(+) T cells trigger a state of tissue-wide pathogen alert. *Science* **346**: 101-105.

Arvind R, Shimamoto H, Momose F, Amagasa T, Omura K, Tsuchida N. 2005. A mutation in the common docking domain of ERK2 in a human cancer cell line, which was associated with its constitutive phosphorylation. *Int J Oncol* **27**: 1499-1504.

Ascierto PA, Kirkwood JM, Grob JJ, Simeone E, Grimaldi AM, Maio M, Palmieri G, Testori A, Marincola FM, Mozzillo N. 2012. The role of BRAF V600 mutation in melanoma. *J Transl Med* **10**: 85.

Ascierto PA, Minor D, Ribas A, Lebbe C, O'Hagan A, Arya N, Guckert M, Schadendorf D, Kefford RF, Grob JJ et al. 2013. Phase II trial (BREAK-2) of the BRAF inhibitor dabrafenib (GSK2118436) in patients with metastatic melanoma. *J Clin Oncol* **31**: 3205-3211.

Balagula Y, Barth Huston K, Busam KJ, Lacouture ME, Chapman PB, Myskowski PL. 2011. Dermatologic side effects associated with the MEK 1/2 inhibitor selumetinib (AZD6244, ARRY-142886). *Investigational New Drugs* **29**: 1114-1121.

Baljuls A, Schmitz W, Mueller T, Zahedi RP, Sickmann A, Hekman M, Rapp UR. 2008. Positive regulation of A-RAF by phosphorylation of isoform-specific hinge segment and identification of novel phosphorylation sites. *J Biol Chem* **283**: 27239-27254.

Ballarò C, Ceccarelli S, Tiveron C, Tatangelo L, Salvatore AM, Segatto O, Alemà S. 2005. Targeted expression of RALT in mouse skin inhibits epidermal growth factor receptor signalling and generates a Waved-like phenotype. *EMBO reports* **6**: 755-761.

Belanger LF, Roy S, Tremblay M, Brott B, Steff AM, Mourad W, Hugo P, Erikson R, Charron J. 2003. Mek2 is dispensable for mouse growth and development. *Mol Cell Biol* **23**: 4778-4787.

Bella J, Hindle KL, McEwan PA, Lovell SC. 2008. The leucine-rich repeat structure. *Cellular and molecular life sciences : CMLS* **65**: 2307-2333.

Bendelac A, Savage PB, Teyton L. 2007. The Biology of NKT Cells. *Annual Review of Immunology* **25**: 297-336.

Bergstresser PR, Sullivan S, Streilein JW, Tigelaar RE. 1985. Origin and function of Thy-1+ dendritic epidermal cells in mice. *J Invest Dermatol* **85**: 85s-90s.

Bertolotti A. 2018. The split protein phosphatase system. *Biochem J* **475**: 3707-3723.

Bichsel KJ, Hammiller B, Trempus CS, Li Y, Hansen LA. 2016. The epidermal growth factor receptor decreases Stathmin 1 and triggers catagen entry in the mouse. *Exp Dermatol* **25**: 275-281.

Bieber T. 2008. Atopic dermatitis. *N Engl J Med* **358**: 1483-1494.

Bissonauth V, Roy S, Gravel M, Guillemette S, Charron J. 2006. Requirement for Map2k1 (Mek1) in extra-embryonic ectoderm during placentogenesis. *Development* **133**: 3429-3440.

Blasco RB, Francoz S, Santamaria D, Canamero M, Dubus P, Charron J, Baccarini M, Barbacid M. 2011. c-Raf, but not B-Raf, is essential for development of K-Ras oncogene-driven non-small cell lung carcinoma. *Cancer Cell* **19**: 652-663.

Bochner BS, Gleich GJ. 2010. What targeting eosinophils has taught us about their role in diseases. *J Allergy Clin Immunol* **126**: 16-25; quiz 26-17.

Boehme P, Doerner J, Solanki M, Jing L, Zhang W, Ehrhardt A. 2015. The sleeping beauty transposon vector system for treatment of rare genetic diseases: an unrealized hope? *Curr Gene Ther* **15**: 255-265.

Bollen M, Peti W, Ragusa MJ, Beullens M. 2010. The extended PP1 toolkit: designed to create specificity. *Trends Biochem Sci* **35**: 450-458.

Boned Del Rio I, Young LC, Sari S, Jones GG, Ringham-Terry B, Hartig N, Rejnowicz E, Lei W, Bhamra A, Surinova S et al. 2019. SHOC2 complex-driven RAF dimerization selectively contributes to ERK pathway dynamics. *Proc Natl Acad Sci U S A* **116**: 13330-13339.

Bonish B, Jullien D, Dutronc Y, Huang BB, Modlin R, Spada FM, Porcelli SA, Nickoloff BJ. 2000. Overexpression of CD1d by keratinocytes in psoriasis and CD1d-dependent IFN-gamma production by NK-T cells. *J Immunol* **165**: 4076-4085.

Bos JD, Kapsenberg ML. 1993. The skin immune system: progress in cutaneous biology. *Immunol Today* **14**: 75-78.

Bos JL, Rehmann H, Wittinghofer A. 2007. GEFs and GAPs: critical elements in the control of small G proteins. *Cell* **129**: 865-877.

Boulton TG, Yancopoulos GD, Gregory JS, Slaughter C, Moomaw C, Hsu J, Cobb MH. 1990. An insulin-stimulated protein kinase similar to yeast kinases involved in cell cycle control. *Science* **249**: 64-67.

Boyartchuk VL, Ashby MN, Rine J. 1997. Modulation of Ras and a-factor function by carboxyl-terminal proteolysis. *Science* **275**: 1796-1800.

Brenan L, Andreev A, Cohen O, Pantel S, Kamburov A, Cacchiarelli D, Persky NS, Zhu C, Bagul M, Goetz EM et al. 2016. Phenotypic Characterization of a Comprehensive Set of MAPK1/ERK2 Missense Mutants. *Cell Rep* **17**: 1171-1183.

Brennan DF, Dar AC, Hertz NT, Chao WC, Burlingame AL, Shokat KM, Barford D. 2011. A Raf-induced allosteric transition of KSR stimulates phosphorylation of MEK. *Nature* **472**: 366-369.

Brockmann L, Giannou AD, Gagliani N, Huber S. 2017. Regulation of TH17 Cells and Associated Cytokines in Wound Healing, Tissue Regeneration, and Carcinogenesis. *Int J Mol Sci* **18**.

Bromberg-White JL, Andersen NJ, Duesbery NS. 2012. MEK genomics in development and disease. *Brief Funct Genomics* **11**: 300-310.

Brunner PM, Guttman-Yassky E, Leung DY. 2017. The immunology of atopic dermatitis and its reversibility with broad-spectrum and targeted therapies. *J Allergy Clin Immunol* **139**: S65-S76.

Burke P, Schooler K, Wiley HS. 2001. Regulation of epidermal growth factor receptor signaling by endocytosis and intracellular trafficking. *Mol Biol Cell* **12**: 1897-1910.

Burnstock G. 2014. Purinergic signalling in the urinary tract in health and disease. *Purinergic Signal* **10**: 103-155.

Burslem GM, Crews CM. 2020. Proteolysis-Targeting Chimeras as Therapeutics and Tools for Biological Discovery. *Cell* **181**: 102-114.

Cabezas-Wallscheid N, Klimmeck D, Hansson J, Lipka DB, Reyes A, Wang Q, Weichenhan D, Lier A, von Paleske L, Renders S et al. 2014. Identification of regulatory networks in HSCs and their immediate progeny via integrated proteome, transcriptome, and DNA methylome analysis. *Cell Stem Cell* **15**: 507-522.

Cai Y, Shen X, Ding C, Qi C, Li K, Li X, Jala VR, Zhang HG, Wang T, Zheng J et al. 2011a. Pivotal role of dermal IL-17-producing gammadelta T cells in skin inflammation. *Immunity* **35**: 596-610.

Cai Y, Shen X, Ding C, Qi C, Li K, Li X, Venkatakrishna, Zhang H-G, Wang T, Zheng J et al. 2011b. Pivotal Role of Dermal IL-17-Producing γδ T Cells in Skin Inflammation. *Immunity* **35**: 596-610.

Cancer Genome Atlas N. 2015. Genomic Classification of Cutaneous Melanoma. *Cell* **161**: 1681-1696.

Candi E, Schmidt R, Melino G. 2005. The cornified envelope: a model of cell death in the skin. *Nat Rev Mol Cell Biol* **6**: 328-340.

Cañedo-Dorantes L, Cañedo-Ayala M. 2019. Skin Acute Wound Healing: A Comprehensive Review. *International Journal of Inflammation* **2019**: 1-15.

Cao H, Alrejaye N, Klein OD, Goodwin AF, Oberoi S. 2017. A review of craniofacial and dental findings of the RASopathies. *Orthod Craniofac Res* **20 Suppl 1**: 32-38.

Carcavilla A, Suarez-Ortega L, Rodriguez Sanchez A, Gonzalez-Casado I, Ramon-Krauel M, Labarta JI, Quinteiro Gonzalez S, Riano Galan I, Ezquieta Zubicaray B, Lopez-Siguero JP. 2020. [Noonan syndrome: genetic and clinical update and treatment options]. *An Pediatr (Barc)* **93**: 61 e61-61 e14.

Carrara M, Sigurdardottir A, Bertolotti A. 2017. Decoding the selectivity of eIF2alpha holophosphatases and PPP1R15A inhibitors. *Nat Struct Mol Biol* **24**: 708-716.

Castellano E, Santos E. 2011. Functional specificity of ras isoforms: so similar but so different. *Genes Cancer* **2**: 216-231.

Caunt CJ, Sale MJ, Smith PD, Cook SJ. 2015. MEK1 and MEK2 inhibitors and cancer therapy: the long and winding road. *Nat Rev Cancer* **15**: 577-592.

Chan LS, Robinson N, Xu L. 2001. Expression of interleukin-4 in the epidermis of transgenic mice results in a pruritic inflammatory skin disease: an experimental animal model to study atopic dermatitis. *J Invest Dermatol* **117**: 977-983.

Chaplin DD. 2010. Overview of the immune response. *J Allergy Clin Immunol* **125**: S3-23.

Cheng Y, Tian H. 2017. Current Development Status of MEK Inhibitors. *Molecules* **22**.

Chiang PM, Ling J, Jeong YH, Price DL, Aja SM, Wong PC. 2010. Deletion of TDP-43 down-regulates Tbc1d1, a gene linked to obesity, and alters body fat metabolism. *Proc Natl Acad Sci U S A* **107**: 16320-16324.

Chiu VK, Bivona T, Hach A, Sajous JB, Silletti J, Wiener H, Johnson RL, 2nd, Cox AD, Philips MR. 2002. Ras signalling on the endoplasmic reticulum and the Golgi. *Nat Cell Biol* **4**: 343-350.

Cho US, Xu W. 2007. Crystal structure of a protein phosphatase 2A heterotrimeric holoenzyme. *Nature* **445**: 53-57.

Chodaczek G, Papanna V, Zal MA, Zal T. 2012. Body-barrier surveillance by epidermal gammadelta TCRs. *Nat Immunol* **13**: 272-282.

Chong H, Lee J, Guan KL. 2001. Positive and negative regulation of Raf kinase activity and function by phosphorylation. *EMBO J* **20**: 3716-3727.

Chotinantakul K, Leeanansaksiri W. 2012. Hematopoietic stem cell development, niches, and signaling pathways. *Bone Marrow Res* **2012**: 270425.

Chovatiya R, Silverberg JI. 2019. Pathophysiology of Atopic Dermatitis and Psoriasis: Implications for Management in Children. *Children (Basel)* **6**.

Chu DH. 2008. *Overview of biology, development, and structure of skin.* New York: McGraw-Hill.

Clark RA, Chong B, Mirchandani N, Brinster NK, Yamanaka K, Dowgiert RK, Kupper TS. 2006. The vast majority of CLA+ T cells are resident in normal skin. *J Immunol* **176**: 4431-4439.

Cleghon V, Morrison DK. 1994. Raf-1 interacts with Fyn and Src in a non-phosphotyrosine-dependent manner. *The Journal of biological chemistry* **269**: 17749-17755.

Coffelt SB, Kersten K, Doornebal CW, Weiden J, Vrijland K, Hau CS, Verstegen NJM, Ciampricotti M, Hawinkels L, Jonkers J et al. 2015. IL-17-producing gammadelta T cells and neutrophils conspire to promote breast cancer metastasis. *Nature* **522**: 345-348.

Cohen PT. 2002. Protein phosphatase 1--targeted in many directions. *J Cell Sci* **115**: 241-256.

Corbalan-Garcia S, Yang SS, Degenhardt KR, Bar-Sagi D. 1996. Identification of the mitogen-activated protein kinase phosphorylation sites on human Sos1 that regulate interaction with Grb2. *Mol Cell Biol* **16**: 5674-5682.

Cordeddu V, Di Schiavi E, Pennacchio LA, Ma'ayan A, Sarkozy A, Fodale V, Cecchetti S, Cardinale A, Martin J, Schackwitz W et al. 2009. Mutation of SHOC2 promotes aberrant protein N-myristoylation and causes Noonan-like syndrome with loose anagen hair. *Nat Genet* **41**: 1022-1026.

Cox AD, Fesik SW, Kimmelman AC, Luo J, Der CJ. 2014. Drugging the undruggable RAS: Mission possible? *Nat Rev Drug Discov* **13**: 828-851.

Cruz MS, Diamond A, Russell A, Jameson JM. 2018. Human alphabeta and gammadelta T Cells in Skin Immunity and Disease. *Front Immunol* **9**: 1304.

Cseh B, Doma E, Baccarini M. 2014. "RAF" neighborhood: protein-protein interaction in the Raf/Mek/Erk pathway. *FEBS Lett* **588**: 2398-2406.

Cubero DIG, Abdalla BMZ, Schoueri J, Lopes FI, Turke KC, Guzman J, Del Giglio A, Filho C, Salzano V, Fabra DG. 2018. Cutaneous side effects of molecularly targeted therapies for the treatment of solid tumors. *Drugs Context* **7**: 212516.

Dai P, Xiong WC, Mei L. 2006. Erbin inhibits RAF activation by disrupting the sur-8-Ras-Raf complex. *J Biol Chem* **281**: 927-933.

Dai Q, Choy E, Chiu V, Romano J, Slivka SR, Steitz SA, Michaelis S, Philips MR. 1998. Mammalian prenylcysteine carboxyl methyltransferase is in the endoplasmic reticulum. *J Biol Chem* **273**: 15030-15034.

Dainichi T, Kitoh A, Otsuka A, Nakajima S, Nomura T, Kaplan DH, Kabashima K. 2018. The epithelial immune microenvironment (EIME) in atopic dermatitis and psoriasis. *Nat Immunol* **19**: 1286-1298.

Dankner M, Rose AAN, Rajkumar S, Siegel PM, Watson IR. 2018. Classifying BRAF alterations in cancer: new rational therapeutic strategies for actionable mutations. *Oncogene* **37**: 3183-3199.

Dard L, Bellance N, Lacombe D, Rossignol R. 2018. RAS signalling in energy metabolism and rare human diseases. *Biochim Biophys Acta Bioenerg* **1859**: 845-867.

de Groot RP, Coffer PJ, Koenderman L. 1998. Regulation of proliferation, differentiation and survival by the IL-3/IL-5/GM-CSF receptor family. *Cell Signal* **10**: 619-628.

Degirmenci U, Wang M, Hu J. 2020. Targeting Aberrant RAS/RAF/MEK/ERK Signaling for Cancer Therapy. *Cells* **9**.

Desideri E, Cavallo AL, Baccarini M. 2015. Alike but Different: RAF Paralogs and Their Signaling Outputs. *Cell* **161**: 967-970.

Dhawan NS, Scopton AP, Dar AC. 2016. Small molecule stabilization of the KSR inactive state antagonizes oncogenic Ras signalling. *Nature* **537**: 112-116.

Dhillon AS, Meikle S, Yazici Z, Eulitz M, Kolch W. 2002. Regulation of Raf-1 activation and signalling by dephosphorylation. *Embo Journal* **21**: 64-71.

Dhurat RP, Deshpande DJ. 2010. Loose anagen hair syndrome. *Int J Trichology* **2**: 96-100.

Dieu-Nosjean MC, Massacrier C, Homey B, Vanbervliet B, Pin JJ, Vicari A, Lebecque S, Dezutter-Dambuyant C, Schmitt D, Zlotnik A et al. 2000. Macrophage inflammatory

protein 3alpha is expressed at inflamed epithelial surfaces and is the most potent chemokine known in attracting Langerhans cell precursors. *J Exp Med* **192**: 705-718.
Diogo LN, Faustino IV, Afonso RA, Pereira SA, Monteiro EC, Santos AI. 2015. Voluntary Oral Administration of Losartan in Rats. *J Am Assoc Lab Anim Sci* **54**: 549-556.
Dmochowski RR. 2005. Bladder outlet obstruction: etiology and evaluation. *Rev Urol* **7 Suppl 6**: S3-S13.
Docherty NG, O'Sullivan OE, Healy DA, Fitzpatrick JM, Watson RW. 2006. Evidence that inhibition of tubular cell apoptosis protects against renal damage and development of fibrosis following ureteric obstruction. *Am J Physiol Renal Physiol* **290**: F4-13.
Doma E, Rupp C, Baccarini M. 2013. EGFR-ras-raf signaling in epidermal stem cells: roles in hair follicle development, regeneration, tissue remodeling and epidermal cancers. *Int J Mol Sci* **14**: 19361-19384.
Downward J, Graves JD, Warne PH, Rayter S, Cantrell DA. 1990a. Stimulation of p21ras upon T-cell activation. *Nature* **346**: 719-723.
Downward J, Riehl R, Wu L, Weinberg RA. 1990b. Identification of a nucleotide exchange-promoting activity for p21ras. *Proc Natl Acad Sci U S A* **87**: 5998-6002.
Drosten M, Barbacid M. 2020. Targeting the MAPK Pathway in KRAS-Driven Tumors. *Cancer Cell* **37**: 543-550.
Drosten M, Lechuga CG, Barbacid M. 2013. Ras signaling is essential for skin development. **33**: 2857-2865.
Dumaz N, Marais R. 2003. Protein kinase A blocks Raf-1 activity by stimulating 14-3-3 binding and blocking Raf-1 interaction with Ras. *J Biol Chem* **278**: 29819-29823.
Dumesic PA, Scholl FA, Barragan DI, Khavari PA. 2009. Erk1/2 MAP kinases are required for epidermal G2/M progression. *J Cell Biol* **185**: 409-422.
Eberle FC, Bruck J, Holstein J, Hirahara K, Ghoreschi K. 2016. Recent advances in understanding psoriasis. *F1000Res* **5**.
Eblen ST. 2018. Extracellular-Regulated Kinases: Signaling From Ras to ERK Substrates to Control Biological Outcomes. *Adv Cancer Res* **138**: 99-142.
Egbuniwe IU, Karagiannis SN, Nestle FO, Lacy KE. 2015. Revisiting the role of B cells in skin immune surveillance. *Trends Immunol* **36**: 102-111.
Ehrenreiter K, Kern F, Velamoor V, Meissl K, Galabova-Kovacs G, Sibilia M, Baccarini M. 2009. Raf-1 addiction in Ras-induced skin carcinogenesis. *Cancer Cell* **16**: 149-160.
Ehrenreiter K, Piazzolla D, Velamoor V, Sobczak I, Small JV, Takeda J, Leung T, Baccarini M. 2005. Raf-1 regulates Rho signaling and cell migration. *J Cell Biol* **168**: 955-964.
Ehrhardt A, Ehrhardt GR, Guo X, Schrader JW. 2002. Ras and relatives--job sharing and networking keep an old family together. *Exp Hematol* **30**: 1089-1106.
Ehrhardt A, Wang B, Yung AC, Wang Y, Kozlowski P, van Breemen C, Schrader JW. 2015. Urinary Retention, Incontinence, and Dysregulation of Muscarinic Receptors in Male Mice Lacking Mras. *PLoS One* **10**: e0141493.
Elbe A, Foster CA, Stingl G. 1996. T-cell receptor alpha beta and gamma delta T cells in rat and human skin--are they equivalent? *Semin Immunol* **8**: 341-349.
Esteban LM, Vicario-Abejon C, Fernandez-Salguero P, Fernandez-Medarde A, Swaminathan N, Yienger K, Lopez E, Malumbres M, McKay R, Ward JM et al. 2001. Targeted genomic disruption of H-ras and N-ras, individually or in combination, reveals the dispensability of both loci for mouse growth and development. *Mol Cell Biol* **21**: 1444-1452.
Estrada CR, Adam RM, Eaton SH, Bagli DJ, Freeman MR. 2006. Inhibition of EGFR signaling abrogates smooth muscle proliferation resulting from sustained distension of the urinary bladder. *Lab Invest* **86**: 1293-1302.
Eyerich K, Dimartino V, Cavani A. 2017. IL-17 and IL-22 in immunity: Driving protection and pathology. *Eur J Immunol* **47**: 607-614.
Fahs S, Lujan P, Kohn M. 2016. Approaches to Study Phosphatases. *ACS Chem Biol* **11**: 2944-2961.
Fay NS, Larson EC, Jameson JM. 2016. Chronic Inflammation and gammadelta T Cells. *Front Immunol* **7**: 210.
Ferraiuolo RM, Tubman J, Sinha I, Hamm C, Porter LA. 2017. The cyclin-like protein, SPY1, regulates the ERalpha and ERK1/2 pathways promoting tamoxifen resistance. *Oncotarget* **8**: 23337-23352.

Fey D, Matallanas D, Rauch J, Rukhlenko OS, Kholodenko BN. 2016. The complexities and versatility of the RAS-to-ERK signalling system in normal and cancer cells. *Semin Cell Dev Biol* **58**: 96-107.

Fischer A, Rosen AC, Ensslin CJ, Wu S, Lacouture ME. 2013. Pruritus to anticancer agents targeting the EGFR, BRAF, and CTLA-4. *Dermatol Ther* **26**: 135-148.

Fischmann TO, Smith CK, Mayhood TW, Myers JE, Reichert P, Mannarino A, Carr D, Zhu H, Wong J, Yang RS et al. 2009. Crystal structures of MEK1 binary and ternary complexes with nucleotides and inhibitors. *Biochemistry* **48**: 2661-2674.

Flaherty KT, Infante JR, Daud A, Gonzalez R, Kefford RF, Sosman J, Hamid O, Schuchter L, Cebon J, Ibrahim N et al. 2012. Combined BRAF and MEK inhibition in melanoma with BRAF V600 mutations. *N Engl J Med* **367**: 1694-1703.

Flaherty KT, Puzanov I, Kim KB, Ribas A, McArthur GA, Sosman JA, O'Dwyer PJ, Lee RJ, Grippo JF, Nolop K et al. 2010. Inhibition of mutated, activated BRAF in metastatic melanoma. *N Engl J Med* **363**: 809-819.

Fremin C, Saba-El-Leil MK, Levesque K, Ang SL, Meloche S. 2015. Functional Redundancy of ERK1 and ERK2 MAP Kinases during Development. *Cell Rep* **12**: 913-921.

Fuchs E. 2009. Finding one's niche in the skin. *Cell Stem Cell* **4**: 499-502.

Fuchs E, Raghavan S. 2002. GETTING UNDER THE SKIN OF EPIDERMAL MORPHOGENESIS. **3**: 199-209.

Galabova-Kovacs G, Matzen D, Piazzolla D, Meissl K, Plyushch T, Chen AP, Silva A, Baccarini M. 2006. Essential role of B-Raf in ERK activation during extraembryonic development. *Proc Natl Acad Sci U S A* **103**: 1325-1330.

Galli SJ, Borregaard N, Wynn TA. 2011. Phenotypic and functional plasticity of cells of innate immunity: macrophages, mast cells and neutrophils. *Nat Immunol* **12**: 1035-1044.

Gençler B, Gönül M. 2016. Cutaneous Side Effects of BRAF Inhibitors in Advanced Melanoma: Review of the Literature. *Dermatology Research and Practice* **2016**: 1-6.

Geng W, Dong K, Pu Q, Lv Y, Gao H. 2020. SHOC2 is associated with the survival of breast cancer cells and has prognostic value for patients with breast cancer. *Mol Med Rep* **21**: 867-875.

Germolec DR, Shipkowski KA, Frawley RP, Evans E. 2018. Markers of Inflammation. *Methods Mol Biol* **1803**: 57-79.

Girardi M. 2006. Immunosurveillance and immunoregulation by gammadelta T cells. *J Invest Dermatol* **126**: 25-31.

Giroux S, Tremblay M, Bernard D, Cardin-Girard JF, Aubry S, Larouche L, Rousseau S, Huot J, Landry J, Jeannotte L et al. 1999. Embryonic death of Mek1-deficient mice reveals a role for this kinase in angiogenesis in the labyrinthine region of the placenta. *Curr Biol* **9**: 369-372.

Glennie ND, Yeramilli VA, Beiting DP, Volk SW, Weaver CT, Scott P. 2015. Skin-resident memory CD4+ T cells enhance protection against Leishmania major infection. *Journal of Experimental Medicine* **212**: 1405-1414.

Gober MD, Fishelevich R, Zhao Y, Unutmaz D, Gaspari AA. 2008. Human natural killer T cells infiltrate into the skin at elicitation sites of allergic contact dermatitis. *J Invest Dermatol* **128**: 1460-1469.

Goleva E, Berdyshev E, Leung DY. 2019. Epithelial barrier repair and prevention of allergy. *J Clin Invest* **129**: 1463-1474.

Golubovskaya V, Wu L. 2016. Different Subsets of T Cells, Memory, Effector Functions, and CAR-T Immunotherapy. *Cancers* **8**: 36.

Gomez de Aguero M, Vocanson M, Hacini-Rachinel F, Taillardet M, Sparwasser T, Kissenpfennig A, Malissen B, Kaiserlian D, Dubois B. 2012. Langerhans cells protect from allergic contact dermatitis in mice by tolerizing CD8(+) T cells and activating Foxp3(+) regulatory T cells. *J Clin Invest* **122**: 1700-1711.

Gray EE, Suzuki K, Cyster JG. 2011. Cutting edge: Identification of a motile IL-17-producing gammadelta T cell population in the dermis. *J Immunol* **186**: 6091-6095.

Gripp KW, Aldinger KA, Bennett JT, Baker L, Tusi J, Powell-Hamilton N, Stabley D, Sol-Church K, Timms AE, Dobyns WB. 2016. A novel rasopathy caused by recurrent de novo missense mutations in PPP1CB closely resembles Noonan syndrome with loose anagen hair. *Am J Med Genet A* **170**: 2237-2247.

Groves MR, Hanlon N, Turowski P, Hemmings BA, Barford D. 1999. The structure of the protein phosphatase 2A PR65/A subunit reveals the conformation of its 15 tandemly repeated HEAT motifs. *Cell* **96**: 99-110.

Guan KL, Figueroa C, Brtva TR, Zhu T, Taylor J, Barber TD, Vojtek AB. 2000. Negative regulation of the serine/threonine kinase B-Raf by Akt. *J Biol Chem* **275**: 27354-27359.

Guggina L, Choi A, Choi J. 2017a. EGFR Inhibitors and Cutaneous Complications: A Practical Approach to Management. *Oncology and Therapy* **5**: 135-148.

Guggina LM, Choi AW, Choi JN. 2017b. EGFR Inhibitors and Cutaneous Complications: A Practical Approach to Management. *Oncology and Therapy* **5**: 135-148.

Gutierrez L, Magee AI, Marshall CJ, Hancock JF. 1989. Post-translational processing of p21ras is two-step and involves carboxyl-methylation and carboxy-terminal proteolysis. *EMBO J* **8**: 1093-1098.

Guttman-Yassky E, Lowes MA, Fuentes-Duculan J, Whynot J, Novitskaya I, Cardinale I, Haider A, Khatcherian A, Carucci JA, Bergman R et al. 2007. Major differences in inflammatory dendritic cells and their products distinguish atopic dermatitis from psoriasis. *J Allergy Clin Immunol* **119**: 1210-1217.

Guttman-Yassky E, Suarez-Farinas M, Chiricozzi A, Nograles KE, Shemer A, Fuentes-Duculan J, Cardinale I, Lin P, Bergman R, Bowcock AM et al. 2009. Broad defects in epidermal cornification in atopic dermatitis identified through genomic analysis. *J Allergy Clin Immunol* **124**: 1235-1244 e1258.

Gutzmer R, Becker JC, Enk A, Garbe C, Hauschild A, Leverkus M, Reimer G, Treudler R, Tsianakas A, Ulrich C et al. 2011. Management of cutaneous side effects of EGFR inhibitors: recommendations from a German expert panel for the primary treating physician. *J Dtsch Dermatol Ges* **9**: 195-203.

Guy GR, Jackson RA, Yusoff P, Chow SY. 2009. Sprouty proteins: modified modulators, matchmakers or missing links? *J Endocrinol* **203**: 191-202.

Ha HL, Wang H, Pisitkun P, Kim JC, Tassi I, Tang W, Morasso MI, Udey MC, Siebenlist U. 2014. IL-17 drives psoriatic inflammation via distinct, target cell-specific mechanisms. *Proc Natl Acad Sci U S A* **111**: E3422-3431.

Haas JD, Ravens S, Duber S, Sandrock I, Oberdorfer L, Kashani E, Chennupati V, Fohse L, Naumann R, Weiss S et al. 2012. Development of interleukin-17-producing gammadelta T cells is restricted to a functional embryonic wave. *Immunity* **37**: 48-59.

Haling JR, Sudhamsu J, Yen I, Sideris S, Sandoval W, Phung W, Bravo BJ, Giannetti AM, Peck A, Masselot A et al. 2014. Structure of the BRAF-MEK complex reveals a kinase activity independent role for BRAF in MAPK signaling. *Cancer Cell* **26**: 402-413.

Hamid Q, Boguniewicz M, Leung DY. 1994. Differential in situ cytokine gene expression in acute versus chronic atopic dermatitis. *J Clin Invest* **94**: 870-876.

Hamilton JA. 2008. Colony-stimulating factors in inflammation and autoimmunity. *Nat Rev Immunol* **8**: 533-544.

Hancock JF, Paterson H, Marshall CJ. 1990. A polybasic domain or palmitoylation is required in addition to the CAAX motif to localize p21ras to the plasma membrane. *Cell* **63**: 133-139.

Hannig V, Jeoung M, Jang ER, Phillips JA, 3rd, Galperin E. 2014. A Novel SHOC2 Variant in Rasopathy. *Hum Mutat* **35**: 1290-1294.

Hansen LA, Alexander N, Hogan ME, Sundberg JP, Dlugosz A, Threadgill DW, Magnuson T, Yuspa SH. 1997. Genetically null mice reveal a central role for epidermal growth factor receptor in the differentiation of the hair follicle and normal hair development. *Am J Pathol* **150**: 1959-1975.

Harder J, Bartels J, Christophers E, Schroder JM. 1997. A peptide antibiotic from human skin. *Nature* **387**: 861.

Harding HP, Zhang Y, Scheuner D, Chen JJ, Kaufman RJ, Ron D. 2009. Ppp1r15 gene knockout reveals an essential role for translation initiation factor 2 alpha (eIF2alpha) dephosphorylation in mammalian development. *Proceedings of the National Academy of Sciences of the United States of America* **106**: 1832-1837.

Harrison PT, Vyse S, Huang PH. 2020. Rare epidermal growth factor receptor (EGFR) mutations in non-small cell lung cancer. *Semin Cancer Biol* **61**: 167-179.

Hatano N, Mori Y, Oh-hora M, Kosugi A, Fujikawa T, Nakai N, Niwa H, Miyazaki J, Hamaoka T, Ogata M. 2003. Essential role for ERK2 mitogen-activated protein kinase in placental development. *Genes Cells* **8**: 847-856.

Heroes E, Lesage B, Gornemann J, Beullens M, Van Meervelt L, Bollen M. 2013. The PP1 binding code: a molecular-lego strategy that governs specificity. *FEBS J* **280**: 584-595.

Higgins EM, Bos JM, Mason-Suares H, Tester DJ, Ackerman JP, MacRae CA, Sol-Church K, Gripp KW, Urrutia R, Ackerman MJ. 2017. Elucidation of MRAS-mediated Noonan syndrome with cardiac hypertrophy. *JCI Insight* **2**: e91225.

Hindley A, Kolch W. 2002. Extracellular signal regulated kinase (ERK)/mitogen activated protein kinase (MAPK)-independent functions of Raf kinases. *J Cell Sci* **115**: 1575-1581.

Hobbs GA, Der CJ, Rossman KL. 2016. RAS isoforms and mutations in cancer at a glance. *J Cell Sci* **129**: 1287-1292.

Holderfield M, Deuker MM, McCormick F, McMahon M. 2014. Targeting RAF kinases for cancer therapy: BRAF-mutated melanoma and beyond. *Nat Rev Cancer* **14**: 455-467.

Horimukai K, Morita K, Narita M, Kondo M, Kitazawa H, Nozaki M, Shigematsu Y, Yoshida K, Niizeki H, Motomura K et al. 2014. Application of moisturizer to neonates prevents development of atopic dermatitis. *J Allergy Clin Immunol* **134**: 824-830 e826.

Horsmanheimo L, Harvima IT, Jarvikallio A, Harvima RJ, Naukkarinen A, Horsmanheimo M. 1994. Mast cells are one major source of interleukin-4 in atopic dermatitis. *Br J Dermatol* **131**: 348-353.

Houben R, Becker JC, Kappel A, Terheyden P, Brocker EB, Goetz R, Rapp UR. 2004. Constitutive activation of the Ras-Raf signaling pathway in metastatic melanoma is associated with poor prognosis. *J Carcinog* **3**: 6.

Hsu V, Zobel CL, Lambie EJ, Schedl T, Kornfeld K. 2002. Caenorhabditis elegans lin-45 raf is essential for larval viability, fertility and the induction of vulval cell fates. *Genetics* **160**: 481-492.

Huang CY, Tan TH. 2012. DUSPs, to MAP kinases and beyond. *Cell Biosci* **2**: 24.

Huser M, Luckett J, Chiloeches A, Mercer K, Iwobi M, Giblett S, Sun XM, Brown J, Marais R, Pritchard C. 2001. MEK kinase activity is not necessary for Raf-1 function. *EMBO J* **20**: 1940-1951.

Hynes NE, Lane HA. 2005. ERBB receptors and cancer: the complexity of targeted inhibitors. *Nat Rev Cancer* **5**: 341-354.

Igyarto BZ, Haley K, Ortner D, Bobr A, Gerami-Nejad M, Edelson BT, Zurawski SM, Malissen B, Zurawski G, Berman J et al. 2011. Skin-resident murine dendritic cell subsets promote distinct and opposing antigen-specific T helper cell responses. *Immunity* **35**: 260-272.

Ikenoue T, Hikiba Y, Kanai F, Aragaki J, Tanaka Y, Imamura J, Imamura T, Ohta M, Ijichi H, Tateishi K et al. 2004. Different effects of point mutations within the B-Raf glycine-rich loop in colorectal tumors on mitogen-activated protein/extracellular signal-regulated kinase kinase/extracellular signal-regulated kinase and nuclear factor kappaB pathway and cellular transformation. *Cancer Res* **64**: 3428-3435.

Ikenoue T, Hikiba Y, Kanai F, Tanaka Y, Imamura J, Imamura T, Ohta M, Ijichi H, Tateishi K, Kawakami T et al. 2003. Functional analysis of mutations within the kinase activation segment of B-Raf in human colorectal tumors. *Cancer Res* **63**: 8132-8137.

Imielinski M, Greulich H, Kaplan B, Araujo L, Amann J, Horn L, Schiller J, Villalona-Calero MA, Meyerson M, Carbone DP. 2014. Oncogenic and sorafenib-sensitive ARAF mutations in lung adenocarcinoma. *J Clin Invest* **124**: 1582-1586.

Imperial R, Toor OM, Hussain A, Subramanian J, Masood A. 2017. Comprehensive pancancer genomic analysis reveals (RTK)-RAS-RAF-MEK as a key dysregulated pathway in cancer: Its clinical implications. *Semin Cancer Biol*.

Infante JR, Fecher LA, Falchook GS, Nallapareddy S, Gordon MS, Becerra C, DeMarini DJ, Cox DS, Xu Y, Morris SR et al. 2012. Safety, pharmacokinetic, pharmacodynamic, and efficacy data for the oral MEK inhibitor trametinib: a phase 1 dose-escalation trial. *Lancet Oncol* **13**: 773-781.

Ise K, Nakamura K, Nakao K, Shimizu S, Harada H, Ichise T, Miyoshi J, Gondo Y, Ishikawa T, Aiba A et al. 2000. Targeted deletion of the H-ras gene decreases tumor formation in mouse skin carcinogenesis. *Oncogene* **19**: 2951-2956.

Jacobsen EA, Helmers RA, Lee JJ, Lee NA. 2012. The expanding role(s) of eosinophils in health and disease. *Blood* **120**: 3882-3890.

Jakubzick C, Gautier EL, Gibbings SL, Sojka DK, Schlitzer A, Johnson TE, Ivanov S, Duan Q, Bala S, Condon T et al. 2013. Minimal differentiation of classical monocytes as they survey steady-state tissues and transport antigen to lymph nodes. *Immunity* **39**: 599-610.

Jameson JM, Cauvi G, Witherden DA, Havran WL. 2004. A Keratinocyte-Responsive TCR Is Necessary for Dendritic Epidermal T Cell Activation by Damaged Keratinocytes and Maintenance in the Epidermis. **172**: 3573-3579.

Jang ER, Galperin E. 2016. The function of Shoc2: A scaffold and beyond. *Commun Integr Biol* **9**: e1188241.

Jang ER, Shi P, Bryant J, Chen J, Dukhande V, Gentry MS, Jang H, Jeoung M, Galperin E. 2014. HUWE1 is a molecular link controlling RAF-1 activity supported by the Shoc2 scaffold. *Mol Cell Biol* **34**: 3579-3593.

Jaumot M, Hancock JF. 2001. Protein phosphatases 1 and 2A promote Raf-1 activation by regulating 14-3-3 interactions. *Oncogene* **20**: 3949-3958.

Jensen JM, Folster-Holst R, Baranowsky A, Schunck M, Winoto-Morbach S, Neumann C, Schutze S, Proksch E. 2004. Impaired sphingomyelinase activity and epidermal differentiation in atopic dermatitis. *J Invest Dermatol* **122**: 1423-1431.

Jeoung M, Abdelmoti L, Jang ER, Vander Kooi CW, Galperin E. 2013. Functional Integration of the Conserved Domains of Shoc2 Scaffold. *PLoS One* **8**: e66067.

Jin H, He R, Oyoshi M, Geha RS. 2009. Animal models of atopic dermatitis. *J Invest Dermatol* **129**: 31-40.

Jin T, Lavoie H, Sahmi M, David M, Hilt C, Hammell A, Therrien M. 2017. RAF inhibitors promote RAS-RAF interaction by allosterically disrupting RAF autoinhibition. *Nat Commun* **8**: 1211.

Johnson L, Greenbaum D, Cichowski K, Mercer K, Murphy E, Schmitt E, Bronson RT, Umanoff H, Edelmann W, Kucherlapati R et al. 1997. K-ras is an essential gene in the mouse with partial functional overlap with N-ras. *Genes Dev* **11**: 2468-2481.

Jones GG, Del Rio IB, Sari S, Sekerim A, Young LC, Hartig N, Areso Zubiaur I, El-Bahrawy MA, Hynds RE, Lei W et al. 2019. SHOC2 phosphatase-dependent RAF dimerization mediates resistance to MEK inhibition in RAS-mutant cancers. *Nat Commun* **10**: 2532.

Jones JC, Renfro LA, Al-Shamsi HO, Schrock AB, Rankin A, Zhang BY, Kasi PM, Voss JS, Leal AD, Sun J et al. 2017. (Non-V600) BRAF Mutations Define a Clinically Distinct Molecular Subtype of Metastatic Colorectal Cancer. *J Clin Oncol* **35**: 2624-2630.

Kamijo S, Hara M, Suzuki M, Nakae S, Ogawa H, Okumura K, Takai T. 2020. Innate IL-17A enhances IL-33-independent skin eosinophilia and IgE response on subcutaneous papain sensitization. *J Invest Dermatol*.

Kaminska R, Helisalmi P, Harvima RJ, Naukkarinen A, Horsmanheimo M, Harvima IT. 1999. Focal dermal-epidermal separation and fibronectin cleavage in basement membrane by human mast cell tryptase. *J Invest Dermatol* **113**: 567-573.

Karnoub AE, Weinberg RA. 2008. Ras oncogenes: split personalities. *Nat Rev Mol Cell Biol* **9**: 517-531.

Kern F, Niault T, Baccarini M. 2011. Ras and Raf pathways in epidermis development and carcinogenesis. *Br J Cancer* **104**: 229-234.

Khavari TA, Rinn JL. 2007. Ras/Erk MAPK Signaling in Epidermal Homeostasis and Neoplasia. *Cell Cycle* **6**: 2928-2931.

Kidger AM, Cook SJ. 2018. De-RSKing ERK - regulation of ERK1/2-RSK dissociation by phosphorylation within a disordered motif. *FEBS J* **285**: 42-45.

Kim D, Kobayashi T, Nagao K. 2019. Research Techniques Made Simple: Mouse Models of Atopic Dermatitis. *J Invest Dermatol* **139**: 984-990 e981.

Kim KB, Kefford R, Pavlick AC, Infante JR, Ribas A, Sosman JA, Fecher LA, Millward M, McArthur GA, Hwu P et al. 2013. Phase II study of the MEK1/MEK2 inhibitor Trametinib in patients with metastatic BRAF-mutant cutaneous melanoma previously treated with or without a BRAF inhibitor. *J Clin Oncol* **31**: 482-489.

Kissenpfennig A, Henri S, Dubois B, Laplace-Builhe C, Perrin P, Romani N, Tripp CH, Douillard P, Leserman L, Kaiserlian D et al. 2005. Dynamics and function of Langerhans cells in vivo: dermal dendritic cells colonize lymph node areas distinct from slower migrating Langerhans cells. *Immunity* **22**: 643-654.

Kobayashi T, Aoki Y, Niihori T, Cave H, Verloes A, Okamoto N, Kawame H, Fujiwara I, Takada F, Ohata T et al. 2010. Molecular and clinical analysis of RAF1 in Noonan syndrome and related disorders: dephosphorylation of serine 259 as the essential mechanism for mutant activation. *Hum Mutat* **31**: 284-294.

Kobe B, Deisenhofer J. 1994. The leucine-rich repeat: a versatile binding motif. *Trends in biochemical sciences* **19**: 415-421.

Koera K, Nakamura K, Nakao K, Miyoshi J, Toyoshima K, Hatta T, Otani H, Aiba A, Katsuki M. 1997. K-ras is essential for the development of the mouse embryo. *Oncogene* **15**: 1151-1159.

Kolarsick KMA, Goodwin C. 2011. Anatomy and Physiology of the Skin: Erratum. *Journal of the Dermatology Nurses' Association* **3**: 366.

Kolch W, Heidecker G, Kochs G, Hummel R, Vahidi H, Mischak H, Finkenzeller G, Marme D, Rapp UR. 1993. Protein kinase C alpha activates RAF-1 by direct phosphorylation. *Nature* **364**: 249-252.

Kolls JK, McCray PB, Jr., Chan YR. 2008. Cytokine-mediated regulation of antimicrobial proteins. *Nat Rev Immunol* **8**: 829-835.

Kolupaeva V, Janssens V. 2013. PP1 and PP2A phosphatases--cooperating partners in modulating retinoblastoma protein activation. *FEBS J* **280**: 627-643.

Komatsuzaki S, Aoki Y, Niihori T, Okamoto N, Hennekam RC, Hopman S, Ohashi H, Mizuno S, Watanabe Y, Kamasaki H et al. 2010. Mutation analysis of the SHOC2 gene in Noonan-like syndrome and in hematologic malignancies. *J Hum Genet* **55**: 801-809.

Konstantinopoulos PA, Karamouzis MV, Papavassiliou AG. 2007. Post-translational modifications and regulation of the RAS superfamily of GTPases as anticancer targets. *Nat Rev Drug Discov* **6**: 541-555.

Kota P, Terrell EM, Ritt DA, Insinna C, Westlake CJ, Morrison DK. 2019. M-Ras/Shoc2 signaling modulates E-cadherin turnover and cell-cell adhesion during collective cell migration. *Proc Natl Acad Sci U S A* **116**: 3536-3545.

Kronenberg M. 2005. Toward an understanding of NKT cell biology: progress and paradoxes. *Annu Rev Immunol* **23**: 877-900.

Krzyzosiak A, Sigurdardottir A, Luh L, Carrara M, Das I, Schneider K, Bertolotti A. 2018. Target-Based Discovery of an Inhibitor of the Regulatory Phosphatase PPP1R15B. *Cell* **174**: 1216-1228 e1219.

Lackner MR, Kim SK. 1998. Genetic analysis of the Caenorhabditis elegans MAP kinase gene mpk-1. *Genetics* **150**: 103-117.

Lake D, Correa SA, Muller J. 2016. Negative feedback regulation of the ERK1/2 MAPK pathway. *Cell Mol Life Sci* **73**: 4397-4413.

Lavoie H, Therrien M. 2015. Regulation of RAF protein kinases in ERK signalling. *Nat Rev Mol Cell Biol* **16**: 281-298.

Lawrence MS, Stojanov P, Mermel CH, Robinson JT, Garraway LA, Golub TR, Meyerson M, Gabriel SB, Lander ES, Getz G. 2014. Discovery and saturation analysis of cancer genes across 21 tumour types. *Nature* **505**: 495-501.

Lee HW, Ahn DH, Crawley SC, Li JD, Gum JR, Jr., Basbaum CB, Fan NQ, Szymkowski DE, Han SY, Lee BH et al. 2002. Phorbol 12-myristate 13-acetate up-regulates the transcription of MUC2 intestinal mucin via Ras, ERK, and NF-kappa B. *J Biol Chem* **277**: 32624-32631.

Leicht DT, Balan V, Kaplun A, Singh-Gupta V, Kaplun L, Dobson M, Tzivion G. 2007. Raf kinases: function, regulation and role in human cancer. *Biochim Biophys Acta* **1773**: 1196-1212.

Leung DY, Boguniewicz M, Howell MD, Nomura I, Hamid QA. 2004. New insights into atopic dermatitis. *J Clin Invest* **113**: 651-657.

Li F, Adase CA, Zhang LJ. 2017. Isolation and Culture of Primary Mouse Keratinocytes from Neonatal and Adult Mouse Skin. *J Vis Exp*.

Li W, Han M, Guan KL. 2000. The leucine-rich repeat protein SUR-8 enhances MAP kinase activation and forms a complex with Ras and Raf. *Genes Dev* **14**: 895-900.

Li X, Huang Y, Jiang J, Frank SJ. 2008. ERK-dependent threonine phosphorylation of EGF receptor modulates receptor downregulation and signaling. *Cell Signal* **20**: 2145-2155.

Li Y, Takahashi M, Stork PJ. 2013. Ras-mutant cancer cells display B-Raf binding to Ras that activates extracellular signal-regulated kinase and is inhibited by protein kinase A phosphorylation. *J Biol Chem* **288**: 27646-27657.

Liang SC, Tan XY, Luxenberg DP, Karim R, Dunussi-Joannopoulos K, Collins M, Fouser LA. 2006. Interleukin (IL)-22 and IL-17 are coexpressed by Th17 cells and cooperatively enhance expression of antimicrobial peptides. *J Exp Med* **203**: 2271-2279.

Lichtenberger BM, Gerber PA, Holcmann M, Buhren BA, Amberg N, Smolle V, Schrumpf H, Boelke E, Ansari P, Mackenzie C et al. 2013. Epidermal EGFR controls cutaneous host defense and prevents inflammation. *Sci Transl Med* **5**: 199ra111.

Lito P, Solomon M, Li LS, Hansen R, Rosen N. 2016. Allele-specific inhibitors inactivate mutant KRAS G12C by a trapping mechanism. *Science* **351**: 604-608.

Liu X, Quan N. 2015. Immune Cell Isolation from Mouse Femur Bone Marrow. *Bio Protoc* **5**.

Long H, Zhang G, Wang L, Lu Q. 2016. Eosinophilic Skin Diseases: A Comprehensive Review. *Clinical Reviews in Allergy & Immunology* **50**: 189-213.

LoRusso PM, Krishnamurthi SS, Rinehart JJ, Nabell LM, Malburg L, Chapman PB, DePrimo SE, Bentivegna S, Wilner KD, Tan W et al. 2010. Phase I pharmacokinetic and pharmacodynamic study of the oral MAPK/ERK kinase inhibitor PD-0325901 in patients with advanced cancers. *Clin Cancer Res* **16**: 1924-1937.

Lou Z, Casali P, Xu Z. 2015. Regulation of B Cell Differentiation by Intracellular Membrane-Associated Proteins and microRNAs: Role in the Antibody Response. **6**.

Lu S, Jang H, Nussinov R, Zhang J. 2016. The Structural Basis of Oncogenic Mutations G12, G13 and Q61 in Small GTPase K-Ras4B. *Sci Rep* **6**: 21949.

Lynch TJ, Bell DW, Sordella R, Gurubhagavatula S, Okimoto RA, Brannigan BW, Harris PL, Haserlat SM, Supko JG, Haluska FG et al. 2004. Activating mutations in the epidermal growth factor receptor underlying responsiveness of non-small-cell lung cancer to gefitinib. *N Engl J Med* **350**: 2129-2139.

Mabuchi T, Takekoshi T, Hwang ST. 2011. Epidermal CCR6+ gammadelta T cells are major producers of IL-22 and IL-17 in a murine model of psoriasiform dermatitis. *J Immunol* **187**: 5026-5031.

MacKintosh RW, Dalby KN, Campbell DG, Cohen PT, Cohen P, MacKintosh C. 1995. The cyanobacterial toxin microcystin binds covalently to cysteine-273 on protein phosphatase 1. *FEBS Lett* **371**: 236-240.

Mak KK, Chan SY. 2003. Epidermal growth factor as a biologic switch in hair growth cycle. *J Biol Chem* **278**: 26120-26126.

Mandala M, Massi D, De Giorgi V. 2013. Cutaneous toxicities of BRAF inhibitors: clinical and pathological challenges and call to action. *Crit Rev Oncol Hematol* **88**: 318-337.

Manousaridis I, Mavridou S, Goerdt S, Leverkus M, Utikal J. 2013a. Cutaneous side effects of inhibitors of the RAS/RAF/MEK/ERK signalling pathway and their management. *J Eur Acad Dermatol Venereol* **27**: 11-18.

-. 2013b. Cutaneous side effects of inhibitors of the RAS/RAF/MEK/ERK signalling pathway and their management. *Journal of the European Academy of Dermatology and Venereology* **27**: 11-18.

Marafioti T, Pozzobon M, Hansmann ML, Delsol G, Pileri SA, Mason DY. 2004. Expression of intracellular signaling molecules in classical and lymphocyte predominance Hodgkin disease. *Blood* **103**: 188-193.

Marais R, Light Y, Paterson HF, Marshall CJ. 1995. Ras recruits Raf-1 to the plasma membrane for activation by tyrosine phosphorylation. *The EMBO journal* **14**: 3136-3145.

Marais R, Light Y, Paterson HF, Mason CS, Marshall CJ. 1997. Differential regulation of Raf-1, A-Raf, and B-Raf by oncogenic ras and tyrosine kinases. *The Journal of biological chemistry* **272**: 4378-4383.

Margolis B, Skolnik EY. 1994. Activation of Ras by receptor tyrosine kinases. *J Am Soc Nephrol* **5**: 1288-1299.

Mascia F, Lam G, Keith C, Garber C, Steinberg SM, Kohn E, Yuspa SH. 2013. Genetic ablation of epidermal EGFR reveals the dynamic origin of adverse effects of anti-EGFR therapy. *Sci Transl Med* **5**: 199ra110.

Mason CS, Springer CJ, Cooper RG, Superti-Furga G, Marshall CJ, Marais R. 1999. Serine and tyrosine phosphorylations cooperate in Raf-1, but not B-Raf activation. *EMBO J* **18**: 2137-2148.

Mason JM, Morrison DJ, Basson MA, Licht JD. 2006. Sprouty proteins: multifaceted negative-feedback regulators of receptor tyrosine kinase signaling. *Trends Cell Biol* **16**: 45-54.

Matejuk A. 2018. Skin Immunity. *Archivum Immunologiae et Therapiae Experimentalis* **66**: 45-54.

Matsui M, Motomura D, Fujikawa T, Jiang J, Takahashi S, Manabe T, Taketo MM. 2002. Mice lacking M2 and M3 muscarinic acetylcholine receptors are devoid of cholinergic smooth muscle contractions but still viable. *J Neurosci* **22**: 10627-10632.

Matsui M, Motomura D, Karasawa H, Fujikawa T, Jiang J, Komiya Y, Takahashi S, Taketo MM. 2000. Multiple functional defects in peripheral autonomic organs in mice lacking muscarinic acetylcholine receptor gene for the M3 subtype. *Proc Natl Acad Sci U S A* **97**: 9579-9584.

Matsunaga-Udagawa R, Fujita Y, Yoshiki S, Terai K, Kamioka Y, Kiyokawa E, Yugi K, Aoki K, Matsuda M. 2010. The scaffold protein Shoc2/SUR-8 accelerates the interaction of Ras and Raf. *J Biol Chem* **285**: 7818-7826.

Maurer G, Tarkowski B, Baccarini M. 2011. Raf kinases in cancer-roles and therapeutic opportunities. *Oncogene* **30**: 3477-3488.

Mauri C, Bosma A. 2012. Immune Regulatory Function of B Cells. *Annual Review of Immunology* **30**: 221-241.

Maust JD, Whitehead CE, Sebolt-Leopold JS. 2018. Oncogenic Mutants of MEK1: A Trilogy Unfolds. *Cancer Discov* **8**: 534-536.

Mazzucchelli C, Vantaggiato C, Ciamei A, Fasano S, Pakhotin P, Krezel W, Welzl H, Wolfer DP, Pages G, Valverde O et al. 2002. Knockout of ERK1 MAP kinase enhances synaptic plasticity in the striatum and facilitates striatal-mediated learning and memory. *Neuron* **34**: 807-820.

McDonald ER, 3rd, de Weck A, Schlabach MR, Billy E, Mavrakis KJ, Hoffman GR, Belur D, Castelletti D, Frias E, Gampa K et al. 2017. Project DRIVE: A Compendium of Cancer Dependencies and Synthetic Lethal Relationships Uncovered by Large-Scale, Deep RNAi Screening. *Cell* **170**: 577-592 e510.

McKay MM, Freeman AK, Morrison DK. 2011. Complexity in KSR function revealed by Raf inhibitor and KSR structure studies. *Small GTPases* **2**: 276-281.

McKay MM, Morrison DK. 2007. Integrating signals from RTKs to ERK/MAPK. *Oncogene* **26**: 3113-3121.

Mestas J, Hughes CC. 2004. Of mice and not men: differences between mouse and human immunology. *J Immunol* **172**: 2731-2738.

Miettinen PJ, Berger JE, Meneses J, Phung Y, Pedersen RA, Werb Z, Derynck R. 1995. Epithelial immaturity and multiorgan failure in mice lacking epidermal growth factor receptor. *Nature* **376**: 337-341.

Mikula M, Schreiber M, Husak Z, Kucerova L, Ruth J, Wieser R, Zatloukal K, Beug H, Wagner EF, Baccarini M. 2001. Embryonic lethality and fetal liver apoptosis in mice lacking the c-raf-1 gene. *EMBO J* **20**: 1952-1962.

Mills CD. 2015. Anatomy of a discovery: m1 and m2 macrophages. *Front Immunol* **6**: 212.

Mischak H, Seitz T, Janosch P, Eulitz M, Steen H, Schellerer M, Philipp A, Kolch W. 1996. Negative regulation of Raf-1 by phosphorylation of serine 621. *Mol Cell Biol* **16**: 5409-5418.

Molzan M, Schumacher B, Ottmann C, Baljuls A, Polzien L, Weyand M, Thiel P, Rose R, Rose M, Kuhenne P et al. 2010. Impaired binding of 14-3-3 to C-RAF in Noonan syndrome suggests new approaches in diseases with increased Ras signaling. *Molecular and cellular biology* **30**: 4698-4711.

Moore GP, Panaretto BA, Robertson D. 1983. Epidermal growth factor delays the development of the epidermis and hair follicles of mice during growth of the first coat. *Anat Rec* **205**: 47-55.

Morrison DK, Cutler RE. 1997. The complexity of Raf-1 regulation. *Curr Opin Cell Biol* **9**: 174-179.

Morrison SJ, Wandycz AM, Hemmati HD, Wright DE, Weissman IL. 1997. Identification of a lineage of multipotent hematopoietic progenitors. *Development* **124**: 1929-1939.

Mossadegh-Keller N, Sarrazin S, Kandalla PK, Espinosa L, Stanley ER, Nutt SL, Moore J, Sieweke MH. 2013. M-CSF instructs myeloid lineage fate in single haematopoietic stem cells. *Nature* **497**: 239-243.

Motta M, Chillemi G, Fodale V, Cecchetti S, Coppola S, Stipo S, Cordeddu V, Macioce P, Gelb BD, Tartaglia M. 2016. SHOC2 subcellular shuttling requires the KEKE motif-rich region and N-terminal leucine-rich repeat domain and impacts on ERK signalling. *Hum Mol Genet* **25**: 3824-3835.

Motta M, Giancotti A, Mastromoro G, Chandramouli B, Pinna V, Pantaleoni F, Di Giosaffatte N, Petrini S, Mazza T, D'Ambrosio V et al. 2019. Clinical and functional characterization of a novel RASopathy-causing SHOC2 mutation associated with prenatal-onset hypertrophic cardiomyopathy. *Human mutation* **40**: 1046-1056.

Muller-Rover S, Handjiski B, van der Veen C, Eichmuller S, Foitzik K, McKay IA, Stenn KS, Paus R. 2001. A comprehensive guide for the accurate classification of murine hair follicles in distinct hair cycle stages. *J Invest Dermatol* **117**: 3-15.

Murillas R, Larcher F, Conti CJ, Santos M, Ullrich A, Jorcano JL. 1995. Expression of a dominant negative mutant of epidermal growth factor receptor in the epidermis of transgenic mice elicits striking alterations in hair follicle development and skin structure. *EMBO J* **14**: 5216-5223.

Nanney LB, Stoscheck CM, King LE, Jr., Underwood RA, Holbrook KA. 1990. Immunolocalization of epidermal growth factor receptors in normal developing human skin. *J Invest Dermatol* **94**: 742-748.

Nazarian R, Shi H, Wang Q, Kong X, Koya RC, Lee H, Chen Z, Lee MK, Attar N, Sazegar H et al. 2010. Melanomas acquire resistance to B-RAF(V600E) inhibition by RTK or N-RAS upregulation. *Nature* **468**: 973-977.

Nekrasova T, Shive C, Gao Y, Kawamura K, Guardia R, Landreth G, Forsthuber TG. 2005. ERK1-deficient mice show normal T cell effector function and are highly susceptible to experimental autoimmune encephalomyelitis. *J Immunol* **175**: 2374-2380.

Nestle FO, Di Meglio P, Qin JZ, Nickoloff BJ. 2009. Skin immune sentinels in health and disease. *Nat Rev Immunol* **9**: 679-691.

Nguyen AV, Soulika AM. 2019. The Dynamics of the Skin's Immune System. *Int J Mol Sci* **20**.

Nikolaev SI, Rimoldi D, Iseli C, Valsesia A, Robyr D, Gehrig C, Harshman K, Guipponi M, Bukach O, Zoete V et al. 2011. Exome sequencing identifies recurrent somatic MAP2K1 and MAP2K2 mutations in melanoma. *Nature genetics* **44**: 133-139.

Nishibu A, Ward BR, Jester JV, Ploegh HL, Boes M, Takashima A. 2006. Behavioral responses of epidermal Langerhans cells in situ to local pathological stimuli. *J Invest Dermatol* **126**: 787-796.

Noeparast A, Teugels E, Giron P, Verschelden G, De Brakeleer S, Decoster L, De Greve J. 2017. Non-V600 BRAF mutations recurrently found in lung cancer predict sensitivity to the combination of Trametinib and Dabrafenib. *Oncotarget* **8**: 60094-60108.

Nomura T, Kabashima K, Miyachi Y. 2014. The panoply of alphabetaT cells in the skin. *J Dermatol Sci* **76**: 3-9.

Nunez Rodriguez N, Lee IN, Banno A, Qiao HF, Qiao RF, Yao Z, Hoang T, Kimmelman AC, Chan AM. 2006. Characterization of R-ras3/m-ras null mice reveals a potential role in trophic factor signaling. *Mol Cell Biol* **26**: 7145-7154.

O'Brien RL, Born WK. 2015. Dermal gammadelta T cells--What have we learned? *Cell Immunol* **296**: 62-69.

Oguro H, Ding L, Morrison SJ. 2013. SLAM family markers resolve functionally distinct subpopulations of hematopoietic stem cells and multipotent progenitors. *Cell Stem Cell* **13**: 102-116.

Ohba Y, Mochizuki N, Yamashita S, Chan AM, Schrader JW, Hattori S, Nagashima K, Matsuda M. 2000. Regulatory proteins of R-Ras, TC21/R-Ras2, and M-Ras/R-Ras3. *J Biol Chem* **275**: 20020-20026.

Ojesina AI, Lichtenstein L, Freeman SS, Pedamallu CS, Imaz-Rosshandler I, Pugh TJ, Cherniack AD, Ambrogio L, Cibulskis K, Bertelsen B et al. 2014. Landscape of genomic alterations in cervical carcinomas. *Nature* **506**: 371-375.

Onishi RM, Gaffen SL. 2010a. Interleukin-17 and its target genes: mechanisms of interleukin-17 function in disease. *Immunology* **129**: 311-321.

Onishi RM, Gaffen SL. 2010b. Interleukin-17 and its target genes: mechanisms of interleukin-17 function in disease. *Immunology* **129**: 311-321.

Ostrem JM, Peters U, Sos ML, Wells JA, Shokat KM. 2013. K-Ras(G12C) inhibitors allosterically control GTP affinity and effector interactions. *Nature* **503**: 548-551.

Pages G, Guerin S, Grall D, Bonino F, Smith A, Anjuere F, Auberger P, Pouyssegur J. 1999. Defective thymocyte maturation in p44 MAP kinase (Erk 1) knockout mice. *Science* **286**: 1374-1377.

Pandit B, Sarkozy A, Pennacchio LA, Carta C, Oishi K, Martinelli S, Pogna EA, Schackwitz W, Ustaszewska A, Landstrom A et al. 2007. Gain-of-function RAF1 mutations cause Noonan and LEOPARD syndromes with hypertrophic cardiomyopathy. *Nat Genet* **39**: 1007-1012.

Pantelyushin S, Haak S, Ingold B, Kulig P, Heppner FL, Navarini AA, Becher B. 2012. Rorgammat+ innate lymphocytes and gammadelta T cells initiate psoriasiform plaque formation in mice. *J Clin Invest* **122**: 2252-2256.

Papke B, Der CJ. 2017. Drugging RAS: Know the enemy. *Science* **355**: 1158-1163.

Park E, Rawson S, Li K, Kim BW, Ficarro SB, Pino GG, Sharif H, Marto JA, Jeon H, Eck MJ. 2019. Architecture of autoinhibited and active BRAF-MEK1-14-3-3 complexes. *Nature* **575**: 545-550.

Pasparakis M, Haase I, Nestle FO. 2014. Mechanisms regulating skin immunity and inflammation. **14**: 289-301.

Payne DM, Rossomando AJ, Martino P, Erickson AK, Her JH, Shabanowitz J, Hunt DF, Weber MJ, Sturgill TW. 1991. Identification of the regulatory phosphorylation sites in pp42/mitogen-activated protein kinase (MAP kinase). *EMBO J* **10**: 885-892.

Peti W, Nairn AC, Page R. 2013. Structural basis for protein phosphatase 1 regulation and specificity. *FEBS J* **280**: 596-611.

Pietras EM, Reynaud D, Kang YA, Carlin D, Calero-Nieto FJ, Leavitt AD, Stuart JM, Gottgens B, Passegue E. 2015. Functionally Distinct Subsets of Lineage-Biased Multipotent Progenitors Control Blood Production in Normal and Regenerative Conditions. *Cell Stem Cell* **17**: 35-46.

Pondeljak N, Lugovic-Mihic L. 2020. Stress-Induced Interaction of Skin Immune Cells, Hormones, and Neurotransmitters. *Clin Ther*.

Poulikakos PI, Solit DB. 2011. Resistance to MEK inhibitors: should we co-target upstream? *Sci Signal* **4**: pe16.

Pritchard CA, Bolin L, Slattery R, Murray R, McMahon M. 1996. Post-natal lethality and neurological and gastrointestinal defects in mice with targeted disruption of the A-Raf protein kinase gene. *Curr Biol* **6**: 614-617.

Proksch E, Brandner JM, Jensen JM. 2008. The skin: an indispensable barrier. *Exp Dermatol* **17**: 1063-1072.

Pylayeva-Gupta Y, Grabocka E, Bar-Sagi D. 2011. RAS oncogenes: weaving a tumorigenic web. *Nat Rev Cancer* **11**: 761-774.

Raguz J, Jeric I, Niault T, Nowacka JD, Kuzet SE, Rupp C, Fischer I, Biggi S, Borsello T, Baccarini M. 2016. Epidermal RAF prevents allergic skin disease. *Elife* **5**.

Razzaque MA, Nishizawa T, Komoike Y, Yagi H, Furutani M, Amo R, Kamisago M, Momma K, Katayama H, Nakagawa M et al. 2007. Germline gain-of-function mutations in RAF1 cause Noonan syndrome. *Nat Genet* **39**: 1013-1017.

Reis LO, Sopena JM, Favaro WJ, Martin MC, Simao AF, Reis RB, Andrade MF, Domenech JD, Cardo CC. 2011. Anatomical features of the urethra and urinary bladder catheterization in female mice and rats. An essential translational tool. *Acta Cir Bras* **26 Suppl 2**: 106-110.

Richardson GD, Bazzi H, Fantauzzo KA, Waters JM, Crawford H, Hynd P, Christiano AM, Jahoda CA. 2009. KGF and EGF signalling block hair follicle induction and promote interfollicular epidermal fate in developing mouse skin. *Development* **136**: 2153-2164.

Ritt DA, Monson DM, Specht SI, Morrison DK. 2010. Impact of feedback phosphorylation and Raf heterodimerization on normal and mutant B-Raf signaling. *Mol Cell Biol* **30**: 806-819.

Ritt DA, Zhou M, Conrads TP, Veenstra TD, Copeland TD, Morrison DK. 2007. CK2 Is a component of the KSR1 scaffold complex that contributes to Raf kinase activation. *Current biology : CB* **17**: 179-184.

Robert C, Karaszewska B, Schachter J, Rutkowski P, Mackiewicz A, Stroiakovski D, Lichinitser M, Dummer R, Grange F, Mortier L et al. 2015. Improved overall survival in melanoma with combined dabrafenib and trametinib. *N Engl J Med* **372**: 30-39.

Rodriguez-Viciana P, Oses-Prieto J, Burlingame A, Fried M, McCormick F. 2006. A phosphatase holoenzyme comprised of Shoc2/Sur8 and the catalytic subunit of PP1 functions as an M-Ras effector to modulate Raf activity. *Mol Cell* **22**: 217-230.

Rodriguez-Viciana P, Sabatier C, McCormick F. 2004. Signaling specificity by Ras family GTPases is determined by the full spectrum of effectors they regulate. *Molecular and cellular biology* **24**: 4943-4954.

Rommel C, Radziwill G, Lovric J, Noeldeke J, Heinicke T, Jones D, Aitken A, Moelling K. 1996. Activated Ras displaces 14-3-3 protein from the amino terminus of c-Raf-1. *Oncogene* **12**: 609-619.

Rosales C, Demaurex N, Lowell CA, Uribe-Querol E. 2016. Neutrophils: Their Role in Innate and Adaptive Immunity. *Journal of Immunology Research* **2016**: 1-2.

Roskoski R, Jr. 2010. RAF protein-serine/threonine kinases: structure and regulation. *Biochem Biophys Res Commun* **399**: 313-317.

Roux PP, Richards SA, Blenis J. 2003. Phosphorylation of p90 ribosomal S6 kinase (RSK) regulates extracellular signal-regulated kinase docking and RSK activity. *Mol Cell Biol* **23**: 4796-4804.

Rushworth LK, Hindley AD, O'Neill E, Kolch W. 2006. Regulation and role of Raf-1/B-Raf heterodimerization. *Mol Cell Biol* **26**: 2262-2272.

Russo I, Zorzetto L, Chiarion Sileni V, Alaibac M. 2018. Cutaneous Side Effects of Targeted Therapy and Immunotherapy for Advanced Melanoma. *Scientifica (Cairo)* **2018**: 5036213.

Sabat R, Wolk K, Loyal L, Docke WD, Ghoreschi K. 2019. T cell pathology in skin inflammation. *Semin Immunopathol* **41**: 359-377.

Sahle FF, Gebre-Mariam T, Dobner B, Wohlrab J, Neubert RHH. 2015. Skin Diseases Associated with the Depletion of Stratum Corneum Lipids and Stratum Corneum Lipid Substitution Therapy. *Skin Pharmacology and Physiology* **28**: 42-55.

Sakaguchi S. 2005. Naturally arising Foxp3-expressing CD25+CD4+ regulatory T cells in immunological tolerance to self and non-self. *Nat Immunol* **6**: 345-352.

Sakamoto KM, Kim KB, Kumagai A, Mercurio F, Crews CM, Deshaies RJ. 2001. Protacs: chimeric molecules that target proteins to the Skp1-Cullin-F box complex for ubiquitination and degradation. *Proc Natl Acad Sci U S A* **98**: 8554-8559.

Samatar AA, Poulikakos PI. 2014. Targeting RAS-ERK signalling in cancer: promises and challenges. *Nat Rev Drug Discov* **13**: 928-942.

Sanchez JN, Wang T, Cohen MS. 2018. BRAF and MEK Inhibitors: Use and Resistance in BRAF-Mutated Cancers. *Drugs* **78**: 549-566.

Sanclemente M, Francoz S, Esteban-Burgos L, Bousquet-Mur E, Djurec M, Lopez-Casas PP, Hidalgo M, Guerra C, Drosten M, Musteanu M et al. 2018. c-RAF Ablation Induces Regression of Advanced Kras/Trp53 Mutant Lung Adenocarcinomas by a Mechanism Independent of MAPK Signaling. *Cancer Cell* **33**: 217-228 e214.

Sandrock I, Reinhardt A, Ravens S, Binz C, Wilharm A, Martins J, Oberdorfer L, Tan L, Lienenklaus S, Zhang B et al. 2018. Genetic models reveal origin, persistence and non-redundant functions of IL-17-producing gammadelta T cells. *J Exp Med* **215**: 3006-3018.

Sato N, Leopold PL, Crystal RG. 1999. Induction of the hair growth phase in postnatal mice by localized transient expression of Sonic hedgehog. *Journal of Clinical Investigation* **104**: 855-864.

Savoia P, Fava P, Casoni F, Cremona O. 2019. Targeting the ERK Signaling Pathway in Melanoma. *Int J Mol Sci* **20**.

Scaltriti M, Baselga J. 2006. The epidermal growth factor receptor pathway: a model for targeted therapy. *Clin Cancer Res* **12**: 5268-5272.

Schneider MR, Antsiferova M, Feldmeyer L, Dahlhoff M, Bugnon P, Hasse S, Paus R, Wolf E, Werner S. 2008. Betacellulin regulates hair follicle development and hair cycle induction and enhances angiogenesis in wounded skin. *J Invest Dermatol* **128**: 1256-1265.

Schneider MR, Schmidt-Ullrich R, Paus R. 2009. The Hair Follicle as a Dynamic Miniorgan. *Current Biology* **19**: R132-R142.

Scholl FA, Dumesic PA, Barragan DI, Harada K, Bissonauth V, Charron J, Khavari PA. 2007. Mek1/2 MAPK kinases are essential for Mammalian development, homeostasis, and Raf-induced hyperplasia. *Dev Cell* **12**: 615-629.

Schwenk F, Baron U, Rajewsky K. 1995. A cre-transgenic mouse strain for the ubiquitous deletion of loxP-flanked gene segments including deletion in germ cells. *Nucleic Acids Res* **23**: 5080-5081.

Sciammas R, Johnson RM, Sperling AI, Brady W, Linsley PS, Spear PG, Fitch FW, Bluestone JA. 1994. Unique antigen recognition by a herpesvirus-specific TCR-gamma delta cell. *J Immunol* **152**: 5392-5397.

Selfors LM, Schutzman JL, Borland CZ, Stern MJ. 1998. soc-2 encodes a leucine-rich repeat protein implicated in fibroblast growth factor receptor signaling. *Proc Natl Acad Sci U S A* **95**: 6903-6908.

Seshacharyulu P, Pandey P, Datta K, Batra SK. 2013. Phosphatase: PP2A structural importance, regulation and its aberrant expression in cancer. *Cancer Lett* **335**: 9-18.

Shimura E, Hozumi N, Kanagawa O, Metzger D, Chambon P, Radtke F, Hirose S, Nakano N. 2010. Epidermal gammadelta T cells sense precancerous cellular dysregulation and initiate immune responses. *Int Immunol* **22**: 329-340.

Shin SM, Kim JS, Park SW, Jun SY, Kweon HJ, Choi DK, Lee D, Cho YB, Kim YS. 2020. Direct targeting of oncogenic RAS mutants with a tumor-specific cytosol-penetrating antibody inhibits RAS mutant-driven tumor growth. *Sci Adv* **6**: eaay2174.

Sibilia M, Wagner EF. 1995. Strain-dependent epithelial defects in mice lacking the EGF receptor. *Science* **269**: 234-238.

Sieburth DS, Sun Q, Han M. 1998. SUR-8, a conserved Ras-binding protein with leucine-rich repeats, positively regulates Ras-mediated signaling in C. elegans. *Cell* **94**: 119-130.

Siegel DH, Mann JA, Krol AL, Rauen KA. 2012. Dermatological phenotype in Costello syndrome: consequences of Ras dysregulation in development. *Br J Dermatol* **166**: 601-607.

Simanshu DK, Nissley DV, McCormick F. 2017. RAS Proteins and Their Regulators in Human Disease. *Cell* **170**: 17-33.

Spangrude GJ, Heimfeld S, Weissman IL. 1988. Purification and characterization of mouse hematopoietic stem cells. *Science* **241**: 58-62.

Sprenkle AB, Davies SP, Carling D, Hardie DG, Sturgill TW. 1997. Identification of Raf-1 Ser621 kinase activity from NIH 3T3 cells as AMP-activated protein kinase. *FEBS Lett* **403**: 254-258.

Stenn KS, Paus R. 2001. Controls of Hair Follicle Cycling. *Physiological Reviews* **81**: 449-494.

Stephens P, Hunter C, Bignell G, Edkins S, Davies H, Teague J, Stevens C, O'Meara S, Smith R, Parker A et al. 2004. Lung cancer: intragenic ERBB2 kinase mutations in tumours. *Nature* **431**: 525-526.

Suarez-Farinas M, Tintle SJ, Shemer A, Chiricozzi A, Nograles K, Cardinale I, Duan S, Bowcock AM, Krueger JG, Guttman-Yassky E. 2011. Nonlesional atopic dermatitis skin is characterized by broad terminal differentiation defects and variable immune abnormalities. *J Allergy Clin Immunol* **127**: 954-964 e951-954.

Sugaya K, Ishihara Y, Inoue S, Hirobe T. 2015. The effects of gamma rays on the regeneration of hair follicles are carried over to later hair cycles. **91**: 957-963.

Sulahian R, Kwon JJ, Walsh KH, Pailler E, Bosse TL, Thaker M, Almanza D, Dempster JM, Pan J, Piccioni F et al. 2019. Synthetic Lethal Interaction of SHOC2 Depletion with MEK Inhibition in RAS-Driven Cancers. *Cell Rep* **29**: 118-134 e118.

Sulcova J, Maddaluno L, Meyer M, Werner S. 2015. Accumulation and activation of epidermal γδ T cells in a mouse model of chronic dermatitis is not required for the inflammatory phenotype. **45**: 2517-2528.

Sumaria N, Roediger B, Ng LG, Qin J, Pinto R, Cavanagh LL, Shklovskaya E, Fazekas de St Groth B, Triccas JA, Weninger W. 2011. Cutaneous immunosurveillance by self-renewing dermal gammadelta T cells. *J Exp Med* **208**: 505-518.

Sun X, Gao H, Yang Y, He M, Wu Y, Song Y, Tong Y, Rao Y. 2019. PROTACs: great opportunities for academia and industry. *Signal Transduct Target Ther* **4**: 64.

Sutton CE, Lalor SJ, Sweeney CM, Brereton CF, Lavelle EC, Mills KHG. 2009. Interleukin-1 and IL-23 Induce Innate IL-17 Production from γδ T Cells, Amplifying Th17 Responses and Autoimmunity. *Immunity* **31**: 331-341.

Suwanpradid J, Holcomb ZE, MacLeod AS. 2017. Emerging Skin T-Cell Functions in Response to Environmental Insults. *J Invest Dermatol* **137**: 288-294.

Tajan M, Paccoud R, Branka S, Edouard T, Yart A. 2018. The RASopathy Family: Consequences of Germline Activation of the RAS/MAPK Pathway. *Endocr Rev* **39**: 676-700.

Tan YH, Liu Y, Eu KW, Ang PW, Li WQ, Salto-Tellez M, Iacopetta B, Soong R. 2008. Detection of BRAF V600E mutation by pyrosequencing. *Pathology* **40**: 295-298.

Taraborrelli L, Peltzer N, Montinaro A, Kupka S, Rieser E, Hartwig T, Sarr A, Darding M, Draber P, Haas TL et al. 2018. LUBAC prevents lethal dermatitis by inhibiting cell death induced by TNF, TRAIL and CD95L. *Nat Commun* **9**: 3910.

Tay SS, Roediger B, Tong PL, Tikoo S, Weninger W. 2014. The Skin-Resident Immune Network. **3**: 13-22.

Taylor SS, Kornev AP. 2011. Protein kinases: evolution of dynamic regulatory proteins. *Trends Biochem Sci* **36**: 65-77.

Terai K, Matsuda M. 2006. The amino-terminal B-Raf-specific region mediates calcium-dependent homo- and hetero-dimerization of Raf. *EMBO J* **25**: 3556-3564.

Terrell EM, Morrison DK. 2019. Ras-Mediated Activation of the Raf Family Kinases. *Cold Spring Harb Perspect Med* **9**.

Threadgill DW, Dlugosz AA, Hansen LA, Tennenbaum T, Lichti U, Yee D, LaMantia C, Mourton T, Herrup K, Harris RC et al. 1995. Targeted disruption of mouse EGF receptor: effect of genetic background on mutant phenotype. *Science* **269**: 230-234.

Tidyman WE, Rauen KA. 2009. The RASopathies: developmental syndromes of Ras/MAPK pathway dysregulation. *Curr Opin Genet Dev* **19**: 230-236.

Tiemessen MM, Jagger AL, Evans HG, van Herwijnen MJ, John S, Taams LS. 2007. CD4+CD25+Foxp3+ regulatory T cells induce alternative activation of human monocytes/macrophages. *Proc Natl Acad Sci U S A* **104**: 19446-19451.

Toulon A, Breton L, Taylor KR, Tenenhaus M, Bhavsar D, Lanigan C, Rudolph R, Jameson J, Havran WL. 2009. A role for human skin-resident T cells in wound healing. *J Exp Med* **206**: 743-750.

Tsai J, Lee JT, Wang W, Zhang J, Cho H, Mamo S, Bremer R, Gillette S, Kong J, Haass NK et al. 2008. Discovery of a selective inhibitor of oncogenic B-Raf kinase with potent antimelanoma activity. *Proc Natl Acad Sci U S A* **105**: 3041-3046.

Uchida Y, Kawai K, Ibusuki A, Kanekura T. 2011. Role for E-cadherin as an inhibitory receptor on epidermal gammadelta T cells. *J Immunol* **186**: 6945-6954.

Umanoff H, Edelmann W, Pellicer A, Kucherlapati R. 1995. The murine N-ras gene is not essential for growth and development. *Proc Natl Acad Sci U S A* **92**: 1709-1713.

Unal EB, Uhlitz F, Bluthgen N. 2017. A compendium of ERK targets. *FEBS Lett* **591**: 2607-2615.

Valledor AF, Comalada M, Xaus J, Celada A. 2000. The differential time-course of extracellular-regulated kinase activity correlates with the macrophage response toward proliferation or activation. *J Biol Chem* **275**: 7403-7409.

van der Fits L, Mourits S, Voerman JS, Kant M, Boon L, Laman JD, Cornelissen F, Mus AM, Florencia E, Prens EP et al. 2009. Imiquimod-induced psoriasis-like skin inflammation in mice is mediated via the IL-23/IL-17 axis. *J Immunol* **182**: 5836-5845.

Van Kaer L, Parekh VV, Wu L. 2011. Invariant natural killer T cells: bridging innate and adaptive immunity. **343**: 43-55.

Vigil D, Cherfils J, Rossman KL, Der CJ. 2010. Ras superfamily GEFs and GAPs: validated and tractable targets for cancer therapy? *Nat Rev Cancer* **10**: 842-857.

Virshup DM, Shenolikar S. 2009. From promiscuity to precision: protein phosphatases get a makeover. *Mol Cell* **33**: 537-545.

Vojtek AB, Hollenberg SM, Cooper JA. 1993. Mammalian Ras interacts directly with the serine/threonine kinase Raf. *Cell* **74**: 205-214.

Von Stebut E. 2007. Immunology of cutaneous leishmaniasis: the role of mast cells, phagocytes and dendritic cells for protective immunity. *Eur J Dermatol* **17**: 115-122.

Vroom TM, Scholte G, Ossendorp F, Borst J. 1991. Tissue distribution of human gamma delta T cells: no evidence for general epithelial tropism. *J Clin Pathol* **44**: 1012-1017.

Vukmanovic-Stejic M, Agius E, Booth N, Dunne PJ, Lacy KE, Reed JR, Sobande TO, Kissane S, Salmon M, Rustin MH et al. 2008. The kinetics of CD4+Foxp3+ T cell accumulation during a human cutaneous antigen-specific memory response in vivo. *J Clin Invest* **118**: 3639-3650.

Vyse S, Huang PH. 2019. Targeting EGFR exon 20 insertion mutations in non-small cell lung cancer. *Signal Transduct Target Ther* **4**: 5.

Wagner VP, Martins MD, Dillenburg CS, Meurer L, Castilho RM, Squarize CH. 2015. Histogenesis of keratoacanthoma: histochemical and immunohistochemical study. *Oral Surgery, Oral Medicine, Oral Pathology and Oral Radiology* **119**: 310-317.

Wan PT, Garnett MJ, Roe SM, Lee S, Niculescu-Duvaz D, Good VM, Jones CM, Marshall CJ, Springer CJ, Barford D et al. 2004. Mechanism of activation of the RAF-ERK signaling pathway by oncogenic mutations of B-RAF. *Cell* **116**: 855-867.

Wang T, Yu H, Hughes NW, Liu B, Kendirli A, Klein K, Chen WW, Lander ES, Sabatini DM. 2017. Gene Essentiality Profiling Reveals Gene Networks and Synthetic Lethal Interactions with Oncogenic Ras. *Cell* **168**: 890-903 e815.

Weaver CT, Hatton RD, Mangan PR, Harrington LE. 2007. IL-17 family cytokines and the expanding diversity of effector T cell lineages. *Annu Rev Immunol* **25**: 821-852.

Wershil BK, Wang ZS, Gordon JR, Galli SJ. 1991. Recruitment of neutrophils during IgE-dependent cutaneous late phase reactions in the mouse is mast cell-dependent. Partial inhibition of the reaction with antiserum against tumor necrosis factor-alpha. *J Clin Invest* **87**: 446-453.

Wheadon H, Roberts PJ, Watts MJ, Linch DC. 1999. Changes in signal transduction downstream from the granulocyte-macrophage colony-stimulating factor receptor during differentiation of primary hemopoietic cells. *Exp Hematol* **27**: 1077-1086.

Whitfield J, Littlewood T, Soucek L. 2015. Tamoxifen administration to mice. *Cold Spring Harb Protoc* **2015**: 269-271.

Whittaker SR, Cowley GS, Wagner S, Luo F, Root DE, Garraway LA. 2015. Combined Pan-RAF and MEK Inhibition Overcomes Multiple Resistance Mechanisms to Selective RAF Inhibitors. *Mol Cancer Ther* **14**: 2700-2711.

Wilson CH, Gamper I, Perfetto A, Auw J, Littlewood TD, Evan GI. 2014. The kinetics of ER fusion protein activation in vivo. *Oncogene* **33**: 4877-4880.

Wohn C, Ober-Blobaum JL, Haak S, Pantelyushin S, Cheong C, Zahner SP, Onderwater S, Kant M, Weighardt H, Holzmann B et al. 2013. Langerin(neg) conventional dendritic cells produce IL-23 to drive psoriatic plaque formation in mice. *Proc Natl Acad Sci U S A* **110**: 10723-10728.

Wojcik SM, Longley MA, Roop DR. 2001. Discovery of a novel murine keratin 6 (K6) isoform explains the absence of hair and nail defects in mice deficient for K6a and K6b. *Journal of Cell Biology* **154**: 619-630.

Wojnowski L, Stancato LF, Zimmer AM, Hahn H, Beck TW, Larner AC, Rapp UR, Zimmer A. 1998. Craf-1 protein kinase is essential for mouse development. *Mech Dev* **76**: 141-149.

Wojnowski L, Zimmer AM, Beck TW, Hahn H, Bernal R, Rapp UR, Zimmer A. 1997. Endothelial apoptosis in Braf-deficient mice. *Nat Genet* **16**: 293-297.

Wolk K, Witte E, Warszawska K, Schulze-Tanzil G, Witte K, Philipp S, Kunz S, Docke WD, Asadullah K, Volk HD et al. 2009. The Th17 cytokine IL-22 induces IL-20 production in keratinocytes: a novel immunological cascade with potential relevance in psoriasis. *Eur J Immunol* **39**: 3570-3581.

Wright TM. 1997. Cytokines in acute and chronic inflammation. *Frontiers in Bioscience* **2**: d12-26.

Wu Y, Han M, Guan KL. 1995. MEK-2, a Caenorhabditis elegans MAP kinase kinase, functions in Ras-mediated vulval induction and other developmental events. *Genes & development* **9**: 742-755.

Wuichet K, Sogaard-Andersen L. 2014. Evolution and diversity of the Ras superfamily of small GTPases in prokaryotes. *Genome Biol Evol* **7**: 57-70.

Yamaoka T, Kusumoto S, Ando K, Ohba M, Ohmori T. 2018. Receptor Tyrosine Kinase-Targeted Cancer Therapy. *Int J Mol Sci* **19**.

Yao Y, Li W, Wu J, Germann UA, Su MS, Kuida K, Boucher DM. 2003. Extracellular signal-regulated kinase 2 is necessary for mesoderm differentiation. *Proc Natl Acad Sci U S A* **100**: 12759-12764.

Yi J, Chen M, Wu X, Yang X, Xu T, Zhuang Y, Han M, Xu R. 2010. Endothelial SUR-8 acts in an ERK-independent pathway during atrioventricular cushion development. *Dev Dyn* **239**: 2005-2013.

Yoon S, Seger R. 2006. The extracellular signal-regulated kinase: multiple substrates regulate diverse cellular functions. *Growth Factors* **24**: 21-44.

Yoshiki S, Matsunaga-Udagawa R, Aoki K, Kamioka Y, Kiyokawa E, Matsuda M. 2010. Ras and calcium signaling pathways converge at Raf1 via the Shoc2 scaffold protein. *Mol Biol Cell* **21**: 1088-1096.

Yoshimura N, Chancellor MB. 2004. Differential diagnosis and treatment of impaired bladder emptying. *Rev Urol* **6 Suppl 1**: S24-31.

Young LC, Hartig N, Boned Del Rio I, Sari S, Ringham-Terry B, Wainwright JR, Jones GG, McCormick F, Rodriguez-Viciana P. 2018. SHOC2-MRAS-PP1 complex positively regulates RAF activity and contributes to Noonan syndrome pathogenesis. *Proc Natl Acad Sci U S A* **115**: E10576-E10585.

Young LC, Hartig N, Munoz-Alegre M, Oses-Prieto JA, Durdu S, Bender S, Vijayakumar V, Vietri Rudan M, Gewinner C, Henderson S et al. 2013. An MRAS, SHOC2, and SCRIB complex coordinates ERK pathway activation with polarity and tumorigenic growth. *Mol Cell* **52**: 679-692.

Young LC, Rodriguez-Viciana P. 2018. MRAS: A Close but Understudied Member of the RAS Family. *Cold Spring Harb Perspect Med*.

Yuan J, Ng WH, Tian Z, Yap J, Baccarini M, Chen Z, Hu J. 2018. Activating mutations in MEK1 enhance homodimerization and promote tumorigenesis. *Sci Signal* **11**.

Zhang B, Hsu YC. 2017. Emerging roles of transit-amplifying cells in tissue regeneration and cancer. *Wiley Interdiscip Rev Dev Biol* **6**.

Zhang BH, Guan KL. 2000. Activation of B-Raf kinase requires phosphorylation of the conserved residues Thr598 and Ser601. *EMBO J* **19**: 5429-5439.

Zhang F, Strand A, Robbins D, Cobb MH, Goldsmith EJ. 1994. Atomic structure of the MAP kinase ERK2 at 2.3 A resolution. *Nature* **367**: 704-711.

Zhang FL, Casey PJ. 1996. Protein prenylation: molecular mechanisms and functional consequences. *Annu Rev Biochem* **65**: 241-269.

Zhang L-J. 2018. Keratins in Skin Epidermal Development and Diseases. IntechOpen.

Zhao H, Liu P, Zhang R, Wu M, Li D, Zhao X, Zhang C, Jiao B, Chen B, Chen Z et al. 2015. Roles of palmitoylation and the KIKK membrane-targeting motif in leukemogenesis by oncogenic KRAS4A. *J Hematol Oncol* **8**: 132.

Zheng CF, Guan KL. 1994. Activation of MEK family kinases requires phosphorylation of two conserved Ser/Thr residues. *EMBO J* **13**: 1123-1131.

Zheng T, Oh MH, Oh SY, Schroeder JT, Glick AB, Zhu Z. 2009. Transgenic expression of interleukin-13 in the skin induces a pruritic dermatitis and skin remodeling. *J Invest Dermatol* **129**: 742-751.

Zhong ZA, Sun W, Chen H, Zhang H, Lay YE, Lane NE, Yao W. 2015. Optimizing tamoxifen-inducible Cre/loxp system to reduce tamoxifen effect on bone turnover in long bones of young mice. *Bone* **81**: 614-619.

Zhou Y, Hancock JF. 2015. Ras nanoclusters: Versatile lipid-based signaling platforms. *Biochim Biophys Acta* **1853**: 841-849.

Zimmermann S, Moelling K. 1999. Phosphorylation and regulation of Raf by Akt (protein kinase B). *Science* **286**: 1741-1744.

Zou Y, Ma D, Wang Y. 2019. The PROTAC technology in drug development. *Cell Biochem Funct* **37**: 21-30.

Appendices

Appendix I

List of publications during the PhD programme

Boned Del Río I, Young LC, **Sari S**, Jones GG, Ringham-Terry B, Hartig N, Rejnowicz E, Lei W, Bhamra A, Surinova S, Rodriguez-Viciana P (2019). SHOC2 complex-driven RAF dimerization selectively contributes to ERK pathway dynamics. Proc. Natl. Acad. Sci. U.S.A. 116(27), 13330–13339.

Jones GG, Del Río IB, **Sari S**, Sekerim A, Young LC, Hartig N, Areso Zubiaur I, El-Bahrawy MA, Hynds RE, Lei W, Molina-Arcas M, Downward J, Rodriguez-Viciana P (2019). SHOC2 phosphatase-dependent RAF dimerization mediates resistance to MEK inhibition in RAS-mutant cancers. Nat Commun. 10(1):2532.

Young LC, Hartig N, Boned Del Río I, **Sari S,** Ringham-Terry B, Wainwright JR, Jones GG, McCormick F, Rodriguez-Viciana P (2018). SHOC2-MRAS-PP1 complex positively regulates RAF activity and contributes to Noonan syndrome pathogenesis. Proc. Natl. Acad. Sci. U.S.A. 115(45), E10576–E10585.

Appendix II

List of license numbers provided by Copyright Clearance Centre (RightsLink)

License number	
4940870758120	Figure 1-1A
4940871324600	Figure 1-1B and 1-2A
1074566	Figure 1-5